

Wind tunnel modelling of atmospheric boundary layer flow over hills

Dissertation

Zur Erlangung des Doktorgrades der Naturwissenschaften im
Fachbereich Geowissenschaften der Universität Hamburg

vorgelegt von

Graciana Petersen

aus

Hamburg

Hamburg

2013

(Jahr der Drucklegung)

Als Dissertation angenommen vom Fachbereich Geowissenschaften
der Universität Hamburg

Aufgrund der Gutachten von Prof. Dr. Bernd Leidl
und Prof. Dr. Michael Schatzmann

Hamburg, den 18. Januar 2013.

Tag der Disputation war am 18. Januar 2013.

Prof. Dr. Jürgen Oßenbrügge
Leiter des Fachbereichs Geowissenschaften

Cover page according to §7.5 of the Doctoral Degree Regulations of the MIN Faculty;

Names of the evaluators:

Prof. Dr. Bernd Leidl

University of Hamburg

Meteorological Institute – EWTl Environmental Wind Tunnel Laboratory

Bundesstrasse 55

D-20146 Hamburg / Germany

Prof. Dr. Michael Schatzmann

University of Hamburg

Meteorological Institute

Bundesstrasse 55

D - 20146 Hamburg

Declaration according to §7.4 of the Doctoral Degree Regulations of the MIN Faculty:

I hereby declare, on oath, that I have written the present dissertation by my own and have not used other than the acknowledged resources and aids.

Hamburg, 26/09/2012

(Signature)

Preface

*“What we observe is not nature itself, but nature exposed to our method of questioning.”
Werner Heisenberg*

How can wind tunnel modelling be applied to the atmosphere of the earth? What has to be considered for modelling hilly terrain? What insights can we hope for using wind tunnel experiments for the improvement of wind energy assessment?

The analysis carried out does not answer the question of whether or not wind tunnel simulation is useful for wind energy assessment in every-day work of wind consulting from economical point of view. Instead, the scientific potential and value of wind tunnel experiments for atmospheric wind flow over hills is investigated. This includes an analysis of the underlying theories, an analysis of the relation between models and reality and extensive analyses of the quality and data of the experiments which were carried out.

It is clear that a scientific analysis concerning the potential and value of a scientific method, such as wind tunnel modelling, is never complete. It is not only a snapshot in time (since modelling techniques advance) it is also always a matter of the focus of the author on certain aspects.

This analysis is inspired by the idea that science is not an isolated endeavour: *“The physicist may be satisfied when he has the mathematical scheme and knows how to use it for the interpretation of the experiments. But he has to speak about his results also to non-physicists who will not be satisfied unless some explanation is given in plain language. Even for the physicist the description in plain language will be the criterion of the degree of understanding that has been reached”*, [Heisenberg, 1958]. That is, science is driven by interaction and communication amongst people with diverse backgrounds.

Serious problems come along with the complexity in scientific work. This comprises for example according to William Rehg (with regard to scientific argumentation) the scientific authority and neutrality, [Rehg 2009, 2011]. His conclusions are that *“given that the multidisciplinary complexity of the technical issues exceeds the expertise of any one person, the cogency of such arguments must be assessed [...] at the level of the argumentative process [...] specifically, assessment must attend to three levels of context: (1) the report content, (2) the local transactions in which reports are constructed and evaluated, and (3) the relevant public networks through which the reports legitimately travel”*, [Rehg 2011, pp. 386]. He argues that for a quality assessment of scientific work, the report content is only one of three levels of the context. The context of production, the use of results and the preparedness for the public perception has to be assessed as well. This fits well with Heisenberg’s opinion and the motivation behind this work. The author of this work believes that multidisciplinary work is not only necessary for quality assurance of scientific argumentation – above all it is the main potential for development in science.

As a teaser for the complexity of modern research in fluid dynamics, see Figure 1, p. 14.

The purpose of this work is to be as focused and exhaustive of the available expert knowledge as necessary whilst being as interdisciplinary und mutually understandable as possible, since the author wants to deliver a compact and coherent analysis on the issue.

This work is divided into 4 key parts:

- **I) Introduction**
- **II) Fundamental work**
- **III) Experimental work**
- **IV) Conclusions and future work**

The outline of the chapters is as follows:

I) Introduction

Chapter 1-3: The *motivation* for this work and an introduction into *atmospheric boundary layer flow* as well as *wind tunnel modelling* is presented.

II) Fundamental work

Chapter 4: The theoretical foundation of fluid dynamics is analysed. This builds the basis for the analysis of wind tunnel modelling within atmospheric science. The analysis is carried out by formal methods of philosophy of science, which are used to structure building blocks and theories of science (structuralism and conceptual spaces). Both methods have been widely applied to a number of scientific disciplines in literature. Here, they are applied to fluid dynamics and target to reveal an innovative point of view for philosophers of science, physicists and mathematicians dealing with the Navier-Stokes Equations.

Chapter 5: The relation between models, theories and applicability of wind tunnel modelling is examined. This will set the stage for what scientifically can be expected of wind tunnel modelling with application for wind assessment. The term “models” is used here in the sense of Cartwright, Morgan and Morrison, meaning *models as mediators between reality and theories*. In modern philosophy of science it is convenient to believe that not only one theory can explain the world, but different *theories competing with each other* [Cartwright 1983, Morgan and Morrison 1999]. This will be explained in detail. Also, the analysis links the ideas of modern philosophy of science with an analysis of the challenges in wind (energy) assessment.

Chapter 6: This chapter is a comprehensive overview of the *physics* of the atmospheric boundary layer flows *over hills* and the challenges which theories, field studies and numerical or physical modelling face. Whereas preceding chapters are written for a more general audience, here the *fundamental concepts* of atmospheric boundary layer flow

over hills are presented in detail. A *literature review* and *historical overview* examines how wind tunnel modelling has been applied to atmospheric boundary layer flow over hills. In addition, specific theories for wind flow over hills, e.g. the *Linear Theory* by Jackson and Hunt, [1975], are explored and field studies for atmospheric flow over hills are reviewed.

III) Experimental work

Chapter 7: The challenges for quality assurance in wind tunnel modelling of atmospheric boundary layer flows are narrowed down further by means of a *concrete example*. In this chapter, the *pilot study* to the main (real) Bolund wind tunnel study is described. In this *pilot study* the *sensitivity* of the geometrical representation of hill *shapes* as well as the impact of the geometrical representation on the *repeatability* of measurements was examined extensively. The aim of the pilot study was to test the aforementioned sensitivity of wind tunnel modelling to prepare for the main wind tunnel study of Bolund in WOTAN.

Chapter 8: In this chapter, the *main Bolund wind tunnel experiment* in the large wind tunnel, WOTAN, of the environmental wind tunnel laboratory (EWTL) Hamburg is described. The selected site is the Bolund hill, an island with steep slopes with an area of 60 x 150 m² in Denmark where a field study was carried out in 2007/2008. The major point in this chapter is to provide a concrete and detailed analysis of the *quality* and *uncertainty* of the experimental results of Bolund in WOTAN. To maximize *accuracy* emphasis was placed on the determination of *plausible meteorological inflow conditions* similar to those of the field study area. Secondly, to maximize *precision* of the experiment emphasis was placed on the assessment and optimisation of the *repeatability of the experiment*. This was based on the *lessons learnt* from the pilot study. In brief, this chapter aims to illustrate the key issues of wind tunnel simulation for flow over hills against the background of the fundamental analyses of the previous chapters.

Chapter 9: Data acquired by laser-doppler-anemometry (LDA), as in the Bolund wind tunnel experiment, consists of non-equidistant time series. For more *advanced statistical* methods of turbulence research with LDA data such as extreme value analysis or tests of theories on turbulence scaling laws, *statistical convergence* of the advanced statistical parameters has to be assured. Recommendations of user manuals for LDA data may not been sufficient. Here, higher order statistics and the influence of sampling duration, sampling rate and LDA-resampling frequencies are examined.

IV) Conclusions and future work

Chapter 10: Results and conclusions are summarized in a guide for wind tunnel modelling of neutral atmospheric boundary layer flows over hills. Remarks are given and open questions are pointed out. Also, modelling based reasoning in the light of Bayesian interference is suggested as a pragmatic approach to deal with model results in the absence of absolute model validation of model results. This closes the loop resulting from the questions posed in this preface.

Microstructure of the text:

- The expert vocabulary is explained where necessary. A list of abbreviations, symbols and selected vocabulary is included following the table of contents. In the case that (mathematical) terminology is not explained further, this is a signal that the understanding of the mathematical details is not crucial for the broader understanding of the text.
- Chapters start with a short introductory paragraph recapitulating how it fits with the larger body of work. At the end of chapters 4 - 9, the main findings, thoughts and future work are summarized. The objective of this is to provide the multidisciplinary reader the option to read the summaries first and then selectively probe the more technical and detailed arguments.

- Quotations in the text are ordered by relevance. In case of equal relevance, they are ordered alphabetically and then by year of publication. References at the end of the book are ordered alphabetically and then by year of publication.
- Words are typed in *light italic font* if they require *special attention*. For a term in inverted commas, a “so-called” can be added in front of the expression.
- The sign: $__ /$ - is used as visual separator after (mathematical) definitions, aligned on the right.

Many parts of this work are submitted to journals, have already been presented at conferences or published in conference proceedings.¹

¹ Parts of chapter 8 are submitted to Boundary Layer Meteorology (Springer), parts of chapter 4 are submitted to History and Philosophy of Science (Elsevier), with F. Zenker; parts of chapter 9 are submitted to Environmental Fluid Mechanics (Springer) with M. Hölling and B. Leitl; parts of chapter 5 are a rewrite of Petersen et al. 2011c, (PHYSMOD 2011 proceedings, Hamburg); parts of chapter 5 and 6 are a rewrite of Petersen et al. 2011a, (EAWC proceedings, Brussels) and Petersen et al. 2011b, (ICWE 13, conference paper, Amsterdam).

Acknowledgements:

The author deeply acknowledges the team of the Environmental Wind Tunnel Laboratory at the University of Hamburg, including Frank Harms, Denise Hertwig, Stephan Werk, Francesco Cuzzola, Rasmus Fischer, Frieso Kipsch and Christine Peeck for help and support. In addition, many thanks belong to Prof. Ulrich Gähde and Martin Hoffmann from the Department of Philosophy, Theoretical Philosophy, University of Hamburg, and Frank Zenker and Prof. Peter Gaerdenfors, Department of Philosophy, Lund University, for giving inspiring insights into the meaning of science. You helped me developing an idea of what models are, how to treat model results in a scientific and real world context, and opened my eyes lastingly in different ways.

Furthermore, thanks to the members of the mathematical department, University of Hamburg, who helped me developing the mathematical tool kit, including Prof. Holger Drees for giving valuable insights for extreme value analysis – and, of course, Prof. Vicente Cortés. Also, many thanks to Prof. Andreas Bechmann, Risø DTU, and Ingo Lange, MI University of Hamburg, for providing field data. Also, many thanks to Prof. Ruedi Kuensch, ETHZ Zürich, for the interesting collaboration on long range dependence² of field and wind tunnel data, and Michael Hölling, for collaboration on higher order statistics.

On top, this work is dedicated to the tax payer who enabled the author to learn about the art of wind tunnel modelling and the exciting and challenging questions of the meaning of theories and models. This led to a journey through atmospheric science, fluid dynamics, quality assurance of data analysis and consistency of research results which was highly appreciated by G.P..

The best for last: Exceptional acknowledgements belong to my supervisors, Prof. Bernd Leitl and Prof. Michael Schatzmann, who - with great wisdom - encouraged me to research openhearted on the critical and detailed questions that tortured me the most

² Long-range dependence is a statistical property which is characteristic for some self-similar processes.

throughout the three years. You provided me with any support I could have wished for. This time has been a great inspiration for me. Thank you.

Altogether, this work is the outcome of a lot of effort and support of more dear people who know in how far they have contributed to this work – and I am thankful for the great time that I was honoured to experience. I hope you enjoy reading.

Hamburg, 10.07.2012

References of the introduction (in order of quotations):

Heisenberg: Physics and Philosophy: The Revolution in Modern Science (1958) Lectures delivered at University of St. Andrews, Scotland, Winter 1955-56

Rehg, W.: Cogent Science in Context. Cambridge: MIT Press, 2009

Rehg, W.: Evaluating complex collaborative expertise: the case of climate change. *Argumentation*, 25, 385-400, 2011

Cartwright, N.: How the Laws of Physics Lie, Oxford University Press, 1983

Morgan, M. S. & Morrison, M.: Models as Mediators: Perspectives on Natural and Social Science Cambridge University Press, 1999

Jackson, P.S. and Hunt, J.C.R.: Turbulent wind flow over a low hill. *Quart. J. R. Met. Soc.*, 101:929–955, 1975.

Petersen, G.; Leitl, B. and Schatzmann, M.: On proper physical simulation of turbulent atmospheric flow over hills, EAWE proceedings, Brussels,, 2011a

Petersen, G.; Leitl, B. and Schatzmann, M.: ABL flow over hills: A review on theory and critics of recent wind tunnel studies, ICWE 13, conference paper, Amsterdam, 2011b

Petersen, G.; Gähde, U.; Hoffman, M.; Leitl, B. and Schatzmann, M.: Models in Wind Energy Assessment, PHYSMOD 2011 proceedings, 2011c

Research in modern fluid dynamics around time series and equation analysis

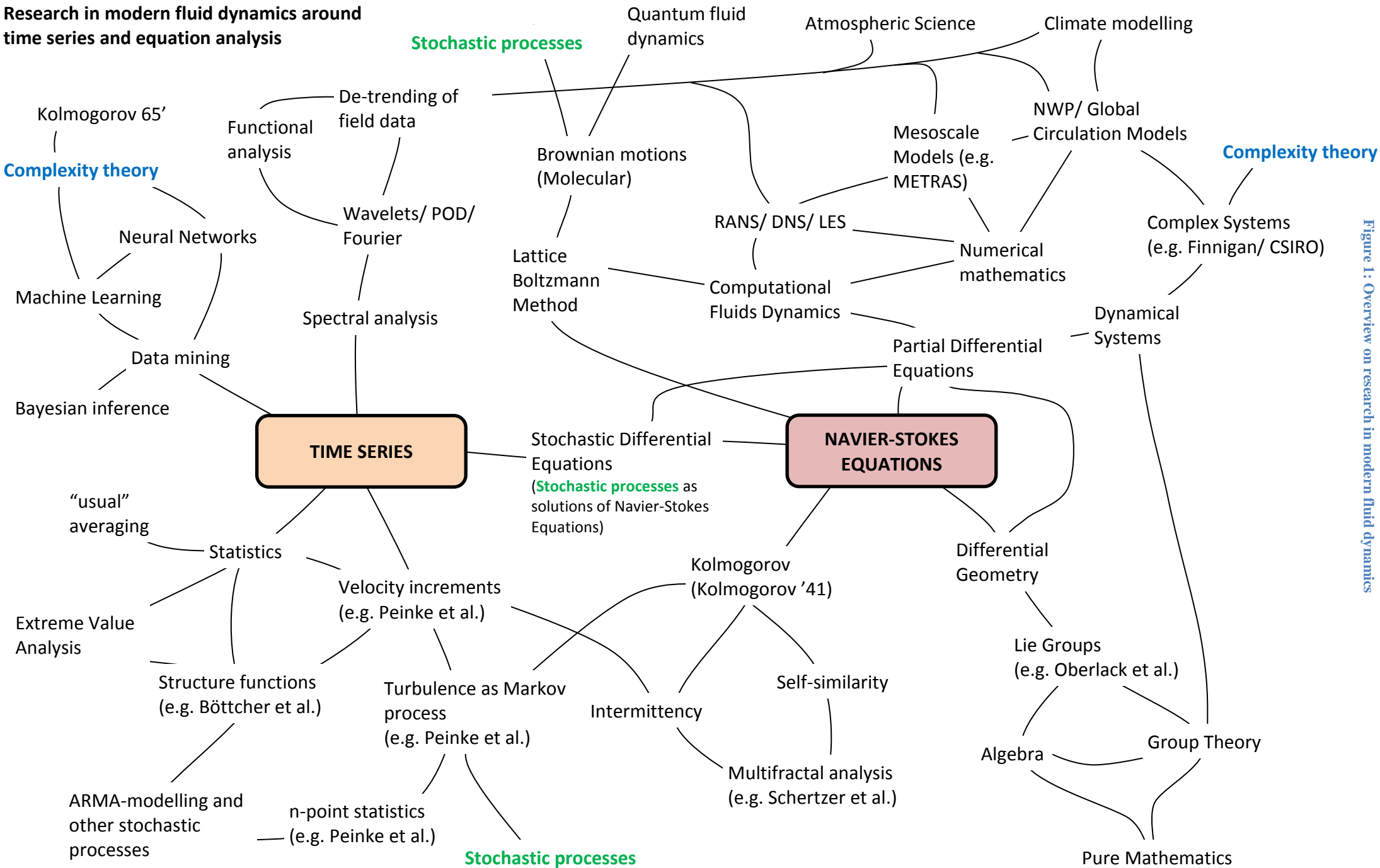


Figure 1: Overview on research in modern fluid dynamics

Research tools and links with each other: phenomenological analysis (time series) and analytical (Navier-Stokes Equations for macroscopic and Boltzmann Transport Equations for microscopic fluid dynamics). This is a heuristic overview based on personal selection by the author.

Table of Content

Introductory practicalities 20

<i>Abstract</i>	<i>20</i>
<i>List of abbreviations</i>	<i>21</i>
<i>List of symbols</i>	<i>22</i>
Fluid dynamics and history of fluid dynamics	22
Mathematical symbols	22
Turbulence characteristics and wind profile	23
Hill characteristics.....	23
Philosophy	23

Part I: Introduction

1. Motivation 25

<i>Definition of the problem “flow over hills”</i>	<i>27</i>
--	-----------

2. Atmospheric boundary layer flow 28

<i>Layers in the atmosphere</i>	<i>28</i>
<i>Equations of motion for fluids</i>	<i>30</i>
<i>Reynolds averaged Navier-Stokes equations (RANS)</i>	<i>31</i>
<i>Logarithmic wind profile.....</i>	<i>32</i>
<i>Boundary layer theory</i>	<i>35</i>

3. Wind tunnel modelling 37

<i>Similarity criterion as fundamental principle</i>	<i>37</i>
<i>The ergodic theorem.....</i>	<i>41</i>
<i>Model simplifications.....</i>	<i>45</i>
<i>Model case restrictions.....</i>	<i>46</i>
<i>Model strengths.....</i>	<i>47</i>

Part II: Fundamental work

4. Theory of fluid dynamics reconstructed in structuralism and conceptual spaces 51

<i>Introduction to this chapter</i>	51
<i>Introduction to structuralist concepts and conceptual spaces</i>	53
<i>Physical foundations of modern fluid dynamics</i>	57
The continuum hypothesis	58
Classic mechanics translated to fluids.....	61
With Stokes and mechanical equilibrium to static pressure.....	63
Gas as a special case	66
Fluid in motion and Euler in the river.....	69
From Euler to Navier Stokes	71
<i>Remarks</i>	74
<i>Summary - Theory</i>	76
<i>Conclusions and outlook – Theory</i>	76

5. Models as mediators in wind assessment 79

<i>Introduction to this chapter</i>	79
<i>Model in science and model development</i>	80
Models in philosophy of science	80
Models, theory, reality and data in wind assessment.....	84
Comparison of models.....	86
Field data	91
Model development and artificial experience	97
<i>Application field: wind energy assessment</i>	101
<i>Summary - Models</i>	103
<i>Conclusions and outlook - Models</i>	104

6. Atmospheric boundary layer flow over hills 106

<i>Introduction to this chapter</i>	106
<i>A review of research on flow over hills</i>	106
Wind tunnel simulation of flow over hills (early years)	107
Wind tunnel simulation of flow over hills (modern times)	108
Discussion of recent wind tunnel studies.....	111
Theory of flow over hills – a rough overview	115
Bernoulli effect	116
Linear Theory by Jackson and Hunt.....	119
Field studies.....	122
Numerical modelling	128
<i>Summary – Flow over hills</i>	130
<i>Conclusions and outlook – Flow over hills</i>	130
<i>Acknowledgement (II)</i>	131

Part III: Experimental work

7. Pilot study to the Bolund wind tunnel experiment 133

<i>Introduction to the experimental part</i>	133
<i>The pilot study “idealized Bolund”</i>	135
Wind tunnel facility BLASIUS	135
Laser-doppler-anemometry (LDA).....	136
The inflow conditions	138
Idealized model hills	140
<i>On error analysis</i>	143
<i>Precision assessment in practice</i>	146
<i>Mean flow dependency on the hill shape representation</i>	159
<i>Summary of the pilot study</i>	164
<i>Lessons learnt from the pilot study</i>	165

8. The Bolund hill wind tunnel experiment 167

<i>Fundamentals and experimental set-up</i>	168
Wind tunnel facility WOTAN	170
Wind tunnel instrumentation and hill model.....	172
<i>Bolund hill inflow conditions</i>	177
Determination of plausible inflow conditions	177
Adjustment of the determined inflow conditions.....	184
<i>Analysis of precision</i>	194
Repeatability and convergence	194
Reynolds number tests	200
<i>Mean flow results for Bolund in WOTAN</i>	205
Mean velocity around the hill.....	205
Mean standard deviations around the hill	208
Skewness and shear stress around the hill.....	215
Speed-up effect above the front edge	218
Deceleration areas around the hill	222
Summary of the flow results	227
<i>Remarks on the Bolund field data</i>	229
<i>Summary of Bolund in WOTAN</i>	243

9. Statistical analysis of the influence of resampling configurations on higher order statistics at the luv edge 246

<i>Statistical representativeness</i>	249
<i>Description of methodology</i>	250
<i>Results of the statistical analysis</i>	252
<i>Discussion of the statistical analysis</i>	261
<i>Conclusion of the statistical analysis</i>	261
<i>Acknowledgement (III)</i>	263

Part IV: Conclusions and future work

10. Final summary and conclusions..... 265

<i>Summary of the main results.....</i>	<i>265</i>
<i>Summary: Suggestions for wind tunnel modelling of ABL flow over hills</i>	<i>268</i>
<i>Remarks</i>	<i>273</i>
<i>Future work.....</i>	<i>276</i>
Open questions.....	276
Modelling based reasoning in the light of Bayesian interference	279

References 287

Appendix 304

<i>Categorisation of changes in terms of conceptual spaces</i>	<i>304</i>
<i>Key figures for the 18th and 19th century fluid dynamics.....</i>	<i>306</i>
<i>Bolund field data analysis.....</i>	<i>307</i>
<i>On basic error metrics.....</i>	<i>318</i>
Standard Deviation	318
Absolute Deviation	318
Spread.....	319
<i>Idealized Bolund hill test (Blasius)</i>	<i>320</i>
Dependence of repeatability assessment on the flow location.....	322
Influence of manual LDA-probe adjustment	324
Reynolds number tests of the pilot study	325
<i>Description of the data structure for main Bolund in WOTAN.....</i>	<i>327</i>
<i>Appendix to the set-up of the inflow-conditions</i>	<i>332</i>
<i>MATLAB program code for filtering Bolund field data</i>	<i>337</i>
<i>Quick Bolund MySQL Query Browser manual</i>	<i>337</i>
<i>Structure function – what is this for?</i>	<i>341</i>
<i>Remarks on the work carried out</i>	<i>342</i>
<i>Standard Bayesian framework</i>	<i>345</i>
<i>Appendix according to §7 paragraph 4 of the Doctoral Degree Regulations of the MIN</i>	
<i>Faculty:</i>	<i>349</i>
Short summary of the results in English:.....	349
Short summary of the results in German:	349
List of any earlier publications derived from the dissertation:	352

Introductory practicalities

Abstract

This work provides a fresh (not exhaustive) analysis on wind tunnel modelling for atmospheric boundary layer (ABL) flow over hills. New insights are developed into the theoretical and practical challenges of modelling flow over hilly terrain. In this work, specific suggestions and examples for *quality assurance* and *consistency* of model results are given, such as for the statistical reliability of measurements, assessment of inflow conditions and the sensitivity of the model results on the geometrical representation of the hill shape.

Analyses are based on a fundamental study of the underlying theories of fluid dynamics and the relationship between models, theories, reality and data. This is completed with the examination and conduction of two wind tunnel experiments: a sensitivity pilot study and a main (real terrain) wind tunnel experiment for flow over a steep hill.

At the end of each chapter, summary, conclusions and an outlook are provided. In the final chapter, suggestions for wind tunnel modelling of ABL flow over hills are summarized, remarks are given and open questions are pointed out.

List of abbreviations

ABL = Atmospheric Boundary Layer

agl = above ground level

CFD = Computational Fluid Dynamics

COST = European Cooperation in Science and Technology

DNS = Direct Numerical Simulation

ESDU = Engineering Science Data Unit

ETWL Hamburg = Environmental Wind Tunnel Laboratory University of Hamburg

IEC = International Electrotechnical Commission

JCGM = Joint Committee for Guides in Metrology

LDA = LASER-doppler-anemometry

LES = Large Eddy Simulation

Lidar = Light detection and ranging (also: LIDAR)

NSE = Navier-Stokes Equations

PDF = Probability Density Function

RANS = Reynolds Averaged Navier-Stokes Equations

SGS = sub-grid scale model (in large eddy simulation)

TPWind = Technology-Platform-for-Wind-Energy

VDI = Vereinigung Deutscher Ingenieure

WAsP = Wind Atlas Analysis and Application Program

WAUDIT = Wind resource assessment audit and standardization

WECS = Wind Energy Converter Systems

List of symbols

Fluid dynamics and history of fluid dynamics

a	= acceleration
δA	= surface element
δV	= Volume element
$\Sigma(n,x,t) = \Sigma$	= surface force with direction perpendicular towards the surface
F	= force
m	= mass
p	= pressure
R	= gas constant
ρ	= density of e.g. a fluid
t	= time
u	= velocity
z	= height of e.g. a measurement position
μ	= viscosity (material property)

Mathematical symbols

∇	= nabla operator
Δ	= difference
$\frac{\partial u}{\partial t}$	= partial derivative (of u with respect to t)
δ_{ij}	= Kronecker delta, i.e. $\delta_{ij} = \begin{cases} 1 & \text{if } i = j \\ 0 & \text{if } i \neq j \end{cases}$
\in	= is element of (" $x \in A$ " means " x is element of A ")
\subset	= is subset of (" $I_g \subset \mathbb{R}$ " means " I is subset of \mathbb{R} ")
\cup	= conjunction with (" $A \cup B$ " means " A conjoint with B ")
\cap	= intersected with (" $A \cap B$ " means " A intersected with B ")
\mathbb{R}	= real numbers
\forall	= "for all"

Turbulence characteristics and wind profile

α	= vertical wind profile power law exponent
BL_δ	= boundary layer depth
g	= gravitational acceleration
$invL$	= inverse Monin Obukhov length
$I_{u,v,w}$	= turbulence intensity of wind speed U,V,W-component
k	= kinetic energy
κ	= von-Kármán constant
L_x	= longitudinal integral length scale (characteristic length of large eddies), e.g. derived from autocorrelation function
\ln	= natural logarithm
Re	= Reynolds number; $Re := \frac{u_R L_R}{\mu}$, with reference velocity, u_R , reference length, L_R
$\bar{\theta}, \theta'$	= mean resp. fluctuation value of potential temperature
T_A	= advection-distortion time scale
T_L	= Lagrangian integral time scale
U_{ref}	= reference wind speed at a certain point (in space-time)
u^*	= friction velocity
z_{agl}	= height above ground level of e.g. a measurement position
z_0	= roughness length

Hill characteristics

agl	= above ground level
H	= hill height
\hat{L}	= characteristic hill length (defined by Jackson-Hunt)
L	= hill length

Philosophy

I	= intended application in Structuralism
K	= theory-core in Structuralism
T	= theory element in Structuralism

Part I: Introduction

1. Motivation

“Courting the sympathy of politicians has its dangers, of course. Let me stress that we must maintain high professional standards, not just in forecasting, but also in the climate and global change business.

Given the extreme difficulty of the problems and the well-known impatience of politicians, this will be a formidable task. We should not run the risk of losing our credibility by jumping on the bandwagon of those who wish to jump to conclusions.”

- [Tennekes, 1988]

Improvement of atmospheric flow models is an on-going question, for example within European projects such as “Wind resource assessment audit and standardization” (WAUDIT), based on the European-Technology-Platform-for-Wind-Energy 3-percent-vision which aims at reducing uncertainties in wind resource assessment and forecasting below three percent by 2030, regardless of the site conditions, [Rodrigo, 2010]. The situation of today’s wind energy assessment is as follows: Predictions are quite erroneous and numbers depend on whom you ask and what kind of “uncertainty” they refer to (manufacturers, investors, politicians, scientist, or wind consulting agencies). In consequence, wind energy assessment quality is hardly provable. On top, data is rarely publicly shared. However: An uncertainty of 30-40 percent in today’s prediction of wind energy output for the next ten years at an average wind energy site can be assumed, [Rodrigo, 2010].

In order to improve wind energy assessment, much money is invested into scientific projects such as WAUDIT (Wind resource assessment audit and standardization) a Marie-Curie action funded by the European Union. The scientific goal of the project is based on the European-Technology-Platform-for-Wind-Energy 3-percent-vision. Whether such aim is within reach remains to be seen and is not to be discussed at this point.

In wind energy, an important question is how to take *complex terrain* into account for the siting of wind energy converting systems (WECS). In addition to *wind speed-up* over hill crest, *turbulence effects* due to topography and *flow separation* are important features for wind

energy assessment. *Turbulence effects* such as *wind shear* can cause in- or decrease of wind energy profit. Turbulence can also have negative effects on the life-time of WECS. In the worst case this leads to *failure* or *damage*.

Ayotte and Hughes, [2004], state that in the commercial arena, the need for *rapid* calculations has led to the development of a number of models in which the *advection* and *turbulent stress terms* are linearized. Linearization of the Navier-Stokes Equations (NSE) is based on Jackson and Hunts *Linear Theory* (see p. 119). However, these models are only valid for *low hills* (i.e. with moderate slopes) – strictly speaking only for *infinitely low* hills. Linear models tend to overestimate the speed-up effect. Berg et al., [2011], remark that this “has led to overly optimistic predictions of power production and thus the economic feasibility of certain wind farms”, [Berg et al., 2011, p. 2020]. Advanced tools such as Large Eddy Simulation (LES) can perform badly on steep terrain, as well, [Bechmann et al., 2011]. Also for regional numerical weather prediction models, flow over non flat topography is challenging, [Wood, 2000; and on-going work in the Wakebench project³]. One objectives of current research is the scaling up of the unresolved effects of flow interactions with the fine-scale topography and combining it with the resolution of regional scale models. This includes the interaction of form drag and shear stress perturbations of hills. For a start, Belcher et al., [1993] argue that form drag is the primary mechanism for the enhanced extraction of momentum, significantly greater than associated shear stress perturbations.

Atmospheric boundary layer flow is important, not only for wind energy assessment. Many applications, such as *determination of air pollution zones*, *predictions of smoke movement* from forest fires or *emergency response to hazardous dispersion accidents* - ask for *models* of atmospheric boundary layer flow over real terrain in the lowest 0-300 meters over ground. In these heights, the atmospheric flow is strongly affected by *surface friction* on the planetary surface and *form drag* by *planetary topography*. Due to the interaction with the *surface*, the lowest atmospheric layer is characterised by *turbulence* (wind fluctuations in all directions) and *vertical mixing*, including mixing of meteorological scalar quantities such as

³ The project Wakebench (“ Benchmarking of Wind Farm Flow Models”) started in 2010 as research tasks of the international energy agency (IEA); [http://www.ieawind.org/summary_page_31.html as of 18/10/2012]

moisture and temperature. This layer is also called *atmospheric boundary layer* (ABL) which extends up to heights of ≈ 1000 m.

In fact, in many cases real terrain is not flat. If the turbulence caused by form drag and surface friction with non-uniform *complex terrain cannot* be neglected (due to the topography) the *complexity* of the modelling increases. Hence, steep and complex terrain is a challenge for numerical models because of the non-linear effects on the flow. In short, open questions in theoretical understanding of flow over complex terrain exist. Furthermore, demand for improvement is present (e.g. for wind energy assessment).

Definition of the problem “flow over hills”

What are the “hills”?

Hills can scientifically be described as land-surface *geomorphological* objects, see e.g. Pike, [1988; 2000], or Deng, [2007]. Land-surface parameters, such as “slope of a hill”, can be used for a *geomorphometrical*⁴ classification. In this work, focus is on a radical confinement of “hills”, mainly on the Bolund case which is a small steep island in Denmark where an extensive field study was conducted in 2007/2008. Other hills that are mainly investigated in literature are “idealized hills”, e.g. bell-shaped or sinusoidal. Concerning the dimensions of the topographic area, the hill area is most commonly assumed to be small enough to *neglect* the effects of the *earth rotation* (Coriolis force) on the flow. This clearly distinguishes the here examined “hills” from “mountains” since the diameter of the model area including the whole hill as land-surface object is assumed to be < 5 km. In literature, “low” and “smooth hills” usually denote hills *with moderate slopes*. This denotation will be used in this thesis.

What is the “flow”?

“The flow” is the *atmospheric boundary layer*. This is the part of the atmosphere which is directly affected by the earth's surface and characterised by high turbulence and a logarithmic vertical mean wind profile. This will be introduced in the following chapter.

⁴ To extract measures and quantify features of topography is objective of investigation in *geomorphometry*.

2. Atmospheric boundary layer flow

“The psalmist’s line ‘I will lift up mine eyes unto the hills from whence cometh my help’ (Psalms 121) is relevant to students of complex turbulent flows. This is because turbulent boundary-layer flows over hills and waves are both controlled by mechanisms that are active in many other perturbed turbulent flows.

Study of these fluid-dynamical problems contributes to our fundamental understanding of mechanisms that control distorted flows and helps to answer practical environmental and engineering questions”
- [Belcher and Hunt, 1998]

The purpose of this chapter is not to give a complete description of the boundary layer theory. Instead, the aim is to introduce the reader to the relevant basic concepts for this work⁵.

Layers in the atmosphere

The *atmospheric boundary layer (ABL)* is the part of the *atmosphere* that is directly affected by the earth’s surface. The height of the *atmospheric boundary layer* is variable. It depends on the particular geomorphology and roughness of the surface and stratification. It can extend from a few hundred meters up to around 1 kilometre radial distance above earth’s surface. Beyond the *atmospheric boundary layer*, the *free atmosphere* extends up to around 11 kilometres. The atmosphere is a layer of gases surrounding the planet, retained by the planet’s gravity. The atmosphere is not strictly bounded to free space. The transition is smooth and can be defined by decreasing density of molecules or decreasing temperature – extending up to around 500 kilometres radial distance above earth surface (including the “thermosphere”). This is below 1/10 of Earth’s radius, which is around 6000 kilometres, Figure 2.

Atmospheric flow (or “wind”) is air in motion. It is driven by a *pressure gradient*. In the atmosphere, pressure gradients are caused by a non-uniform global *thermal energy*

⁵ This is based on Stull, [1988], and Schatzmann, [2008].

distribution. This is caused by different angles of incident of solar radiation that lead to thermal energy differences (more heating at the equator than at the poles). In the *free atmosphere* wind flows from high to low pressure in balance with the Coriolis force (caused by the rotation of the earth) parallel to the isobars (= lines of constant pressure). This is the “geostrophic wind”. Friction with earth surface can be neglected at this level.

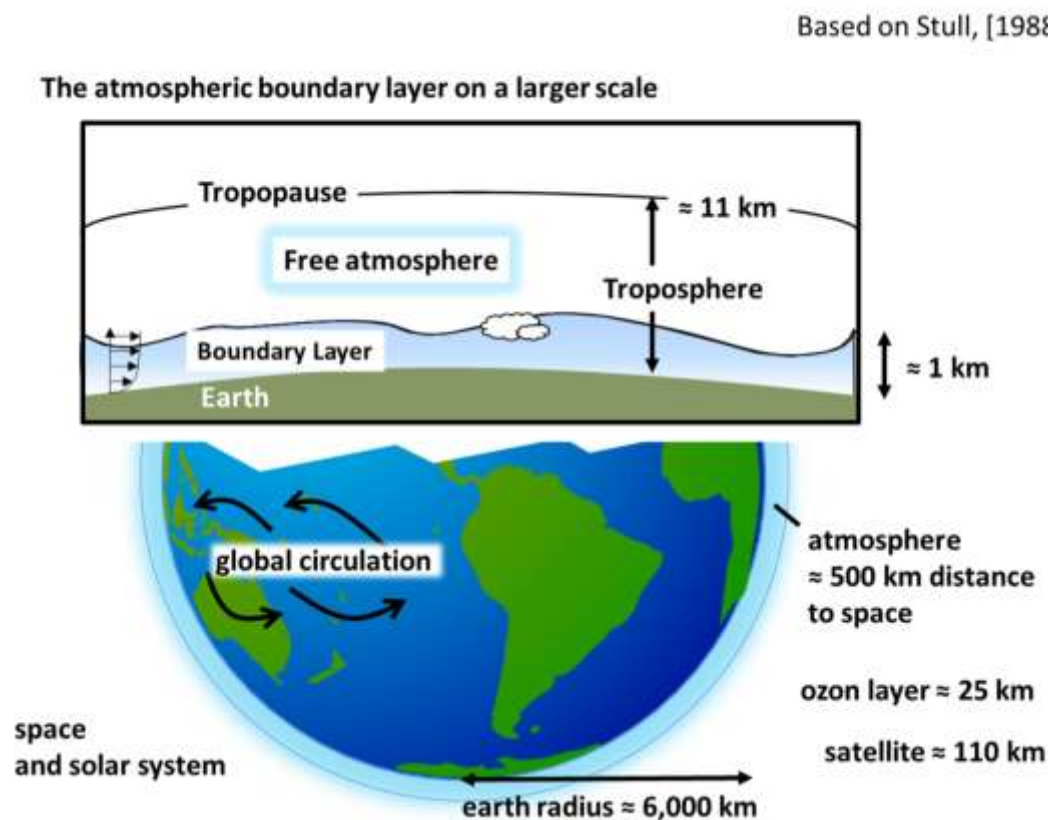


Figure 2: Basic scales of atmospheric flow

Close to the ground, the surface friction cannot be neglected. This defines the *atmospheric boundary layer*. Wind speed decreases down to zero relative to the (solid) surface boundary. The lowest layer is the *viscous* or *laminar* sublayer, being only a few millimetres thin and dominated by molecular interaction with the wall (or boundary). Beyond is the *Prandtl layer*, (also: *surface layer*), consisting of approximately 10 percent of the total boundary layer.⁶

⁶ It is named in honour of the German scientist Ludwig Prandtl (1875-1953).

The top 90 percent of the *atmospheric boundary layer* are called *Ekman layer*. In this layer, the balance between pressure gradient force and Coriolis force is disturbed and the wind vector differs from the geostrophic wind. The influence of surface friction *decreases* with *increasing* height. Due to this, the wind vector rotates towards the direction of the geostrophic wind with increasing height. This rotation is called the *Ekman spiral*.

Equations of motion for fluids

The basic laws of fluid mechanics are the mass conservation law, the momentum conservation (*Navier-Stokes equation*) and the energy conservation law. The Navier-Stokes equation is a nonlinear partial differential equation of 2nd order.

The *Navier-Stokes Equations* in *instantaneous* form, i.e. with the wind velocity, u , as a function which maps time to *instantaneous* wind speeds, are⁷:

$$\rho \left(\frac{\partial u_i}{\partial t} + u_i \cdot \nabla u \right) = a_i \rho - \frac{\partial}{\partial x_j} [p \delta_{ij} + 2\mu (S_{ij} - 1/3 S_{ii} \delta_{ij})] \quad , i, j = 1, 2, 3 \quad (\text{NSE}),$$

summed over $j = 1, 2, 3$, with

t := time, $t \in \mathbb{R}$

x := point, i.e. $x: (t) \mapsto (x_1, x_2, x_3)^t(t) \in \mathbb{R}^3$

u := the speed, i.e. $u: (x, t) \mapsto (u_1, u_2, u_3)^t(x, t) \in \mathbb{R}^3$

a := acceleration⁸, i.e. $a: (x, t) \mapsto (a_1, a_2, a_3)^t(x, t) \in \mathbb{R}^3$

p := pressure, i.e. $p: (x, t) \mapsto p(x, t) \in \mathbb{R}$

ρ := density, i.e. $\rho: (x, t) \mapsto \rho(x, t) \in \mathbb{R}$

μ := material property denoting the viscosity, i.e. $\mu: (x, t) \mapsto \mu(x, t) \in \mathbb{R}$

$$\delta_{ij} := \begin{cases} 1 & \text{if } i=j \\ 0 & \text{if } i \neq j \end{cases}$$

$$S_{ij} := \frac{1}{2} \left(\frac{\partial u_i}{\partial x_j} + \frac{\partial u_j}{\partial x_i} \right), \text{ i.e. } \frac{\partial u_i}{\partial x_j} = \frac{\partial}{\partial x_j} u_i : \mapsto \frac{\partial}{\partial x_j} u_i(x, t) \in \mathbb{R} \text{ derivative at a certain point } (x, t).$$

⁷ See e.g. Schatzmann, [2008]

⁸ Acceleration due to volume forces such as gravitation or Coriolis force

This will be explained further in chapter 4. The mathematical complexity of the NSE for turbulent flows with $\mu \neq 0$ leads to a complexity in the physical description. Practical (deterministic) description of turbulent flow is usually handled *statistically*. This means that the flow geometry is described in (time or space) averaged flow values.

Reynolds averaged Navier-Stokes equations (RANS)

Splitting u into *statistical* features, i.e. the time *average*, \bar{u} , and *fluctuations*, u' , and averaging all terms in the equation over *time*, leads to the *Reynolds averaged Navier-Stokes equations* (RANS), summed over $j = 1, 2, 3$:

$$\rho(\bar{u}_i \cdot \nabla \bar{u}) = a_i \rho - \frac{\partial}{\partial x_j} [p \delta_{ij} + 2\mu(S_{ij} - \frac{\partial}{\partial x_i} \overline{u'_i u'_j})] \quad , i, j = 1, 2, 3 \quad (\text{RANS}),$$

with $u = \bar{u} + u'$, and $\overline{u'_i u'_j}$ denoting the cross correlation⁹ (not divided by the product of the standard deviations). RANS describes *statistically stationary* turbulent flow, i.e. the instantaneous flow field is understood as a *stochastic process*, the velocity *time series*, $u(x, t)$ are *realisations* of the stochastic process at a point x , and the probability density functions of $u(x, t)$ are constant over time at x , for all x . Thus, \bar{u} and $\overline{u'_i u'_j}$ are constant over time at a point, x . Static pressure, p , forces, F , and density, ρ , in the above RANS denote *time averaged mean values*. The new generated tensor, $\overline{u'_i u'_j}$, (the *Reynolds stress* term) leads to an *underdetermined* system of equations (more variables than equations). This is the *closure problem* of the Reynolds equations. This means that the equations *remain empirical* (further information is needed to close the gap). To *close* the Reynolds equations, many competing *turbulence models* exist for the *Reynolds stress term*.

Prandtl's mixing length ansatz is based on the idea of “eddy viscosity” which parameterizes the turbulent fluctuations in terms of the *local* flow gradients. For *isotropic* flow, (= “eddy

⁹ Let $u_1(t)$ and $u_2(t)$ be two discrete time series with $t \in T$ and time average \bar{u}_1 and \bar{u}_2 . Then $\overline{u'_i u'_j}$ is defined as $1/|T| \sum_{t \in T} [(u_1(t) - \bar{u}_1)(u_2(t) - \bar{u}_2)]$. Later in this work, cross correlation will be regarded as a function of the time lag and normalized with the product of the standard deviations of u_1 and u_2 as in Dias et al, [2004]. Accordingly, the autocorrelation function of a time series will be regarded as the cross correlation function of the time series with itself.

viscosity" is assumed to be independent of direction), the *mixing length ansatz* leads to the form

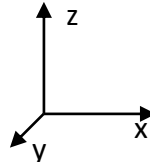
$$\overline{u_i' u_j'} = \nu_t S_{ij} - 2/3 k \delta_{ij}.$$

The scalar quantity *turbulent viscosity*, ν_t , is introduced with traditional reference to the *material viscosity*, μ , which was historically introduced to step from the Euler to the Navier-Stokes equations, see chapter 4. Here, k denotes the kinetic energy (per unit mass), $k = \frac{1}{2} \sum_{i=1}^3 (\overline{u_i' u_i'})$.

Logarithmic wind profile

With Prandtl's boundary layer theory and the RANS (or NSE), *boundary layer equations* for an *idealized atmosphere* can be derived. In the *idealized atmosphere*, flow is assumed to be *horizontally homogeneous* and *statistically stationary*. The "Boussinesq approximation" introduces simplifications for the vertical *density gradient* in the atmosphere. The simplifications yield equations for the *free atmosphere* and the *Ekman layer*. The equations can be specified for the derivation of the *logarithmic wind profile* in the *Prandtl Layer*. In the *Prandtl layer*, gravitational and Coriolis force is neglected since *shear stress* is assumed to be the dominant generator of momentum.

With $u := u_1$, $w := u_3$, $\nu := \mu/\rho$, the equations of the *idealized atmosphere* for *neutral stratification* yield:

$$0 = \frac{\partial}{\partial z} (-\overline{u'w'} + \nu \frac{\partial u}{\partial z}).$$


Integration over z and the introduction of empirically useful quantities such as the *friction velocity*, u_* , the *von Kármán constant*, κ , the *roughness length*, z_0 ,

$$u_*^2 := \overline{u_i' u_i'},$$

and the relationship

$$\frac{\partial u}{\partial z} = \frac{u_*}{\kappa z}$$

leads to the *logarithmic wind profile*:

$$u(z) = \frac{u_*}{\kappa} \ln \left(\frac{z}{z_0} \right)$$

By this *log law* the *mean wind speed* is estimated for *atmospheric boundary layer* flow in the lowest 50-100 m above ground level in the *idealized atmosphere*. This means that Prandtl's concept of boundary layer fluid mechanics is transferred to atmospheric boundary layer flow. For further reading see Schatzmann, [2008]. A scheme is given in Figure 3 and Figure 4.

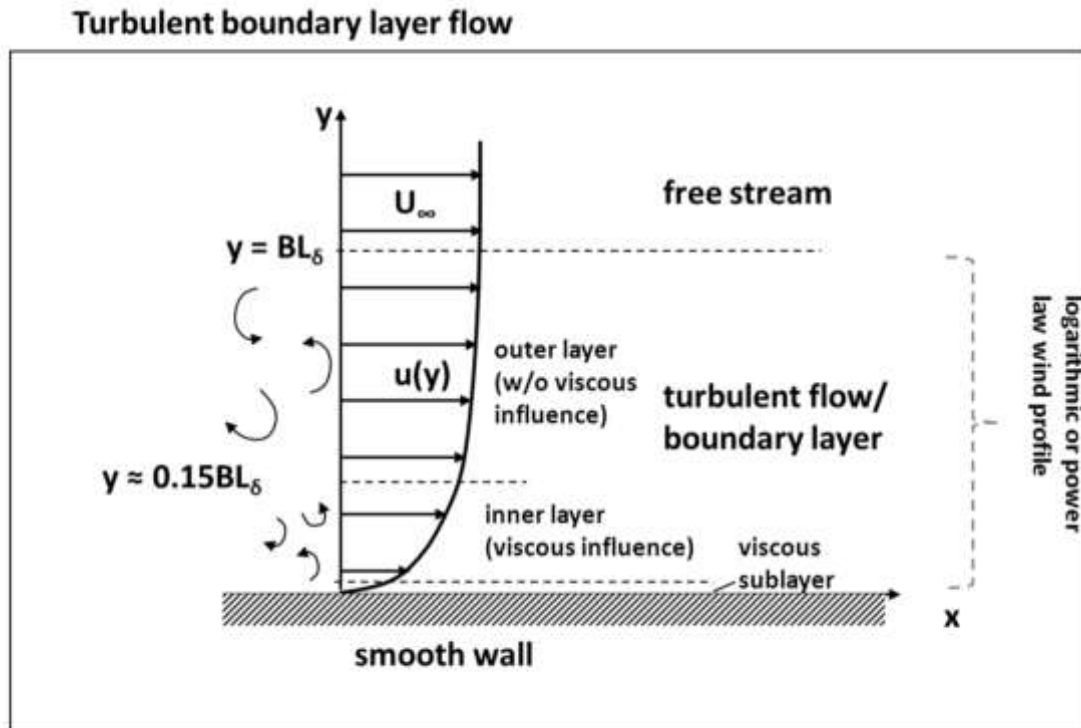


Figure 3: Wall log law and Prandtl boundary layer scheme

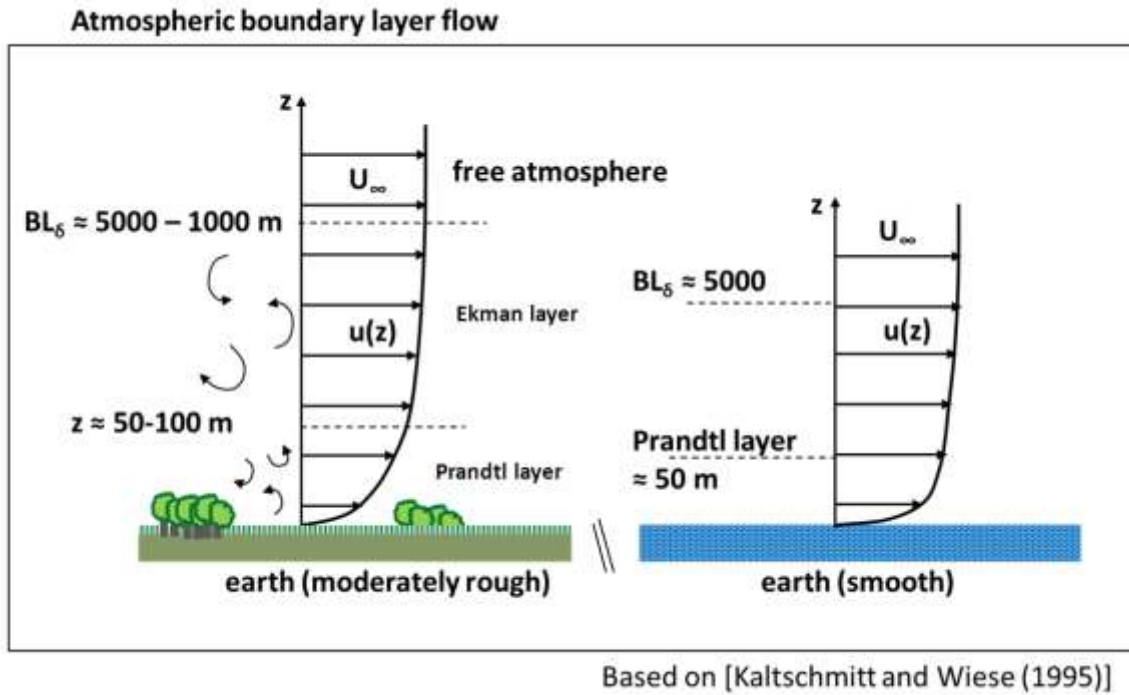


Figure 4: Wall boundary layer transferred to the atmospheric boundary layer for different roughness lengths

The introduced empirical quantities for the log law can be understood as integration constants. The *roughness length*, z_0 , can be related to surface roughness features in the real world geomorphology. It influences the shape of the wind profile. (Theoretically, z_0 is the height with zero wind speed). The *roughness length* and the *log law* are the main tools for the rough estimation of wind energy production.¹⁰ For example, wave-less water or an airport runway is classified as very *smooth* with z_0 between 0.0002 m and 0.002 m. (In the context of wind energy consulting this reassembles a “roughness class between 0 and 0.5”).

For moderate to high wind speeds, it can be assumed that *turbulence* induced by *shear stress* outreaches *buoyancy production or decay* of turbulence. This means that for moderate to high wind speeds, the boundary layer is assumed to be well-mixed and neutrally stratified. The *local* relation of the *buoyancy* to the *shear induced turbulence* is indicated by the *Monin Obukhov length*, of which the *inverse* is:

¹⁰ In the sense that wind velocities from a given height are extrapolated to heights which are relevant for wind energy production.

$$\text{invL} := -\frac{g\overline{kw'\theta'}}{u_*^3\bar{\theta}}.$$

The indicator invL is derived from the *transport equation* for turbulent kinetic energy with interpretation of

$$\overline{gw'\theta'}/\bar{\theta}$$

as the buoyancy production (or elimination) term and

$$u_*^3/\kappa$$

as the production term of shear turbulence, with g , the gravitational acceleration, and $\bar{\theta}$, θ' the mean respectively fluctuation value of the potential temperature, and w , u_* and κ as above. The invL is used for the analysis of field data and determination of the inflow conditions for the wind tunnel experiment in chapter 8.

Boundary layer theory

Boundary layer theory originally describes the influence of a *boundary* (e.g. a wall) on any flow, e.g. flow in pipes. Prandtl was a pioneer in *boundary layer theory* with a background in experimental engineering. Much of his work is based on wind tunnel and water tank experiments, e.g. in Göttingen where he worked from 1904 to his death and developed a mathematical rigorous approach to the *boundary layer theory*, [Davidson et al., 2011].

A key point is that boundary layers *are dependent* on the consistency of the boundary. If a boundary is added to a *free stream (boundary free stream)* the boundary layer in the flow first needs to develop. This means that the boundary layer grows with increasing fetch of the flow over the boundary until it reaches an *equilibrium* height in which *molecular* and *turbulent stresses* are balanced. The *molecular* and *turbulent stresses* are induced by friction in the fluid (in case of the atmosphere: gas) and the requirement of *zero velocity* relative to the boundary directly at the boundary.

To reach equilibrium, the flow passes through a *turbulent* regime after a certain fetch over the boundary (the length depends on fluid material and velocity). *Turbulent* 3dimensional flow is characterised by *irregular, 3dimensional fluctuations* of velocity, *rotation* and

dissipation, and *intensive mixing* of scalar quantities such as temperature or pollutants. This is assumed to characterise the Prandtl layer in the atmosphere. For the derivation of the log law, it needs to be assumed that the Prandtl layer is in equilibrium (fully developed). Homogeneous boundary consistency (flat and constant roughness length) is also assumed. A roughness change induces a *transition area* in which the boundary layer needs to adjust to a *new* equilibrium according to the *new* boundary consistency.

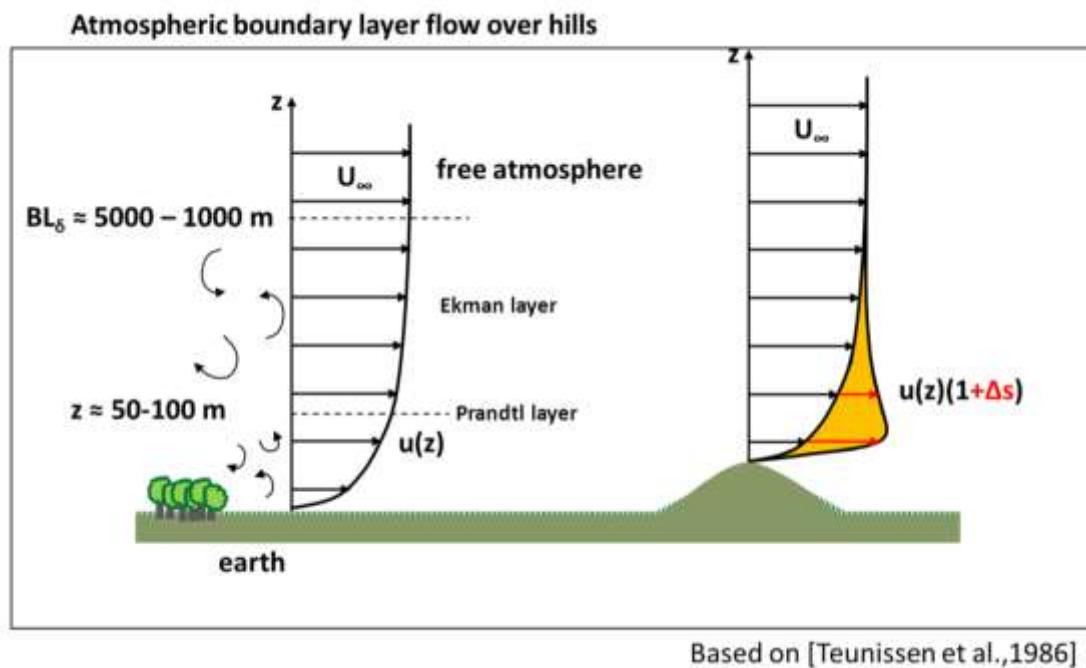


Figure 5: Topography induced distortion of vertical log law

This is one reason why the log law and usual boundary layer theory is in general *not applicable* for atmospheric flow over *complex topography*. *Complex terrain (including flow over hills)* can be defined as cases in which usual boundary layer concepts fail, such as when a non-negligible wind *speed-up effect* (Figure 5) and *terrain-induced turbulence* is to be expected. This will be analysed in depth in chapter 6 and chapter 7.

For further reading on turbulence in the atmosphere, turbulent closure models and boundary layer flows, Pope, [2009], or Wyngaard, [2010], are recommended. For boundary layer- and micro-meteorology Stull, [1988], and Arya, [2001] are classic references and for fluid mechanics Batchelor, [1970], or Rotta, [1972].

3. Wind tunnel modelling

*“Turbulence data for flow over topography from a single height, however, are rather difficult to interpret.”
- [Walmsley and Taylor, 1996, p. 298]*

This chapter briefly introduces the fundamental principles for fluid modelling of atmospheric boundary layer flow (in general) as introduced by Snyder, [1981], and Cermak, [1984]. Furthermore, simplifications, case restrictions and model strengths are discussed.

In the following, the rigorous definitions of the *Joint Committee for Guides in Metrology* (JCGM) are used. “Errors” in statistics are *not* “mistakes”, instead they are a measure of uncertainty. Different types of errors are distinguished from one another. “Absolute error” or “accuracy” is the degree of closeness of measurements of a quantity to its actual (*true*) value. The latter is *not a number*, since the *true value* cannot be known, [JCGM 200, 2008]. The *true value* is part of the *reality*. (This is further discussed in chapter 5.) The “relative error” or “repeatability” is also called “precision”, that is the degree to which *repeated measurements* under *unchanged conditions* show the *same* results.

Similarity criterion as fundamental principle

The purpose of physical flow modelling is to accurately simulate the dynamics of the flow in reality. Thus, a *similarity criterion* has to be formulated: “If x then the dynamics of the flow in the fluid model can be called similar to those in reality.” The generally accepted *similarity criterion* for fluid modelling of atmospheric phenomena is described in detail by Snyder, [1981], or Cermak, [1984]. The main idea is to convert the Navier-Stokes Equations (NSE) into a *dimensionless* form by insertion of *reference quantities* and stating that *every atmospheric flow* that can be described by the *modified equations of motion* can be modelled by *another flow*, provided that the characteristic coefficients are equal and *dimensionless boundary conditions correspond* [Snyder, 1981].

For NSE (p. 30), neglecting Coriolis force and gravity, the quality dimensions x , u , p and t can be identified sharing three standard (SI) units (m, s, kg). This means that for the following dimensional analysis and according to the Buckingham π -theorem [Buckingham, 1914; Rayleigh, 1915], one characteristic dimensional number is expected to properly describe the above NSE equation ($4-3 = 1$). The non-dimensional variables can be defined in the following form:

$$x_{ND} := x/L_R ;$$

$$u_{ND} := u/u_R ;$$

$$p_{ND} := p/\rho u_R^2 ;$$

$$t_{ND} := u_R t/L_R$$

yielding:

$$\begin{aligned} & \frac{u_R^2}{L_R} \left(\frac{\partial u_{NDi}}{\partial t_{ND}} + u_{NDi} \cdot \frac{u_R}{L_R} \nabla u_{ND} \right) \\ & = \\ & \frac{\rho u_R^2}{\rho L_R} \frac{\partial}{\partial x_{ND}} \left(- p_{ND} \delta_{ij} + 2 \frac{\mu u_R}{L_R} \left(S_{NDij} - \frac{1}{3} S_{NDii} \delta_{ij} \right) \right), i=1,2,3 \end{aligned}$$

Hence:

$$\begin{aligned} & \frac{\partial u_{NDi}}{\partial t_{ND}} + u_{NDi} \cdot \nabla u_{ND} \\ & = \\ & \frac{\partial}{\partial x_{ND}} \left(- p_{ND} \delta_{ij} + 2 \frac{\mu}{u_R L_R} \left(S_{NDij} - \frac{1}{3} S_{NDii} \delta_{ij} \right) \right), i=1,2,3 \end{aligned}$$

As a characteristic number, the Reynolds number can be extracted:

$$Re := \frac{u_R L_R}{\mu}.$$

The procedure can be amended to the NSE with the Coriolis force and the gravitation¹¹, leading to further characteristic numbers, e.g. the *Rossby* and *Froude* number, [Snyder, 1981, p.5].

That is, if and only if the characteristic numbers as well as the *boundary conditions* formulated in *non-dimensional variables* are identical, then solutions of the modified set of equations are also identical. In other words, dynamics of flows with the *same characteristic numbers* and *non-dimensionalised boundary conditions* are *similar*.

The similarity criterion is embedded in general symmetries of the NSE in terms of Lie group analysis. The transformations under which solutions of NSE *remain invariant* include: *rotation, time translation, space translation* and *Galilean transformations*. This is extensively discussed in Oberlack, [2000]; Boisvert et al. [1983]; Oberlack and Rosteck, [2010]; Rosteck and Oberlack, [2011] and Frisch, [2004].

Is the *similarity criterion* usable as a basic law for wind tunnel modelling? The criterion gives proof that wind tunnel flow is equivalent to real scale flow provided that certain similarities are matched. Furthermore, the Navier-Stokes Equations are assumed to be valid¹². However, the crucial viscosity term in NSE is based on empirical observation in water tanks and wind tunnels. Thus, in the worst case, the similarity criterion is only the mathematical manifestation of what has been physically assumed by wind tunnel observation. In practice the requirement is softened in boundaries which are empirically observed to be legitimate. For example, the *Reynolds numbers* of the atmosphere cannot be matched in the wind tunnel. Let geometrical scaling be 1:250 and u_{AS} , u_{WT} the characteristic velocity in the atmosphere, respectively in the wind tunnel. The wind tunnel is (usually) operated at the same temperature and pressure as the *atmospheric boundary layer*, yielding similar viscosity, μ , of the fluid in the wind tunnel (e.g. air) as in the atmosphere. This yields a relation of atmospheric Reynolds number, Re_{AS} , and wind tunnel Reynolds number, Re_{WT} :

¹¹ It can also be extended to the continuity equations of mass and thermal energy (e.g. yielding the Peclet number).

¹² Consider that flow over hills in another planet's atmospheric boundary layer can contradict the assumptions of the continuum hypothesis (due to the low density of the gas).

$$\frac{Re_{AS}}{Re_{WT}} = 250 \frac{u_{AS}}{u_{WT}}$$

This means that wind tunnel reference velocity would need to be 250 times faster than the reference speed in the atmosphere, i.e. in the order of around 10^3 m/s. This is not feasible.

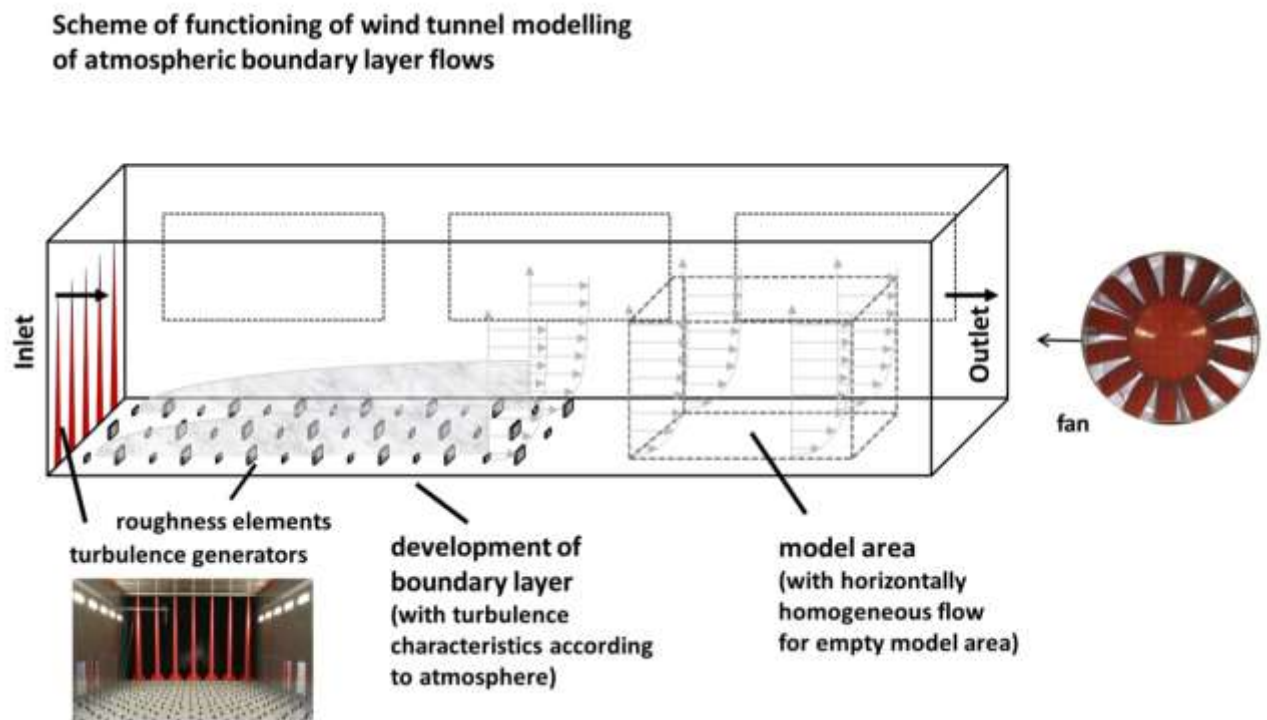


Figure 6: Schematic view on wind tunnel modelling of atmospheric boundary layer flow

On the other hand, by empirical observation fluid dynamics are assumed to be nearly similar for “fully developed turbulence” hence independent of the Reynolds number beyond a finite *critical Reynolds number*. The finite *critical Reynolds number* determines the transition point of laminar or turbulent flow to *fully turbulent* flow. The empirical evidence on the *Reynolds number independency* for fully turbulent flow is crucial for wind tunnel modelling. Instead of matching the atmospheric Reynolds number, *fully turbulent atmospheric boundary layer flow* is modelled by *turbulence generators* at wind tunnel intake and *roughness elements* on the ground. (For a scheme see Figure 6.) Then, Reynolds number tests are conducted in order to give the empirical evidence that the flow is Reynolds number independent and that

the regime of fully developed turbulence is reached. *Reynolds number tests* are repetitions of measurements with different wind tunnel mean velocities (measured at a reference location in the wind tunnel). This gives evidence whether the non-dimensional measurements vary with wind tunnel mean velocity at the reference location.

The ergodic theorem

The similarity criterion is not a sufficient condition for obtaining meaningful *measurement data* extracted from the flow geometry. Theoretical background for recording and interpretation of wind tunnel data is provided by the *ergodic theorem*, [Frisch, 2004]. Consider that the wind speed time series can be interpreted as a stochastic process:

Definition: σ -algebra¹³

Given a set Ω , a σ -algebra on Ω is a set of subsets of Ω that contains Ω and is closed under complementation and countable union, i.e.:

$$(\sigma 1) \sigma \subseteq \wp(\Omega) \quad ^{14}$$

$$(\sigma 2) \Omega \in \sigma$$

$$(\sigma 3) \text{ If } A \in \sigma \text{ then } \bar{A} \in \sigma$$

$$(\sigma 4) \text{ If } \{A_i\}, \text{ is a countable collection of subsets of } \sigma, \text{ then } \bigcup \{A_i\} \in \sigma.$$

—/

Definition: Probability function

Given a set Ω equipped with the rules of a σ -algebra, a *probability function*, p , on the ordered pair (Ω, σ) is a total, real valued function on σ , satisfying the following three axioms:

$$(p1) p(A) \in [0,1] \text{ for each } A \in \sigma$$

$$(p2) p(\Omega) = 1$$

$$(p3) p(A \cup B) = p(A) + p(B) \text{ whenever } A \cap B = \{\}$$

—/

¹³ This is mentioned for completion and the final outlook and not necessary in detail for the ongoing text. For a motivation of this definition see also p. 249.

¹⁴ Let $\wp(\Omega)$ denote the power set of a set Ω , i.e. the set containing all subsets of Ω including the empty set and Ω itself. For following definition, according to Zermelo-Fraenkel axiomatic system for set theory (ZFC), it will be assumed that the power set always exists.

The ordered pair (Ω, σ) is also called *outcome space*. The ordered triple (Ω, σ, p) is also called *probability space*.

Definition: random variable

Consider (Ω, σ, p) . A random variable on (Ω, σ, p) is a map

$$\begin{aligned} u : \Omega &\rightarrow \mathbb{R} \\ \omega &\mapsto u(\omega) \end{aligned}$$

such that

$$\{\omega \mid u(\omega) \leq r\} \in \sigma, \forall r \in \mathbb{R}.$$

—/

For example, the u -component of the velocity of turbulent flow at a certain time and location with initial condition, ω , is a *random variable*.

The second part of the definition is the technical requirement that it can always be assigned the *probability* for (ranges of) values of the random variable. For example, the *probability* that wind speed is below a certain value, a , i.e. $u(\omega) \leq a$, is the probability for the event $A := \{\omega \mid u(\omega) \leq a\}$ and can be denoted as $p(u \leq a) =: P(a)$. P is also called *cumulative probability function* of u , and p *probability density function*.

Definition: stochastic process

A stochastic process (or random function) is a family of (scalar or vector-valued) random variables depending on one or several space and time variables, e.g. the velocity field, $u(t, x, y, z, \omega)$, [Frisch, 2004].

—/

Definition: statistically stationary

Here, a flow will be called statistically stationary iff¹⁵ for all points in the flow and all t , ω it holds:

$$u(t+h, \omega) = u(t, \omega_h), \forall h \geq 0,$$

and appropriately shifted ω_h .

—/

That is, for appropriate boundary conditions (e.g. statistically stationary), solutions of NSE are *statistically stationary* by the symmetry of *time translation* for NSE solutions.

Consider a wind tunnel experiment with constant mean wind tunnel reference velocity. After switching on the device and a few seconds or minutes for the boundary layers to come to equilibrium, the flow can be expected to be *statistically stationary* – by experimental set-up.

Let $\langle u \rangle$ denote the *ensemble mean value* of the statistically stationary stochastic process $u(t, \omega)$. This is the mean value of all possible realisations of $u(t, \omega)$. From the *ergodic theorem* it follows, [Frisch, 2004, p.49], for a stationary function $u(t, \omega)$ and almost all ω ,

$$\lim_{T \rightarrow \infty} \frac{1}{T} \int_0^T u(t, \omega) dt = \langle u \rangle$$

This means that *time averages* of a *statistically stationary stochastic process* converge against *ensemble averages*. Thus, *time averaged* values of a statistically stationary wind tunnel time series with *sufficiently long sampling duration* can be regarded as *representative* for the underlying *stochastic process*.

This means that for every measurement position and given *starting conditions* ω , one has to find a sampling duration T' sufficiently large, such that

¹⁵ “iff” := if and only if

$$\langle u \rangle = \lim_{T \rightarrow \infty} \frac{1}{T} \int_0^T u(t) dt \approx \frac{1}{T'} \int_0^{T'} u(t) dt \approx \frac{1}{T'} \sum_0^{T'} u(t).$$

The $u(t)$ in the sum is the discretised time series corresponding to the continuous $u(t)$, which idealizes the flow motions as being continuous.

By the *mean square ergodic theorem*, Frisch, [2004], points out that a sufficient *sampling duration* can be estimated with $T \gg T_{\text{int}}$, with the *integral time scale*, T_{int} , based on the autocorrelation function of $u(t)$. However, the abstract integral autocorrelation function is *not* accessible from a *finite measurement* and has to be *assessed* via a finite sum. Let t_{max} denote the *sampling duration*. If $T' \rightarrow t_{\text{max}}$ and $\tau \rightarrow T'$, then the *statistical error* of the autocorrelation computed for the finite time series *increases* significantly. Also the standard deviation is computed from the finite time series. The errors cannot be computed.

However, the convergence properties of the empirical time series can be examined by computing statistical quantities obtained from the empirical time series for a discrete set of increasing sampling times, $T' \rightarrow t_{\text{max}}$.

For example, let \bar{u} be the *time averaged value* for the empirical time series with measurement duration t_{max} . Then, the level of convergence for the mean value in dependence of the measurement duration can be assessed by:

$$\left| \bar{u} - \frac{1}{T'} \sum_0^{T'} u(t) \right|,$$

for discrete values of T' , $T' \rightarrow t_{\text{max}}$. This was extensively examined for the Bolund wind tunnel study, see pp.244. To obtain statistically representative measurements is one of the key goals (and opportunities) of wind tunnel modelling.

Model simplifications

Simplifications of wind tunnel modelling towards reality for *intended applications* such as wind energy assessment are:

- The *Coriolis force* in the model does not reassemble the *Coriolis force* in reality. The larger the area modelled in the wind tunnel, the larger the error due to the mismatch of the *Coriolis force*. For many applications it is assumed that the effects of the *Coriolis force* for atmospheric length scales smaller than 5 kilometres are negligible.
- The model area within the wind tunnel is physically restricted by walls. Thus, atmospheric turbulence larger than the wind tunnel dimension cannot physically be reproduced. This is why the *wind tunnel size* matters with respect to the *geometrical scaling* of the experiment. For example, in a 1 m wide and 1 m high wind tunnel at length ratio 1:100, the largest reproducible eddy is of about 100 m width and length in full scale¹⁶.
- The Kolmogorov length scale in the wind tunnel translated to full scale is too large (depending on the Reynolds number and the model length scaling). In other words, the smallest eddies are not resolved in the wind tunnel model. For example, for a scaling of 1:500 and a spatial LDA probe volume uncertainty of around 0.1 mm, eddies of around 50 mm in full scale are not resolved in the wind tunnel model. (For comparison: A value of around one millimetre is given as an example for a field scale Kolmogorov length scale in Stull, [1988, p. 167].) However, macroscopic fluid dynamics are mainly driven by *large eddies*. Thus, compared to large eddies which carry the main part of the flow energy, small eddies are assumed to be negligible.

¹⁶ Assuming that turbulence is isotropic and homogenous, and mean advection time of the eddy is 10 m/s, wind turbulence of more than 10 seconds length does not occur in the time series.

Summarizing latter two points, the turbulence spectrum in the wind tunnel compared to that of the field is cut at low and at high frequencies. This has to be considered with regard to the choice of the *length scale ratio*.

Model case restrictions

The restrictions of wind tunnel modelling are:

- Most wind tunnels are not built for simulation of *thermal effects*. Thus, in the majority of cases, wind tunnel modelling is restricted to *neutral stratification*.
- *Inflow conditions* can exist which are impossible to be modelled, e.g. flow over very smooth surfaces due to the scaling of the large eddies. The scaling of the inflow conditions also restricts the size and scaling of the areas which can be modelled.
- *The size of the real terrain model area* is also restricted with respect to the effects of the Coriolis force (see “Model simplifications”).
- *Inflow* and “meteorological boundary” conditions in the model are *statistically stationary*. This is both a weakness and strength because most numerical models need *statistically stationary* reliable flow data for comparison or validation. On the other hand it is clear that the models are not made to predict the variability of the atmosphere.
- Alteration of wind direction is possible. However, in practice, this is labour-intensive. The model area can be turned on a turntable. In case that the inflow conditions are distinct for different inflow directions, the inflow conditions have to be adjusted carefully for every change of the wind direction.

In conclusion, it has to be examined carefully whether or not an atmospheric flow can be meaningfully modelled in the wind tunnel. This is part of the *accuracy* assessment that needs to happen prior to the experimental set-up (see also chapter 10 pp. 265).

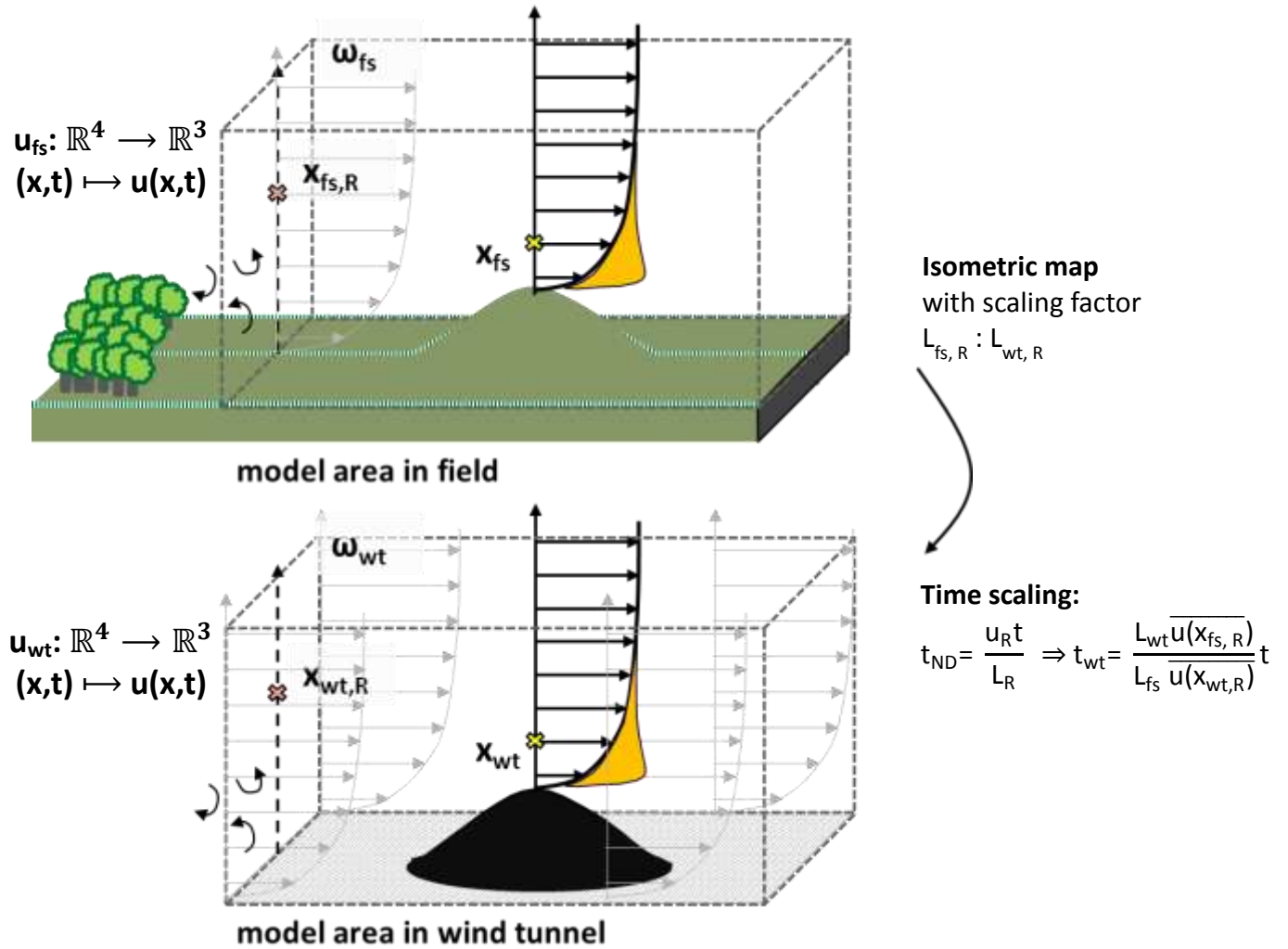
Model strengths

The Navier-Stokes Equations (NSE) do not need to be solved for wind tunnel modelling. This is the main advantage since the NSE existence and smoothness problem is one of the seven most important open problems in mathematics. The NSE are only needed for deduction of the similarity criterion.

- Instead of solving equations with epistemic uncertainty, the physical model uses *real flow* to replicate flow.
- Wind tunnel measurements can be conducted with high *spatial*- and *time-resolution*. Compared to field data, wind tunnel data is cost-effective and rapidly available.
- Inflow conditions in wind tunnel modelling are well defined in the sense of completeness of information. They can be measured with high spatial and temporal resolution.
- As stated before, boundary conditions are statistically stationary. This is both a weakness and strength. However, boundary conditions are controllable which is very important with regard to *model comparison*, as will be examined in more detail in chapter 5.

Finally, the conclusions of the ergodic theorem and the up-scaling of wind tunnel flow measurements to field (full) scale based on the symmetries of the Navier-Stokes Equations is illustrated in Figure 7, p. 48.

An illustration of non-dimensional wind speed and the flow similarity



Variables:

u := velocity; x := position in 3dimensional space; t := time; ω := boundary conditions;
 L := length; p := pressure; ρ := density

Meaning of the indices:

fs := “full scale”; ND := “non-dimensional”; R:= “reference” (length resp. velocity); wt := “wind tunnel”;

For u_{fs} , u_{wt} as stochastic processes and solutions of the Navier-Stokes Equations with the same non-dimensional boundary conditions ω_{ND} .

Non-dimensional wind velocity:

$$u_{ND} = \frac{u(x_{fs}, t)}{u(x_{fs, R}, t)} = \frac{u(x_{wt}, t_{wt})}{u(x_{wt, R}, t_{wt})}$$

Figure 7: Scaling of wind tunnel flows

Part II: Fundamental work

4. Theory of fluid dynamics reconstructed in structuralism and conceptual spaces

“Every word or concept, clear as it may seem to be, has only a limited range of applicability.”

- Werner Heisenberg

“A theory that predicts a particular value for U is almost certain to be wrong”

– [Pope, 2009, p. 37]

This chapter gives the theoretical background on the Navier-Stokes Equations. The objective is to embed the art of wind tunnel modelling into the triangle of theories, reality and models.

Introduction to this chapter

No methodological framework for general model comparison in fluid dynamics exists so far. The interest in an establishment of frameworks increases. This is indicated by recent projects such as Wakebench (Benchmarking of Wind Farm Flow Models, started in 2010) or WAUDIT (Wind resource assessment audit and standardization, started in 2009), Rodrigo, [2010]. Reconstruction of fluid dynamics in structuralism and conceptual spaces can provide new insights for the philosopher of science but also for the scientist active in this field¹⁷. This is in particular true in the area of atmospheric flow modelling (for the complexity of models and inter-scientific links involved).

In this chapter, *fundamentals* of fluid dynamics are analysed. It starts with the continuum hypothesis, leads via classical mechanics to the Euler Equations. Finally the Navier-Stokes Equations are derived. Main parts of this analysis can be found in the historical and structural analysis of fluid dynamics in Petersen and Zenker, [2012].

¹⁷ As far is known by the author, a reconstruction of fluid dynamics beyond the Euler-Equations by use of the structuralist framework or by means of conceptual spaces has not been published by summer 2012. This work was partly discussed at the conference “Perspectives on Structuralism” in Munich, February 16 – 18, 2012.

The formal analysis tools are *structuralism*, [Balzer et al., 1987; Sneed, 1971; Stegmüller, 1976; Balzer et al., 1984; 2000; Gähde, 2002 and Moulines, 2002], and *conceptual spaces*, [Gärdenfors, 2000; Gärdenfors and Zenker 2011; Petersen and Zenker, 2012]. No technical knowledge of *structuralism* and *conceptual spaces* is required a priori.

The motivation is to build a *methodological framework* in which scientific models can be compared and scientifically embedded for facilitation of scientific development. *Models* in this sense refer to the understanding of *models as mediators between theories and reality* as introduced by Morgan and Morrison, [1999]. This notion includes the type of models which are used in fluid dynamics and atmospheric modelling (for examples see chapter 5, “Models as mediators in wind assessment.”)

Note that the improvement of assessment tools is based on the *comparison of model data* with *data of other models* or with *field data*. Scientists which are involved in the comparison of numerical models need to know about pitfalls for the *application* of wind tunnel or field data as *validation data* for their models (e.g. concerning the *statistical representativeness* of the data). This requires a broad scientific knowledge in various disciplines including physical modelling, computational methods and meteorology. This is in full detail not possible in a real scientist’s life. A compact information base is needed for communication among specialists together with the establishment of a *methodological framework*. For the *validation*¹⁸ and improvement of flow models concerning wind energy assessment, no commonly established methodological framework exists.

An important starting point for building a methodological framework is the identification and analysis of the *theories*¹⁹ which are involved in the *models*. Cartwright, [1983], states that *theories* are one tool *amongst others* for the *construction of models*. This supports the argument that for the clarification of the inter-model relationship in practical science, the

¹⁸ Be aware of the meaning of *validation*. *Validation* in a rigorous sense is impossible, as it will be argued later. However, comparison of adequate data can *increase the belief* into the validity of a model.

¹⁹ For explicitness, “theories” are denoted in plural although “theories” could be interpreted as part of the set called “theory”. This is to emphasise the fact that, even for the same part of the set called “theory” (e.g. for a specific theoretical question) different “theories” can exist.

examination of the *theories* which are involved in the construction of the models is a *necessary* condition.

Here it is found that the framework of *structuralism* and *conceptual spaces* is a practical basis for clarifying the inter-scientific relation of models that are used in practice. Both concepts illustrate the fundamental *building blocks* of theories and *assumptions*²⁰. This is of key importance if the theories are implemented or assumed for the construction of the models.

Introduction to structuralist concepts and conceptual spaces

The author is aware of the fact that both approaches, *structuralism* and *conceptual spaces*, are too complex to be presented in detail in this dissertation which is primarily focused on wind tunnel modelling of atmospheric boundary layer flow over hills. Hence, the modest scope in this section is to introduce the minimal technical toolkit of notions and definitions which is necessary for the following analysis of modern fluid dynamics by means of *structuralism* and *conceptual spaces*. Furthermore, structuralism is applied with a strongly reduced degree of formalization. The hope is that this simplifies the accessibility for readers without profound experience in formal methods²¹. On the other hand, alas, the author has to skip many interesting parts and questions which come about by the use of structuralism in plain formalism. Especially, no complete formal reconstruction of fluid dynamics in structuralist terms is delivered in this chapter.

The *structuralist framework* aims to analyse the *structure* of a theory in a formal and precise way. In contrast to conventional approaches for axiomatizations of empirical theories, the *structuralist framework* seeks to also precisely specifying variants of a theory. Namely, these variants are obtained by formulating the basic principles of a theory first and then successively adding more specific laws which are applied for some but not for all *intended applications* of the theory. More explicitly, Balzer et al. use “structure species” for the

²⁰ The notions of the structuralist framework which are used in the following are mainly based on Balzer et al., [1987]. The ideas of conceptual spaces are those being introduced in Gärdenfors, [2000]; Gärdenfors and Zenker, [2011]. Terms are explained as detailed as necessary for the analysis of fluid dynamics in the following.

²¹ However, the author is aware of the fact that this might be more difficult or unsatisfactory for those which are familiar with formal methods.

axiomatization of their idea of *models of empirical theories* which is obviously inspired by the seminal mathematical work of Bourbaki, [Balzer et al., 1987 p.11]. Note that the *models of empirical theories* in the sense of Balzer et al. somewhat differ from the general use of the notification *model* in this dissertation. Namely, Balzer et al. “understand the term ‘model’ here in the sense of modern logic and model theory. [...] Logicians and mathematicians consistently use ‘model’ in the sense of the thing depicted by a ‘picture’ (= by a *theory*). [...] Therefore, instead of saying that certain equations are a model of subatomic or economic phenomena, we propose to say that the subatomic or economic phenomena are models of the theory represented by those equations”²² [Balzer et al., 1987 p.11]. More explicitly, models in the sense of Balzer et al. are set-theoretical entities which are depicted by a theory **T** and share the same structure which consists of the same “conceptual framework” and the compliance of “laws”²³. Balzer et al. distinguish between those set-theoretical entities which fulfil *the same conceptual framework* and those which, additionally, fulfil *the same laws*. In structuralist terms, former are called *potential models* or *possible realizations* of the theory **T**, latter (*actual*) *models* of the theory **T**. The distinction of *potential models* and *models* is necessary to pursue the specialisation of theories on a formal level.

For example, if the theory consists of a law given by the equation $a=bx$, the *possible realisations* of the theory could be regarded as all triples (a,b,x) which exist *regardless of the above equation*. However, all triples (a,b,x) which actually fulfil above equation would be regarded as (*actual*) *models* of the theory.

A *constraint of the set of all potential models* rules out certain combinations of potential models. More explicitly, a constraint is a (non-empty) subset of the power set of all potential models and hence serves as a specification of the theory, namely on the level of combinations of all *possible realizations* of the theory.²⁴

²² Highlighting in the quotation are maintained as of Balzer et al., 1987.

²³ It should be remarked that Balzer et al. note in a different part of the publication that “in spite of much discussion on lawlikeness within traditional philosophy of science, we still lack an adequate set of precise necessary and sufficient conditions as a criterion for a statement to be considered a ‘law’”. [Balzer et al., 1987, p. 15]

²⁴ There are more granularities to consider with respect to constraints, such as the compliance or non-compliance of transitivity. This could be worth to discuss and is skipped, here.

One of the most important notions in structuralism is that of a *theory-element* **T** which is understood to be the simplest kind of a set-theoretical structure that may be identified with, or serve as, a logical reconstruction of an empirical theory, [Balzer et al., 1987 p.36.] Described in a very condensed way, a theory-element **T** is defined by its *theory-core* **K** and its *intended applications* **I**. The *theory-core* **K** is constructed against the background of set theory, and amongst other it consists of the *potential models* as well as the (*actual*) *models* which fulfil the theory.

The *intended applications*, **I**, are the informal description of what the theory is about and aim at identifying those systems on which the theory can be applied. “Informal” reads that the *intended applications*, **I**, of a *theory-element*, **T**, should be formulated in everyday language or at least without use of the terminology of the theory which later describes the theory. In other words, **I** should be formulated at most independently of the vocabulary of the theory.

A *specialisation* of a theory-element in a structuralist view is the refinement of the theory. A theory-element being the specialisation of another theory-element *gives a more detailed picture* or is *less fundamental* or *less basic*, etc. [Balzer et al., 1987, p.170]. This means on the level of the theory-core, **K**, a specialisation can be obtained by the refinement of the equations contained in **K**. This can also refine the *intended applications*, **I**. In other words, “Specializations apply to ‘special cases’ of the initial range of intended applications **I**.” [Balzer et al., 1987, p.170]. Also, the distinction of *potential models* and *models* is used to trace specialisations of theories on a formal level: *potential models* of theories with a *specialisation relation* fulfil equality; however, on the *level of (actual) models*, the *specialisation relation* induces a set-theoretical *inclusion relation*, analogically to the chain of inclusions for the *intended applications*. (The inclusions of the sets are, in both cases, not necessarily strict.)

In brief, the formal *specialisation relation* of structuralism imposes a structure on certain sets of theory-elements within an area of theories, telling which theory-elements are

specializations of which others in that set, [Balzer et al., 1987, p.172]. This structure can graphically be depicted as a net and is called *theory-net* in the structuralist framework.

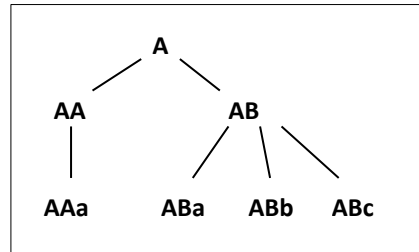


Figure 8: Schematic view on a theory net

Recall that a *theory-element* in structuralism generally refers to the *smallest* structure of an empirical theory. From the author's point of view, the *Navier-Stokes Equations* define the *theory-core* of modern fluid dynamics. The Navier-Stokes Equations are non-linear partial differential equations in three dimensions and can be interpreted as part of a purely mathematical theory. Hence, fluid dynamics can be understood as a purely *mathematical theory*. However, the *interpretational power* of the Navier-Stokes Equations is the application of the equations on real world phenomena, namely the motion of fluids, and is based on empirical observation (as will be shown later). In this point of view, fluid dynamics associated to its application on real world phenomena is an *empirical theory*. For this reason in the following analysis, fluid dynamics is to be understood as an *empirical theory*.

The idea of conceptual spaces as pointed out in Gärdenfors, [2000], Gärdenfors and Zenker, [2011], can be seen as following the tradition of analysing variables and dimensions involved in physical equations, such as by e.g. Buckingham, [1914], and Rayleigh, [1915]. However, Gärdenfors's spaces are much more flexible and broader in scope. They can, on the one hand, be applied for structural analysis of learning mechanisms and cognitive phenomena dealing with cognitive structures such as perceptions and memory. On the other hand, Gärdenfors's spaces are applicable for the *precise structural* analysis of scientific *theories*. Here, conceptual spaces are used in latter meaning. Conceptual spaces provide a meta-framework by means of which theory frameworks can be reconstructed.

The basic components of a conceptual space are its *dimensions*. The notion of a *dimension* should be understood literally. Usually, it is assumed that each *dimension* is endowed with a certain *geometrical structure*, [Gärdenfors and Zenker, 2011]. This means that the structures of theories are illustrated geometrically with *space and dimensions*. This is (at first sight) in contrast to the set-theoretic approach of structuralism. However, since the mathematical treatment of spaces contains set theory, the author of this thesis regards both concepts as being complementary and synergetic in combination.

As a remark it can be added that in the case of fluid dynamics, Gärdenfors's spaces are closely related to the differential geometry (mathematical) *manifolds*. This is due to the assumptions for the variables and (differential) equations that are involved. On the other hand, as stated above, Gärdenfors's spaces are related to the dimensional analysis by Buckingham, [1914], or Rayleigh, [1915], which has been extensively used in fluid dynamics. In terms of Gärdenfors and Zenker, theory development which is analysed in conceptual spaces can be classified into five types of theory change²⁵. Here, it will be focused on the *addition or deletion of laws* and the *addition or deletion of dimensions*²⁶.

Physical foundations of modern fluid dynamics

In this section, first the *continuum hypothesis* is considered as starting point of modern fluid dynamics. Then, forces are introduced by transfer of classic mechanics to fluids. In the section "With Stokes and mechanical equilibrium to static pressure", pressure is derived by the use of differential calculus and the continuum-mechanical notion of mechanical equilibrium. Gas as special fluid and the theory link to thermodynamics is drawn in "Gas as a special case". The major step onwards from fluid in rest to fluid in motion is examined in "Fluid in motion" and "From Euler to Navier Stokes." The outline is as follows: first the Euler-Equation is introduced. Second, the evolution from Euler-Equations to Navier-Stokes

²⁵ For details see appendix "Categorisation of changes in terms of conceptual spaces", pp. 304

²⁶ In the following, extensive use will be made of the fundamental work by Batchelor, [1970]. Since neither reconstruction in structuralism nor conceptual spaces is unique, the aspects considered here are based on personal selection.

Equations is illustrated by the transfer of the stress tensor from solids in continuum mechanics to fluids, (“from Euler to Navier Stokes”).

The continuum hypothesis

The *continuum hypothesis* is the basis for continuum mechanics. Here, the application is focused on *fluids* and not on solids although many scientific concepts are transferred from solids to fluids (e.g. the stress tensor, as will be seen later). Fluids can be of *liquid* or *gaseous* material. The *continuum hypothesis* states that the distances of molecules in liquids are much *larger* than the molecules itself. This is based on the empirical evidence that the macroscopic behaviour of fluids is the same as if they were *continuous*. Thus, the discrete structure of fluids is *neglected* and “physical quantities such as the mass and momentum associated with the matter contained within a given small volume will be regarded as being spread uniformly over that volume instead of, as in strict reality, being concentrated in a small fraction of it.” [Batchelor 1970, p.6]

Note that on the one hand, the particle structure of the fluid is *neglected*, on the other hand *points* are considered for the mathematical characterisation of the *fluid in the space*. For example, the *trajectory* (= the history of movement of particles as volume-less parts of the continuous concept) is considered in modern fluid dynamics. This seems to be contradictory to the fact that this trajectory does *not exist* in the microscopic molecular *reality*. The crucial assumption of the *continuum hypothesis* is that the *macroscopic* behaviour of the fluids is the same as if they were perfectly *continuous*. “Indeed the structure and properties of air and water are so obviously continuous and smoothly varying, when observed with any of the usual measuring devices, that no different hypothesis would seem natural”, [Batchelor 1970, p.5]. Concluding, particle dynamics are *by assumption* excluded due to the demand for continuity.

Particle dynamics are for example taken into account by the *Boltzmann equation*, [Hirschfelder et al. 1964]. The *Einstein kinetic model* or other stochastic processes are considered for molecular motions as well, [Einstein, 1905; Smoluchowski, 1906; Erdős, 2010]. Also, a *linear Boltzmann equation* can be formulated, coupling Boltzmann’s particle

distribution function with a random process (random jump process on the sphere of velocities), [Erdős, 2010].

There is a *key conceptual difficulty* behind the combination of the *microscopic* and the *macroscopic* fluid scale. This is the collision of *reversible* and *irreversible* processes. Hamiltonian mechanics (classic mechanics) is *reversible* and *deterministic*. The Boltzmann equation is *irreversible*. Due to Erdős, the key point is the *loss of information* on macroscopic scale: “there is a permanent loss of information along their evolution [...]. The continuous fluid equations live on the macroscopic fluid scale: they are obtained by neglecting (more precisely, integrating out) many degrees of freedom on short scales. Once we switch to the fluid description, the information of these degrees of freedom is lost forever”, [Erdős, 2010, p.7]. Despite of these conceptual difficulties, macroscopic quantities can be derived from thermodynamic statistics: with the assumption of small deviations from thermodynamic equilibrium, the Boltzmann equations converge to the Navier-Stokes Equations (via the Chapman-Enskog expansion), for details see Hänel, [2004, pp. 131]

However, the *continuum hypothesis* is necessary as foundation of the Navier-Stokes Equations as used in modern fluid dynamics. The previous paragraph created an understanding of the conceptual incompatibilities which arise by assumption of the continuum hypothesis.

In structuralist terms, the continuum hypothesis can be interpreted in different ways. The set of *potential models* for fluid dynamics, could be understood as being the “amorphous everything of the reality” corresponding to the (level of) *unprepared observation* as described by e.g. Cartwright, [1983]. However, in a formally correct way, the potential models need to *be the same* for more specialized and less specialized theory elements of the same theory net. Hence, in a formal correct way, the basic theory element of Fluid dynamics necessarily contains all variables which appear in the Navier Stokes equations, especially all variables of Newton’s classic mechanics. It would contain all these variables without

limitation of range and format.²⁷ If so, then the continuum hypothesis can be regarded as a restriction excluding those potential models which do not fulfil continuum hypothesis. Also, the continuum hypothesis restricts the space of *intended applications*, namely to applications that fit into the *concept* of continuity. One might understand the *continuum hypothesis* as a *theory element* which introduces *density* as a *theoretical term* (based on the idea of a continuously uniformly spread mass). This means that a certain “mass density”²⁸ is taken into account while its specific molecular structure is averaged out. However, for didactic reasons we will leave it open which perspective the reader wants to share. In brief, she can choose the structuralist formal correct way for a today’s snapshot of the theory net of modern fluid dynamics or a rather didactic perspective in which the mass of “blind” variables is not carried along the theory net.²⁹ In the former case, the *potential models* of the basic theory contain all variables of the Navier-Stokes Equations and all variables which exist *today* for all specialisations of the Navier-Stokes Equations. In the latter case, the “empty variables” which only become relevant in later steps of specialisations are left out for the moment. This is the informal approach which will be continued over the next sections.

In conceptual spaces, *density* can be introduced as the *quality dimension* of the one-dimensional *conceptual space* containing the *continuum hypothesis*. At this point, the mathematical notion of three-dimensional (e.g. Euclidean) space might not be needed in any elaborate way, as stated above. Similarly, in the case of a structuralist reconstruction, Balzer et al., [1987], state: “Space and time are not needed to display thermodynamics’ formal structure nor to provide a general interpretation of its basic concepts”, [Balzer et al. 1987, p. 129].³⁰ Hence, space at this stage can be considered as part of some *abstract* schematic concept of *density*.

²⁷ It would also need to include all variables which are deduced from the various specialisations of the Navier-Stokes Equations. Moreover, it would be a snapshot in time or an open list because the specialisations of the Navier-Stokes Equations with regard to turbulence theories are ongoing research.

²⁸ Historically, mass was derived from mass density and volume by Newton

²⁹ If the reader wants to transfer the informal to the formally correct way she needs to “add back” the variables of modern fluid dynamics along the course of this text, especially the variables of Newton’s classic mechanics. (She will need to have the full set of the variables already in the beginning in order to handle specialisation relations formally correct on the level of the potential models.)

³⁰ Density can be linked to thermodynamics at this stage. “Expressions for all these bulk properties in terms of molecular properties and intermolecular forces can be obtained from statistical mechanics.”[Hirschfelder et al., 1964, p.1]

Classic mechanics translated to fluids

Historically, *classic mechanics* was applied on the “continuitized” fluid object for examining how forces act on fluids. In classic fluid mechanics, *long range forces* are distinguished from *short range forces*. The former include gravity, electromagnetic forces and fictitious ones, such as the centrifugal forces brought about by the global movement of the continuous space in which a fluid is located. (Imagine you are walking through the hallway with your cup of coffee in hand. The fluid in the cup will move back and forth while walking.)

Long range forces are also called volume- or body-forces. They are assumed to act equally on all matter contained in a (given small) volume of fluid and to be proportional to the *size* of the volume element and the *density* of the fluid. This means that *density*, ρ , is now specified by the notion of *matter* and *volume*. The molecules of the fluid are assumed to be *idealized continuous matter equally* distributed within the volume element, δV .

The above definition is compatible with the *continuum hypothesis*. In terms of *conceptual spaces*, the *dimension* (or *domain*) of *force* is added to the conceptual space of *continuum mechanics*. This dimension (or domain) can be split up into more specific dimensions, namely *long range forces* and *short range forces*.

In *structuralist terms*, introduction of forces can be interpreted in different ways, for example as an instance of a *theory evolution* of the *continuum hypothesis*, or as a *specialisation* of classic continuum mechanics towards classic fluid mechanics.

Let us consider the body forces (or long range forces) in more detail. Assuming force as a function of space and time, proportional to the *density* and the *volume* of a volume element, the total of all body forces that, at time t , have an impact on the volume δV with density ρ associated to the position x , can be given by:

$$\text{Total body forces} = a(x,t) \rho \delta V.$$

For example, consider $a(x,t)$ as an *acceleration* acting on the fluid volume element in position, x , at time, t . The link to Newton’s second law, *force* = ma , is obvious, since the product $\rho \delta V$ gives the mass, m , of the volume element (and $a(x, t)$ denotes acceleration, a).

Note that not only *force* is added as a *quality dimension*, but also the *quality dimensions* of (Euclidean) *space*. At this point, the *conceptual space* consists of at least either three or four quality dimensions. This includes (a, ρ , space) or, respectively (a, ρ , space, time). Strictly speaking, at this point, time is not needed as a quality dimension and space could be considered as 1dimensional. However, space can also be thought of as \mathbb{R}^3 . \mathbb{R}^3 is a flat 3dimensional vector space or, in other words, the common Cartesian coordinate system. For the common mathematical treatment of long *range forces* acting on a fluid, the abstract *mathematical definition* of *vector spaces* is needed.

Let us consider further the specification of the forces, starting with *short range forces*. In contrast to long range forces, these are assumed to have a direct *molecular* origin, “decreas[ing] extremely rapidly with increase of distance between interacting elements, and are applicable only when that distance is of the order of the separation of molecules of the fluid”, [Batchelor 1970, p.7]. This means that within a volume element, both the *gravitational* acceleration of, and any *collisions* between molecules may be *neglected* (as matter is assumed to be distributed *continuously* and *equally*). This is consistent with the *continuum hypothesis*.

The new step is to consider interaction with materials *outside* the volume element which tend to *deform* the volume element. This is assumed to be conceptually analysable as *surface force*, and directly transferred from the *continuum mechanics of solids*. Surface force is assumed to be proportional to the surface involved, δA , and *directed*. This means that the surface force on δA with direction perpendicular towards the surface at time, t , for an element at position, x , is denoted as:

$$\Sigma(n,x,t) \delta A.$$

The *surface force per unit area* is also called *stress* and assumed to be an odd function³¹ of the vector pointing in a perpendicular direction to the surface, n .

³¹ Definition: Let $f(x)$ be a real-valued function of a real variable. Then f is odd if $-f(x) = f(-x)$ for all x in R .

This is expressed as:

$$\Sigma(-n,x,t) \delta A = - \Sigma(n,x,t) \delta A.$$

For the *total deforming forces on a volume element in rest*, only the *deforming forces perpendicular* to the surface are considered. This means that the new *conceptual space* can be constructed of five integral *quality dimensions* – or in the sense of Gärdenfors and Zenker as domains (x, t, ρ, a, Σ) , since x and a can be considered as elements of \mathbb{R}^3 . Concretely:

x element in $(= \in) \mathbb{R}^3$

$t \in \mathbb{R}$,

$\rho \in \mathbb{R}$

$a \in \mathbb{R}^3$

$\Sigma \in \mathbb{R}^3$.

This leads for (x, t, ρ, a, Σ) to a total of 11 dimensions.

The natural link of Gärdenfors's spaces to the mathematical *manifolds* becomes now clear, provided that the above space is diffeomorphic to \mathbb{R}^{11} and equations within (x, t, ρ, a, Σ) will cut out *manifolds* in \mathbb{R}^{11} .

With Stokes and mechanical equilibrium to static pressure

Let us denote the 11dimensional conceptual space introduced in the previous section, with G . It can be analysed further. The definition of *mechanical equilibrium* can be transferred from *solid* mechanics to *fluid* mechanics.

“A rigid body is in equilibrium when the resultant force and the resultant couple exerted on it by external agencies are both zero. The conditions for equilibrium of a fluid are less simple, because the different elements of fluid can move relative to each other and must separately be in equilibrium”, [Batchelor 1970, p.14].

In *structuralist* terms, the transfer of the mechanical equilibrium (ME) can be interpreted either as a *specialisation* of continuum mechanics, or as a *theoretical link* between fluid mechanics and solid mechanics (unless, mechanical equilibrium is introduced independently). In brief, *mechanical equilibrium* introduces a *condition* for the fluid to remain at rest, namely that volume forces and surface forces are in *balance*.

Further, a special case of Stokes theorem, itself being part of the *integral calculus*, is applied. (This is the so called “divergence theorem”.) The *divergence theorem* “converts” the directed surface forces $\Sigma(n,x,t)\delta A$ into a non-directed force which acts on the Volume δV . This introduces the quantity *static pressure*. More precisely, the *surface force* is translated into terms that express the *divergence of a scalar quantity*, called *pressure*. Formally, this is expressed as:

$$ap = \nabla p \quad (\text{ME}),$$

where, a , is the *acceleration* due to the surface force and, ∇p , denotes the vector of partial derivatives of, p , namely

$$\nabla p = \begin{pmatrix} \frac{\partial p}{\partial x_1} \\ \frac{\partial p}{\partial x_2} \\ \frac{\partial p}{\partial x_3} \end{pmatrix}.$$

Equation (ME) is the necessary and sufficient condition for a fluid to be *in equilibrium*.

Recall that the volume forces and surface forces acting on the fluid are interpreted as acting *on average* on the volume element. Such averaging does *not* result in a “loss of epistemic accuracy” since from the start the location of, x , was already “somewhere in the volume”. From a technical point of view, averaging itself is *linked to the mathematical integration* (in differential calculus).

When viewed against the background of the above 11dimensional space, G , the *mechanical equilibrium* means that certain tuples of elements are excluded by the equation (ME). The other way around, elements of G which satisfy the equation for *mechanical equilibrium* form

a *subspace* (or *region*) in G . Following Gärdenfors, a *convex region* of a *conceptual space* is a *natural concept*, [Gärdenfors 2000], making *mechanical equilibrium* a generic example of a natural concept in G .

In the *structuralist* framework, the quantity *static pressure* can be analytically introduced using *theory elements* of the *continuum hypothesis*, *Newton's second law*, *surfaces forces* and *mechanical equilibrium* (all as part of continuum mechanics) – and the *divergence theorem* (as part of integral calculus). In the structuralist framework, a *concept* or *term* which is *determined dependent* on a theory, T , is called **T-theoretical**.

“Traditional philosophy of science attempted to draw a universal distinction between ‘theoretical’ and ‘observational’ terms in a way relative to our total system of knowledge. [...] According to our view such a universal account is inadequate for the task of reconstructing single theories and their empirical bases. [...] The really fruitful task is to distinguish between concepts which can be determined and therefore controlled independently of a given theory and those for which is not so.” [Balzer et al. 1987, pp.48]

The distinction is always *relative* to a theory, T , and can be understood as *local view* on a scientific *term* or *concept*. An analysis of *theoreticity* requires examining the *minimum* amount of theory (in a local context of other theories) which is necessary in order to (re-)construct a concept. Structuralists are aware of the fact that, in other local context of other theories, the same term might be (re-)constructed in a *different* way. Structuralists emphasise that one or another local concept can be *linked theoretically*.

In summary, assume that *divergence-theorem* can be used as a synonym for the mathematical theory of integral-calculus (which includes the divergence theorem). Further, let *continuum-mechanics* consist of the continuum hypothesis, Newton's second law, surfaces forces and mechanical equilibrium. Then the concept of static pressure for

macroscopic fluid dynamics in structuralist point of view can be denoted as **divergence-theorem continuum-mechanics-theoretical**³².

Gas as a special case

With regard to gases, let us consider a specialisation of the above theories. Gases are a special fluid, whence a structuralist reconstruction would render them as a subset of the *intended applications* of fluid mechanics. In Gärdenfors's terms, the restriction to gases can be understood as a restriction on the quality dimension, ρ , to a particular range of values, because the density of gases is different from that of liquids.

Gas can be introduced as a *concept* in G , since the restriction to certain density values defines a region in G . Furthermore, the new region can be interpreted as new space G_g being the conceptual space for fluid mechanics applied on gases only.

The form of G_g depends on the values that are allowed for the density. For example, it may be assumed that the density of some gas is represented as an element of a certain interval of gas density, I_g in \mathbb{R} , (in notation: $I_g \subset \mathbb{R}$). From a mathematical point of view, if I_g is assumed to be an open interval in \mathbb{R} , then $G_g \cong G$. Hence, the spaces G and G_g are *diffeomorphic* in the mathematical sense of the term.

Now consider the introduction of new *quality dimensions* through application of thermodynamics on G_g . From a structuralist point of view, this can be understood as a *theory link* between fluid mechanics and thermodynamics. A fundamental point is: the wide separation of the molecules in gases and weak intermolecular forces leads to the assumption of *dynamically independent* molecules. This stands in *contrast* to liquids and solids, where intermolecular relations are *stronger*.

³² This is in accordance to Alcalde, [1984], who reconstructed hydrodynamics up to the level of the Euler Equations. The author is thankful to Prof. Moulines for sending the document. Alcalde, [1984] is the only reconstruction of hydrodynamics in structuralist terms, so far. Alcalde argued that pressure is hydrodynamic-theoretical and not thermodynamic-theoretical for historical and systematic reasons, [ibid, p. 101]. However, here, it might be insisted that static pressure can also be derived in statistical thermodynamics without taking fluid dynamics into account.

“The notion of a gas as an assemblage of molecules moving almost freely except at occasional collisions is the basis of the kinetic theory of gases. It is found convenient in that theory to consider the properties of a perfect gas whose molecules exert no force on each other except at collisions and have negligible volume”, [Batchelor 1970, p.37].

To establish G and G_g , the molecular movements of single particles are “averaged out”, when viewed from a macroscopic point of view. The new step consists in *re-considering* the microscopic structure of gases and linking previous considerations to thermodynamics. The main point which links the previous (macroscopic) considerations with thermodynamics is the quantity *pressure*. In the conceptual space of thermodynamics, *temperature* and *internal energy* are quality dimensions. Thus, the notion of a *perfect gas* can be introduced as a gas for which the following equation of state (EoS) holds:

$$p=R\rho T \text{ (EoS)}$$

Here, R is the so called *gas constant*, depending on the internal energy per temperature and average mass of the molecules of the specific gas. Note that, historically, the equation was derived empirically via $\frac{pV}{T} = \text{constant}$. Of course, perfect gases do not exist in reality. The concept denotes a simplification of reality, but remains to some extent based on empirical observation. Note further that from a structuralist point of view, the *macroscopic* concept of pressure for fluids in mechanical equilibrium is linked to the *microscopic* concept of pressure in *thermodynamics*, e.g. Hirschfelder et al., [1964].

In brief, as was stated so far, fluid mechanics can be linked, via the equation of state (EoS) with thermodynamics (and thus with statistical mechanics and quantum mechanics.) More precisely, the mechanical concept of *force* is linked via *pressure* with the thermodynamic concepts of *temperature* and *internal energy*.

Is the *continuum hypothesis* compatible with the equation of state (EoS)? The continuum hypothesis is involved in the sense that *pressure*, *density* and *temperature* are assumed to be represented as smooth (or at least continuous) scalar fields in the spatio-temporal

coordinate system (x,t) . Strictly, assigning a value for the *density* at a single point (x, t) is *not* readily meaningful, since an averaged value is assumed for a volume that is homogeneous with respect to density and temperature. So, continuity is a mathematical “trick” to “make” the equations “work”.

The thermodynamic *quality dimensions* enable further specialisations of *intended applications*. The *equation of state* for gas mixtures can be *specialised*, since the gas constant, R , depends on the material properties of the gases. For instance, consider *moist air*. It can be defined as a mixture of dry air and gaseous phases of water (water vapour), both of which are treated as *perfect gases*. Additionally, the idea of *moist air* can be simplified such that the gas constant for the gas mixture is assumed to be the weighted average of the gas constants involved for the different gases.

This means in equations:

$$R=R_1 m_1+R_2 m_2,$$

R_1 := gas constant of dry air

R_2 := gas constant of water vapour

m_1 := fraction of molecular weight of dry air

m_2 := fraction of molecular weight of water vapour

and

$$m_1+ m_2= 1.$$

Note that R_1 is already an average gas constant, since dry air is a mixture of different gases.

Then the equation of state for moist air can be derived as:

$$p=(R_1 m_1+R_2 m_2) \rho T.$$

This example illustrates the directions of *specialisations* for fluid dynamics. Fluid mechanics and thermodynamics are *theoretically linked*. This link is important if fluid dynamics is applied to real world phenomena such as atmospheric flows.

Fluid in motion and Euler in the river

Strictly speaking all considerations so far are based on the observations of *fluids in rest*. Motion (velocity) is conceptually described in physics as how an object or particle changes its *position* in *space* during a *time interval*. From mathematical point of view this is computing differences in the space-time concept. Consideration of infinitesimal differences leads to *differential calculus* in mathematics.

The motion of a fluid (a flow) can be considered in two different ways: either *remaining* in one *point* or *following* the *streamlines* of the flow. This is also known as *Lagrangian* and *Eulerian* perception of flow. Lagrange sits in the boat, *follows* the motion of a particle in the fluid, tracing its dynamic history. Euler stands in the river, remains at one fixed *point* in the reference coordinate system observing the velocity of the particles passing through this point (- the reference coordinate system is the riverbed). Both are *equivalent*. Here, it will be focused on the Eulerian view.

While observing the flow of a river, actually, the fluctuations of the velocities during time are observed. These are differences of velocities, leading to the quality dimension *acceleration*. In brief, the continuum hypothesis, the Eulerian perception of flow and the differential calculus leads to the description of fluid dynamics in terms of *differential calculus*. The Eulerian perception can be treated as follows:

Let u be the *velocity* of a particle in point x in the fluid at time t . The *acceleration* of the particle in x at time t can be denoted with the partial derivative $\partial u / \partial t$. The flow direction in the neighbourhood of x at time t has to be considered since the *velocity distribution* in the surrounding *determines* which particles with associated velocities will pass next through the fixed point x . The mathematical description of the so called “convective change” or

“advective acceleration” is analytically treatable in the framework of differential calculus, leading to u times the divergence of u , namely:

$$\sum_{i=1}^3 u_i \frac{\partial u_i}{\partial x_i} (=u \cdot \nabla u).$$

The acceleration in point x at time t is the sum of both variations considered above, thus:

$$\frac{\partial u}{\partial t} + u \cdot \nabla u.$$

For technical reasons it is useful to consider the dynamics of the *continuously* spread mass as being two times differentiable with respect to t . Thus, “continuum hypothesis” is not enough anymore. Moreover, a “differentiable hypothesis” is needed if above equation is considered for *practical mathematical* use.

In terms of *conceptual spaces*, above considered space G is extended with *velocity* as a new *quality dimension*.

Linking the notion of *acceleration in point x at time t in a flow* with Newton’s second law and above consideration on forces acting on the fluid volume leads to

$$\rho \left(\frac{\partial u}{\partial t} + u \cdot \nabla u \right) = \rho a - \nabla p \quad (EE)$$

Previous considerations on forces acting on fluids in *rest* are *transferred* to fluids in *motions*. In addition with the law of conservation of mass, equation (EE) is also known as *Euler-Equations governing the motions of fluid*³³.

³³ Alcalde, [1984], defined the *models of hydrodynamics* (in structuralist terms) in the following way:

- He denoted with F and T the space, respectively time-domain and with v , velocity, ρ , density and G the gravitational force, and v , ρ , G being suitable functions of F and T
- Then he defined the *models of hydrodynamics* (in structuralist terms) to be the tuples (F, T, v, ρ, G) which solve (EE) for all $f \in F$, $t \in T$.

This means that Alcalde reconstructed (EE) and defined the models as the manifolds which solve (EE).

From Euler to Navier Stokes

The assumption of *surface forces* acting on the fluid volume element in a *perpendicular* direction only, was (and is) motivated for fluids *in rest*. The crucial step from the Euler-Equations to the Navier-Stokes Equations is to consider deformation forces acting *tangential* and *torsional* as surface forces on the volume element due to the *motion of the fluid*. The term “surface force” might be misleading at this point since the “viscosity effects” can be physically interpreted as being effects of the “internal friction”.

The quality dimension for *viscosity* can be introduced with the following two assumptions:

(A1) is motivated by the empirical evidence that the *deviatoric stress tensor* is approximately proportional to (= approximately a linear function of) the various components of the *velocity gradient*.

(A2) demands the *statistical isotropy* of the fluid, meaning that the deviatoric stress generated in an element of the fluid is *independent* from the spatial *direction* of the velocity gradient by which it was generated. For illustration of what this excludes: “[...] suspensions and solutions containing very long chain-like molecules may exhibit some directional preferences owing to alignment of these molecules in a manner which depends on the past history of the motion”, [Batchelor 1970, p. 143].

Fluids that are assumed to (exactly) match the linearity assumption of (A1) are called *Newtonian*. Water and air are generally assumed as being *Newtonian* fluids. Gases in general and simple fluids such as water are assumed to be *statistically isotropic*. (This is due to their “simple” or disorganised molecular structure.) Hence, gases and water match (A2).

The step from (EE) to Navier-Stokes Equations with the assumptions (A1) and (A2) is conceptually as follows (historically based on Saint-Venan, 1843, and Stokes, 1845): Consider the stress tensor of fluids in motion to be of a certain format – that is a 3x3 matrix according to the stress tensor for solids in continuum mechanics.

This can be interpreted as *transformation matrix* deforming the *infinitesimal* fluid volumes of the fluid in motion. Remember that the *perpendicular* directed surface forces (also called normal stresses) can be considered in terms of the *static pressure*. It is convenient to regard the total of the surface forces as sum of the *normal* stresses, having the same form as the stress tensor in a fluid at rest, plus a *new part* contributing *torsion* and *shear* stress. The new part is also called *deviatoric stress tensor*.

The stress tensor for fluids is the analogous to the *Cauchy stress tensor* in *solid* continuum mechanics. The diagonal of the 3x3-matrix σ_{ij} , $i,j=1,2,3$ denotes the normal stresses. As stated above, the normal stresses are assumed to be given by the pressure. Thus, the diagonal of σ_{ij} , $i,j=1,2,3$ is given by p .

Tensor analysis with the assumption (A1) and (A2) leads to a specific format of the stress tensor σ_{ij} , $i,j=1,2,3$, for fluids in motion:

$$\sigma_{ij} = -p\delta_{ij} + 2\mu(S_{ij} - 1/3 S_{ii}\delta_{ij}) \quad ,$$

with

p := pressure

μ := material property denoting the viscosity

$$\delta_{ij} := \begin{cases} 1 & \text{if } i=j \\ 0 & \text{if } i \neq j \end{cases}$$

$$S_{ij} := \frac{1}{2} \left(\frac{\partial u_i}{\partial x_j} + \frac{\partial u_j}{\partial x_i} \right).$$

(The mathematical details are skipped here.) Note that the introduction of the *viscosity*, μ , is essentially based on *empirical observation*. The *viscosity*, μ , is the *linear coefficient* by which the Newtonian assumption (A1) is motivated *empirically*. Furthermore, note that μ depends in general on temperature and thus is linked to thermodynamics. Here it is integrated over the molecular inhomogeneity of viscosity which leads to a loss of molecular *information* on reversibility, as stated before.

Above steps can be reconstructed in terms of conceptual spaces. First, velocity is introduced as a new dimension to \mathbf{G} yielding to the conceptual space \mathbf{G}_{EE} in which the Euler-Equation holds³⁴. The conceptual space \mathbf{G}_{EE} is extended by the *viscosity*, μ , namely adding the dimension *viscosity* within the concepts of (A1) and (A2). This means in geometrical sense that (A1) and (A2) define a region in \mathbf{G}_{EE} which can be interpreted as new Gärdenfors space $\mathbf{G}_{EE}^* \subset \mathbf{G}_{EE}$. The dimension μ is added to \mathbf{G}_{EE} yielding to a new Gärdenfors space \mathbf{G}_{NSE} with domains $(u, x, t, a, \sigma_{ij}, \rho, \mu)$.

For the concrete equations, this means that the stress tensor σ_{ij} , $i, j=1,2,3$, for fluids in motion, replaces the stress tensor in (EE) yielding the Navier-Stokes Equations. The general Navier-Stokes Equations are of the form

$$\rho \left(\frac{\partial u_i}{\partial t} + u_i \cdot \nabla u \right) = a_i \rho - \frac{\partial}{\partial x_j} [p \delta_{ij} + 2\mu (S_{ij} - 1/3 S_{ii} \delta_{ij})] \quad , i, j=1,2,3 \quad (\text{NSE})$$

for each of the three components of $u = (u_1, u_2, u_3)$, summed over j .

In structuralist terms, (NSE) can be seen as specialisation of (EE), incorporating the constraints (A1) and (A2) and providing the option for specifying the *intended applications* by choosing values for μ . *Viscosity* can be seen as **Newtonian-theoretical** since it is empirically introduced in (A1). On the other hand, its scientific meaning in nowadays' fluid dynamics is based on the total of (A1), (A2) and (NSE), so it can be called Newtonian-isotropic-Navier Stokes-theoretical, too.

As a remark, the normal stresses (pressure) in a fluid at rest are not necessarily the same as for the same fluid in motion (e.g. flow with non-zero divergence). Note that for above considerations, *density* and *viscosity* might be functions of space and time and do not need to be constant.

³⁴ It is noteworthy that Alcalde's models in structuralist formalism, [Alcalde, 1984], coincide exactly with \mathbf{G}_{EE} . Both are the manifolds which solve (EE). This means, for the special case of fluid dynamics, the set-oriented structuralist formalism coincides with the geometrical approach of conceptual spaces.

Remarks

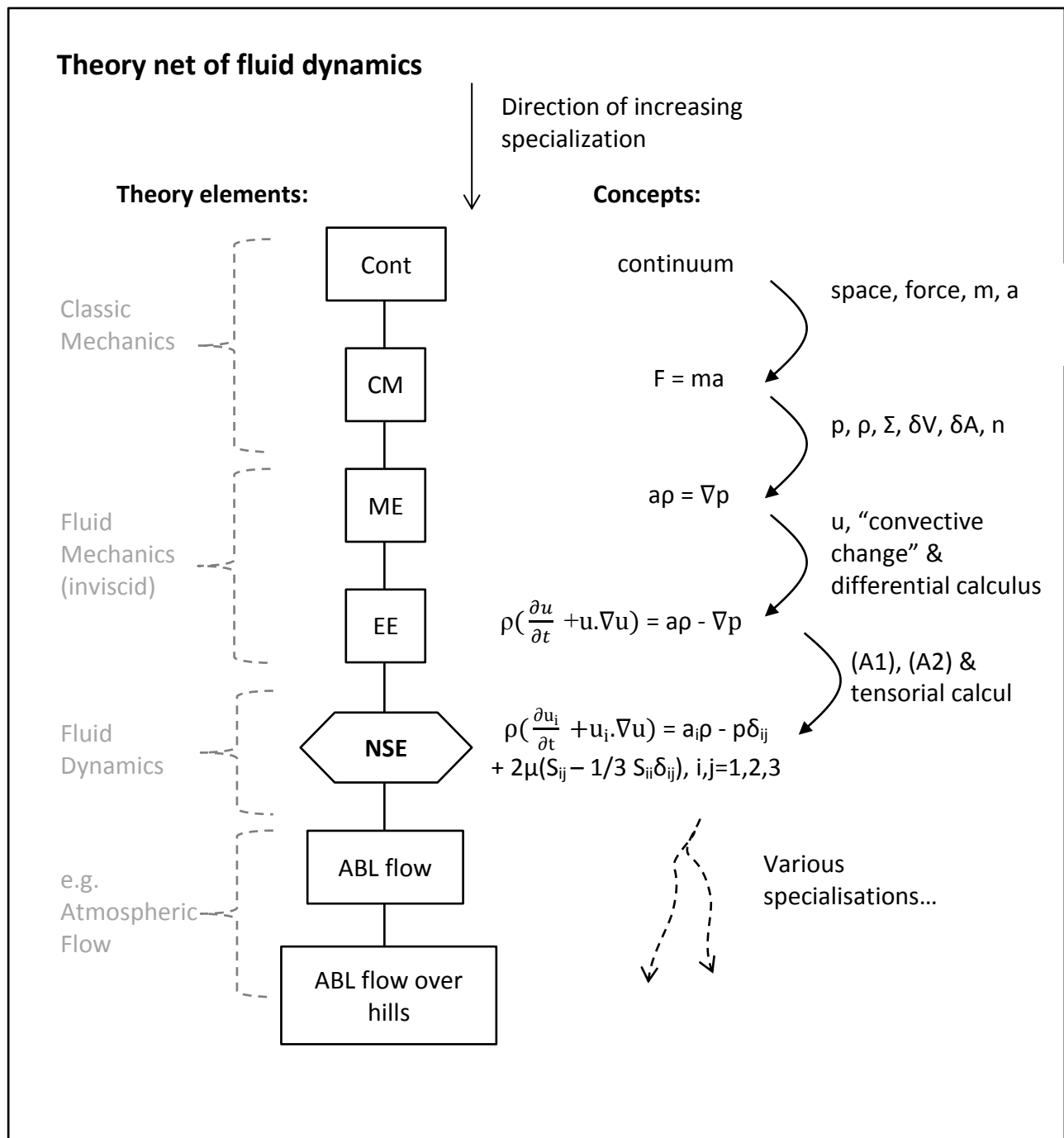
The continuum hypothesis is the basis for fluid mechanics and *neglects* the molecular structure of the fluid. The quality dimension of *viscosity* encrypts the molecular effects of friction in the macroscopic scale for fluid dynamics. The *viscosity* can be seen as the follow-up of the *density* which encrypts the molecular structure of the resting fluid as uniformly averaged spread mass. The *turbulent viscosity*, introduced for RANS on p. 31, is derived by similar assumptions focusing on the dynamics of turbulent flow – another *follow-up of* encryption.

Encryption of the molecular structure of the fluid by scalar quantities for obtaining better understanding of the fluid dynamics on a macroscopic level can be seen as the “generic” step of *theory evolution* in fluid dynamics.

In applied fluid dynamics, density, ρ , and viscosity, μ , are often considered as being constant. Further simplifications are being made, such as conservation of mass. Note that (NSE) and the equation for the conservation of mass is a set of four equations with four unknown variables, namely $\mathbf{u} = (u_1, u_2, u_3)$ and p , whereas ρ and μ are determined empirically. This means that (NSE) and the equation for the conservation of mass build a complete set of equations (=same number of variables as equations) provided that adequate boundary conditions are known. The term “Navier-Stokes Equations” often refers to this complete set of equations.

It is mathematically not yet proven that in three dimensions solutions of (NSE) always *exist* or that if they do exist then they do not contain any singularity. This means that the symmetry assumptions for NSE solutions, as used before, are strictly speaking *hypotheses*, assuming the *existence* of NSE solutions.

Methods for the approximations of solutions for atmospheric flow modelling include for example averaging methods based on the Reynolds averaged Navier-Stokes equations (RANS), numerical approximation in terms of direct numerical simulation (DNS) or Large Eddy Simulation (LES) or considering statistical features of turbulence, such as probability density functions (PDFs), [Pope 2009].



Abbreviation key:

Cont := Continuum hypothesis, p. 58

CM := Classic Mechanics, p. 61

ME := Mechanical Equilibrium, p. 63

EE := Euler Equation, p. 69

NSE := Navier-Stokes Equations, p. 71

ABL flow := Atmospheric boundary layer equations

Figure 9: Theory net of fluid dynamics based on historical evolution

Summary - Theory

The *continuum hypothesis* is introduced as fundamental assumption for modern fluid dynamics. Furthermore, classical mechanics is translated to fluids introducing the notion of force and *mechanical equilibrium*. Forces are split into body and surface forces acting on a volume fluid element respectively its surfaces. This leads to the conceptual space **G** which consists of elements of the form (x, t, ρ, F, Σ) . With help of integral calculus and the assumption of mechanical equilibrium, static pressure is derived in a divergence-theorem continuum-mechanics-theoretical way.

The Euler-Equation is derived for fluids by linking former analysis of forces acting on fluids in rest with Euler's perception of acceleration in point x at time t in a flow and Newton's second law, $F = ma$. The crucial step from Euler-Equations to Navier-Stokes Equations is to transfer of the stress tensor from solid mechanics to fluid dynamics. Tensor analysis translates the stress tensor into a certain shape under the idealizing assumptions of statistically isotropic and Newtonian fluids, (A1) and (A2). A compact illustration of these steps is given in Figure 9, p.75.

Also, gas as a subset of *intended applications* for fluid dynamics was examined by means of theoretical links to thermodynamics. Moist air was given as an example for directions of specialisations of fluid dynamics.

Conclusions and outlook – Theory

The Navier-Stokes Equations are based on assumptions for the underlying fluid, as discussed. Integration over the molecular structure leads to “material properties” on macroscopic scale, such as *density* and *viscosity*. However, *density* and *viscosity* depend on temperature. In the limit of scales approaching infinitesimals (on molecular level where dissipation occurs) temperature will alter locally. One could interpret *viscosity* also as a “flow characteristic property on molecular level” instead of “fluid property” on macroscopic level.

For future work, the analysis of turbulent atmospheric boundary layer flow by means of formal analytical concepts such as *structuralism* and *conceptual spaces* can provide further insights for modern fluid dynamics, especially *turbulence research*. Several explicit examples for theory evolution in structuralist terms can be given. This includes the RANS-Equations (Reynolds Averaged Navier Stokes) which encrypt turbulence into *averaged values* (namely into the sum of a mean flow value plus standard deviation). This also includes the Kolmogorov's theory on *self-similarity of locally idealized turbulence* (homogenous and rotational invariant). Furthermore, purely mathematical investigation which focuses on specific aspects of *chaotic dynamical systems* can be considered as part of fluid dynamics. Also, it can be examined further how physical and computational models are linked to the theory net of modern fluid dynamics. Finally, in 20th century, theories on turbulent flows advanced remarkably and a structural analysis could provide fruitful hints for scientific synergies. A few theory links are worked out in Figure 10.

The structural theory evolution from the Euler-Equations to the Navier-Stokes equations can also be embedded into the historical context, [Petersen and Zenker, 2012]. The historical development of fluid dynamics and fluid mechanics throughout the 19th century is far from linear. For instance, the Navier-Stokes Equations have reportedly been derived at least five times, sometimes by authors working independently of each other.³⁵ A table with key figures for the 18th and 19th century development of fluid dynamics is given in the appendix (based on Darrigol, [2005] and Tokaty, [1971]).

For this chapter, G.P. acknowledges especially the participants and organisers of “Perspectives on Structuralism” (Munich, 2011) for fruitful discussion, as well as the organisers and participants of “Conceptual Spaces at Work” (Lund, 2012), especially F. Zenker and P. Gärdenfors, both Lund University, M. Hoffmann from the University of

³⁵ In 1821, C.L.M.H. Navier derives the Navier-Stokes Equations (NSE) as the viscosity extension of the Euler Equations. In 1829, S.D. Poisson provides a new derivation of the NSE, inspired by Laplace's molecular physics, yet mentioning neither Navier nor Cauchy's 1821 elasticity theory. In 1837, A.B. de Saint-Venant provides a derivation of the NSE and, in 1859, H. Helmholtz provides an independent derivation of the NSE, based on internal friction. The NSE finally count as established through Maxwell's kinetic theory of gases in 1866 and the review of H. Lamb and the studies on turbulent flow by Reynolds and Boussinesq in the 1880s; see Darrigol, [2005]. A more compact historical overview is provided by Tokaty, [1971].

Hamburg for encouraging support and K. Lux from the University of Arizona for building communicative bridges in fluid-dynamics.

Extended theory net for fluid dynamics

Abbreviation key:

Cont := Continuums hypothesis, p. 58

CM := $F = ma$ (Classic Mechanics), p. 61

ME := Mechanical Equilibrium, p. 63

EE := Euler Equation p. 69

NSE := Navier-Stokes Equations p. 71

ABL flow := Atmospheric boundary layer flow

EoS := Equation of State, p. 67

BTE := Boltzmann Transport Equation

RANS := Reynolds Averaged Navier Stokes

*Prob/ Stat := Probability theory/ Statistics
(Mathematical theory)*

*Diff := Differential Calculus
(Mathematical theory)*

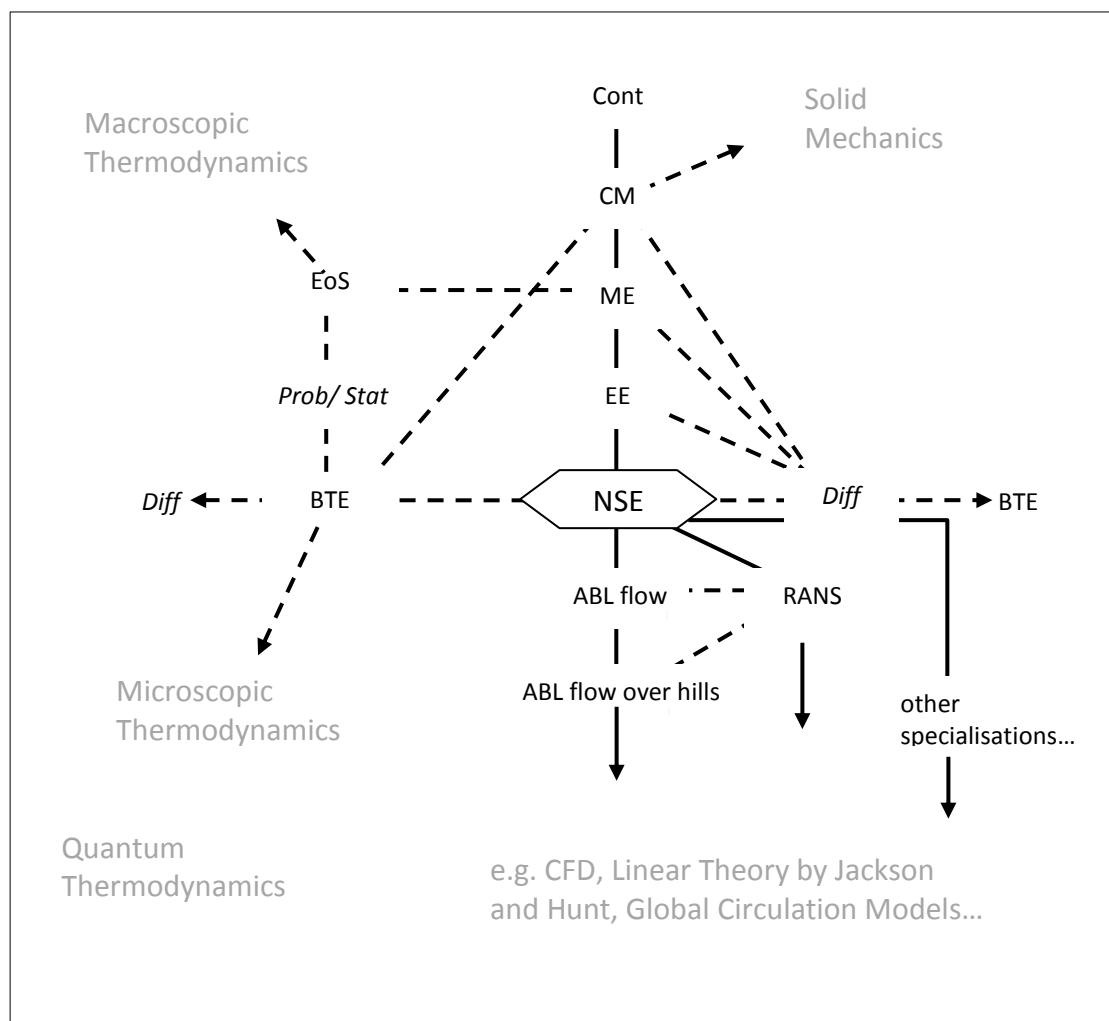


Figure 10: Fluid dynamics with exemplary theory links; solid arrows denote directions of specialisations; dashed arrows exhibit theory links

5. Models as mediators in wind assessment

“Verification and validation of numerical models of natural systems is impossible. This is because natural systems are never closed and because model results are always non-unique. [...] The primary value of models is heuristic.”

- [Oreskes et al., 1994, p. 641]

This chapter builds the bridge between theories³⁶, models and reality and introduces the notion of *models as mediators*. It will set the scope for what scientifically can be expected of wind tunnel modelling with application for wind assessment.

Introduction to this chapter

The previous chapter raised the awareness of the many simplifications and assumptions on which the theories of fluid dynamics are built upon. The available theoretical foundation of fluid dynamics was reviewed in detail. For wind flow predictions in the *real world*, the *complexity* of fluid dynamics increases. Concretely, *meteorological* conditions and *physics of the atmosphere* have to be taken into account. This includes global circulation, radiation, and inhomogeneous material of the fluid (e.g. clouds) and inhomogeneous surface of the earth.

It is not surprising that *increasing* complexity of influencing factors *increases* the uncertainty of results of (or predictions derived from) theories. Wind, weather and climate predictions mainly rely on numerical models – and in most of them, *the fundamental equations* of fluid dynamics (in previous chapter) are indirectly or directly *implemented*. *Uncertainty* of wind assessment models is the *symptom* of the underlying *theoretical challenge* of fluid dynamics and the *complexity* of the *influencing factors*.

³⁶ Recall that the plural is used to emphasise the fact that competing theories can exist for *the same* theoretical question within the set of theories which can be called “theory”.

In the following chapter, modelling in science with regard to wind assessment will be discussed. To conclude, the chapter “Application field: wind energy assessment” shortly illustrates how such models practically are involved into wind farm building projects.

Model in science and model development

For introduction, the meaning of *models* in science and the relation between theories, models, reality and data is analysed³⁷. Furthermore, the role of *model comparison* in *model development* will be examined. Also, the *adequacy of reference data* will be discussed. It is illustrated by an example with regard to the Bolund wind tunnel experiment (filtering of the *Bolund field data*). The *inverse non-stationarity* measure will be proposed as an assessment tool for the *variability of the atmosphere* and for the adequacy of reference data.

Models in philosophy of science

Although *theory* is one of the most often used terms in science, the term is not easily definable. In the 1960s, theory is assumed to represent the world. “Models were there to tell us how to change the theory. [...] Theory itself was supposed to be a formal system of internal principles on the one hand – axioms and theorems – and of bridge principles on the other, principles meant to interpret the concepts of the theory, which are only partially defined by the axioms”, Cartwright in Morgan and Morrison, [1999, p. 241].

This explanation is not practical in the sense that it does not give a rigorous answer for specific cases, for differentiation between something that can be denoted as *theory* and something that cannot. Between 1960s and 1980s, a new approach was tried: the *semantic view of theories* – lining out the idea that a model provides a realization in which the *theory* is satisfied. The discussion was thus shifted towards a discussion on *models*. It had to be clarified how the relation between the *model* and the real system is characterized. Many questions needed to be addressed, such as: what is a *model* in scientific terms? What is the relation between *models*, *reality* and *theory*?

³⁷ In this work, the term “models” is used in the sense of Magnani et al. [1999], and Morgan and Morrison, [1999], namely as models as mediators between theories and reality.

From nowadays point of view, *theory* is no longer the *ultimate truth* with regard to reality. *Theory* is related to reality and takes part of science but it does not directly depicture *reality*. Furthermore, there is not *one* theory, explaining the world, but *many theories*, competing with each other.

Theories are part of an abstract world which is built with axioms and abstract concepts. The abstract world is not necessarily *isomorph* (one-to-one and structure-preserving) to the real world. *Models* are needed to represent the *reality*.

This comprehension of *theory* is supported by contemporary philosophers of science, such as Nancy Cartwright in Morgan and Morrison, [1999]: theories give purely abstract relations between abstract concepts and this does not generally represent what happens in the world. It is stated that only *models* represent what happens in the world.

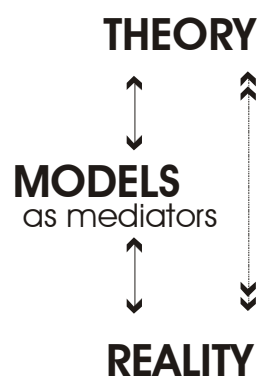
This definition is still not very specific. One Problem in defining *theories* is obvious: the term covers a very inhomogeneous set of scientific building blocks. These can, for example, be analysed by means of *structuralism* or *conceptual spaces*, as done for the Navier-Stokes Equations in chapter 4. Further discussion about the examination of theories will be skipped here. For the purpose in this work, the comprehension of theories as part of an abstract world which is built of axioms and abstract concepts (and can be used as building blocks for models which represent the world) serves as a sufficiently exact delimitation of the term *theories* towards *reality* and *model*.

From the model's perspective: what is the relation of *models* with *reality* and *theories*? To start with a practical approach, consider the statements of Arturo Rosenblueth, a Mexican physiologist, and Norbert Wiener, a US-American mathematician: "No substantial part of the universe is so simple that it can be grasped and controlled without abstraction. Abstraction consists in replacing the part of the universe under consideration by a model of similar but simpler structure". [Rosenblueth and Wiener, 1945, p. 316]

That is, models *simplify* reality³⁸. Furthermore, they state that scientific progress consists in a progressive *adding of variables* to a model – hence from relatively *simple*, highly *abstract* to more *complex*, more *concrete* theoretical structures. They claim, if the model approached asymptotically the complexity of the original situation, in limit, it would become identical with the original system. However, Rosenblueth and Wiener admit that the *ideal model* can never be achieved. This is in line with the point of view of structuralists. Additionally, it is pinpointed that models are always imperfect and limited:

“(Partial) models, imperfect as they may be, are the only means developed by science for understanding the universe. This statement does not imply an attitude of defeatism but the recognition that the main tool of science is the human mind and that the human mind is finite.” [Rosenblueth and Wiener, 1945, p. 321]

This is a practical point of view on models. In Morgan and Morrison, [1999], an extensive contemporary study on models in science is given. It is considered how models are *constructed*, how they *function*, what they *represent* and how it can be *learned* from them. Models are considered as *mediators* between theory and reality, in illustration:

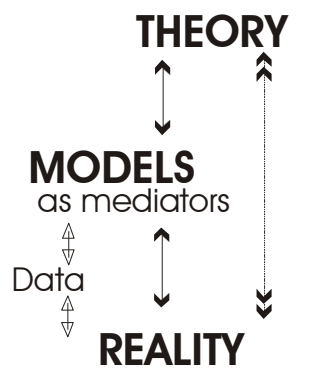


The considerations in Morgan and Morrison, [1999, pp. 11], can be summarized as follows:

³⁸ It has to be mentioned that with models in this conclusion, Rosenblueth and Wiener refer to “material” as well as to “theoretical” models. “Material models”, from their point of view, are linked to experiments whereas “theoretical models” or intellectual models are denoted with theory by other authors – or models by the structuralists. Key point is: Rosenblueth and Wiener emphasize that imperfection holds for both, for models as well as for theory.

- Regarding construction of models, models are *neither theory nor data*, “*but typically involve some of both (and often additional ‘outside’ elements), that they can mediate between theory and the world*” [Morgan and Morrison, 1999, p11].
- Models *mediate* between things and can often be used for different tasks. The point concerning representation is that scientific models work like an *investigative* tool. Investigative in this context means that models can be differentiated from simple tools by their property to represent: “*models typically represent either some aspect of the world or some aspect of our theories about the world, or both at once*” [ibid, p11]. That is to say, a model is not just like a “hammer”, that functions instrumentally, but it is an instrument which teaches us something about the world.
- We learn from building the model and manipulating it. “*In this sense, they have the quality of a technology – the power of the model only becomes apparent in the context of its use*” [ibid p.12].

The process step of data generation, in the context of concrete use, can also be a crucial point. Addition of *data* as output of model experiments and output of field studies can be illustrated as follows:



This is, *models* mediate between *theory* and *reality* and represent parts of both. In this

sense, models are closer to reality than theory. It can be seen as a remarkable statement since it might be in contrast to nowadays common view in many parts of science.

The author feels that Morrison and Morgan's definition has weak points. They are not precise regarding the term *world*. It is not correct to just identify *data* with *reality*. No observation is possible without *manipulation* of the observed object, (the observer-effect). Secondly, measurements require *technical equipment* and introduce further uncertainties into the data. Uncertainties are for example induced by the experimental equipment, by the human users and by the measurement set-up. Also statistical features come into play such as the *statistical representativeness*. Thus, it is clear that *data* as result of measurements and observations is only another *representation* of the world. Data is *not* reality.

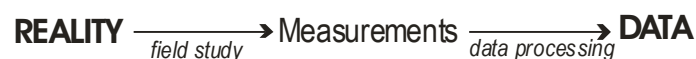
The role of *data* is analysed more deeply in the following paragraph. It is an extension of Morrison and Morgan's analysis.

Models, theory, reality and data in wind assessment

Every day model development in science (or application of models in real world) is difficult with respect to the epistemological meaning and benefit of modelling. What does *models as mediators* mean in practice?

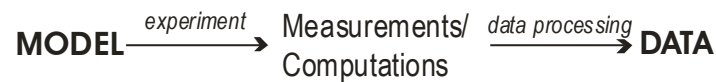
As mentioned before, data is not reality. *Data* only represents the world. It is one way of observing nature, "What we observe is not nature itself, but nature exposed to our method of questioning" [Heisenberg].

The *process chain* to obtain field data is as follows:



Field data modifies the relation between *model* and *reality* and imposes a *bias* on what is observed of *reality*. Bias of field data is caused by the choice of observable and measurement error. Equivalently, *model data* is biased.

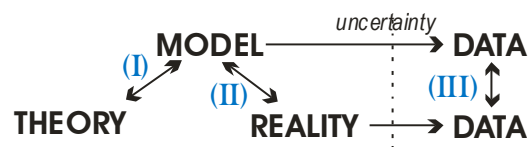
In scientific practice, a model predicts *data*. This means for example in wind energy application that a model is used for predictions of wind speeds at a certain site. In order to predict the wind velocities an experiment is conducted – physically or numerically. The measurement- or computational output is *data*. Analogously to field measurements every step induces *uncertainties* and *errors*. In illustration of the process:



In order to consider the relation between *model* and *reality*, comparison is commonly done between model-*data* output with field-*data* output, for example:

- The relation between *model* and *theory* is examined (I).
- Then, in order to understand the relation between *model* and *reality* (II), data is compared (III).

In illustration:



How can different models be compared with each other? This question is examined in the following paragraph.

Comparison of models

In wind energy assessment, it can be assumed that competing models for wind assessment exist at the same time. The importance of *adequacy and quality of data* is connected to the problem of *model comparison*.

In practice, the problem in choice of models is as follows: Needed is a wind prediction for a certain site, x. Meteorological data is only available from an airport which is 50 kilometre far away. Let us assume model 1 performs well for cases, A, model 2 for cases, B. Consider a scientist who wants to make predictions for the atmospheric flow at x, and let him run model 1 and model 2. Then, two sets of data are generated. How can be known, which model performs better if it is not known if, x, belongs to, A, or to, B, – or to case, C, which is neither A or B?

In practice, the answer is that a *blind comparison* of the *models* can be conducted. “Blind” indicates that physical and numerical modellers get a certain restricted set of field data (e.g. starting and inflow conditions) and are asked to reproduce the remaining data-set. In case of Bolund hill, inflow conditions serve as restricted *starting set* and measurements from the masts are to be *reproduced*, [Berg et al., 2011; Bechmann et al., 2011]. Another example for a study on model comparison is the COST-Action³⁹ 732, [COST 732. 2010]. An analysis for *model* comparison can also be derived from a models-as-mediators perspective and related to the COST procedure⁴⁰, as it will be done in the following.

How can *models* be compared? What mostly is done in practice is the following: modellers let their numerical model or the wind tunnel run and obtain *data*. Then *data* is compared (I), for a scheme see Figure 11.

³⁹ COST is an intergovernmental European framework for international cooperation between nationally funded research activities.

⁴⁰ Objective of COST 732 was to improve and assure the quality of microscale meteorological models for predicting flow and transport processes in urban or industrial environments. Although urban and industrial environments are not wind energy sites, wind energy community can learn methodically from the COST action. Within COST 732, a structured quality assurance procedure was developed, based on data for model validation and consensus of the community.

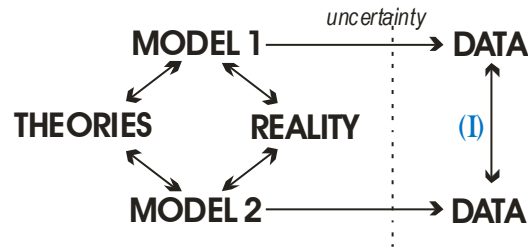


Figure 11: Model comparison by data comparison

In practice, the relation between *model* and *reality* is not perfectly clear. Moreover: the relation between *model* and *reality* is deduced from the relation between *data*-output of the model and *field data*. That is, the relation between the *model* and *reality* is approached by the relation between the *model* and *field data* (I). The relation (I) is deduced from the relation between the *model data-output* and *field data* (II), and from the process of *model* to *model data-output* (III). Furthermore, there is a relation between *model* and *theories* (IV). For a scheme see Figure 12.

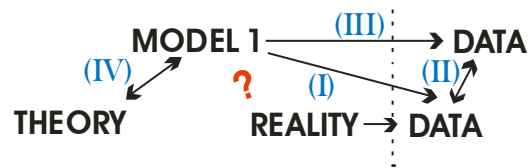


Figure 12: Model comparison I-IV

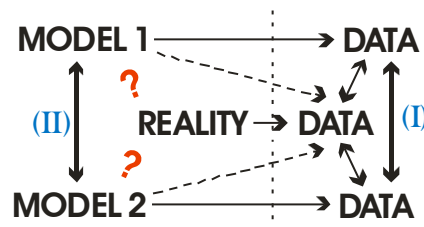
In consequence, if different models exist, say model 1 and model 2, the models are linked by the *relation of their data* towards the data that represent *reality*. Additionally, model 1 and model 2 are linked with each other by their *relation towards theories*. In practice, relation towards theories differs extremely from model to model.

Concerning the comparison of data of models, a crucial point of the comparison is the *comparability* of the model *output*. It is very tempting to just *compare numbers* and forget about the *meaning*. Instead, one should consider that application of quality metrics (which

are certain differences or relations of numbers) can only be interpreted reasonably if it is taken into account where the numbers come from⁴¹.

Lemma 1: Data of model 1 and model 2 is only comparable if model 1 and model 2 are comparable.

Hence, it can be claimed: in order to compare data of models, the relation between the models has to be examined.⁴² This includes the question whether or not both models are built to replicate *statistically stationary flow*, and how the *boundary conditions* are set. The structure is following:



In other words: Comparison between output data of model 1 and model 2 (I) is only possible if model 1 and model 2 are comparable (II). This leads to the Lemma.

What does *comparability of models* mean in practice? Simply, models are *comparable* if a comparison can be done (and *is* done). Here, a five step comparison will be suggested. It starts in the above structure on the left hand side and shifts towards the right. At the end it takes into account the whole picture. The five steps of model comparison are practicable for two models and more than two:

⁴¹ In the Bolund blind comparison, quantification of data comparison is mainly done with the differences of ensemble averages of wind speed mean values and wind speed standard deviations. Thus, comparison can be quantified 'easily'. The problem is: nothing is learnt from comparison of data if the models are unknown from which the data was generated. In Bolund, the main properties of the models were analysed.

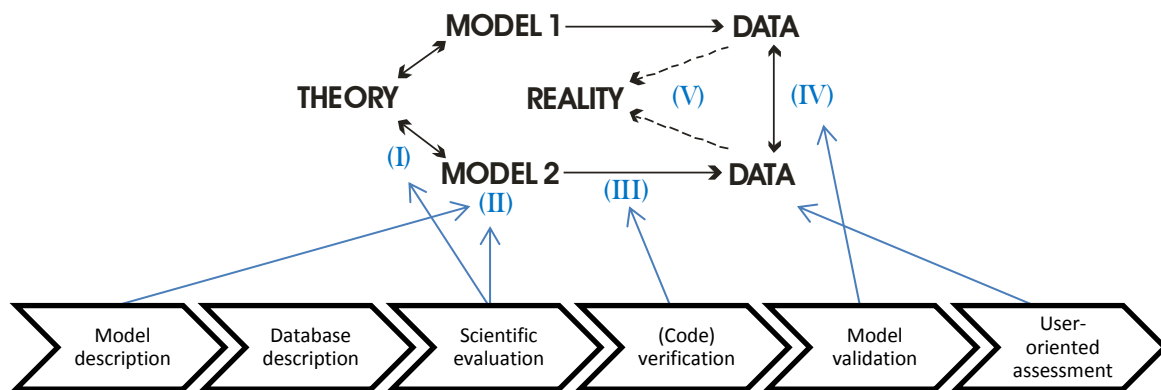
⁴² In most cases, relation between models and reality is not known exactly and can only be guessed by means of comparing the model output-data with field data. In practice, the focus then often remains on the data: data of the models is compared – instead of stepping back and first considering the structure.

- (I) Relation between *models* and *theories* has to be made clear: What theories are applied for the models?
- (II) *Assumptions* for the models need to be compared.
- (III) *Experimental conditions* need to be clarified. A detailed *documentation* of the experimental set-up is obviously the precondition for a comparison. (In practice, this has not always been the case. This is shown extensively in the chapter “A review of research on flow over hills”.)
- (IV) *Output data* needs to be compared. The quantification of comparison has to be done well-thought-out and with regard to underlying *theories* and *assumptions*. Comparison of model results, (e.g. computation of quantitative differences of data), depends in general on the specific *choice* of the *quality metric*.
- (V) Comparison of data (e.g. the quantitative differences) needs to be *interpreted* with regard to *reality* and its dependence on the *choice of the quality metric*. If field data is available it is used for comparison with model output-data. The aim of the interpretation is to obtain a *quantitative diagnosis* how the model data relates, how the models *qualitatively correspond* and how the results of the comparison can be *interpreted with regard to theory and reality*.

Is this feasible in reality? Yes. The comparison of the models within COST 732 was named “model evaluation procedure” and is a good example, although it was dedicated to microscale flow dispersion models and not to wind (energy) assessment. It consisted of the following six steps: model description – database description – scientific evaluation – code verification – model validation⁴³ and user-oriented assessment.

⁴³ In terms of COST 732, “model validation” is *a structured comparison of model predictions with experimental data and is based on statistical analysis of selected variables. It seeks to identify and quantify the differences between the model predictions and the evaluation (validation) datasets; it provides evidence as to how well the model approximates to reality*; [COST 732, 2010, p.9, additions in “()” by the author]. This fits the understanding as in the *International vocabulary of metrology — Basic and general concepts and associated*

These five steps fit well to COST 732's model evaluation procedure. The latter is the *process-oriented* formulation of the former, which is based on a *structural* approach and derived from the analysis of models as mediators between reality and theories:



The step “database description” refers to the fact that the participants of COST 732 agreed on the use of a database as *validation data set*. It was employed for the validation of the model and was a combination of field with wind tunnel data. Thus, “database description” means to consider (I) - (V) for the validation data set.

Key point of this paragraph is: if different *models* exist and are to be *compared* it is not sufficient to compare *model data-output*. Data is only comparable if models are comparable. Also, a structured approach for a comparison in five steps was suggested. Furthermore, there are model comparison procedures of which the structure can be used in more general sense and transferred for wind energy application, such as COST 732.

Recall that the motivation for model-comparison in the case of wind energy assessment was the *improvement of the models*. This is examined in the following two chapters.

terms by the Joint Committee for Guides in Metrology, [JCGM 200, 2008]. In the following, the term *validation* is used in the meaning of the COST 732 definition.

Field data

In order to build “good” models for wind prediction, “good” quality of *reference* or *field data* is a crucial point for *model validation* (and hence *development*), see e.g. COST 732, [2010], or Ross et al. [2004].⁴⁴ Key points for quality assurance of wind tunnel data will be examined in the chapter on the “Bolund Wind Tunnel Experiment”. Here, it will be given a short insight on the epistemic challenges for *field data* as validation foundation.

Field data needs to be interpreted for the adjustment of the *inflow conditions* for models, for example those of the Bolund field experiment [Berg et al., 2011; Bechmann et al., 2011]. The Bolund experiment can be regarded as a field study that provides a unique dataset for validating models designed for flow over a steep hill⁴⁵. The experiment was conducted from December 2007 to February 2008 on the Bolund hill located 1 km north of Risø DTU, National Laboratory for Sustainable Energy, [Berg et al., 2011; Bechmann et al., 2011]. Not only is the measurement process challenging but also the *planning*. Explicitly, it has to be agreed on *measurement methods*, on *location*, overall *equipment* and on *funding*. The *conduction* of the measurement, *storage* and *post-processing* of the *data* is another challenge. In the case of the Bolund field study, nine masts were mounted on and around the Bolund hill and equipped with instruments. The *inflow conditions* which are determined by the Bolund field measurements for the use by numerical and wind tunnel modellers consist of *a mean wind profile* and *turbulent kinetic energy* (computed from autocorrelations of wind fluctuations) as inflow conditions. The Bolund values can be checked for consistency against values of the literature – this is done in chapter “Determination of plausible inflow conditions”, pp. 177. The key point here is that the field data and out-coming information is *ambiguous*. The reason for this is the *variability of the atmosphere* provided that the

⁴⁴ Ross et al., [2004], clearly state: “When validating the results from analytical or numerical models it is essential to have good quality measurements of both mean and turbulent quantities over the hill. Making measurements at a range of heights and locations over a real hill can be difficult to achieve. The inability to control the upstream conditions also makes it hard to compare the results with numerical models. For these reasons experimentalists have often made use of wind tunnels to carry out experiments on flow over hills.” [ibid. pp. 428]

⁴⁵ The Bolund field experiment is also a key topic in “Field studies”, pp. 122 and in the experimental chapter “Pilot study to the Bolund wind tunnel experiment”, pp.133.

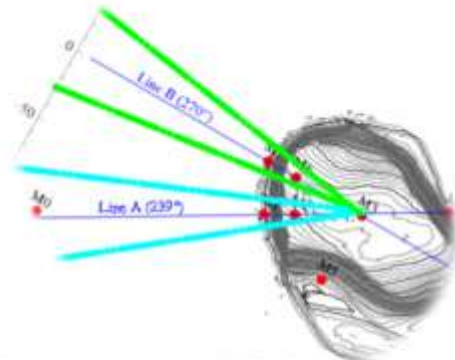
structural error of the measurement instruments, the precision of measurement location and further measurement errors are already taken into account.

The *variability of the atmosphere* can be illustrated for example by filtering the field data for nearly constant boundary conditions such as *mean wind direction*, *meteorological stratification* (in this case *neutral*) and *mean wind speed*. The reference location is M0 in 5 m above ground level around 120 m south-west of the hill. As it can be seen in Figure 13 and Figure 14, the ensemble of wind velocity data for the Bolund mean wind inflow direction Line A ($239^\circ \pm 8^\circ$ degrees) consists of time series with an overall record length of 160 hours. The *sampling size* (= *overall record length*) is the same for 10 minutes respectively 30 minutes averaging intervals. Figure 13 shows that less than five percent of the time for Fetch A fulfils nearly neutral conditions. It results in absolute 7 hours sampling size for 10 minutes means (8 hours for 30 minutes means).

How does the sampling size depend on filtering methods? 1/2

Line A, 10 min. mean, M0_S_5:

wind direction $239^\circ \pm 8^\circ$	160 h
AND nearly neutral conditions i.e. $ABS(ss.invL) < 0.002^\circ$	7 h
$ABS(ss.invL) < 0.004^\circ$	18.5 h
$ABS(ss.invL) < 0.006^\circ$	31 h



Line A, 30 min. mean, M0_S_5:

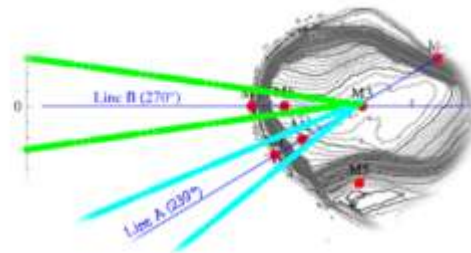
wind direction $239^\circ \pm 8^\circ$	160 h
AND nearly neutral conditions i.e. $ABS(ss.invL) < 0.002^\circ$	8 h

Figure 13 Filtering Bolund field data for inflow direction A

How does the sampling size depend on filtering methods? 2/2

Line B, 10 min. mean, M0_S_5:

wind direction 270 ° +/- 8°	120 h		
AND nearly neutral conditions i.e. _ABS(ss.invL)<0.002°	23 h	AND 4-6 m/s	1.2 h
		AND 6-8 m/s	2.5 h
		AND 8-10 m/s	4 h
		AND 10-12 m/s	5 h



Line B, 30 min. mean, M0_S_5:

wind direction 270 ° +/- 8°	118 h		
AND nearly neutral conditions i.e. _ABS(ss.invL)<0.002°	24.5 h	AND 4-6 m/s	1 h
		AND 6-8 m/s	2.5 h
		AND 8-10 m/s	4.5 h
		AND 10-12 m/s	4.5 h

Figure 14 Filtering Bolund field data for inflow direction B

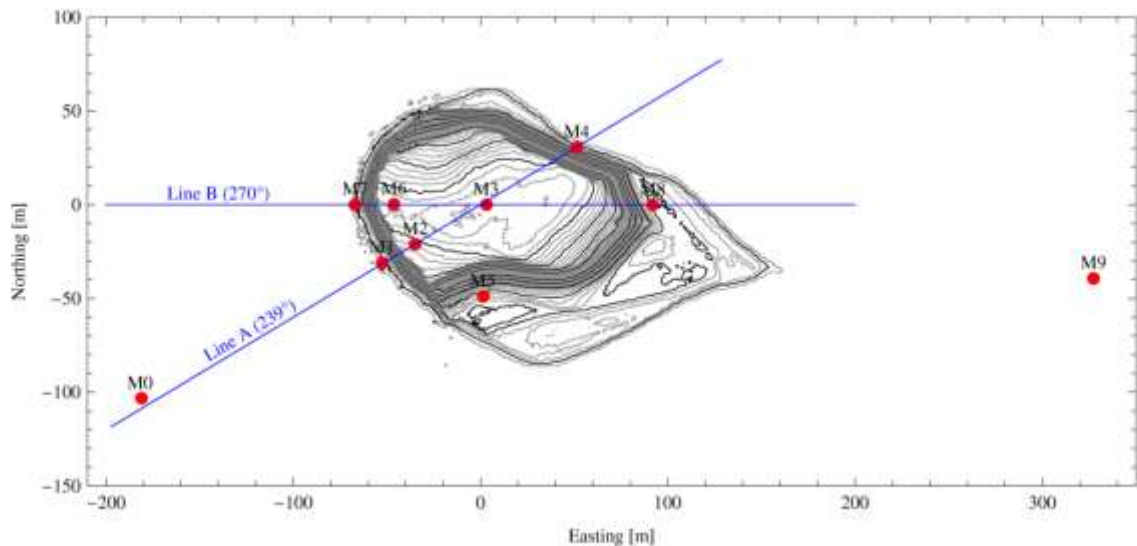


Figure 15: Bolund hill field study measurement positions and inflow directions with friendly permission by Bechmann et al., [2011].

The “neutrality” range, measured by the inverse Monin Obukhov Length, $invL$, also influences the sample: *doubling* the interval for the inverse Monin Obukhov Length *more than doubles* the sampling size. The absolute sampling time for Line B, which is $270^\circ \pm 8^\circ$, yields 120 hours of measurement data, 40 hours *less* than for Line A. For inflow direction B, around 23 hours fulfil *nearly neutral* stratification. Narrowing down the result to mean wind speeds in an interval of 4-6 m/s leads to a final ensemble size of one hour of sampling duration. This is *below* one percent of the Line B full sample (inflow $270^\circ \pm 8^\circ$). The wind energy relevant mean wind speeds of 8-10 m/s and 10-12 m/s give 4.5 hours, which is below four percent of the overall record length for inflow direction B. For the *inflow directions* and position of *reference mast* M0 see Figure 15.

The question is whether a few hours of field data can serve as *statistically reliable and meaningful data* for being used as *reference data* for model validation.

For *statistically stationary* flow, the claim for Reynolds independence (Re-independence) of fully turbulent flow (= Reynolds number sufficiently large) can be applied⁴⁶. That is,

- for all x in the flow and
- a fixed reference speed position, x' ,
- and $u(x)$, $\tilde{u}(x)$ time averaged wind velocities in x with time averaged reference wind velocity $u_{ref}(x')$ respectively \tilde{u}_{ref}

it holds:

$$u(x)/u_{ref}(x') = \tilde{u}(x)/\tilde{u}_{ref}(x') \quad [*].$$

(I.e.: The *non-dimensional* wind velocities are the same at the same location, x . For the use of the *non-dimensional* wind velocity recall pp. 37.)

⁴⁶ If the flow is not statistically stationary the meaning of the average wind velocity is not clear.

What does this mean for field data? The key point is that the deviation from this rule, $[*]$, will quantify the *deviation from a stationary Re-independent flow*⁴⁷. If atmospheric flow is assumed to be fully turbulent (due to its large Reynolds number) then the deviations from this rule serve as a measure for the *non-stationarity* of the field time series. Explicitly, the *inverse non-stationarity measure* which is suggested here can be defined as follows:

$$|u(x)/u_{\text{ref}}(x') - \tilde{u}(x)/\tilde{u}_{\text{ref}}(x')|$$

- With x , x' , $u(x)$, $\tilde{u}(x)$, u_{ref} and \tilde{u}_{ref} defined as above.

This means in words that the *inverse non-stationarity measure* can be defined as the velocity deviations at the measurement position x for all (in the data set available) reference velocities \tilde{u}_{ref} .

The deviation can be expressed *in percentage of the average non-dimensional wind speed* at x . The spread is shown in Figure 16 for characteristic flow locations around the Bolund hill: In the centre point of the hill in 2 m and 5 m above ground level (M3_S_2 and M3_S_5); at the front edge of the hill (M6_S_2 and M6_S_5); in front of the luv slope of the hill (M7_S_2 and M7_S_6) and in the lee of the hill at M8 (Figure 17).

As shown in Figure 16, the *inverse non-stationarity measure* for the Bolund field data gives deviations around ± 10 percent along the hill and shows a slight *positive linear dependence* between the reference velocity, U_{ref} , and the non-dimensional velocity. At M6_S_2 (which is 2 m above the steep front slope of the hill) the variability spread of the field data yields around ± 50 percent (values between 0.4 and 1 in units of non-dimensional velocity). This reassembles a spread of up to 9 m/s (at 15 m/s reference velocity) in field scale. In the lee of the hill the spread is around ± 35 percent (Figure 17). This indicates that the ambiguity is not satisfyingly reducible for this data set.

⁴⁷ With “stationarity”, in this work, it is always referred to statistical stationarity; recall the technical definition on p. 43.

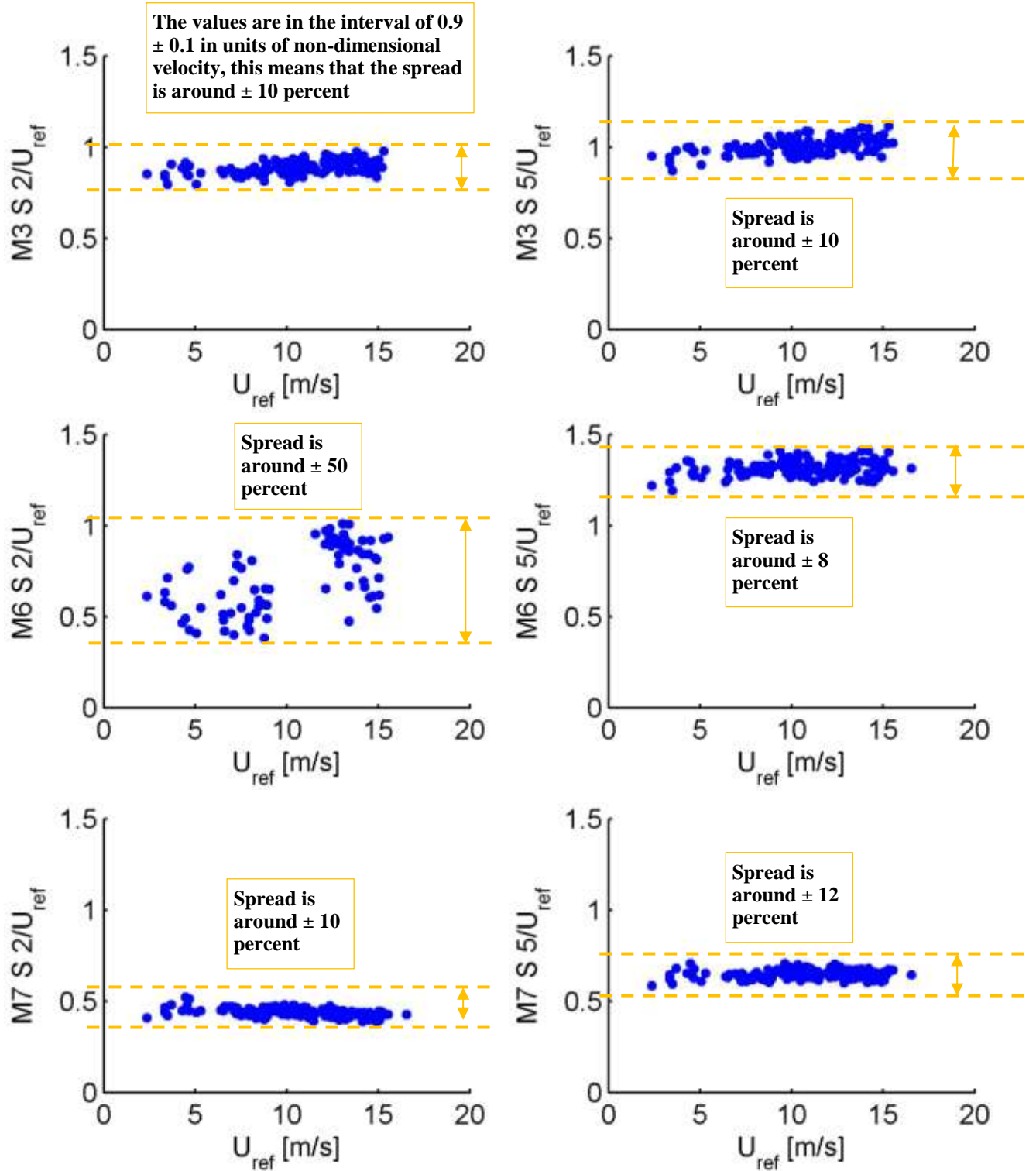


Figure 16: Inverse non-stationarity measure for wind speed divided by reference wind speed measured at M0 at characteristic points around the hill, x-axis denotes reference wind speed, y-axis denotes 10 minutes averaged wind speeds and location. Location name in format “MX S Z” denotes MX= mast position; S = sonic (S); Z = height above ground level in [m]. [Data request as of October 2012] The data was filtered for $|\text{invL}| < 0.002$ and inflow direction between 162 and 178 degrees.

Data quality is not only a matter of the measurement *precision and accuracy*. Equally important is the analysis of the *adequacy* of the data. Field data is not *adequate* if its *ambiguity* (with respect to the *theories* which are implemented into the models) is too *large* for provision of *narrow reference intervals* for model results. If the *reference interval* for model validation is too *large* the meaning of the validation is questionable. Furthermore, an *increase of the model accuracy* with such data is *not possible* if the properties of the field data differ drastically from the theoretical assumptions of the model.

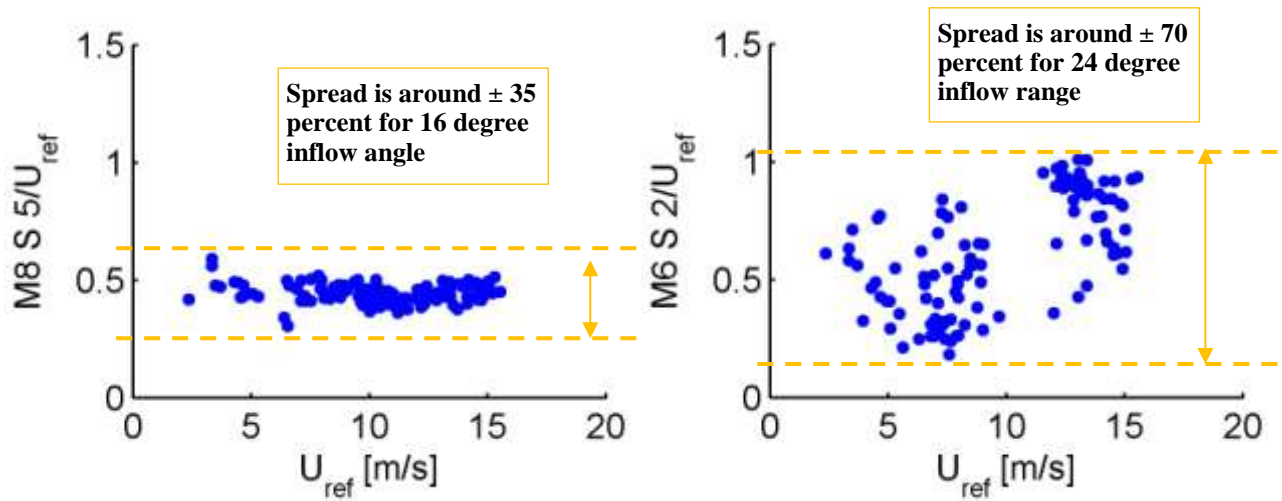


Figure 17: Inverse non-stationary measure at the lee of the hill (left) and at the front edge of the hill for a larger interval of mean inflow directions with $270^\circ \pm 12^\circ$ instead of $270^\circ \pm 8^\circ$ (right)

Also, filtering of field data leads to a *selection of data sets*. If the *filtering assumptions* are too strict (small filtering intervals) the resulting *ensemble size* is too small and hence the *statistical error increases*. The other way around, increase of the filtering intervals can increase the *spread of the data*. For example the increase of the interval for the mean inflow direction by eight degrees (from $270^\circ \pm 8$ to $270^\circ \pm 12^\circ$) increases the spread at the front edge of the hill in 2 m above ground level (in field scale) from 50 percent to 70 percent (Figure 17).

Model development and artificial experience

In wind energy assessment, a model is considered to be “good” if it fits reality, i.e. the model reproduces and predicts correctly what is observed in reality.

Assume there are again two models - say model 1 and model 2. Assume again that model 1 performs well in specific cases, A, and model 2 in specific cases, B. An obvious idea is to *merge* both models. The problem is: models are not necessarily addable. Also, *addition* does not necessarily lead to improvements. Alternatively, partial synergy effects can be the aim, for example: model 1 learns from model 2 for cases B, and model 2 learns from model 1 for cases A. Linked to this is the idea of *model validation*. Models are validated by data comparison with *reference data*. Schlesinger, [1979], Oreskes et al., [1994], and Sargent, [2009], use a rigorous vocabulary for *model verification* (= to ensure that the model is built the right way) and *model validation* (= to ensure that the right model is built) with regard to numerical models. (They also distinguish *models* from *conceptual models* which are the models to be implemented into a computer to become the *computerized model* [Sargent, 2009, p. 164].)

In some cases, *model development* and *model validation* seems to be not strictly distinguishable with respect to *long term* improvement of models. Concretely, this is the case if models are validated with reference data and improved. The process of model validation and recursive improvement is neither directly *machine learning*, nor *artificial intelligence*, but a sort of gaining *artificial experience*⁴⁸. This can be understood as a three-stepped loop: input data is used for the model run (step one), the results are validated with a reference data set (step 2) and on the long term the model is improved due to this experience (step 3), see Figure 18. If model data is used as reference data, this is the same as a *comparison of model data-output*.

In order to approximate the validation data set with the model output, *parameters* can be *added, deleted, adjusted or recombined*. In this way, model improvement is an *empirical and recursive process*. In other words, model improvement can be regarded as a learning process by models that are fed with evaluation data, which is a mixing of *fundamental theories* and *empirical theories*.

⁴⁸ There exist exotic prognosis tools that work with neural networks, hence relying on *artificial intelligence*. In most cases, this process is not automated but a mixture of machine and human learning based on model data-output comparison.

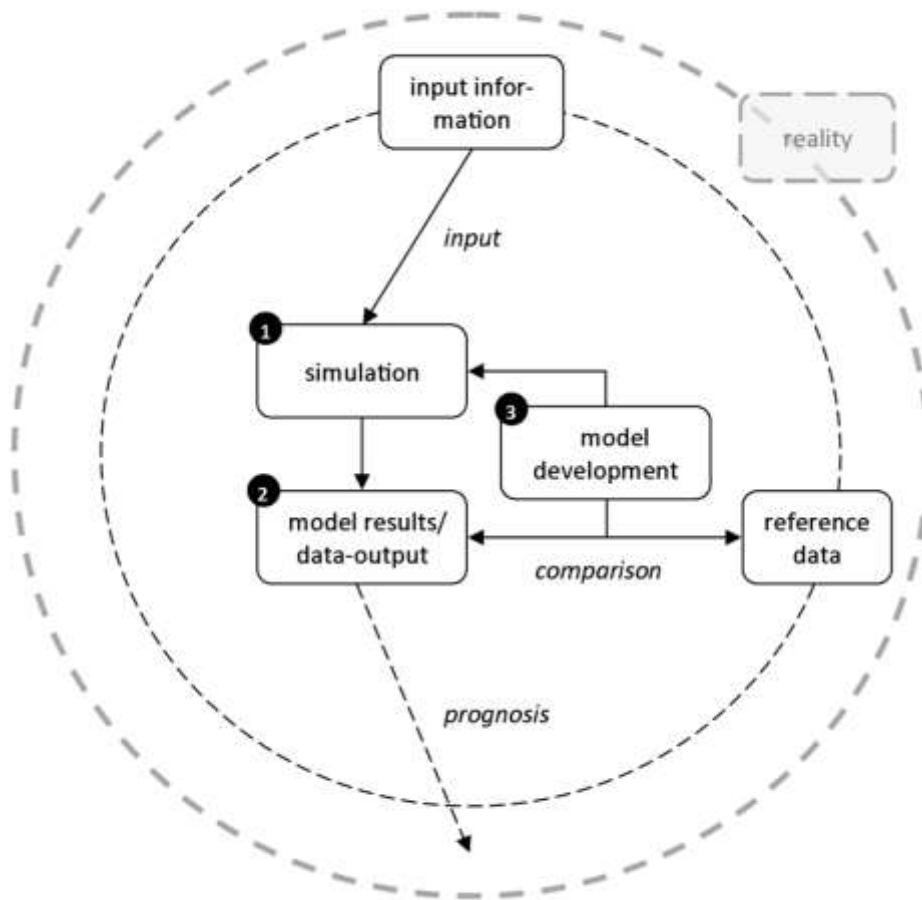


Figure 18: Improvement of models in a three-stepped loop

In conclusion, *reference data-sets* that are used as *validation data* have to be of good quality. Model improvement on the long term, is strongly based on a *recursive adjustment process*. Furthermore, reference data sets have to match the requirements of the model. If boundary conditions have to be guessed the model adjustment does not make sense. The model data-output depends on the model-input-data. In order to gain useful *artificial experience* and improve models in wind assessment, coherent, solid and reasonable validation data is necessary.

Previous considerations lead to two strong applications for wind tunnel modelling for wind (energy) assessment:

Lemma 2: Wind tunnel data in wind energy assessment can

1. serve as adequate validation and input data for generation of artificial experience in compatible numerical models.
2. predict roughly atmospheric flow for certain sites and in a certain range of meteorological boundary conditions.

Ad 1: As stated before, for *improvement*, models are compared with *validation data* and adjusted recursively. Therefore, reference data sets have to match the *requirements* of the model, for example *statistically stationarity* or *information on the set of boundary conditions*. Since wind tunnel modelling delivers data with *high spatial* and *time-resolution* and by construction *statistically stationary* flow, it can serve as coherent, solid and reasonable validation data for corresponding numerical models.

Ad 2: Provided that the *similarity criterion* is fulfilled and that the *atmospheric boundary conditions* are adequately matched, wind tunnel flows are *realisations of possible states of atmospheric flow*. For example around steep hills, no generally accepted turbulence closure model exists. Thus, physical modelling is specifically useful in cases where flow behaviour cannot be solved adequately by numerical models, yet. Thus, with respect to model restrictions and simplifications, wind tunnel modelling can predict atmospheric flow at certain sites and in a certain range of meteorological boundary conditions.

Application field: wind energy assessment

Before constructing a wind farm, potential investors request *engineering or renewable energy consultancies*⁴⁹ to predict the *wind energy output* for potential Wind Energy Conversion System (WECS) sites. Typically, those agencies use standard *wind assessment tools* such as the Wind Atlas Analysis and Application Program WAsP or WindPRO. These standard tools are *not* suited for *complex flow* situations. WAsP estimates the *long-term energy production* of wind turbines and wind farms and was developed by Risø National Laboratory over 20 years ago. It is based on wind data measured at stations in the same region. Based on WAsP is WindPRO, developed by the Danish energy consultant “EMD International A/S”. It uses wind flow modelling inputs from WAsP or Computational Fluid Dynamics (CFD) software and makes predictions about *energy production, turbine noise levels, turbine wake losses* and *turbine suitability* of planned wind farms. Predictions about energy production are deficient, Rodrigo, [2010]. The reason is that WAsP and similar tools are only meant for *simple terrain* and are *inaccurate* with respect to flow physics, for example turbulence and atmospheric stability. So, more appropriate simulation of the atmospheric boundary layer is requested. This is how the academic research on atmospheric flow models, such as in the WAUDIT project, comes into play.

Within WAUDIT, a major question is how to assure the *quality* of wind assessment *models*. For this purpose, models need to be compared. Hence, considering the methodological frameworks in which models are embedded is not only an academic exercise. *Models* in the WAUDIT project are *numerical* models and *physical* models. The numerical *models* within WAUDIT are nine models for micro-scale numerical modelling and three mesoscale wind

⁴⁹ Wind engineering consultancies are typically responsible for a number of tasks. Rodrigo, [2010], summarizes as follows:

- “1. Site prospecting: site selection from cartography and onsite evaluation
2. Measurement campaigns: design, monitoring and quality-check data filtering
3. Post-processing of wind measurements for energy assessment: analysis of wind distribution, vertical velocity profile, correlation with nearby measurements, etc.
4. Simulation of the wind resource over the site of interest using numerical model(s)
5. Wind farm layout design, considering geographical constraints and wake interaction
6. IEC site classification: analysis of extreme winds and effective turbulence intensities for determining the technical viability of a wind turbine class according to the IEC norm.”

IEC is the “International Electrotechnical Commission” that sets standards for energy production and distribution.

condition assessment tools. (For an insight into *mesoscale modelling* the publication of Pielke, [1984], is recommended)

Finally, the role of wind prediction in wind farm building projects is briefly considered.

A wind energy investment project consists of three main steps:

- Determination of a *manufacturer* who is able to produce and install the wind turbine.
- Funding/ Attraction of an (or multiple) *investor(s)*.
- Identification of the *location* in which building wind turbines is possible and profitable. The choice of site is driven by legal, social, economic and scientific consideration.

Manufacturing, investment and choice of *location* are linked together in a wind energy project, [Berkhuizen, 1988]. Investors provide money only if they are convinced of the success of the project. On the other hand, investors are only convinced if both, the manufacturer and the site are *promising*.

For the purpose of this work, the determination of an appropriate manufacturer and the process of attracting investors will not be analysed further. Instead, the term of a *promising location* is examined for its link to wind assessment.

In general, a *promising location* has five main properties:

1. It is *legally permitted* to build wind turbines in this location.
2. The location is *socially accepted* as wind energy site. (This means that the adjacent population agrees to the installation of wind turbines.)
3. *Meteorological conditions* are good. For a reliable economic analysis of wind turbines, detailed information about the wind frequency distribution is necessary. Wind resources are characterized by wind-power density classes, ranging from class 1 (the lowest) to class 7 (the highest). Good wind resources are class 3 and above, which have an average annual wind speed of at least 20 km/h (over 5 m/s).
4. The location is *accessible* for installation and maintenance of wind turbines.

5. The location is *close to demand* of energy (since the transport of energy is still inefficient and expensive).

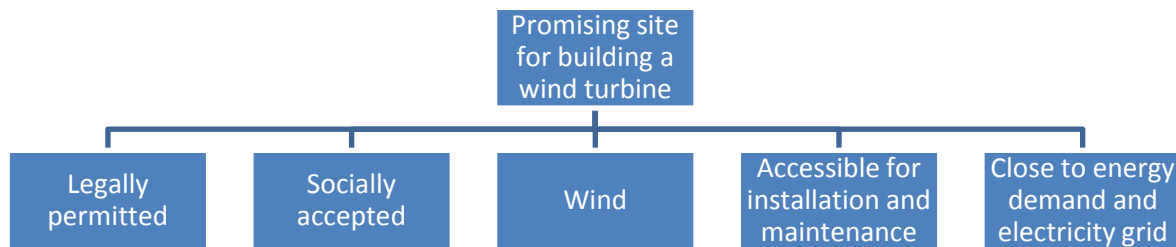


Figure 19: Five key points for determination of a promising location for a wind energy project

In other words, wind assessment is a key factor for the suitability of a WECS site although only one factor amongst others. It can be added that for economical consideration not only *wind speed mean values* are interesting. Wind turbines are classified according to the analysis of *extreme winds* and *turbulence intensities* at the installation site, as well. For the specific needs of wind predictions, *flow models* are needed that correctly depict these required flow properties.

Summary - Models

In summary, *models as mediators between reality and theories* are a modern perception of models in science. It is found, that in practice, model-output *data* is compared with field *data* and field data is not reality. It turns out, that data of different models is only comparable if the models are comparable, (Lemma 1). Based on the structural approach of models as mediators between reality and theories, a five-step *model comparison* is suggested and related to the process-oriented model evaluation procedure of COST 732. The COST 732 action concerning quality assurance and improvement of microscale meteorological models is used as example for model comparison in practice.

Adequacy of reference data was examined and the *inverse non-stationarity measure* is proposed as an estimation tool for deviation of atmospheric wind data from statistical stationarity flows. Furthermore, it is found that model improvement is an empirical and

recursive process and demands high quality (adequate) validation data. It turns out that field data might not be adequate (for its statistical spread of up to ± 60 percent).

Fundamental principles, case restrictions and strengths of wind tunnel modelling were reviewed shortly. It is concluded that wind tunnel data in wind energy assessment can serve as adequate validation and input data for the generation of experience with physically adequate numerical modelling (artificial experience). Additionally, it predicts atmospheric flow for certain sites and in a certain range of meteorological boundary conditions, (Lemma 2).

Conclusions and outlook - Models

It seems that models are used to bridge the gap between *theories* and *observational data* and that model validation and comparison generates some sort of *artificial experience* (combining theories and model and field data in a complexity which goes beyond the capacity of data handling and computing of the human brain). In the author's opinion, models are "dangerous" tools in different ways. The devil is in the details: *wrong* models can produce correct data (right for the wrong reasons). This means that the model can be *wrong* even if the model data-output fits well to the reference data (which is assumed to be "correct", i.e. statistically reliable and within reasonable bounds of measurement errors). In other words, "model results are always non-unique", [Oreskes et al., 1994, p. 641]. This is why the following fact was emphasised in this chapter, namely: the throughout *qualitative analysis* of the *relation of a certain model to theories* is crucial for a *proper model comparison*.

Furthermore, models are in general user dependent. As much as models *simplify* reality, they introduce a *new complexity*. This is allocated on the *user* and *interpretation* level. To prevent abuse the model developer needs to *communicate* the adequate model use and *accuracy* to the model user. This is difficult since a highly specialised research field, such as atmospheric flows and wind prediction, is already complex by its theories and *accuracy cannot be quantified* in absolute terms. Interpretation of model results is even more complex if models and real world application (model users or public communication) is

involved. Hence, special attention needs to be drawn to models which are used as decision basis in politics and economy by “non-scientists”.

It could be claimed, that model-developers should be more actively asked for communicating their model *restrictions* and *simplifying assumptions* including *measurement (or computational) errors* and further *uncertainties*.

As interesting open question remains how the learning process of models or *artificial experience* can be epistemically related to the evolution of *fundamental theories* and how the epistemic benefit of models can be quantified, e.g. by means of probabilistic tools such as Bayesianism (see outlook pp. 279).

6. Atmospheric boundary layer flow over hills

*“The approach [...] has been based on linear thinking – meteorologically the prophecy of Isiah that ‘every mountain and hill shall be made low’ has come true.”
- [Wood, 2000]*

This chapter gives an overview on the state of the art of research on atmospheric boundary layer *flows over hills*. This includes the challenges which theories, field studies and numerical or physical models are facing.

Introduction to this chapter

Whereas previous chapters provided a more general perspective, the following focuses on *atmospheric boundary layer flow over hills*. In a *literature and historical overview* it is examined how wind tunnel modelling has been applied to atmospheric boundary layer flow over hills, so far. In addition, *specific theories* for wind flow over hills are explained and *field studies* for atmospheric flow over hills are reviewed.

A review of research on flow over hills

The more detailed outline of this chapter is as follows: In “Wind tunnel simulation of flow over hills (early years)” the *physical modelling of topography in a wind tunnel* in the 1920s, until the 1990s, is summarized. In “Wind tunnel simulation of flow over hills (modern times)”, a short review is given on *physical modelling of hills in a wind tunnel*. The section is structured by *keywords* such as *experimental set-up*, *surface of hill models*, a remark on *error sources*, and an example of a wind tunnel study from 1998 concerning flow over a *tree covered hill*. More *details* of wind tunnel studies are *summed up* in “Discussion of recent wind tunnel studies”, p.111. An historical overview of the *theoretical development* for flow over hills is given in pp.115, whereas in “Linear Theory by Jackson and Hunt”, p. 119, the interested reader finds an excursion on the probably *most important* step stone of theoretical achievements on flow over low hills: the Linear Theory. In “Field studies” an overview of “must-know” field studies, from Askervein (1982) to Bolund (2008) is provided,

p.122. The most important options of nowadays numerical modelling are discussed briefly in pp.128.

Wind tunnel simulation of flow over hills (early years)

For a broad historical review of *laboratory modelling* of flow over complex terrain, Meroney's literature review on "wind tunnel modelling of hill and vegetation influence on wind power availability", [Meroney, 1993], is recommended to the reader.

Briefly, *Field and Warden* as well as *Abe and Putnam* are mentioned to be the *pioneers* in simulation of *steep topography in a wind tunnel*. Field and Warden examined in the years 1929 and 1930 neutral flow over the *Rock of Gibraltar* in length scale ratio 1:5000. Abe studied 1941 mountain clouds and topographic effects of *Mount Fujiyama* in Japan, and Putnam examined 1948 topographic effects of Mount Washington and Pond Glastenberg with scale 1:5280. More details on the experiments are outlined in Meroney, [1993].⁵⁰

Since the 1950s, it is expedient to differentiate between experiments with *stratified* and those with *neutral* flow over hills. For *stratified* flows: Long, [1953, 1954, 1955], examined flow with two layers over simple obstacles, Wei et al., [1975], conducted towing tank experiments, and Kitabayashi, [1977], simulated stratified flow over smooth hills with maximum slope of 10° and 15° in a wind tunnel. In 1980, Hunt and Snyder formulated with "towing tank experiments for stable and neutral conditions and a model 3dimensional hill" a seminal work in investigation on stratified flow over hills, [Hunt and Snyder, 1980]. The *dividing streamline concept* has widely been used since then and no remarkably new developments of the theoretical concepts are known to the author so far. More on *stratified flow over hills* can be found in Snyder, [1985], Snyder et al., [1985], and R.B. Stull, [1988, p. 62]

Concerning *neutral flow over hills*, an important work is contributed by Britter, Hunt and Richards, [1981]. They examined the *wind speed-up* of 2dimensional hills, turbulence effects

⁵⁰ It can be added that nowadays quality requirements are distinct from those of that time. This concerns for example the chosen length scales.

and the impact of roughness. In 1983, several wind tunnel simulations were made in relation with the *Askervein Hill Project*, [Teunissen et al, 1987; Taylor and Teunissen, 1987].

One of the first *wind energy* related *wind tunnel simulations* was carried out in the University of California, Davis, ABL wind tunnel, namely a *wind resource assessment* for a proposed wind farm site in the Pacheco Pass, California, USA in 1985, [Migliore et al., 1985]. The study consists of the construction of a model of a potential wind farm site, surveying the *wind distributions* in the *wind tunnel* and comparing to the few available field measurements. Since then, numerous more *wind tunnel* simulations have been carried out. Some of them are analysed in the following.

Wind tunnel simulation of flow over hills (modern times)

Not only the art of wind tunnel modelling has developed since the beginnings of the 20th century due to increase of experience in methods and technical advance of measurement instrumentation, also wind tunnels have *grown in size*. In the following chapter, state of the art of modern wind tunnel simulation of flow over hills is summarized along key questions such as *purpose of measurements*, *surface roughness* and *tree covers*.

Experimental set-up depends on the purpose of measurements

Wind tunnel simulation of turbulent flow over complex terrain in literature can be classified according to different purposes of measurements. Also, the experimental set-up depends on the reference data that is available. (This comprises e.g. data which can be used for the determination of consistent *inflow conditions*.) One aim can be to obtain *general information* about the structure of ABL flow over hills. In this case, emphasise can be taken on the *hill-model shape*, it can be shaped in an “academic” format (e.g. sinusoidal) or *certain parameters* can be varied to conduct a *sensitivity study* (such as the Bolund hill pilot-study, “idealized Bolund hill”, see chapter 7). Alternatively, for modelling *real existing terrain*, questions are amongst others how to choose the *full-scale detail* to ensure an expedient *scaling rate* in conjunction with matching *flow characteristics* of a *given* full-scale atmospheric boundary layer flow. This problem is analogue to the computer modellers’

problem of matching small-scale models to *boundary conditions*. (An overview on the different purposes of measurements is given in chapter 10, pp. 268.)

As a recent example, at the University of California (UC Davis, USA), a starting point to model the existing wind farm in the Altamont Pass, California, was a full-scale power-law exponent α , estimated by field measurements, [Cheng et al. 2004]. According to him, in the UC Davis wind tunnel $\alpha \approx 0.19$ can be matched by a certain arrangement of *roughness elements* on the floor in the development section. In addition, the approaching mean velocity profile was tested to agree with the *log law wind* profile being valid in the lower 10 – 15 percent of the boundary layer, in the surface layer. Briefly, the vertical mean velocity profile of the inflow was configured as boundary conditions.

Surface of hill models needs to be aerodynamically rough

To maintain fully turbulent flow and thus *Reynolds independency* along the model topography, the model surface must be *sufficiently rough*, i.e. *aerodynamic rough in order to prevent relaminarisation*. In other words, the model must not be *aerodynamically smooth* such that the turbulence breaks down. This can happen if the wind speeds are e.g. decreased by topographic effects – and thus friction is decreased with the smooth surface. To ensure *model roughness* and prevent relaminarisation, the model surface can be coated or covered with a suitable material. Gong and Ibbetson, [1989], used for example studded *rubber sheets*, Baker et al., [1985], used uniformly *spread sand*, Carpenter and Locke, [1999], used *textured wall paper* and Kim et al., [1997], as well as Lubitz and White, [2007], used *artificial grass*.

Another opportunity to achieve *aerodynamic roughness* (i.e. maintaining a turbulent boundary layer) is to integrate *steps* or *terraces* in the model hill. The maximum *step size* depends on the *scale of the properties* which are aimed to be modelled, since *larger* steps cause a *larger* departure from *geometric similarity*. This means, if steps become too large they *distort* the properties of the flow.

This has been observed, for example, by Neal et al., [1981], who modelled Gebbies Pass in New Zealand at a 1:4000 scale. They used both, *stepped* and *smooth* surface, and found the *stepped* model performed *inadequately*. The reason can be that the step size of 1 cm in model scale was relatively *large* as geometrical resolution (4 m in full scale). *Steps* have also been used by Lubitz and White, [2007], for their *circular* and *elliptical* 3dimensional hill models. The models were 38 mm high and furnished with 2.5 mm steps – and the steps “did not seem to cause absurd results”⁵¹.

The sufficient amount of *roughening of model surface* on flow over topography can be answered only partially. This is since the two tasks “*roughening the surface to maintain aerodynamic roughness*” and “*modelling real roughness of the field terrain*” are not clearly separated. Further consideration on *smooth hills* in comparison with *rough hills* can be found in the experiments by Cao and Tamura, [2006; 2007]. These are also further discussed in “Discussion of recent wind tunnel studies”, pp. 111. Effects of stepped slopes versus slopes without steps are shown in the sensitivity study in chapter 7. Besides effects of *surface-roughening* on *speed-up ratio* and *vertical mean velocity profiles*, most mentioned impacts of *surface roughness* are those on *flow separation*. That is, the exact location of *separation points* and its downstream areas can be influenced by *surface-roughening*. This is because the exact location of separation points is a strong function of *perturbations* in the local flow and model geometry (and *not necessarily constant* in time).

Special example: wind flow over tree covered hills

With regard to *wind power availability*, wind flow over *tree covered hills* and ridges were examined by Neff and Meroney, [1998]. Firstly, *wind tunnel* measurements of hill-top wind speed profiles were conducted in a 2dimensional setting. (Hill-top wind speed profiles as a function of *surface roughness*, *hill shape* and *hill slope*.)

They found that the effect of *vegetation* was generally limited to the region immediately above the ground except when the presence or absence of vegetation induced *flow*

⁵¹ However, due to lack of reference values it can only be qualitatively estimated whether or not the results “make sense”.

separation. Concerning examination of effects of *tree cutting*, it was seen that the wind velocity near the ground *increased* substantially for even small clear cut operation at the crest, but over steeper hills, clear cutting provided only *marginal speed-up*. Secondly, wind flow over a scale model of a *proposed wind energy site* in the north-eastern United States, Kibby Mountain area, Maine, was simulated with a variety of *clear-cut options*. Speed up in the 3dimensional case was *lower* than that which was found for equivalent slope and shape in the 2dimensional case. *Non-linear* flow interactions were observed when *another* hill or ridge was placed directly *upwind* of a measurement site which resulted in deviations from the 2dimensional results. Finally, Neff and Meroney, [1998], concluded, that a “crew cut” type approach to tree cutting and removal was an adequate strategy for most *forested hills* if an *increase of wind speed-up* was the aim to achieve.

Discussion of recent wind tunnel studies

In this section, a detailed *table of information* about the following *wind tunnel studies* is provided:

1. Ferreira et al., [1995], examined flow over *2dimensional* hills as well as impact of *hill shape* on the *recirculation* zone, and compared the results with those of a RANS k- ϵ -model.
2. Flow over *3dimensional steep* hills was investigated by Ishihara et al., [1999], with an emphasis on *turbulence profiles* and *flow separation*. Also, a comparison of split-fibre and cross-wire probes was made.
3. Athanassiadou and Castro, [2001], examined *neutral flow* over a *series* of *sinusoidal, 2dimensional, low* hills in comparison with *steep* ones.
4. Ayotte and Hughes, [2004], examined *neutrally stratified* turbulent flow over *2dimensional isolated* ridges of *varying steepness* and *roughness* with the aim to understand better the transition of cases for which *Linear Theory* is valid to those for which it is not.

5. Cao and Tamura, [2006; 2007], conducted measurements concerning the impact of *roughness changes* for *2dimensional steep* and *2dimensional low* hills. In former case, variation of the *separation bubble* and roughness effects on the *speed-up* ratio was examined. In the low-hill experiment, emphasis was put on effects of roughness change on *mean* and *turbulent* flow.
6. *Lateral* speed-up and effect of *wind-direction* on speed-up over *3dimensional elliptical* and *circular* hills respectively a *sinusoidal 2dimensional* barrier was examined by Lubitz and White, [2007].

Table 1: Recent wind tunnel experiments, people, time and location (unavailable information is assigned with a question mark)

Who?	When?	Where?	Open/ closed wind tunnel	Size l , w ,H [m]
Ferreira et al.	1995	Coimbra (Portugal)	A: ? B: open working section	A: 9, 0.46, 0.45 B: 8.55 , 4
Ishihara et al.	1999	?	„return winnd tunnel“	7, 1.1, 0.9
Athanassiadou, Castro	2001	University of Surrey (UK)	„EnFlo A“, „blowing wind tunnel“	4.2, 0.9, 0.6
Ayotte and Hughes	2004	CSIRO Land and Water, Canberra	Open return blower type	17, 1.78, 0.7
Cao, Tamura	2006	Tokyo Institute of Technology	Open circuit	7.0, 1.0, 0.8
Cao, Tamura	2007	Tokyo Institute of Technology	Open circuit	7.0, 1.0, 0.8
Lubitz, White	2007	University of California	Open return	3.7, 1.2, 1.7

Table 2: Recent wind tunnel experiments, inflow conditions

Who?	ABL	Wind profile	Turbulence intensity $\sigma u/u$	z_0 [mm]	α	Int. length scale
Ferreira et al.	✓	neutral	A: 5 percent B: 12 percent	?	A: 0.16 B: 0.24	?
Ishihara et al.	✓	neutral/ power/ log	$\sigma u/u^*0$ 2.4 $\sigma v/u^*0$ 1.6 $\sigma w/u^*0$ 0.8	0.01	0.135	?
Athanassiadou, Castro	✓	neutral	$\sigma u/u^*0$ 2.19 $\sigma w/u^*0$ 1.12	0.337	?	?
Ayotte, Hughes	✓	neutral	?	0.03 – 0.8	?	?
Cao, Tamura	✓	neutral	Smooth: $\sigma u/u_0^*$ 2.35 $\sigma v/u_0^*$ 1.1	0.004 smooth 0.2 rough	?	?
Cao, Tamura			Rough: $\sigma u/u_0^*$ 2.15 $\sigma v/u_0^*$ 1.13 3 percent free stream 8.93 percent smooth at HT 15.1 percent rough at HT			
Lubitz, White	✓	neutral	?	?	0.19	?

Table 3: Recent wind tunnel studies, measurement instruments directly cited from the articles:

Ferreira et al.	Pitot-static tube (3mm diam) for pressure measurements, const.temp. hot-film anemometer with 70 μ m wire for vertical and longitudinal velocity profiles, Irwin-tube type for shear-stress measurements and a 7-hole probe with 60° aperture angle for wind direction.
Ishihara et al.	Split-fiber probes, designed for measuring flows with high turbulence and separation since X-wire probe anemometers cannot be used, when turbulence intensity is larger than 0.3 (Tutu, Chevray 1975). Constant temperature hot-wire anemometers with XW probes were used to measure the flow in the undisturbed boundary layer
Athanassiadou, Castro	For mean flow and turbulence statistics: SW (single hot wire) and XW (cross hot wire) in conjunction with PSI [sic!] 6100 const temp anemometer system. PW (pulsed wires) were used over large hills, in areas of flow separation.
Ayotte and Hughes	TSI 3dimensional laser Doppler velocimeter system to measure flow, angle between the probes: 60 degrees → spherical measurement volume with a diameter \approx 100 μ m. Air flow was seeded with small particles \approx 5 μ m diameter by a Rosco 1600 theatrical fog machine. Shift frequency of 1 MHz → no directional ambiguity in the recorded velocity data.
Cao, Tamura	Mean flow and turbulence statistics were measured in the upper part, $y/H > 1$, by an X-wire probe (55P61) in conjunction with a constant temperature anemometer system. In the lower part, $y/H < 1$, by a split-fiber probe (55R55), since measurements of highly turbulent flow with different angles cannot be measured properly with X-wire probes.
Cao, Tamura	
Lubitz, White	Mean flow and turbulence statistics were measured by single wire, end flow hot wires (TSI Model 1210-20) in conjunction with a const. temp. anemometer (thermal anemometry has been widely used in measuring turbulent flow for its ability to sample flow velocity at frequencies up to 1000 Hz.) Close to the surface, hot wire measurements have typically an uncertainty of less than \pm 5 percent. Sampling rate: 1000 Hz 90s.

Some of the details listed in the tables above are *not available* in the papers and were only available due to written conversation with the authors. Nevertheless, the amount of question marks assigning “lost” and not available information is *not satisfying*. *Repeatability* of experiments is one of the *basic* demands of *proper* science and research. Without an accurate *documentation* of the experimental set-up reproducibility is *not warranted*.

Further remarks concerning the experiments listed above, are the following:

- Ferreira et al.: The *ceiling* of wind tunnel B could not be deformed and led to 10 percent *velocity decrease* along the test section. Also, experiments in wind tunnel A were *not* Reynolds number independent.
- Ishihara et al.: The experiments were *not* Reynolds number independent.
- Athanassiadou, Castro: *No* experimental test of Re-independence was made. Also, a longitudinal *pressure gradient* existed.
- Ayotte and Hughes: It is not clear *where* the flow characteristic over flat surface was measured. Furthermore, *lateral uniformity* is not tested.
- Cao, Tamura (2006): Re-independence was *not* experimentally tested.
- Cao, Tamura (2007): Speed-up for smooth hill in rough flow leeward the hill was greater than 1. The authors think that there is no problem of energetic balance, since “it is not >1 for the whole region behind the hill...”, however, this fact was *not* shown in the wind tunnel.
- Lubitz, White: It is not known anymore by the authors *where* the reference velocity and the undisturbed boundary layer characteristics (without hill influence) have been measured.

As a conclusion, in this section, *seven* wind tunnel studies from the recent years were reviewed and *no uniform practice* of documentation was found. Furthermore, it turned out that most of the experiments were *not completely documented* in order to assure *repeatability*. Also one of the most important features of wind tunnel simulation was not assured: the *similarity criterion* which is tested by the variation of *Reynolds number*.

Theory of flow over hills – a rough overview

For a comprehensive review on *theories* for flow over hills within a *historical* context, the article “Wind Flow over Complex Terrain: A Historical Overview and the Prospect for Large-Eddy Modelling” by N. Wood, [2000], is highly recommended to the reader.

As Wood points out, *phenomenological* examination of *lee waves* exists since the 1930s. But, according to him, in 1948, Queney’s review of theoretical models of *inviscid* flow over hills pushed the research area.

In the 1950s, theoretical work on wind flow over hills became more popular but was concerned to *lee wave* phenomena with regard to *stratification* effects and upper level winds, not on the wind speed within say 50 m above the surface of the hill. Corby, [1954], gives a review on the work of Queney, Lyra, Scorer and Long on flow over hills with respect to that research area. Wood, [2000], states that the reasons for the rise of interest in the topic may have been the development of *numerical weather prediction* and general *circulation models* and the growing awareness of the importance of mountain flows due to the increasing *popularity of skiing*, *advent of satellites* and an increased interest in *wind energy applications*. According to Wood, [2000], at the end of the 1960s, there was an improved understanding of *inviscid* flow dynamics over hills in *stable stratification*, mainly with regard to *streamline curvature*.

It must be emphasised that at that time *mean flow properties* were discussed and not those of *turbulent flow* (which is nowadays objective of modelling atmospheric boundary layer flow). One should keep in mind that only 1922, Richardson had the idea of turbulence as a

hierarchy of eddies, cached up in 1941 by *Kolmogorov* who introduced nowadays understanding of the *cascade process* of atmospheric boundary layer flow based on computations for homogenous and isotropic turbulence.

Pursuant to Wood, in the *mid-seventies* there was a revival of interest in flow over hills. One step-stone was *Jackson and Hunt's* paper on "Turbulent wind flow over a low hill", published in 1975. Jackson and Hunt pointed out, that although stratification usually had an important effect on wind over *low hills*, there were many instances when high winds occurred and stratification had a *small* effect on the flow, especially near the surface of the hill. Their paper can be seen as the attempt to formulate a simple *analytical* theory which was able to predict the general features of a small hump on a turbulent boundary layer and to demonstrate the influence of changes in the basic physical parameters determining the flow, [Jackson and Hunt, 1975].

Since then, with increase of computational capacities, *numerical modelling* has become more and more important. For example, since the 1980s, the understanding of momentum transfer and energy balance (the temperature and moisture balance) has been worked on and in the last 20 years, *large eddy simulation* has become more and more important. The interested reader is once again referred to Wood, [2000], for a start on this topic. The following chapter will focus on the most well-known achievement of *theoretical* work on flow over hills, namely Jackson and Hunt's *Linear Theory* based on the *Bernoulli effect* (wind speed-up effect over hills).

Bernoulli effect

As mentioned before, Jackson and Hunt's paper in 1975 aimed to build up a simple *analytical* theory which was able to predict the *general features* of the effect of a small hill on a turbulent boundary layer flow. The *main* effect underlying all advanced theories concerning flow over hills is the *Bernoulli effect*. Disregarding Coriolis force, gravitation, buoyancy and radiation, assuming air to be an *ideal* gas with *constant* density and temperature, then, for a *steady state*, *2dimensional* flow over a *low* hill, it holds approximately: If air passes the hill it follows the *shape* of it. This means that in a

surrounding, D, of the hill the originally horizontal flow is *deformed*. Further away, outside of D, the flow remains *undisturbed*. In the outside region usual pressure and horizontal flow are observed. In D, at *upwind*-slope of the hill, the curvature of the trajectories is *positive*, over hill top it is *negative* and turns to *positive* curvature again at *lee*-slope of the hill.

This holds as long as no *flow separation* occurs which is excluded by assumptions. In physical terms, a *positively curved* trajectory means that the streaming air is *accelerated upwards*.

By Bernoullis law, the sum of *static* and *dynamic* pressure remains constant, that is with above mentioned simplifications (e.g. disregarding gravity):

$$p + \rho/2 v^2 = \text{const.},$$

with

p := static pressure,

$\rho/2 v^2$:= dynamic pressure

ρ := air density

and v := wind speed.

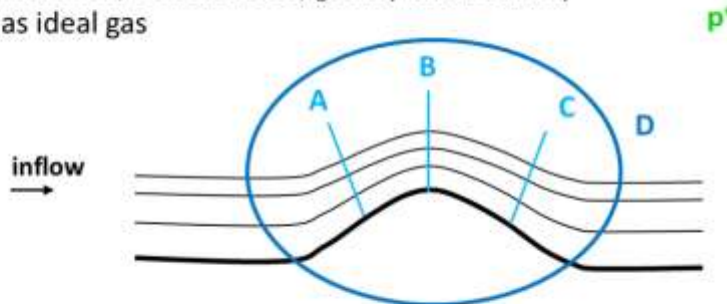
This means that the *acceleration upwards* is linked to a pressure gradient (high pressure at the ground). The same holds at the lee-slope of the hill. In other words, since outside of D the vertical pressure gradient has to *match* asymptotically a *given* pressure p_0 , by *continuity* it can be concluded that at the bottom on upwind- and lee-slope of the hill pressure must be *higher* than p_0 . By analogue reasons, pressure on the hill top must be *lower* than p_0 . Thus, by flow *deformation*, a nonzero vertical *pressure gradient* occurs - with change of sign from upwind to top to lee of hill. This leads (once again by *continuity*) to the pressure gradient *along* trajectories.

In summary, at the upwind-slope of the hill, the air is expected to *decelerate* relative to wind speed outside of D. Then it *accelerates* over hill-top, *decelerate* at the lee-slope and finally accelerate slightly until it recovers to its *undisturbed* flow geometry outside of D. Thus, “speed-up” over hills is, as a basic principle, driven by *pressure gradients* that occur due to flow deformation. (For an illustration, see Figure 20.)

The Bernoulli effect over hills

Assumptions

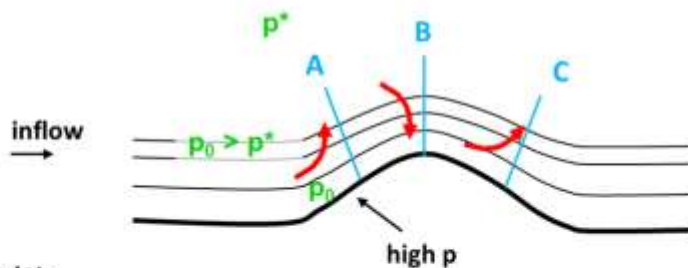
1. steady state 2dimensional flow over a hill with gentle slope
2. horizontally constant air density and temperature
3. no radiation, Coriolis force, gravity and bouancy
4. air as ideal gas



Explanation

Step (1/2):

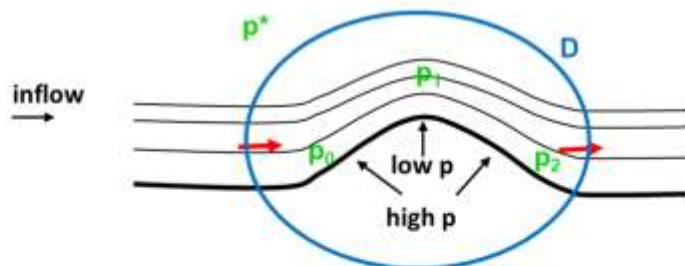
vertical acceleration along A, B, C
(Bernoulli equation, continuity and p^* → vertical pressure gradient)



Bernoulli equation:
 $p + \rho/2 v^2 = \text{const.}$
i.e.
the sum of static
and dynamic pressure
is constant

Step (2/2):

continuity → pressure gradient along streamlines
Bernoulli equation → „speed-up“.



Based on [Weltner and Ingelmann-Sundberg, 1999]

Figure 20: On top, the assumptions of the (basic) Bernoulli effect are summarized; Middle: Vertical acceleration induced by hill shape (1/2); Bottom: Induced pressure gradient leads to horizontal acceleration (1/2)

Linear Theory by Jackson and Hunt

Let us draw the attention first to the assumptions, Jackson and Hunt's theory is built upon. As in the case above, Jackson and Hunt restricted their considerations to *2dimensional, isolated, low* hills, with a *gentle* slope, example given bell shaped or sinusoidal hills. In addition, stratification was supposed to be *neutral* and approaching flow to be *logarithmic* in mean vertical wind profile.

Furthermore, the ratio between *characteristic hill length*, \hat{L} , and *roughness length*, z_0 , was assumed to be very large, i.e.

$$\hat{L}/z_0 \rightarrow \infty.$$

The *characteristic hill length*, \hat{L} , was defined as the horizontally *projected* distance from hill *top* to the point on the hill with *half of the top height*.

Additionally, boundaries were set for the ratios H/\hat{L} and BL_δ/\hat{L} . Let BL_δ denote the *height of the boundary layer*. Example given, for a rural terrain with say $BL_\delta = 600$ m, the restrictions implied $10^2 \text{ m} < \hat{L} < 10^4 \text{ m}$ and $H/\hat{L} < 0.05$. Later on, these restrictions were undermined by many authors. Amplification then was often justified with empirical observation.

Due to the *assumptions* and the *Bernoulli effect*, close to the hill surface, in an *inner region*, the horizontal mean velocity component $u(x,z)$ was deduced to have following form:

$$u(x,z) = u_0(\Delta z) + \Delta \hat{u}(x, \Delta z) = (u_*/\kappa) \ln(\Delta z/z_0) + \epsilon u_* \hat{u}(x/\hat{L}, \Delta z/l)$$

whereas $u_0(\Delta z)$ is the *horizontal* component of the *undisturbed mean upwind flow* in relative height Δz and $\Delta \hat{u}(x, \Delta z)$ is its *perturbation* due to hill effects at point $(x, \Delta z)$, u_* and κ are *friction velocity* and *von-Kármán constant* respectively, $\epsilon \ll 1$ is a small parameter which is introduced to provide a scale for the *perturbation velocities*, and l is the thickness of the *inner region* which is unknown.

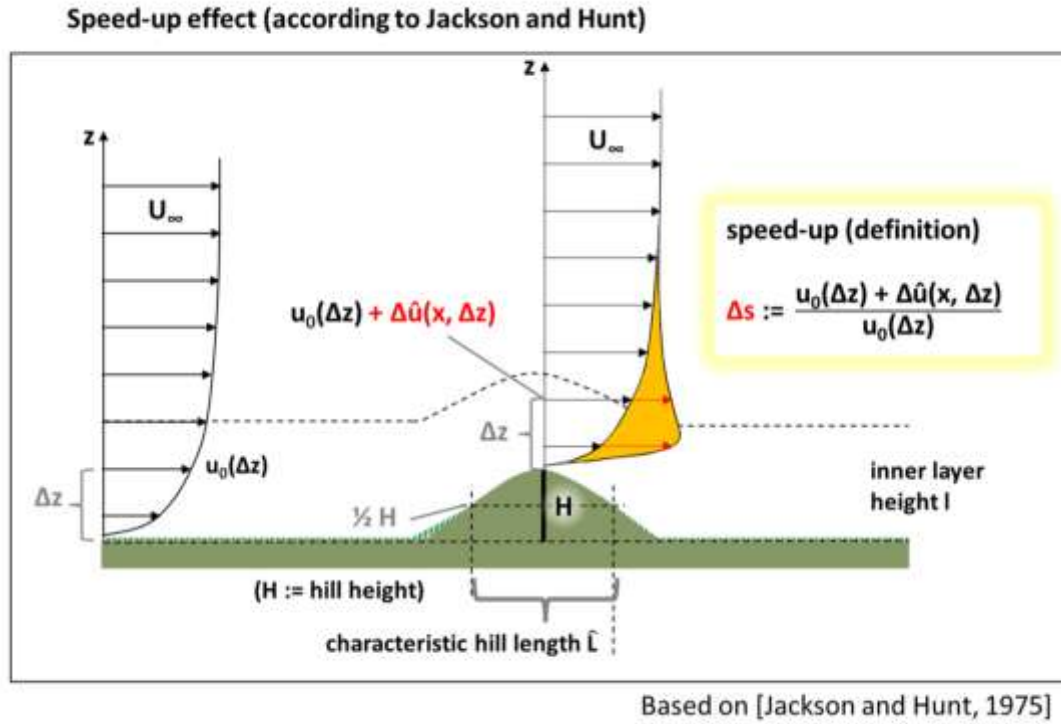


Figure 21: Jackson and Hunt formulated the speed-up over low hills in neutral stratification as first order perturbation problem to the mean flow and introduced the characteristic hill length which has been widely used in literature, since then.

The equation holds due to the assumption of a *logarithmic approaching* flow⁵² combined with a *perturbation expansion ansatz* of first order, [Jackson and Hunt, 1975, Claussen, 1988]. Recall that only *2dimensional* flow is considered.

In combination with the *continuity equation*, a first order perturbation formula is derived for the *vertical mean velocity component* $v(x, z)$. With this expressions for u and v , the horizontal component of the equation of motion for steady-state 2dimensional flow turns into a “nasty” term. However, *adding* all terms of first order perturbations and assuming l to be the height of the *inner layer*, in which the perturbation stress gradient, induced by flow over the hill, is of *same magnitude* as the non-linear advection term leads to the formula

$$(l/\hat{L}) \ln(l/z_0) = \text{const. } O(1).$$

Applying a *mixing length ansatz* on above equation leads to the formula, [Jackson and Hunt, 1975]:

⁵² *Logarithmic approaching* flow means that the vertical mean flow profile fulfills the logarithmic wind profile (pp. 32).

$$(l/\hat{L})\ln(l/z_0) = 2\kappa^2. \quad [**]$$

Expressions for the right hand side of equation [**] can also be deduced differently, e.g. by Claussen, [1988], Beljaars and Taylor, [1989] and Taylor, [1998].

A distinct ansatz that leads to the same formula $(l/\hat{L})\ln(l/z_0) = 2\kappa^2$, is given by Belcher and Hunt, [1993]. They start from a different point of view and introduce two time scales: The *advection-distortion time scale*,

$$T_A := \hat{L}/(U(z) + \Delta u) \approx \hat{L}/U(z) [1 + O(\Delta u/U(z))],$$

often just denoted by

$$T_A = c \hat{L}/U(z), \quad c \in \mathbb{R}^+,$$

and the *Lagrangian integral time scale*,

$$T_L := \kappa z/u_*,$$

whereas κ denotes the von-Kármán constant and z the height above ground.

In other words, T_A characterizes (in theory) the time in which turbulent eddies in the air flow are *distorted* by straining motions associated with perturbations to the mean flow *caused by the hill*. The *Lagrangian integral time scale*, T_L , characterizes (in theory) the *decorrelation* time scale of the large energy-containing eddies and the time scale at which the turbulence comes into equilibrium with the surrounding mean-flow conditions. [Britter et al., 1981 ; Belcher and Hunt, 1998; Poggi et al. 2007].

By definition, T_A decreases with increasing z whereas T_L is proportional with height, see also Tennekes and Lumley, [1972, chapter 2]. So, it can be differentiated between an *inner layer*, with $T_L < T_A$, and an *outer layer*, with $T_A < T_L$. In the *inner layer*, turbulent eddies adjust to equilibrium with the surrounding mean-flow velocity gradient *before* they are advected over

the hill. Hence, it can be named “local-equilibrium layer” and an eddy viscosity is used to relate the Reynolds stress perturbations to the local mean-velocity gradient, [Townsend 1961; Belcher and Hunt, 1998].

By contrast, in the *outer region*, with $T_A < T_L$, the mean flow advects turbulent eddies over the hill *more rapidly* than they interact nonlinearly. This is, distortion of the upstream turbulence, by the cumulative mean strain, determines local properties of the turbulence in the so-called “rapid-distortion” outer region. More on *rapid distortion theory* can be found in e.g. Batchelor and Proudman, [1954]; Hunt, [1973]; Hunt and Carruthers, [1990], and Belcher and Hunt, [1998]. However, *rapid distortion theory* has lost its popularity within the last decade.

Jackson and Hunt’s Linear Theory is the historical most important framework concerning turbulent flow over low hills in neutral stratification. At least one extension of it should be known by the reader. Hunt et al., [1988], divided the inner layer further into two layers. Firstly, adjacent to the ground into a very thin “inner surface layer”, of the order of the roughness element height, where velocity goes to zero and viscous forces dominate. Secondly, a deeper “shear stress layer” was defined that extends from the top of the inner surface layer to top of the inner layer where the mean flow is affected by the perturbation shear stress. The (inviscid) outer area is divided into a “middle rotational layer” and an “upper rotational layer”. In their analysis of 1988, Hunt et al. improved the Linear Theory from 1975 in the sense that pressure and horizontal and vertical velocity components then *matched continuously* across each of the layers. This can be regarded as the “actual” theory to which it is referred, today, with the terminus “Linear Theory”.

Field studies

Thanks to Jackson and Hunt’s theoretical achievements, in the 1980s a field study boom came up in order to prove the theoretical predictions. The most prominent example is the *Askervein Hill project* (in 1982 and 83), it will be shortly summarized below, as well as the already mentioned *Bolund* campaign in Denmark (2007 and 2008). Some additional

information will be given on Black Mountain (Canberra, Australia 1977), Kettles Hill (Alberta, Canada 1984) and Nyland Hill (Somerset, United Kingdom 1984), among others.

Askervein Hill

The *Askervein Hill project* was an extensive study of flow over hills conducted in 1982, as preliminary test study, and in 1983 as main study. Its main focus was to measure the spatial characteristics of mean wind and turbulence over a typical hill site that is adequate for siting of wind energy conversion systems.

Askervein is located in the Outer Hebrides, an island chain off the west coast of Scotland. During the experiment, over 50 towers were instrumented for wind measurements, most of them simple 10 m posts with cup anemometers. In the 1983 study, equipment consisted of two 50 m towers, a 30 m tower, and thirteen 10 m towers instrumented for 3-component turbulence wind measurements.

The project was carried out as a task of the International Energy Agency Program of Research and Development on Wind Energy Conversion Systems. Since it is not meaningful in this work to describe the *Askervein Hill Project* in detail, the interested reader is referred to the elaborate and illustrated original literature. An overview of the measurements for example is given by Taylor and Teunissen, [1987], containing necessary background information including location maps and details of experimental runs. Additional details and many of the data are given in the reports by Taylor and Teunissen, [1983; 1985]. A report on vertical profiles of mean wind speed and turbulence at upwind and hilltop locations can be found in Mickle et al., [1988]. Also, Askervein has widely been used as a test case for numerical models. This was for example Zeman and Jensen, [1987], who used a second-order turbulence model formulated in streamline coordinates which includes both the effects of rapid distortion and of streamline curvature on the turbulence field; or by Castro et al., [2003] with RANS-simulation; or Lopes et al., [2007], with LES-simulation – just to name a few.

The popularity of the Askervein Hill as numerical test case is based on different aspects. First of all, the hill is “nice”, i.e. geometrically “easy shaped” so to say. It can be approximated by

the function of “Witch of Agnesi” with *characteristic hill length* $\hat{L} = 250$ m and height $H = 113$ m, (some say 116 m). Zeman and Jensen, [1987], have used a Gaussian shape as well. Secondly, inflow conditions are well-defined (relative to other field areas) and the roughness length $z_0 = 3$ cm can be assumed to be uniform. Furthermore, hill slope ranges from 0.25 to 0.12 depending on wind direction which was assumed to be smooth enough for the application of Jackson and Hunt’s Theory.

The conclusions that were drawn in the literature from the Askervein Hill Project were:

- Simple, linear models appear to predict speed-up well on the upwind side of the hill and at hilltop locations.
- In contrary, at the lee side of the hill the measurements indicate that flow separated against expectance, this can be a reason why linear models fail to describe the flow properly in this area.
- Furthermore, strong speed-up was observed near the ground on top of the hill, namely doubling of the wind speed. For wind energy application more interesting is, though, the value at around 100 m above ground level (agl) of the top of the hill. Here, a 10 – 20 percent increase of the wind-speed was measured (with respect to the wind speed at the same height agl upwind the hill).
- Last but not least, Askervein Hill has widely been used as test case for computer modellers and can probably only be outstripped by the recently conducted Bolund Experiment, see next paragraph.

Bolund Hill

Bolund is a 12 m high, 130 m long and 75 m wide hill, located approximately 3 km north of Roskilde, in Denmark. It is surrounded by water and has a steep escarpment. Its inflow conditions are well-examined; the uniform upstream fetch over water is long. It is 4-7 km depending on main wind direction. Additionally, Bolund is uniformly covered by grass.

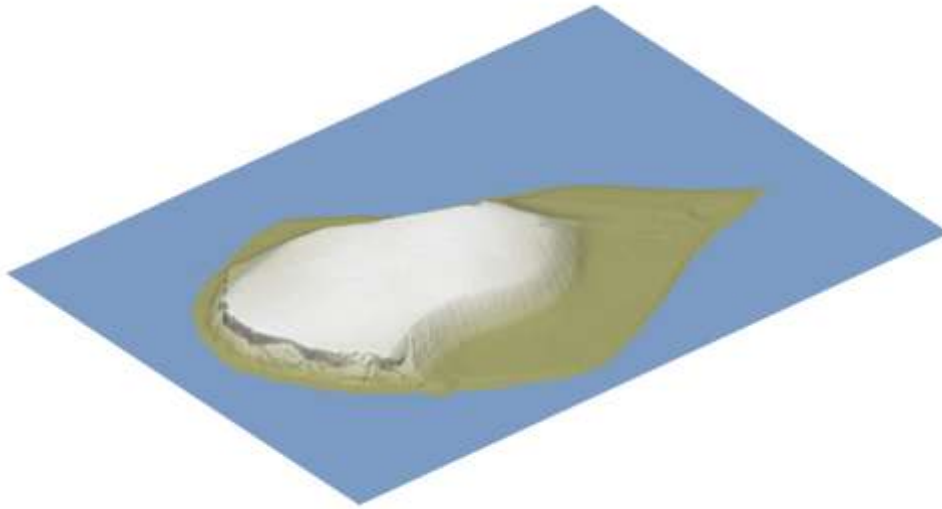


Figure 22: Bolund tilted view from south-west



Figure 23: Bolund lateral view from west



Figure 24: Bolund lateral view from south

The Bolund Hill measurements were conducted in January and February 2008 and are part of a three year project concerning three major topics: to identify *characteristic flow conditions* over *complex terrain* for reliable estimation of power production and wind turbine loads, to develop remote sensing techniques, such as Lidar (Light Detection and Ranging) for measuring wind conditions in complex terrain, and to *apply and validate* Computational Fluid Dynamics (CFD) methods.

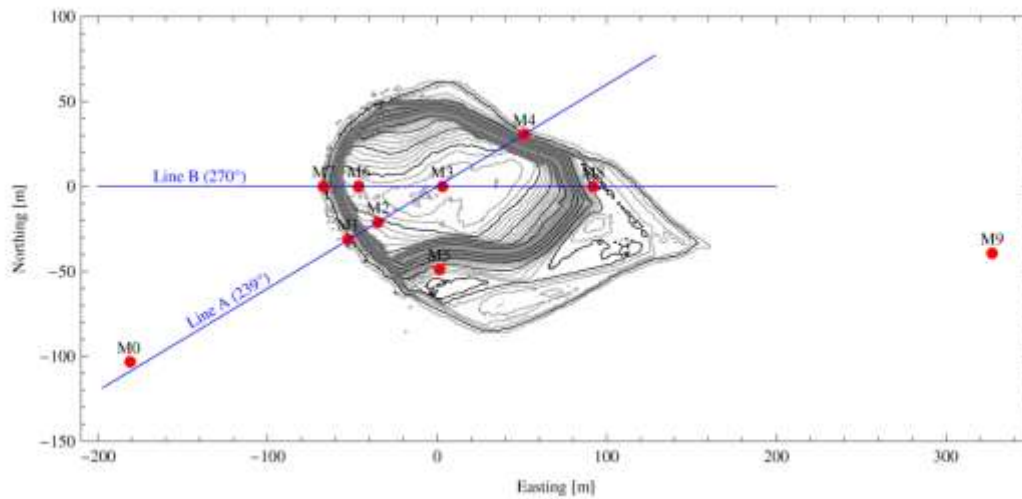


Figure 25: Bolund measurement positions of field study and corresponding wind tunnel study, with friendly permission by Bechmann et al., [2011].

Table 4: Bolund instrumentation (symbol description in text box)

	1m	2m	5m	9m	16m
0		0	0X	0	0
M1		X	X		
M2*	X	X	X	0	
M3		X	X	0	
M4		X	X	X	
M5		X	X		
M6		X	X	0	
M7		X	X		
M8		X	X	0	
M9*		0	0X	0	0

- 12 cup anemometers: marked with < 0 >
Mean wind speed, direction (5Hz)
- 21 sonic anemometers: < X >
Wind speeds, direction and turbulence (10-35 Hz)
- 2 Lidars (*)
wind speed, direction and turbulence at 10m-150m, 25 Hz, 3 scans at 5 heights
- 1 prototype Lidar
wind speed, direction and turbulence in vertical plane, 380 Hz
- Temperature

Within the Bolund Project, a *blind comparison* of 52 models was made. Two of the models are wind tunnel facilities, one is a flow channel, 9 are linearized flow models and 37 are non-linear CFD codes. Bechmann et al., [2011; 2009], give an overview of the results and conclude that *physical models* predict *mean velocity* well but *underestimate turbulent kinetic energy* whereas *linear models* give the *largest error*. Top ten predictions lie within the CFD codes but the *spread* amongst the others was so *large* that the *user* seems to be *more important than the conceptual model*. More information on the Bolund hill can be found in Berg et al., [2011] and Bechmann et al., [2011; 2009], and on Bolund in the large atmospheric boundary layer wind tunnel, WOTAN, in chapter 8.

More field studies

- Bradley, [1980], investigated the flow over *Black Mountain* near Canberra, Australia, using a 100 m high tower on the summit of the mountain and a 25 m high tower upstream of it. Black Mountain is covered by eucalyptus trees which yields a high surface roughness. The parameters of the topography are $\hat{L} = 275$ m, $H = 170$ m, $z_0 = 1.14$ m.
- *Blashaval hill* is an isolated, roughly circular hill with half-length at half-height $\hat{L} = 160$ m, height $H = 100$ m, and roughness length $z_0 = 1$ cm. The measurements were analysed by Mason and King, [1985].
- *Cooper's Ridge* is a north-south oriented quasi two-dimensional ridge located north-west of Goulburn in New South Wales, Australia. Pursuant to Coppin et al., [1994], the ridge is around 115 m high and has a characteristic length $\hat{L} = 400$. The ridge is located in an east-west oriented river valley that turns south at the foot of the ridge. The prevailing winds in the region are generally in the westerly sector. According to Coppin, the river valley tends to channel these winds into a narrow range of directions about the normal to the ridge and a flat farmland fetch can be assumed.
- *Kettles hill* is located in the south of Alberta, Canada, at $49^\circ 30' \text{ N}$, $113^\circ 50' \text{ W}$. It is an isolated hill with hill height 105 m, length 600 m and smooth slopes of around 0.1, approximately bell-shaped. The inflow conditions are smooth with z_0 around 0.003-0.01 m and an uniform upstream fetch of around 20 km, Salmon et al., [1988], and Taylor et al., [1983].
- Mean flow and turbulence statistics over the summit of *Nyland hill* are reported in Mason, [1986]. Nyland is an isolated, roughly circular hill, located in Somerset, UK, $51^\circ 15' \text{ N}$ and $2^\circ 47' \text{ W}$. It rises 70 m above the surrounding terrain and has a base diameter of about 500 m. Flow speed increased by a factor of 2 at 8 m relative height and at the lee of the hill flow separation occurs.

- Finally, *Ailsa Craig* is located off the coast of Ayrshire in south-west Scotland. The island has a base diameter of roughly 1 km, a height of 330m, and is situated 20 km from the nearest coast. Apart from the 100 m high cliffs on the western and southern sides, the terrain is fairly smooth with grass and heather but no trees. As slopes are about 30-45°, *Ailsa Craig* cannot be assumed to be low in order to apply Linear Theory. The flow field 4 m above the surface showed a speed-up around the sides and over the summit, with reverse flow on the lee slope, [Jenkins et al., 1981].

Numerical modelling

As aforementioned prior to constructing a wind farm, potential investors employ engineering consultants to predict the wind energy output for potential WECS sites. However, wind assessment tools applied in economical practice are distinct from those which are being developed in science. This is mainly due to the time and money requirements of computation and the development of numerical models. In this paragraph, it will be focused on the available academic flow models. Academic research of computational fluid dynamics in geometric scales which are suitable for flow over hills can effectively be divided into three main areas: Direct Numerical Simulation (DNS), Large Eddy Simulation (LES) and Reynolds Averaged Navier-Stokes Models (RANS).

In DNS, the Navier-Stokes Equations are numerically solved *without* any turbulence model or averaging. This means that *all* spatial scales of the turbulence must be resolved in the computational mesh, which includes the *Kolmogorov length* (*smallest* eddies) as well as the *integral scale* of the *largest* eddies. At present, DNS is nearly computationally impossible for modelling of realistic ABL flows and it is very costly in terms of time and money. RANS models, on the other hand, solve *averaged* Navier-Stokes Equations and thus provide *average* solutions. In other words, they do not compute turbulent fluctuations at all but consider turbulence effects on mean flow values. The averaging process leads to a significant decrease of computation time in comparison to DNS.

LES is based on Kolmogorov's theory of *self-similarity*. In brief, large eddies in the ABL are assumed to depend on the flow geometry whereas small eddies are assumed to be self-similar and have *universal character*. Thus, it is supposed that small eddy effects can be nested in parameterized form into the dynamics of the larger ones. Thence, LES solves Navier-Stokes Equations for large scale motion. The effects of small eddies are often modelled using a sub-grid scale model (SGS). How to adjust the SGS can be one of the key questions in modelling flow over hills with LES.

Comparing DNS, RANS and LES, it is not astonishing that *complexity* and *computational costs* are anti-proportional to each other. This means with regard to the *level of detail* that DNS is more detailed than LES, and LES is more detailed than RANS, or:

DNS > LES > RANS.

This is the other way around for the computational costs:

DNS > LES > RANS.

Since DNS is in terms of time and money *not* yet suitable for application in siting of wind turbines and RANS models do not feature turbulent flow statistics, LES seems to be the most promising *candidate* for atmospheric (micro- and meso-scale) flow modelling. LES aims at predicting *instantaneous* flow characteristics and at resolving a large portion of the *turbulence spectrum* as well as representing *complex flow regimes* such as *separation*, *wakes*, *stability transitions* and *stable boundary layers*. Furthermore, sub-grid scale models can by assumption be universally applied (this is not necessarily an advantage). Disadvantages of LES in comparison with standard tools for wind assessment (such as WAsP or WindPro) are the still *high computational costs*. There are also attempts to mix LES with RANS to decrease computational costs, called detached eddy simulation (DES), [Spalart, 2008]. For further readings on LES with respect to *complex terrain*, the interested reader is referred to Wood, [2000].

Summary – Flow over hills

In this chapter, a (literature) review on *wind tunnel* studies, development of *theories* and a brief overview on *numerical models* was given. It turned out, that *wind tunnel* studies for flow over hills (mountains) exist since around end of the 1920s and that *stratified* flow over hills turned into an active research area since the 1950s. The *dividing stream line concept* was one major achievement. However, mean flow values (and not the time resolution of the turbulent fluctuations) were the target of the investigations at that time.

In the review of “modern times” of experiments for flow over hills, it turned out that neither uniform *quality assurance* nor uniform *documentation* practice exists so far. This includes a lack of *repeatability* and of *Reynolds tests* in physical experiments which are reported in the literature. Result is that *repeatability* and *similarity* to large scale flow geometry of those experiments is *not* assured.

As main *theoretical* achievement, the *Linear Theory* was identified, developed by Jackson and Hunt in 1979. It initiated a boom of *field studies* in the 1980s – of which the *Askervein* hill project is a well-known example, also often used as reference test case for numerical models. The Linear Theory is strictly speaking only valid for infinitely *low* hills. For prediction of wind flow over *any type* of hills, there is still no comprehensive numerical tool or analytical theory commonly accepted.

Conclusions and outlook – Flow over hills

The numerous examples of research on flow over hills in this chapter provided a concrete illustration for the building blocks of chapter 5, i.e. *models as mediators* between *reality* and *theories* by means of *data*. This means that the Bernoulli’s law and the Linear Theory (LT) by Jackson and Hunt are part of the *theories* for flow over hills. The set of *models* consist of numerical models and physical models. The *reality* can be understood as being approached by the means of *field studies*.

The *specialisation* of fluid dynamics for flow over hills can be analysed according to chapter 4 in *structuralist* terms, as well as in *conceptual spaces*, i.e.: further quality dimensions are added to the *conceptual space* of the Navier-Stokes Equations, such as *characteristic hill*

length, \hat{L} , *roughness length*, z_0 , *hill height*, h , and *height of the boundary layer*, BL_δ . Also, the use of the Bernoulli equation as a *concept* narrows down the set of solutions, such as the restrictions for e.g. boundaries of h/\hat{L} and BL_δ/\hat{L} do. In *structuralist* terms, the Linear Theory, (LT), is a *specialisation* of the Navier-Stokes Equations and narrows down the *intended applications* of general NSE to flow over low hills in neutral stratification (combined with further assumptions as mentioned in the specific section). Of course, many steps in between would be needed for a complete reconstruction of LT, e.g. the introduction of the *logarithmic wind profile* or the *mixing length* ansatz on top of the NSE.

Since the *repeatability* of experiments is a necessary condition for meaningful physics, and a lack of *documentation* and appropriate *quality tests* was found in the review of *wind tunnel studies for atmospheric boundary layer flow over hills*, it can be concluded that the increase of attention for *quality assurance* of wind tunnel measurements is desirable. In the author's opinion, the *users* of wind tunnel data need to be aware of the importance of quality assessment for wind tunnel experiments. This includes, from the author's point of view, *repeatability* tests, tests for *Reynolds* number influence, sensitivity tests on the representation of the hill *shape* and analysis on the *statistical representativeness* of wind tunnel measurements. (For an extensive list see chapter 10, pp. 268)

Acknowledgement (II)

For the fundamental part, G.P. acknowledges especially Frank Zenker for warm-hearted support, filling its surrounding with enthusiasm, having the admirable ability to connect people - and on top letting G.P. experience cheerful and smooth cooperation with inspiring expertise – equally many thanks to Martin Hoffmann for always being ready for philosophical problem solving, testing new ideas with surprising results and wise advice, and giving a measure of strength and courage in motivating meetings at the favourite café. Many thanks belong to Prof. U. Gähde for attracting the interest for models as mediators in science and with his work, paving the way for all following philosophical activities of G.P. Equally, many thanks to Prof. J. Franke, University of Siegen, for repeatedly giving highly welcome literature recommendations. Thank you!

Part III: Experimental work

7. Pilot study to the Bolund wind tunnel experiment

"In all affairs it's a healthy thing now and then to hang a question mark on the things you have long taken for granted."

- Bertrand Russell

In the previous chapters, general aspects for the *quality assurance* and *adequacy* of models and data were analysed and derived. Part III of the thesis, namely the experimental work, translates the general aspects which were found in the previous analyses into *concrete procedure examples* and *quality tests for physically modelling of atmospheric boundary layer flows over hills*. The experimental conduction and quality assurance is based on the EWTL Hamburg *quality guidelines* and *best practice* for modelling wind flow and pollutant dispersion in industrial and urban landscapes, [Harms 2010; Leitl, 2008; Leitl et al. 2003; 2005; 2009; Schatzmann and Leitl, 2011].

Introduction to the experimental part

First of all, let us shortly recall the analysis carried out so far: In chapter 1–3, a brief introduction into atmospheric boundary layer flow was given. Also, hills as *geomorphological objects* in an atmospheric boundary layer flow were introduced as well as the theoretical *foundations of wind tunnel modelling*. The Navier-Stokes Equations as *theory-core* of modern fluid dynamics (and flow over hills) in terms of philosophy of science were analysed in chapter 4. The *embedding of modelling* into a scientific frame, namely its relationship with reality, theories and data, was analysed in chapter 5. The state of the art for wind tunnel modelling of atmospheric boundary layer *flow over hills* was examined in a literature review in chapter 6. Also, open questions and areas for improvement of quality assurance or documentation were discovered. The results will now be applied concretely, in chapter 7 - 9, for two wind tunnel studies for flow over hills. The two studies consist of the *pilot study "idealized Bolund"* in chapter 7, and the main *Bolund hill wind tunnel study* in chapter 8. A more detailed *statistical analysis* of resampling features and *relative statistical convergence* is carried out in chapter 9. Here, an introductory overview on the two experiments is given:

The pilot study “idealized Bolund”:

In 2010/2011 an extensive study was conducted in the BLASIUS wind tunnel with four configurations of an “idealized” Bolund hill⁵³. The purpose of the pilot study was to analyse the *sensitivity* of the model results on the representation of the hill *shape*. The BLASIUS wind tunnel was chosen due to its availability in the time schedule of the Environmental Wind Tunnel Laboratory (EWTL) in Hamburg. To be clear: the scope of the pilot study was *not* to model the real Bolund hill field study conditions. The scope was to *gather information* in order to design and plan the main (real) Bolund wind tunnel study in the large atmospheric boundary layer wind tunnel, WOTAN, according to the lessons learnt. The pilot study is described on pp. 135.

The (real) Bolund hill wind tunnel study

The case study for modelling real terrain in the WOTAN wind tunnel, chosen here, is the Danish steep island, the Bolund hill, [Bechmann et al. 2011, Berg et al. 2011]. This terrain was previously introduced (see pp. 91 for the variability of the Bolund field data and pp. 122 for an introduction to the field study). Bolund was chosen due to its impact in the literature and *complexity as a hill test case* (steep slopes). It was modelled in the large boundary layer wind tunnel facility, WOTAN, at the University of Hamburg in 2011. An Emphasise was put on carrying out an extensive quality analysis because of the results of the pilot study. Further on, for the main study of Bolund in WOTAN, a main goal was to model the atmospheric boundary layer flow according to the *meteorological conditions* of the *real Bolund location*. The full documentation and results of the Bolund in WOTAN study are given in chapter 8, pp. 167.

⁵³ “Idealized” with respect to symmetry and easily producible hill shape, based on the real Bolund shape.

The pilot study “idealized Bolund”

In this section, the pilot study is described. First, the *experimental set-up* is lined out, including the wind tunnel specification of BLASIUS and the geometry of the “idealized” hill shapes. Remarks on *error analysis* (deviation metrics) are given on pp. 143. The deviation metrics are used to examine the *precision* (repeatability) of the experiment regarding the *location* of the measurement and the *time gap* between the measurements, pp. 146. The dependence of the mean flow on the *representation of the hill shape* is analysed in pp. 159. *Reynolds number* tests with regard to the *location in the flow geometry* are analysed in pp. 158. An analysis on the influence of the *manual adjustment* of the LDA-probe is added in the appendix. The pilot study is summarized in pp. 164. *Lessons learnt* as the starting point for the design of the main Bolund wind tunnel study in WOTAN are concluded in pp. 165. *Further details* of the pilot study are given in the appendix, “Idealized Bolund hill test (Blasius)”, pp. 320.

Wind tunnel facility BLASIUS

The BLASIUS wind tunnel is a conventionally designed *closed test section/ open return boundary layer wind tunnel*. The 16 m long facility consist of an air intake with honeycombs and screens, an approximately 7.5 m long fetch *upwind of the test section* and an approximately 4 m long *test section*, see Figure 26. BLASIUS is driven by a blower operated in suction mode preventing possible flow disturbance generated by the wind tunnel drive to be propagated through the test section. *Wind speeds* are adjustable between 0 and 15 m/s and the wind tunnel is equipped with an *adjustable ceiling* in order to compensate for possible blockage effects caused by models mounted in the test section. The latter enables the *longitudinal pressure gradient* along the test section to be *minimized* and allows for a physically consistent modelling of the constant flux layer. Along the test section, the tunnel is equipped with a computer controlled 3D probe *positioning system* which enables automated consecutive *point wise* measurements with a positioning accuracy of about 0.1 mm.

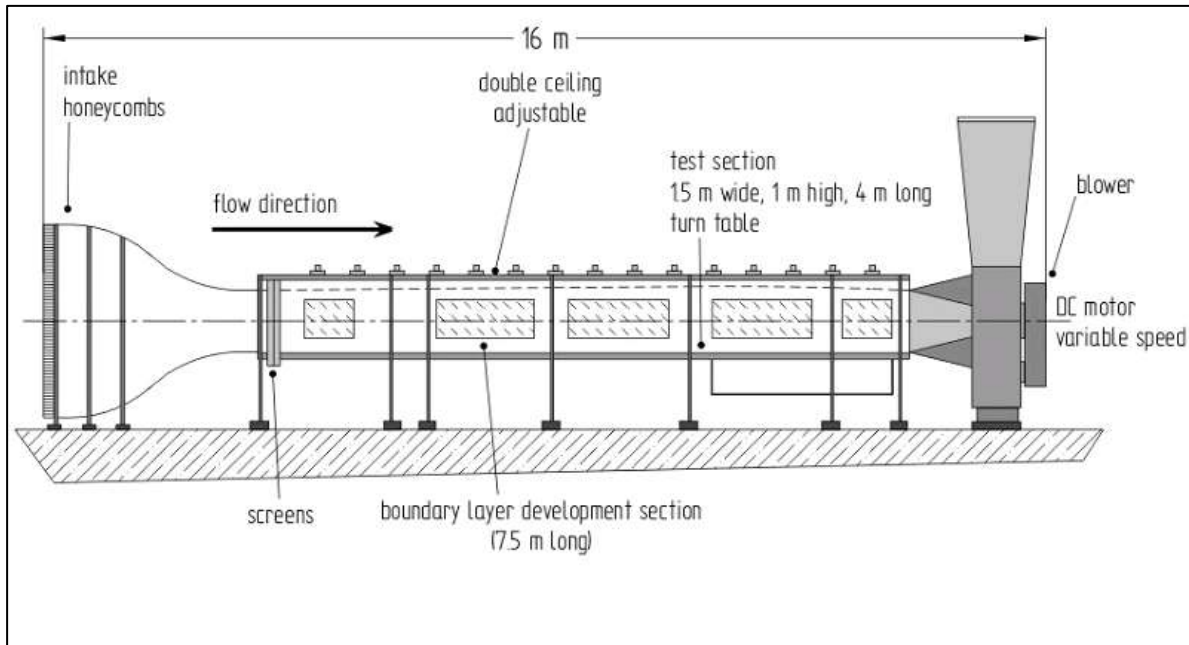


Figure 26: BLASIUS wind tunnel for "Idealized Bolund"

Laser-doppler-anemometry (LDA)

For the measurements in this study, a 2D fibre-optic probe with an outer diameter of 27 mm and a fairing was used to ensure *nonintrusive flow measurements*, see Figure 27. A homogeneous seeding of flow with *tracer particles* was generated by means of a commercial grade hazer. *Seeding particles* have a diameter of 1-2 μm and a negligible descent rate below 0.01 m per minute.

It can be noticed that laser-doppler-anemometry (LDA) has been used for fluid dynamical investigations in gases and liquids for more than three decades [Dantec, 2006]. The flow velocity is measured by the *scattered light* from the seeding particles which move with the flow through a *probe volume*, spanned by *intersecting laser beams*. The probe volume is typically up to a few *millimetres* long. The basic configuration of an LDA consists of a *continuous wave laser*, *transmitting optics*, including a beam splitter and a focusing lens, and furthermore *optics for reception of the scatter light*, comprising a focusing lens, an interference filter and a photo-detector [Dantec, 2006].

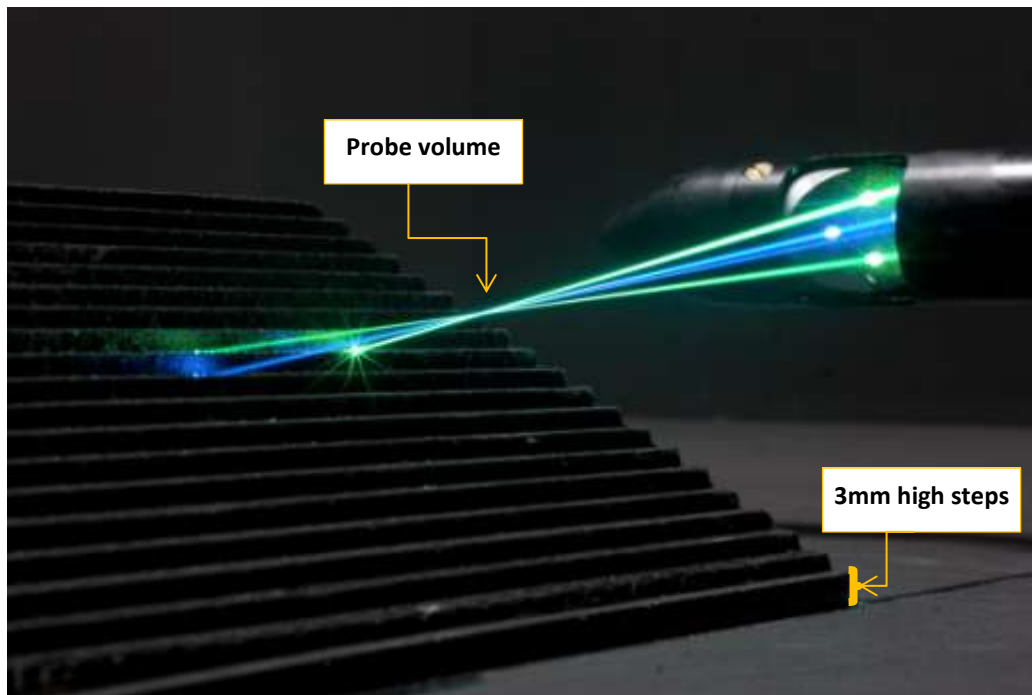


Figure 27: LDA probe in horizontal set-up (for UW measurements), laser beam intersections and front slope of a stepped hill model (3mm-steps)

For measurements of 3dimensional flow velocities with a 2D probe, the following procedure can be applied: the UW velocity components are measured (in a horizontal set-up), and then UV components are measured (in a vertical set-up), after rotation of the probe⁵⁴. Due to the *asymmetry* of the probe volume, the set-up can have influence on the measurement results in flow areas with large velocity gradient. This was also remarked in COST 732, [2010]: “[...] due to the shape and the small but finite size of the measurement control volume of an LDA system, the measured U-velocity component for consecutive UV- and UW-measurements at exactly the same location differs because the measurement volume has a different orientation in space.” [COST 732, 2010; p. 14].

The *sampling frequency* (also: data rate) of LDA data depends on the *density of the particle seeding*, as well as on the *mean flow velocity*. Furthermore, LDA time series are *not equidistant*. The time steps between the measurements depend on the (velocity of the) particles which arrive and pass through the laser beam intersection.

For the computation of mean values, standard derivation or turbulence spectra, it is convenient to demand equidistant time series. Hence, LDA data needs to be resampled.

⁵⁴ UV components can also be measured first.

Often, zero-order-sample-and-hold is used as a resampling method for LDA data. This means that the velocity is kept constant until a next measurement value indicates that the velocity has changed: let $u_{\text{resamp}}(t)$ be the resampled time-series and $u(t_i)$ be the raw-time series. Then, the sample-and-hold method is:

$$u_{\text{resamp}}(t) = u(t_i), t_i < t < t_{i+1}, i \in \mathbb{N}.$$

Depending on the application of the data, it is necessary to determine an appropriate *resampling frequency* and *resampling method* for LDA data. This is further discussed in chapter 9.

The inflow conditions

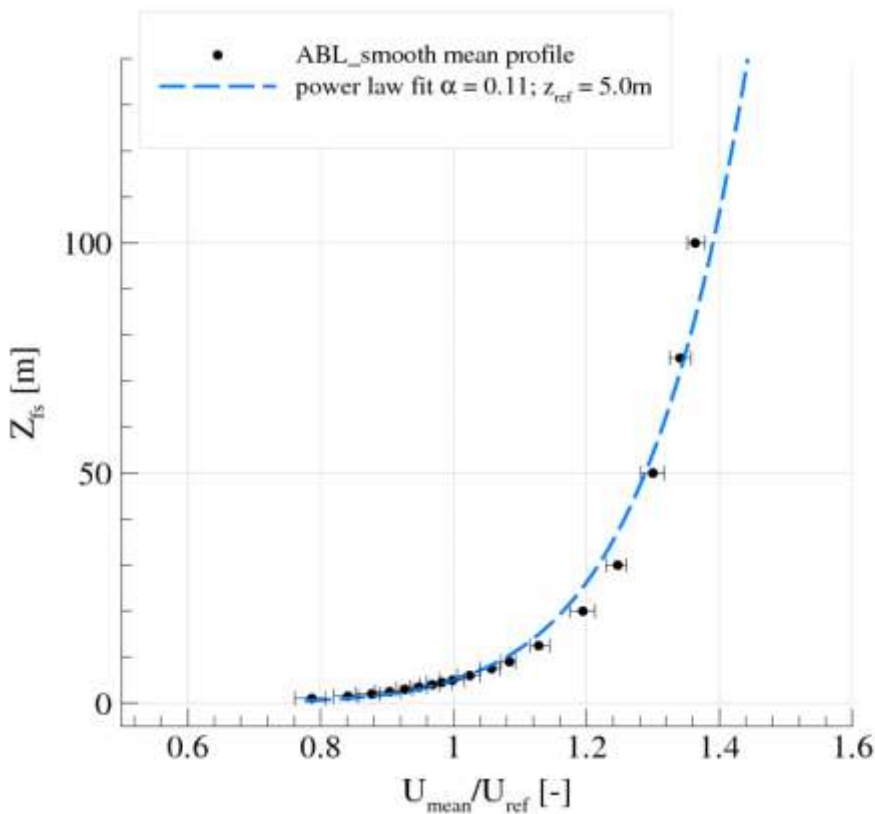


Figure 28: Mean vertical profile over all measurements of the stream wise velocity component. Error bars indicate the value range.

As stated before, it was *not* the aim of the pilot study to adjust the wind tunnel inflow according to the real Bolund field conditions. However, a *meteorologically consistent*

smooth boundary layer was achieved in the scale 1:500. The smooth boundary layer was modelled by Denise Hertwig in BLASIUS for a previous study and was adopted for the idealized Bolund hill study. In Figure 28 and Figure 29 the estimated power law exponent and the estimated roughness length of the inflow for idealized Bolund in BLASIUS are given. Many thanks belong to Denise Hertwig for providing the figures. Further information on the inflow is given in her internal report (“ABL smooth results, 2010”). The full documentation contains the *lateral profile of the stream wise velocity component* at three heights for $X = 0$ mm, the *mean turbulence intensity* for all three components, the *mean integral length scales* in stream wise direction at different heights, and the *mean vertical profile* of the Reynolds shear flux in the lowest parts of the boundary layer.

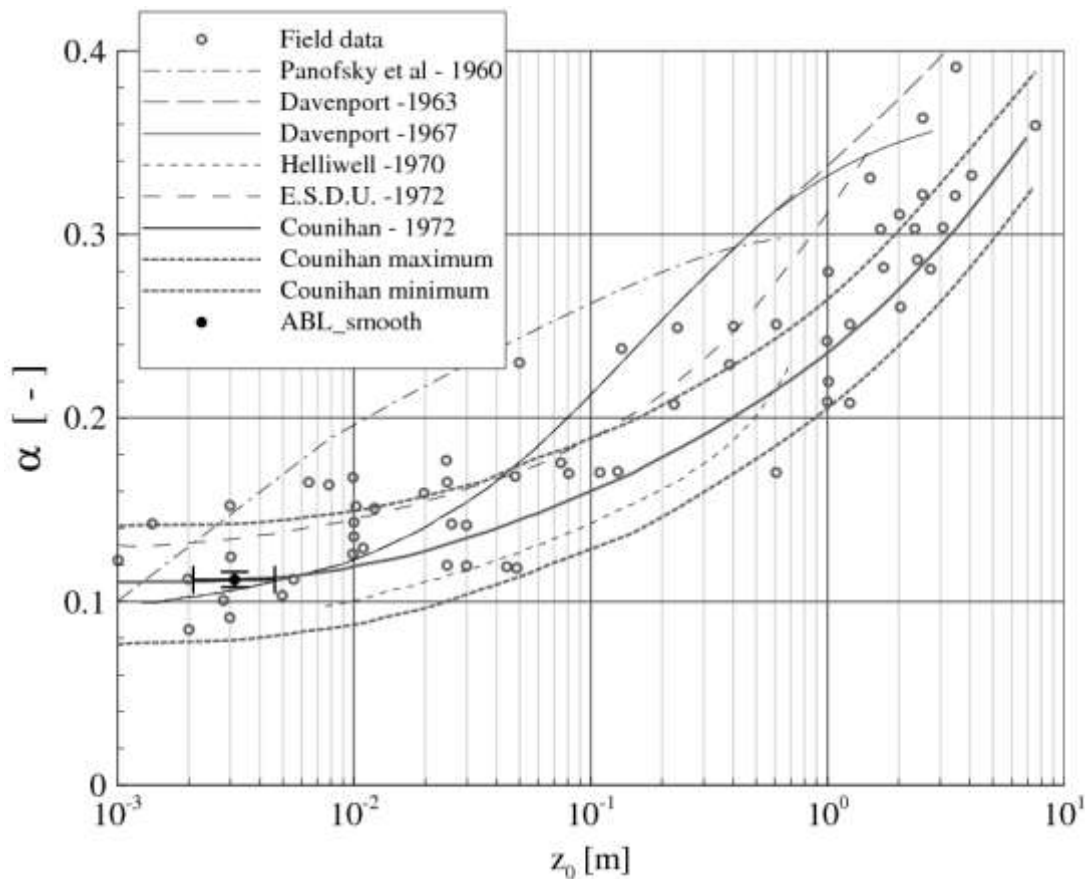


Figure 29: Mean profile exponent α and roughness length z_0 . Error bars indicate the value range.

Idealized model hills

The basis hill model for the pilot study “idealized Bolund” in BLASIUS was designed with reference to the *characteristic features* of the Bolund hill. For this, a 60° inclination at the front and the lateral slopes was chosen and a 30° inclination at the lee slope. Furthermore, the overall shape of the real Bolund was idealized with respect to *symmetry along the middle axis* in flow direction. The ratio of length, width and height was approximately preserved (800 mm : 400 mm : 60 mm), see Figure 30. In order to achieve a compromise between the *restrictions* of the BLASIUS wind tunnel (the model scale for the atmospheric boundary layer cannot be as large in a small large boundary layer wind tunnel as for a large one) and the *geometrical resolution* of the measurements and the hill model, the scaling factor was set to be 1:500 and the idealized hill models were assumed to be *twice as large* as the real Bolund hill.

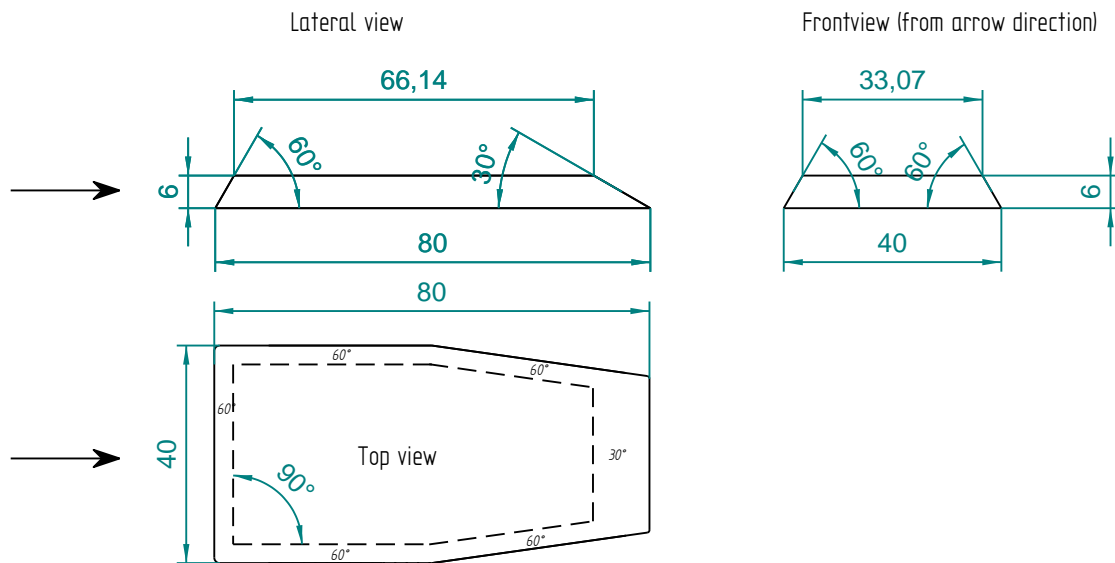


Figure 30: Technical drawing of basis hill model "idealized Bolund". All length scales are in "cm" model scale, which refers to approximately twice the size of Bolund in the meteorologically consistent boundary layer of scaling 1:500.

The “idealized” Bolund hill model was built in *four configurations*: With slopes without steps (A1), with stepped slopes (3-mm-steps) (A2), with smoothed edges (A3) and with strongly smoothed edges (A4), for a scheme see Figure 31- Figure 33.

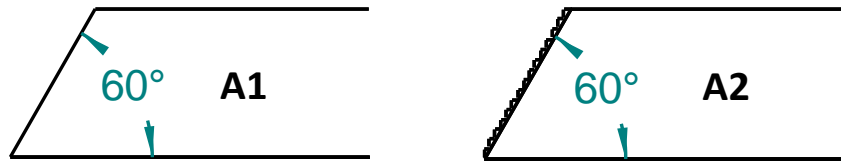


Figure 31: Schematic view on the luv slope of idealized Bolund; left: model A1, without steps; right: model A2, stepped slopes with 3mm height (all slopes stepped)

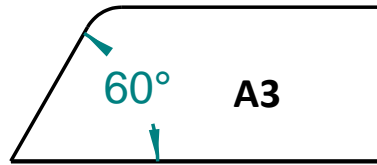


Figure 32: Schematic luv slope of idealized Bolund model A3: smoothed front edge; radius ≈ 5 mm

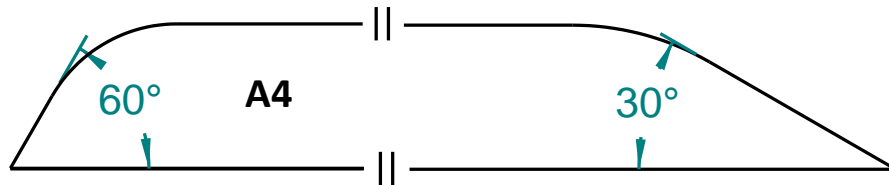


Figure 33: Luv and lee slope of model A4: strongly smoothed front and lee edge; radius $\gg 5$ mm

The tests for geometric representation were chosen according to the *level of detail* in which topography is spatially resolved by numerical models. For example, a slope as in the model A3, can be approximated in a numerical model as *slope with steps*, which is A2. It can also be approximated by A2, if the spatial grid is adjusted accordingly and if the *spatial resolution* is below the radius of the rounded off front part. For the reasonable comparison of a wind tunnel model with a numerical model, the sensitivity of the (measured or computed) *flow geometry* on the choice of the *geometrical resolution* and *representation* is important.

Furthermore, in the wind tunnel, relaminarisation of the boundary layer due to an *aerodynamically smooth* model hill surface needs to be prevented, recall the discussion on pp. 109. In brief, the challenge for the physical modeller is to build an *aerodynamically rough* model without violating the *geometrical similarity* (e.g. by mounting too large roughness elements on the hill). Steps can lead to both increase and decrease of aerodynamical roughness. Hence the variation of no steps (A1) to steps (A2) is interesting not only for the comparison with numerical models but also from a purely physical modeller's point of view.

Finally, with hill model A4, the effects of the bluff bodies (A1 to A3) in comparison to the rounded off body (A4) are examined.

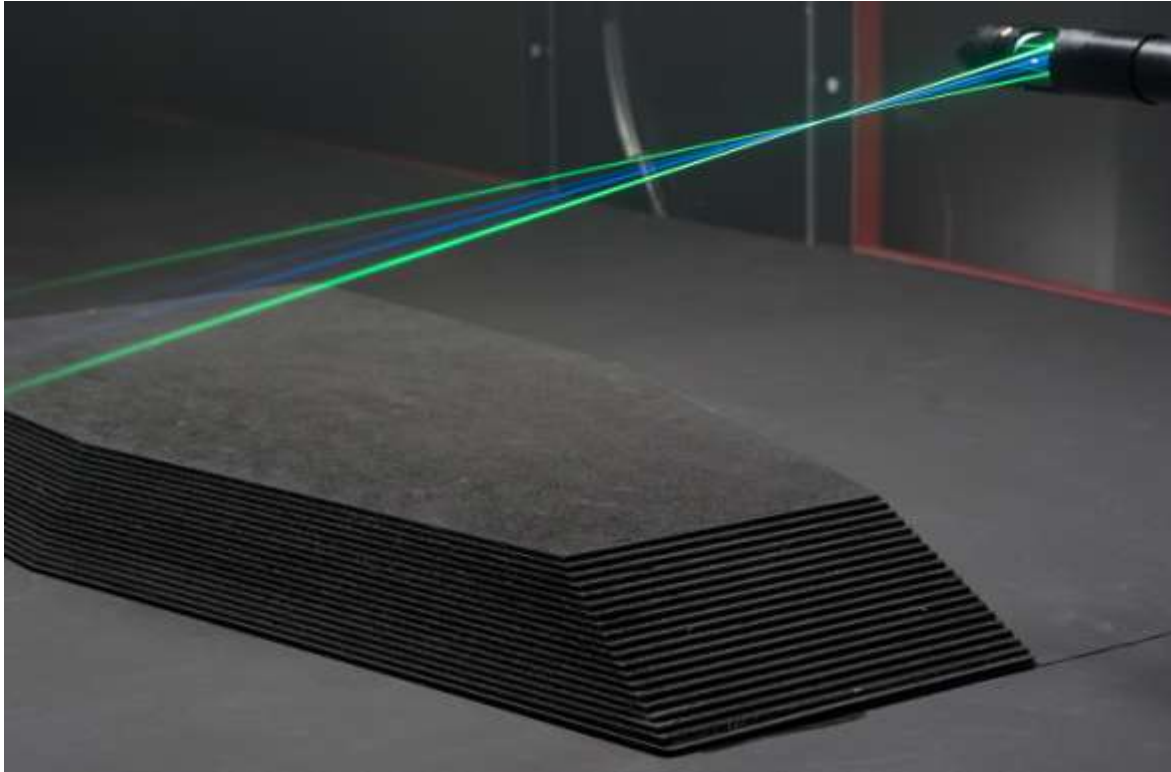


Figure 34: Hill model A2 in BLASIUS with LDA probe in horizontal set-up

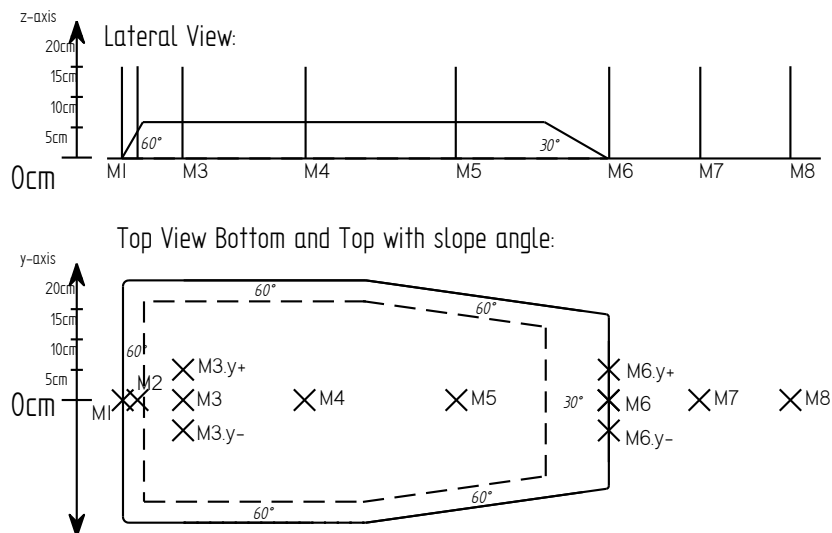


Figure 35: Naming of the measurement positions of the pilot study “idealized Bolund”.

Hill model A2 in BLASIUS is shown in Figure 34. The name of the *measurement positions* and the spatial *resolution of the measurements* are illustrated in Figure 35 and Figure 36. All

models were painted with *black, matt colour* for *minimising noise* in measurements due to reflection of LDA measurement beams.

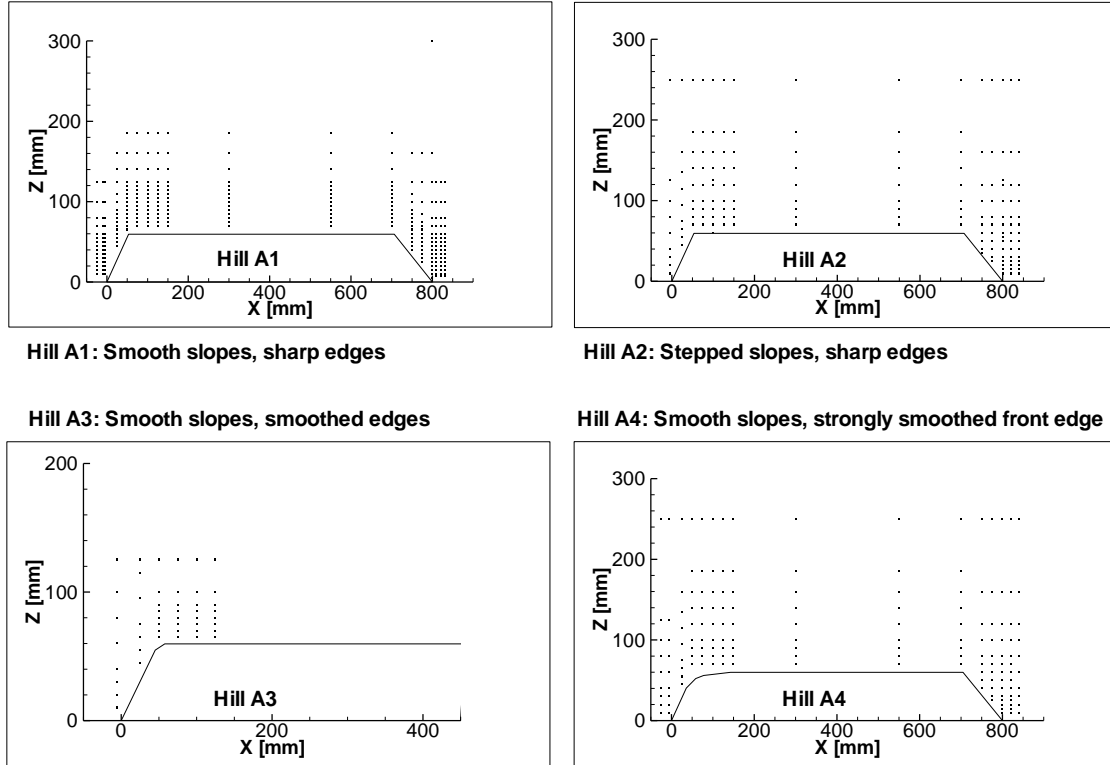


Figure 36: Measurement positions of hill models A1-A4 (in UW probe set-up)

On error analysis

Recall that the “absolute error” or “accuracy” of a physical experiment with respect to reality is not quantifiable (chapter 3)⁵⁵. Recall further that the “relative error” or “repeatability” can also be called “precision”, denoting the degree to which *repeated measurements* under *unchanged conditions* show the *same* results. Please note that, in this work, “repeatability” is distinguished from “reproducibility” in the following meaning: “Repeatability” denotes the degree of *repeatability* of measurements taken in the *same experimental set-up with the same ambient conditions*⁵⁶. “Reproducibility” denotes the

⁵⁵ “Accuracy” was the degree of closeness of measurements of a quantity to its actual (*true*) value.

⁵⁶ This is never perfectly possible as time goes by, but variation in a certain range is negligible. The precise details of the term “repeatability” and “reproducibility” need to be based on the specification of the model.

variation of the test results with different experimental set-up, e.g. operators (human factor), test apparatus, and laboratory locations⁵⁷. Here, it will be focused on *repeatability*.

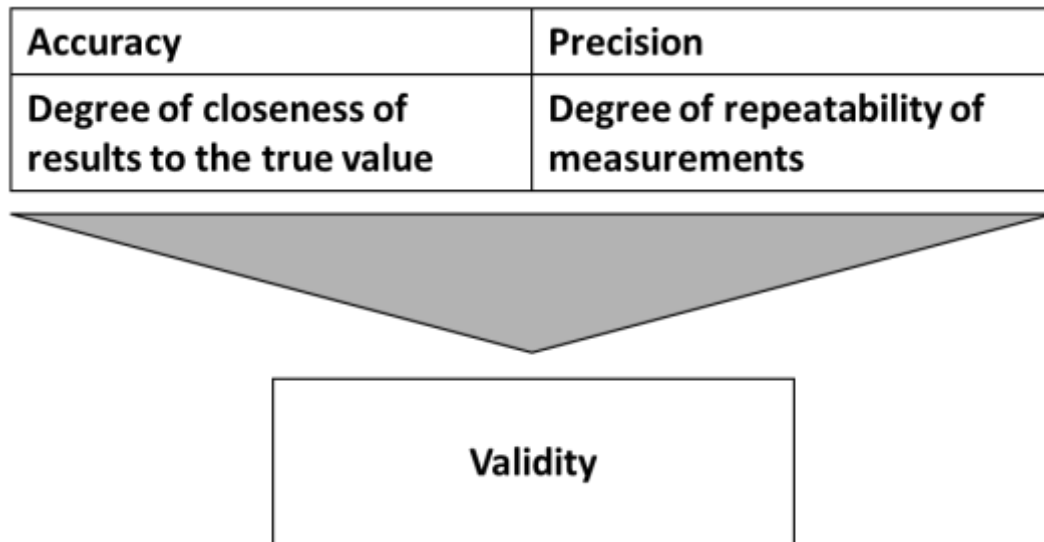


Figure 37: Illustration to the epistemological meaning of “validity of measurements”

Only experimental results which are *accurate and precise* to a certain degree are called “valid”. There can obviously be *accurate* experiments that are *not precise* and the other way around. Hence, only the combination of the analysis of *precision* and *accuracy* leads to the estimation of the *validity* of the experiment, see Figure 37. Since *accuracy* cannot be strictly quantified models (also numerical models) cannot be *validated* in a *rigorous* manner.

In practice, two different ways of error analysis can be differentiated: the *bottom-up* and the *top-down* method. In the *bottom-up* method, *sources* of error are analysed as well as its *interferences* and, at the end, errors are quantified. In other words, the error sources and their relation towards each other are first considered qualitatively – then quantitatively. The bottom-up method is also the only method to qualitatively assess the accuracy of data.

⁵⁷ As an example, the deviation of a series of measurements for model Hill A1 at point M1 with reference wind speed almost 7 m/s with almost no changed ambient conditions serves as measure for *repeatability*. It is sometimes also called “test-retest reliability”. On the other hand, the deviation of measurements for model hill A1 at point M1 with *different* reference wind speeds serves as a measure for *reproducibility* of test results at different Reynolds numbers.

The *top-down* method works the other way around. *Quantitative differences* in measurement results are analysed first. Obviously in this method, *not* accuracy of the experiment is assessed but an *internal uncertainty* of the measurements. In other words, the estimation of the *repeatability* within the same experimental set-up is useful for the *precision* assessment. The measure of repeatability can simply be the *standard deviation* as “repeatability standard deviation”. Other mathematical deviations can be used as well for example the *mean absolute deviation* or the *spread*. A review and remarks on basic measures of repeatability are given in the appendix on pp. 318. An overview on advantages and disadvantages is given in Table 5, p. 146.




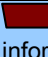
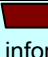

Concluding, for an in-depth error analysis in this work, a top-down approach is combined with a bottom-up approach in order to get an estimation of both, the *precision* and *accuracy* of the measurements. First, in chapter 4 -6, a (not exhaustive) *top-down error analysis* on the modelling of hills in an atmospheric boundary layer flow was given. In the outlook, chapter 10 pp. 279, further ideas for the assessment of *accuracy* are introduced. Then a combination of both approaches is used for the error analyses of the concrete experiments, the *pilot study* and the *main Bolund wind tunnel study*. This means that the *quantitative differences* of repeated time series are computed (top-down) with regard to *expected sources of structural errors*⁵⁸ (bottom-up).

The details of the conditions of *repetition* are the crucial point. For example, the Reynolds number in the wind tunnel is smaller than in the atmosphere (*structural error*), and by means of repeated measurements at the same location with different Reynolds number (here also called “*Re-tests*”) the error is quantified (namely by computation of *quantitative differences*). Based on the *quantitative deviations*, it can be decided whether or not the error is *significant* for the *purpose of modelling*.

Here, the repetitions with different *mean wind tunnel reference velocities* (Re-tests) are not classified as a different *experimental set-up* (reproducibility), they are rather classified into *repeatability assessment (precision)*.

⁵⁸ “Error” is not meant in a negative sense, here. It refers to the “structural error” or “accuracy deviation from reality” which every model has.

Table 5 Summary of different types of deviation

Standard Deviation	Mean Absolute Deviation	Spread
Formula Let $x_i, i = 1, \dots, N$ be a finite data set with mean value \bar{x} and maximum x_{\max} and minimum x_{\min} .		
$s_N = \sqrt{\frac{1}{N} \sum_{i=1}^N (x_i - \bar{x})^2}$	$D = \frac{1}{N} \sum_{i=1}^N x_i - \bar{x} $	$\xi = x_{\max} - x_{\min} $
Properties		
 +: gives rough information whether values are clustered around the mean or if there are many far away from the mean. +: very useful in case of normal distribution	 +: gives rough information on the mean difference between points in the data set and its mean value. +: can also be used for other mean values such as the median for example	 +: gives information on the absolute difference between maximum and minimum value of a given data set. +: can be used also if the computation of an average value does not make sense
 -: does not give information on the shape of distribution -: can lead to false conclusions if data is not normal distributed	 -: does not give information on the shape of the distribution -: does not weight the absolute values of the distances	 -: can lead to false conclusions if (single) extreme deviations occur -: does not give information about the shape of the distribution

Precision assessment in practice

As aforementioned, in order to determine the *precision* of an experiment the differences of *repeated* measurements can be computed.

For the idealized Bolund hill, *repeatability* is analysed with respect to the *location of the measurement* and the *time gaps* between the repeatability tests. The latter means that the *mean values* of *immediately* repeated time series (time gap below 1 hour) are compared with measurements repeated at *different days* at characteristic points around the hill. A wind tunnel study usually takes several days or weeks. In a time span of ten days, changes of external experimental conditions are larger than within an hour. Changes that have to be considered are for example *meteorological variations* such as pressure, humidity, temperature – which prevent the experiment from being perfectly *closed*⁵⁹. Additionally, *time* has a natural effect on measurement instruments and on any kind of technical

⁵⁹ Theoretically, a laboratory experiment is a *closed (physical) system*.

equipment. Hence, the question is whether or not a repeatability test *in the beginning of the experiment* is *sufficient* to estimate the precision for the conjunction of the experimental data set – or whether repeatability tests need to be conducted *along the whole period of the study*. Hence, in this paragraph, immediate repetitions ($\Delta t < 1$ h) are compared with measurement repetitions that have a time gap of more than 24 hours.

Standard deviation and *spread* are computed and analysed. Also, *Reynolds number variation* at different *characteristic points* around the hill is examined. It will be focused on the U-component of *model Hill A1*, i.e. slopes without steps, with sharp 60° degree front edge.

Immediate Repeatability ($\Delta t < 1$ h)

In hill model A1, points M1z10 and M1z300 are chosen to compute *immediate repeatability*. 3-minute time-series (in model scale time⁶⁰) are taken with data rate between 614 Hz and 1015 Hz. The criterion here was to obtain the maximum data rate possible (the variation of the maximum depends on the measurement location). Each data series is repeated five times within 1 hour in the experimental process ($\Delta t < 1$ h).

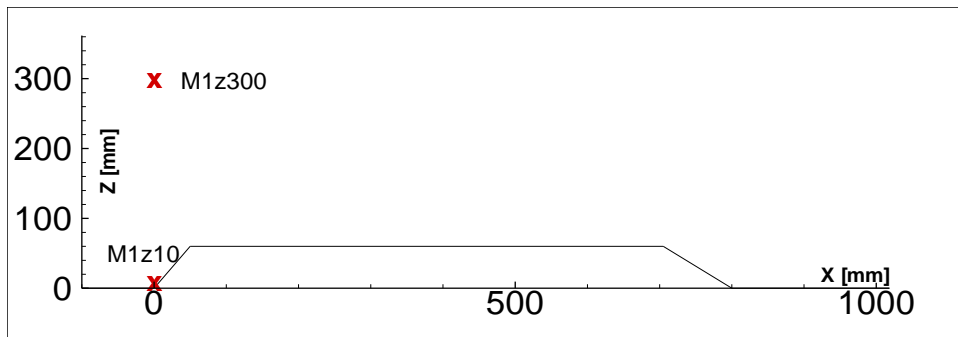


Figure 38: Measurement positions

In order to estimate the quantitative dependence of repeatability on the *measurement locations*, the points represent different *characteristic* flow conditions. Concretely, M1z10 is located at the *bottom* in *front* of the hill in $z = 10$ mm (5 m full scale) height whereas M1z300 is located in front of the hill but *five times the hill height* above ground level, see Figure 38.

⁶⁰ With geometrical scale 1:500 and full scale free stream velocity of 10 m/s, a 3-minute wind tunnel time-series with wind tunnel free stream velocity of $U_{\text{ref}} = 8$ m/s reassembles 20 hours of full scale measurements. In this set-up, 800 Hz wind tunnel measurements reassemble 2 Hz in full scale. For the basis of computation, recall the chapter “Similarity criterion as fundamental principle”, on pp. 18.

In field scale the location of M1z300 reassembles 150 m height in full scale and the hill height = 60 mm model scale reassembles 30 m in full scale.

At M1z10, the mean flow is pointed *backwards* due to the *blockage* effect of the hill. Additionally, the *absolute* value of the wind speed is *small* in relation to the *reference velocity*, U_{ref} , at the Prandtl tube. For example, in numbers, extracted from the raw data this yields:

$$\begin{aligned} u(\text{M1z10}) &= -0.35 \text{ m/s} \\ \text{for } U_{\text{ref}} &= 7.8 \text{ m/s,} \end{aligned}$$

which reassembles $u(\text{M1z10}) = -0.045$ in units of *non-dimensional* wind speed (or for comparison with field data, this reassembles -0.45 m/s in full scale for a free stream reference velocity of 10 m/s)⁶¹. This means that the absolute value of the mean velocity at M1z10 is below 5 percent of the absolute value of the mean reference velocity.

In contrast to this at M1z300 the flow is nearly *undisturbed* by the hill and the absolute value of wind speed is *almost equal* to U_{ref} . This means for explicit values extracted from the data:

$$u(\text{M1z300}) = 8.8 \text{ m/s for } U_{\text{ref}} = 9 \text{ m/s,}$$

this means that $u(\text{M1z300}) = 0.98$ in units of non-dimensional wind speed and hence around 98 percent of the reference velocity. Hence, M1z10 (blockage area) and M1z300 (free stream) have *distinct flow properties* with respect to the *value relative to the reference velocity*, the *location* around the hill and the *direction of the mean velocity vector*. At both points, the repetitions are made for *lower* and *higher* reference velocities in order to examine the *immediate repeatability*. (In the here tested interval of the mean reference velocities between $5 \text{ m/s} - 9 \text{ m/s}$, the increase of the reference velocity in the wind tunnel is achieved by the increase of the *revolutions per minute of the wind tunnel drive*. The interval

⁶¹ For the ease of reading, in this chapter the non-dimensional wind speeds can be multiplied by the factor 10 for assessment of full scale wind velocities in m/s.

of the mean reference velocities between 5 m/s – 9 m/s corresponds to 60 – 80 percent of the maximum revolutions per minute of the wind tunnel drive). The key facts on M1z10 and M1z300 are summarized in Table 6.

Table 6 Key facts on M1z10 and M1z300; the revolutions per minute of the wind tunnel drive are given in percentage of the maximum frequency frequency

M1z10		M1z300	
Position [mm]			
X = 0, Y = 0, Z = 10		X = 0, Y = 0, Z = 300	
Impact of hill			
High		Low	
Flow properties			
Reverse flow, U << U _∞ due to hill blockage		Almost free stream flow, U ≈ U _∞	
Wind tunnel drive (revolutions per minute)			
≈ 50 percent	≈ 70 percent	≈ 60 percent	≈ 80 percent
Mean wind tunnel reference velocity			
≈ 5.5 m/s	≈ 8 m/s	≈ 6.5 m/s	≈ 9 m/s

In conclusion, *four* set-ups of measurement repetitions are compared, each is repeated five times: M1z10 with the mean wind tunnel reference velocity (at the Prandtl tube) of around 5.5 m/ and 8 m/s and M1z300 with the mean wind tunnel reference velocity of around 6.5 m/s and 9 m/s. See from left to right in the *immediate repetition multiplot* below (Figure 39). In the *multiplot*, results of the comparison are visualized, namely:

- In Figure 39, the *spread* and the *standard deviation* of the repeated measurements are visualized as *green*, respectively *blue*, bars in units of *normalized* wind speed.
- Furthermore, its *percentage* on the *mean* wind speed is allocated by the *light green* and *light blue* bars⁶². For example, the *standard deviation* for M1z10 with mean wind

⁶² How is the term “standard deviation” used here? What does it mean for field data? Consider e.g. a 3-minute time-series (in wind tunnel time, this reassembles 20 hours in field scale as stated before). Assume the *mean*

tunnel reference velocity of around 5.5 m/s is 26 percent, whereas the standard deviation for M1z300 with the mean wind tunnel reference velocity of around 9 m/s is 0.1 percent. (This is a remarkable difference of *over 25 percentage points*.)

- The *reference velocity* is assigned with *red right-pointed triangles*. For example, at M1z10 there are $U_{\text{ref}} = 5.5 \text{ m/s}$ and $U_{\text{ref}} = 7.9 \text{ m/s}$.
- The average sample rate (depending on the measurement location) is denoted by *black little squares*. For example, in M1z10 at $U_{\text{ref}} = 5.5 \text{ m/s}$, the *average* amount of samples for each 3-minute time series is 77.087#. (# is the cardinality = the number of elements of a set.)

wind speed u at point p , to be $u(p) = 0.1 \text{ m/s}$, and the reference wind speed $U_{\text{ref}} = 5 \text{ m/s}$. This results in the *non-dimensional* wind speed of 0.02. Assume that a five times repetition of the measurement yields to a *standard deviation* of 0.01 m/s in field scale (with $U_{\text{ref}} = 5 \text{ m/s}$). This is 0.002 in units of *non-dimensional* wind speed. Often, the deviation is related to the *mean value* in order to express the *percentage of error*. In both cases, 0.01/0.1, respectively 0.002/0.02, yields to an error of 10 percent. In other words, the *standard deviation* in relation to the mean wind speed is 10 percent which holds for both, the field scale and the non-dimensional velocities.

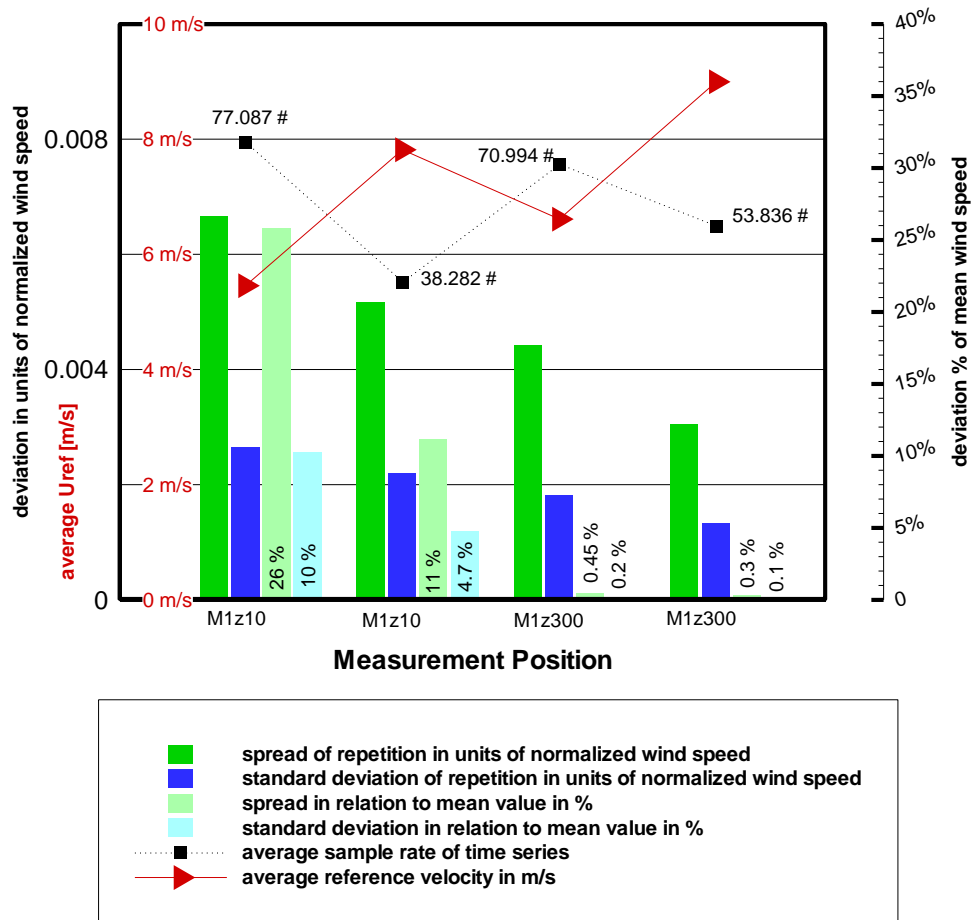


Figure 39: Immediate repeatability tests as M1z10 and M1z300 with different U_{ref} ; the x-axis shows the measurement position, the left hand red axis denotes the values of the different U_{ref} in m/s (red triangles, connected for visual reasons); the left hand black axis denotes the values of the deviation in units of non-dimensional wind speeds for the spread (dark green bars) and the standard deviation (dark blue bars); the right hand black axis denotes the values of the deviation in percentage of the mean value of all samples at that point with given reference velocity in terms of spread (light green bars) and standard deviation (light blue bars); the values of the sample size are explicitly given next to the black squares in order to estimate whether the influence of the sampling size on the precision exceeds the influence of the reference velocity (it does not, as it is shown for the here tested configuration)

Summary of the immediate repeatability for M1z10 and M1z300

- The *spread* is by about a factor of 2 larger than the *standard deviation*.
- All types of errors are *larger* at M1z10 than at M1z300 for both, low and high reference velocities.
- Differences of the error analysis can yield 2.5 -3.75 m/s differences in full scale wind speed. This means e.g. that a 4.75 m/s error can be obtained instead of 1 m/s error. (An explicit example is given in the appendix “Dependence of repeatability assessment on the flow location”, pp. 322.)
- *Values in percentage* can *distort* the results, e.g. if the reference wind speeds are low. In this case, this can lead to over *70 times of overestimation* of the empirical spread, (more details in the appendix, pp. 322.)
- Thirdly, in this case a *higher data rate*, respectively *sampling rate*, does *not* influence the measurement precision *positively* (or this effect is *superimposed* by others).
- *Sampling rate* and *reference wind speed* are anti-proportional (as expected for constant laser adjustment). This means that the sampling rate at low mean wind tunnel reference velocity is high and *decreases* with *increasing* reference velocity. This was found in a *range* of mean wind tunnel reference velocities of 5.5 m/s – 9 m/s and as long as the LDA setting, especially the laser power, remained *identical*.

The next analysis compares different *precision metrics* for *four* measurement positions in 10 mm above ground level around the hill. The measurement positions are M1z10 (in the blockage area), M3z70 (above the front edge), M4z70 and M5z70 (both further downstream above the hill), see Figure 40. The results are exhibited in Figure 41 and described in the following summary.

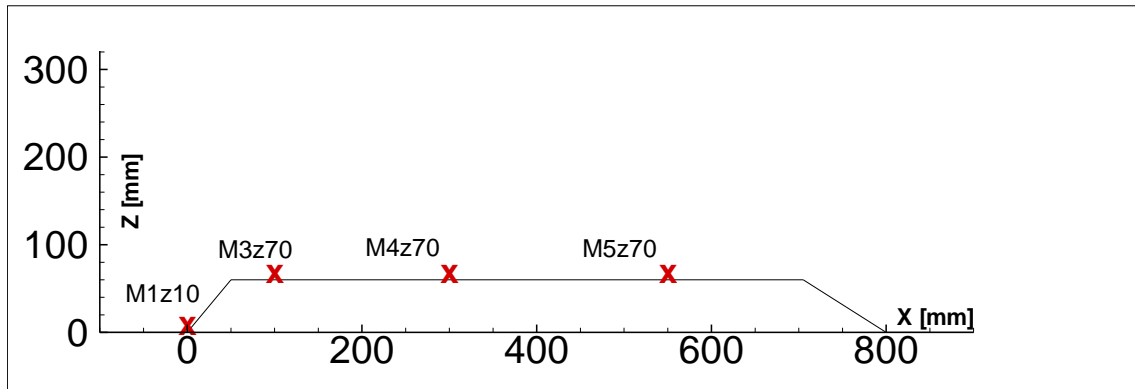


Figure 40: Characteristic measurement locations along the hill

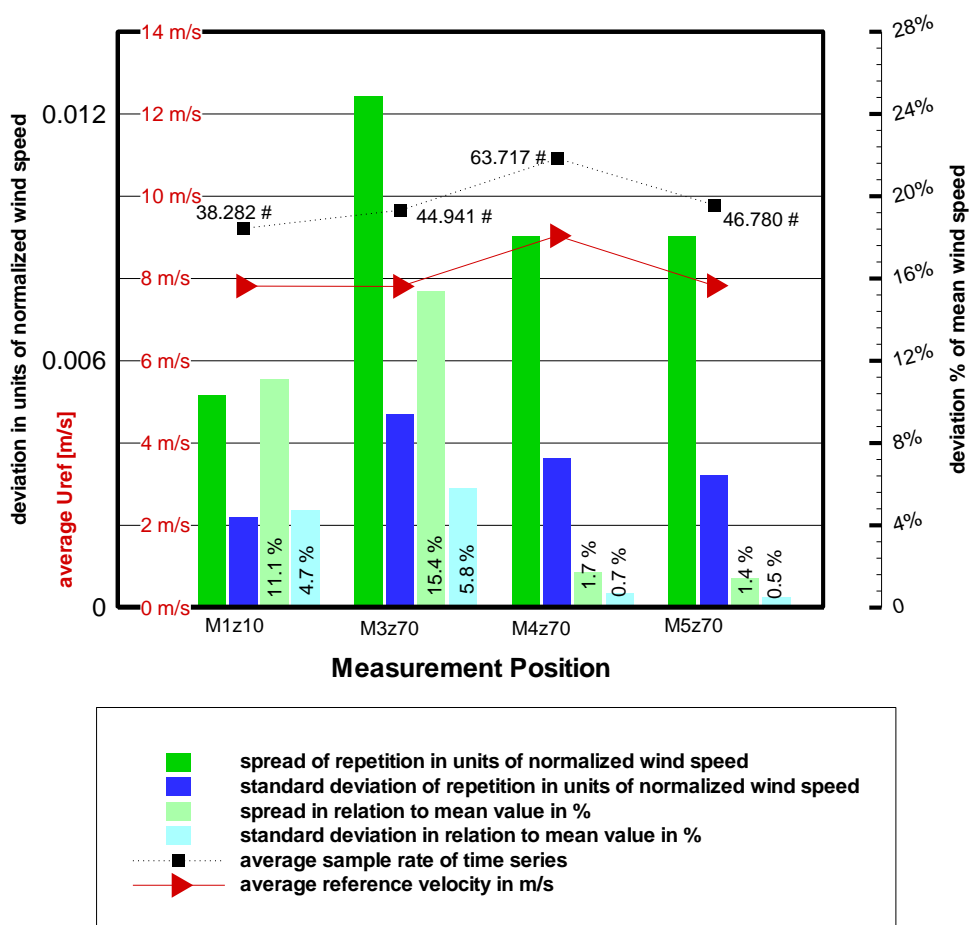


Figure 41: Immediate repeatability tests for 4 different characteristic points, a detailed description of the multiplot is given in the previous figure

Summary immediate repeatability for 4 different characteristic points

- As expected, the *spread* is always larger than the *standard deviation* for all 4 points. The factor is around 2.
- Errors are largest at M3z70, followed by M4z70 and M5z70. *Standard deviation* of the immediate repeatability is between 0.002 and 0.005 in units of *non-dimensional* wind speed.
- As in the case of Multiplot 1, it does not make sense to average the *percentage* of the standard deviation or the *percentage* of the spread. Both depend on the *mean wind speed* at the point. For example, the percentage of the standard deviation yields between 0.5 percent for M5z70 and 15.4 percent for M3z70. This means that the difference of error assessment of both points yields around 15 percentage points. However, both standard deviations are between 0.002 and 0.004 in units of non-dimensional wind speed (of which the *difference* is below 0.002 in units of non-dimensional wind speed). Hence, the repeatability in both cases is below 0.5 m/s in field scale (with $U_{\text{ref}} = 10 \text{ m/s}$) and the deviation in percentage points would distort the results for applications in which 0.5 m/s mean wind velocity are negligible.

Summary of immediate repeatability

- The *best* precision (repeatability) is achieved 5 times *above* hill top with high mean wind tunnel reference velocity, *lowest* precision (repeatability) occurs *close* to hill *surface* right behind the *front edge* of the hill.
- An average of the percentages of calculated standard deviations at different locations might not be representative, since it can have variation of up to 25 percentage points relative to the mean value of that location.
- *Different (plausible) methods* of error analysis can yield around 2.5 - 3.75 m/s differences for error bars of the full scale wind velocity results. This can be significant in certain applications. Hence the *purpose of modelling* is a crucial factor for the *choice of the error metrics*.
- The *spread of the immediate repeatability* is more than twice the standard deviation.

- The variation of the *data rate* in the range of 600 Hz – 1000 Hz LDA measurements has not influenced the repeatability in this experiment.

Conclusions

- In conclusion, the measurement position and the absolute value of the mean wind speed as well as the meaning of the deviation metric have to be considered carefully, in order to obtain a meaningful description of *measurement precision* in terms of deviations. Description in percentage can be *misleading*.
- Future measurement error analyses with *larger* error samples are desirable. This was taken into account for the main Bolund in WOTAN wind tunnel study. However, these analyses can still be extended in order to figure out whether the influence of the *location* on the measurement precision is a special problem for flow over hills or whether it can be solved by an extension of the *measurement duration*, for example⁶³.

Different-day Repeatability ($\Delta t > 24h$)

To assess the influence of the *time gap* between *repeatability measurements*, immediate repetitions of are compared with those at different days during the “idealized Bolund” hill study in BLASIUS. For this, measurements in the locations M1z10, M1z30 and M1z100 (Figure 42) were repeated every day during the experiment period. For consistency, only model hill A1 was used. The sample size consists of eight time series of different-day repetitions within ten days.

⁶³ That means points close to the ground could require *longer* measurement duration in order to be of the same level of *statistical representativeness* as other points with shorter measurement duration.

Results

The results of the analysis of the *different-day repeatability*, Figure 43, can be summarized as follows:

- Increase of the *time gap* reduces the repeatability precision of measurements for the here tested time gaps. In case of M1z10 the *absolute spread* increases of about *seven times*. M1z10 is a “difficult” point close to the ground in front of the hill with *low wind speeds*. The measurement spread here is of the order of 10^{-2} m/s in field scale. (This is low as absolute value, however, the relative deviation is large; hence, once again the significance depends on the purpose of modelling.)
- For “more easy” points, 30 mm respectively 100 mm (model scale) above the ground, calculated measurement spreads reduce to the order of 10^{-3} m/s. Reason can be that the *data rate* is larger at these points. (This is only the calculated repeatability value.)
- *Average reference wind speed* is almost constant whereas the *data rate* changes. The reason for the *differences of the data rate* at different points can be the height of the measurement position and a change of the hazer density adjustment. Close to the ground or at low hazer density, *fewer particles* are available at the measurement position and thus the data rate is *reduced*.
- As shown in Figure 43, in case of *immediate repeatability* it does not make sense to denote the >24h-repeatability by *percentage* values since this can lead to absurd conclusions. For example, at M1z10 the spread of multiday repetitions is more than 90 percent. However, with regard to the *low mean wind speed* at M1z10, the absolute spread is of order 10^{-2} m/s and thus can be sufficiently precise (this, again, depends on the *purpose of modelling*.)

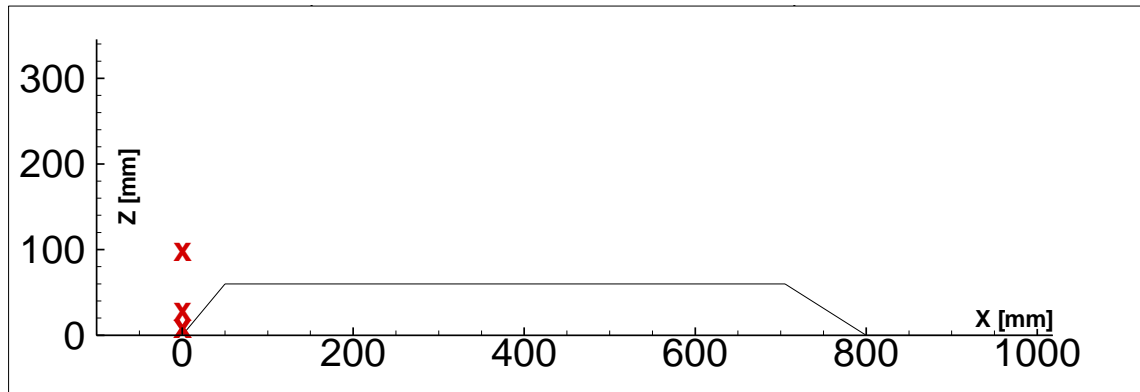


Figure 42: Measurement positions M1z10, M1z30, and M1z100

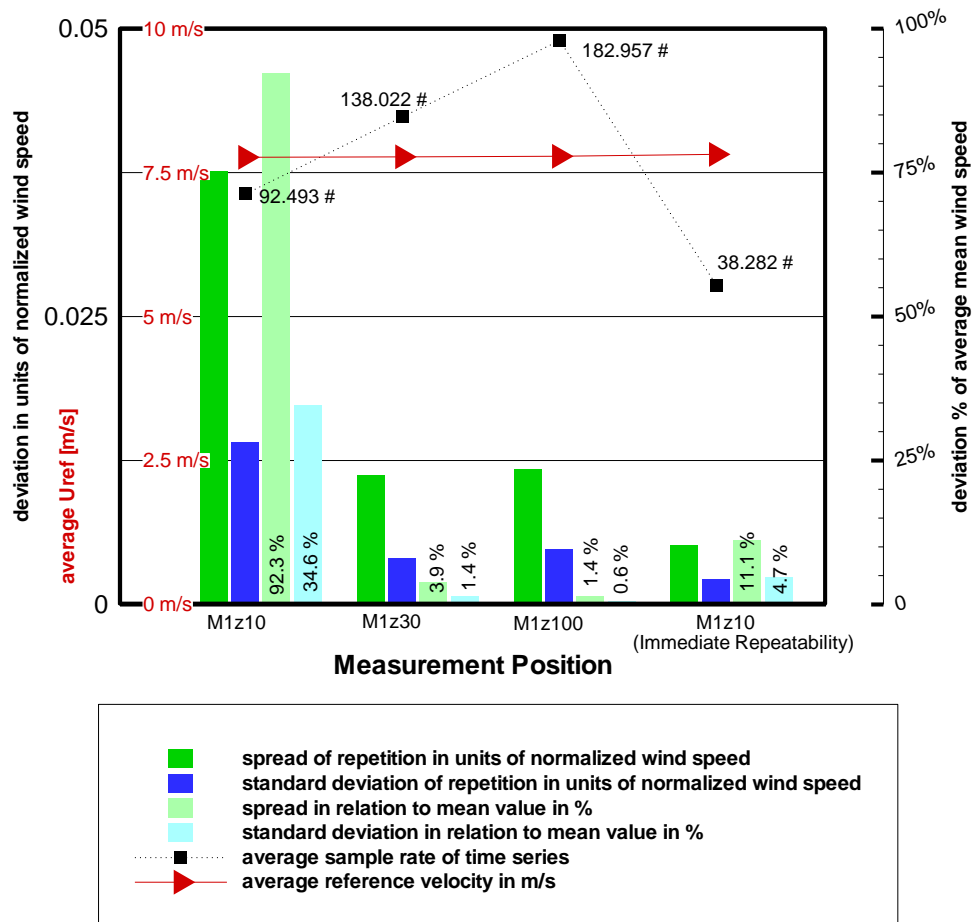


Figure 43: Different day repeatability of different characteristic points compared with immediate repeatability; a detailed description of the axes of the figure is given in the first multiplot

Conclusions

- For an assignment of the *precision* of wind tunnel modelling of flow over hills the dependence of the precision on the *time gap* and the measurement *locations* between the repetitions should be taken into account for each topographical experiment separately. The repetition *spread* can increase by 7 times for different locations. Its absolute value for this experiment is in the order of 10^{-3} in units of *non-dimensional* wind speed, in worst cases up to 10^{-2} . (Whether this is sufficient depends on the *purpose of modelling*.)
- The description of the measurement deviations *in percentage* without the information of the measurement location, can *distort* the results *significantly*. This is especially the case for measurement points with very *low mean wind speeds* such as backwards pointed mean flow at the bottom in front of the hill (over 90 percent spread because of low wind speeds around zero in this flow area.).

Independence of reference velocity and LDA probe set-up

Extensive *Reynolds tests* are conducted for the pilot study in BLASIUS and the influence of the *manual adjustment* of the horizontal LDA probe angle is tested, see appendix, pp. 322. In summary, it turns out, that the error due to manual adjustment of the horizontal angle of LDA-arrangement is *small* with comparison to measurement repeatability error and thus can be neglected. As stated before, this can be different for the *rotation of the probe* due to the asymmetry of the probe volume, (see p. 136 on laser-doppler-anemometry.)

The result for the *Reynolds tests* is not satisfying: in the *blockage area* in front of the hill and *above* the front *edge* of the hill, Reynolds number influence yields between 10 percent and 50 percent deviations in the interval of 7 m/s to 9 m/s as reference wind speeds at the Prandtl tube, (Figure 44 and appendix pp. 325). This can be regarded to be significantly large. This is why much emphasise was taken for the assessment of *repeatability* and *Reynolds influence* of the flow measurements in the *main* Bolund wind tunnel study in WOTAN.

Reynolds number tests in Summary:

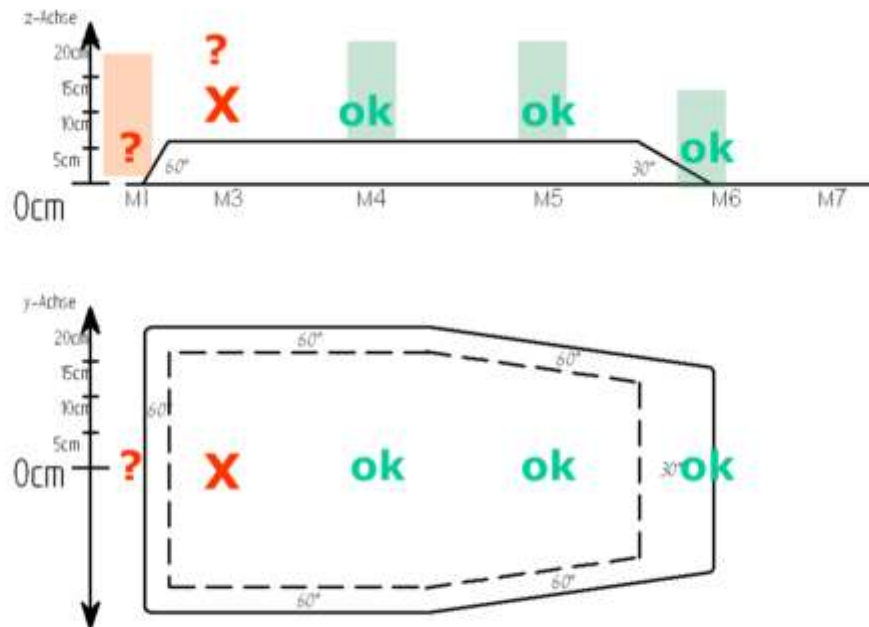


Figure 44: Reynolds number influence test results for characteristic points in the flow geometry around the hill

Mean flow dependency on the hill shape representation

In order to estimate the influence of the representation of the *hill shape* on the flow properties and to substantiate the choice of an appropriate representation of the real Bolund hill, the mean flow results of the *hill models* A1 - A4 were compared with each other, Figure 45.

Figure 45 shows that the *separation vortex* as *averaged* flow pattern at the *lee of the hill* is a phenomenon which can be observed for all hill configurations: for *stepped* slopes as for slopes *without steps* and also for model A4, with *strongly smoothed front and lee*⁶⁴ *edge*. This is according to theoretically expected values, since in all cases lee slope is steeper than the commonly assumed *critical slope* of 16 degrees. In case of the strongly smoothed lee edge, the separation area is slightly smaller.

⁶⁴ "lee" denotes the slope which is turned away from the inflow.

Normalized mean velocity U component for A1 - A4

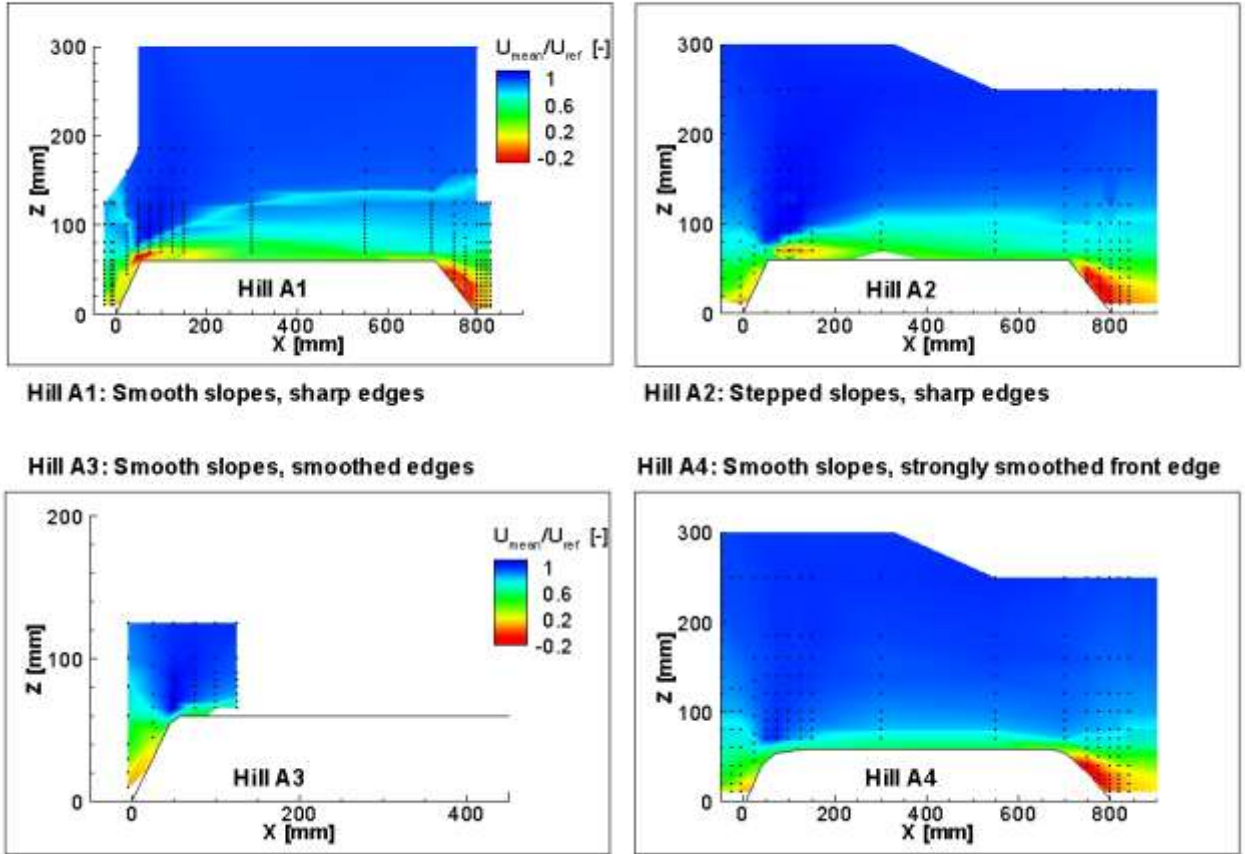


Figure 45: Comparison of hill shape representation

Another “stable” phenomenon (= invariant under the change of the here tested representations of the hill shape) is the *blockage effect* in *front* of the hill. This means that slopes with 3 mm steps (1.5 m in field scale) for the model height of 60 mm (30 m in field scale) give the same *flow geometry* for the *blockage effect* as slopes *without* steps or modifications at the hill *lee* slope. In contrast to this, the *separation* at the front edge depends on the here tested hill shape representation. This means that for hill A1, *without* steps, *separation* occurs right at the *front* edge. In case of the stepped slopes, the front edge separation zone moves *down stream*. Also, the area of the mean reverse flow is *smaller*. This is remarkable since A1 and A2 can be assumed as being “geometrically equivalent” for the spatial resolution of 1.5 m in full scale. (This reassembles in non-dimensional numbers

relative to hill height, H, or hill length, L, a spatial resolution of 0.05H respectively below 0.005L.)

In conclusion, the result of this analysis shows that A1 and A2 are *not* geometrically equivalent and that attention has to be drawn to the question, whether a model hill is built with or without steps. In case of hill A3, with *smoothed* front edge, the flow does *not* separate above the front edge. The same holds for the *strongly smoothed* front edge, hill A4. Reason can be that the flow can follow the *smoothed* contours. However, the result is still remarkable, since for A3 the front edge is only smoothed *slightly*. Thus, it can be deduced from this observation that the flow separation is very *sensitive* with regard to the *sharpness of edges* of terrain at steep *luv*⁶⁵ slopes for the here tested inflow.

Speed-up at one half hill height above the front edge occurs for *all* four hill configurations. In case of the *strongly smoothed* front edge speed-up is slightly *less*. Furthermore, in the latter case flow deceleration along the hill is less and the deceleration area is *flat* above hill level. The *influence* of the representation of the *hill shape* on mean flow characteristics was also analysed in the Bachelor thesis by Gillmeier, [2011]. As an example for the analyses of Gillmeier, [2011], Figure 46 - Figure 48 show the influence of the hill shape on the *wake of the hill* at measurement position M6, (see Figure 35, p. 142). Furthermore, the variability of statistical features of 10-minute (field scale) wind velocity records along hills is analysed in Gillmeier, [2011]. For this purpose the 3-minute wind tunnel time series recorded in BLASIUS (reassembling around 20 hours of full scale records) are divided into 10 minute mean values based on the 1:500 geometrical scaling of the wind tunnel model and an assumed field scale reference velocity of 12 m/s. The spread of the *time averages* of the 10-minute subsamples (blue crosses) are shown as well as the *mean values* of the ensemble (red crosses).

Figure 46 - Figure 48 illustrate that the spread of the mean values behind the hill is largest at around hill height and decreases with height, except for the area at the *bottom in the lee of the hill*. For A1, (no steps), the spread of the mean values at the bottom of the hill wake is distributed around zero, for the stepped model, A2, the mean values are negative (reverse

⁶⁵ "luv" is synonym to "front slope" and opposite of "lee"

flow), and for the strongly smoothed model, A4, the mean values are positive. Furthermore, in hill height the mean value of the smooth model, A4, is largest, followed by the stepped model, A2, and the bluff body, A1. This can be partly consequence of the size of the reverse flow area at the front edge, namely: Largest area of mean reverse flow at A1 (lowest recuperation at hill height), smaller area of mean reverse flow at A2 (larger recuperation at hill height), and no reverse flow at A4 (largest recuperation at hill height). Accordingly, the *speed-up*, *blockage* and the *mean flow development along the idealized hill* for its variation of 10-minute mean values (full scale) are analysed in Gillmeier, [2011], (see also p. 273 for further analysis of the spread of the statistical properties of 10-minute averages.)

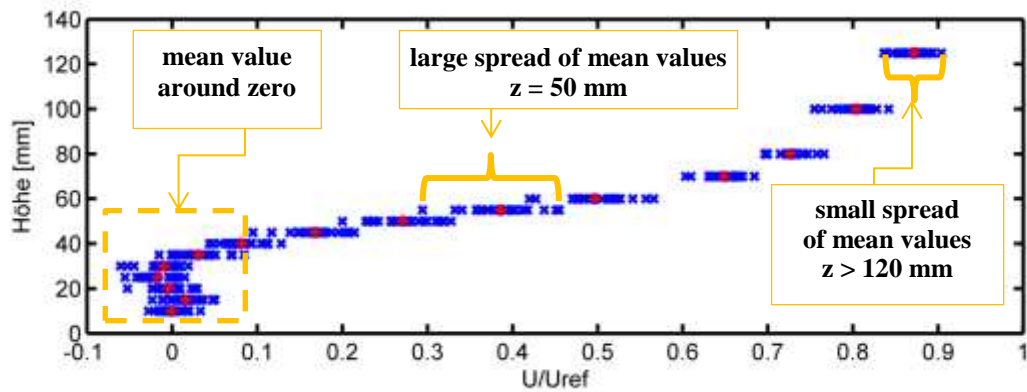


Figure 46: 10-minutes averages vertical profile in hill wake for hill model A1 (sharp edges, without steps), measurement position M6, see Figure 35, results based on Gillmeier, [2011]

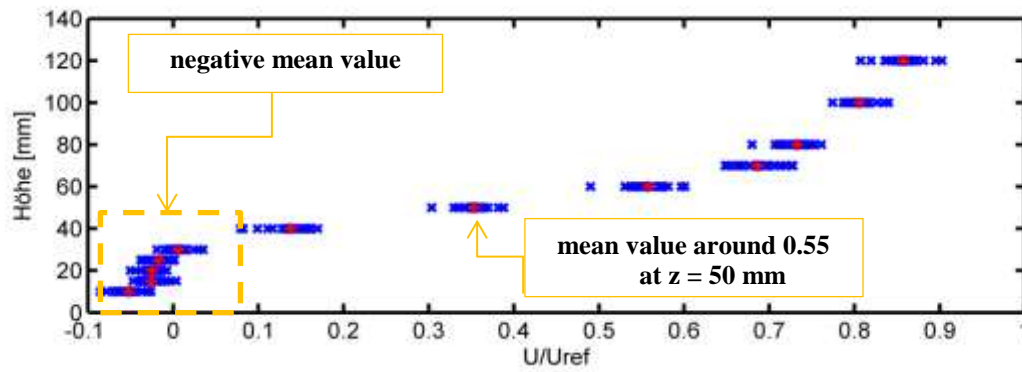


Figure 47: 10-minutes averages vertical profile in hill wake for hill model A2 (sharp edges, with steps), [Gillmeier, 2011]

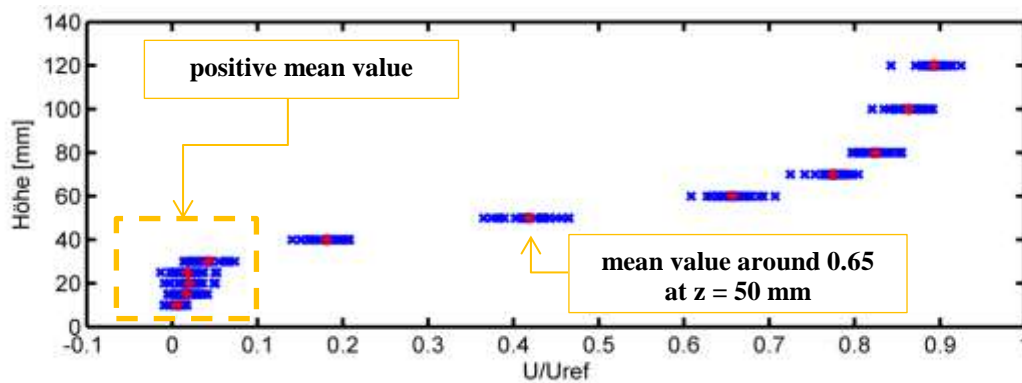


Figure 48: 10-minutes averages vertical profile in hill wake for hill model A4 (no steps, smoothed edges), [Gillmeier, 2011]

Summary of the pilot study

The sensitivity study illustrates that the interpretation of wind tunnel results for hills in an atmospheric boundary layer without testing *repeatability of the experiment* with respect to *different locations* is questionable. The results can be summarized in following five points:

- The *repetition spread* (as a measure of precision) can increase by *7 times* for different *locations*. (Whether or not this is dramatic depends on the purpose of measurements)
- *Different (plausible) methods* of error analysis can yield around 2.5-3.75 m/s difference for error bars in full scale wind speed. This can be e.g. the case for the description of measurement deviations in percentage at locations with very *low* mean wind speeds such as backwards pointed mean flow at the bottom in front of the hill. Hence the *purpose of modelling* is the basis for the *choice of the error metrics*.
- Negative *Reynolds number dependency* tests were found in *certain flow areas* of which the reason can be a lack of *statistical representativeness of the measured time series*.
- *Modelling of sharpness of topography* with spatial resolution of 5 mm (here 2.5 m in field scale) was found to determine *whether or not a separation vortex* occurs *above the front edge*. Hence, modelling *sharp edges* instead of the *real topography* due to low resolution influences the speed-up effect and the whole flow geometry around the hill. (In non-dimensional numbers for hill height, H , and hill length, L , this resolution reassembles around $0.1H$ respectively $0.01L$).
- *Modelling of slopes* with spatial resolution lower than 3 mm (here 1.5 m in field scale; or $0.05H$ respectively $0.01L$) was found to have a distorting effect on the *location* and *size* of the *speed-up area* as well as the *wake region* (and on the mean velocities which were measured in these areas.)

Considering the results of the *precision assessment* (repeatability), it can be concluded that the documentation of the wind tunnel studies on hills in atmospheric boundary layer flows

which was found *in the literature* (see “Discussion of recent wind tunnel studies” pp. 111) is unsatisfying for a detailed understanding of the *experimental quality* of these experiments (for modern requirements). A detailed *quality assessment* and *documentation* of wind tunnel studies for hills in atmospheric boundary layer flow can help in understanding the value of wind tunnel experiments.

Lessons learnt from the pilot study

In summary, the following conclusions can be drawn for the study on (real) Bolund in WOTAN:

- Three main points for the assessment of *repeatability* need to be taken into account:
 - The longer the time step between the measurements the larger the deviation the of measurement results in the here tested periods. Hence, repeatability should be assessed for both, with short time gaps (for the Reynolds tests) and every day along the experiment.
 - Different *measurement locations* in the flow can have different results for precision. This can have different reasons (e.g. the lack of statistical representativeness due to different sampling size or frequency at different locations; or the statistical turbulence properties itself; or the spatial orientation of the LDA-probe volume). Hence, tests for statistically representativeness are crucial for flow over hills (see below).
 - The choice of the *repeatability metric* (type of deviation metric) and extrapolation of the values to other flow areas has influence on the result for the assessment of the “overall” precision of the experiment. Hence it needs to be clearly distinguished between different types of metrics. This includes the choice of the *unit* (*absolute* non-dimensional values versus values in *percentage*) and for *relative measures* the choice of the *reference value*.
- *Reynolds number* tests need to be conducted in *different flow areas*. This can be a crucial point for *vortex* or *deceleration areas* around the hill (e.g. above the front edge or in the blockage area in front of the hill.)

- Emphasis has to be taken on recording *statistically representative* data. This should be tested in “difficult” flow areas with respect to the *precision results* (e.g. in the blockage area in front of the flow.)
- The *maximum possible spatial resolution* should be used for the geometrical representation of real Bolund in WOTAN in order to prevent the distortion effects which were shown in the pilot study. The models of the pilot study were assumed to be sufficiently aerodynamically smooth since no problems of Re-dependence were found along the hill and in the wake of the hill. (For real Bolund in WOTAN a *geometrical resolution* of 1 mm in model scale could be achieved. This reassembles 0.25 m in field scale and is a six times finer resolution than 1.5 m which was tested in the pilot study.)

Based on the conclusions of the pilot study, the main Bolund wind tunnel experiment was planned and conducted (details are provided in the next chapter).

8. The Bolund hill wind tunnel experiment

„Big is beautiful in wind tunnel modelling.“
– Michael Schatzmann, 28.03.2011

“Experimenters are the shock troops of science.”
– Max Planck, 1949 [Planck, 1949, p. 325]

The scope of the *main Bolund hill wind tunnel experiment* is to analyse how well the real Bolund hill can physically be modelled in the large atmospheric boundary layer wind tunnel WOTAN at the University of Hamburg. One main *purpose of modelling* is to increase the knowledge on how the quality of wind tunnel modelling of hills in an atmospheric boundary layer can be assessed and maximized in terms of *accuracy* and *precision*. This goal is to establish a foundation for future physical modelling of atmospheric boundary layer flow over topography in WOTAN. The analysis is embedded into the fundamental considerations of part I and II of the thesis and based on the explicit results from the pilot study on “idealized Bolund hill” in BLASIUS (which was described in chapter 7).

For the maximisation of the *accuracy*, emphasis is taken on the determination of *plausible* meteorological field conditions similar to those of the field Bolund area. This analysis is based on the Bolund field study, [Bechmann et al., 2009; 2011; Berg et al., 2011] and other references, [VDI-3783 part 12, 2000; Snyder, 1985; Counihan, 1975; Davenport, 1963; ESDU 85020, 2008]. Furthermore, emphasis is taken on the correct actual *implementation* (the physical modelling) of the determined inflow conditions in the wind tunnel (hence the adjustment of the inflow conditions). Secondly, it is focused on the maximisation and assessment of the *precision* of the experiment (with respect to the *lessons learnt* from the pilot study, see previous chapter).

The next chapter can be outlined as follows: First of all, *foundations* are briefly recalled, pp. 147, the *wind tunnel facility* is introduced, pp. 170, and the *wind tunnel instrumentation and hill model* is documented, pp. 172. The structure of the *data storage* is described in the appendix, pp. 327. The *determination* and the *adjustment of plausible inflow conditions* are documented in the chapter “Bolund inflow conditions”, pp. 177. Also, a wind tunnel process

loop for the *adjustment of meteorologically consistent inflow conditions* illustrates the procedure until the quality of the *boundary conditions* of a wind tunnel experiment can be assured. Different assessments of the *repeatability of the experiment* are introduced and the importance of the *convergence of time series* is examined. In addition, *Reynolds number tests* are analysed. Concerning the fluid dynamical model output of the Bolund hill experiment the effect of the hill on the atmospheric boundary layer flow is analysed. This comprises the effects on the *mean flow velocity* for the longitudinal component, the *standard deviations* for lateral, longitudinal and vertical components and the *shear stress* as well as the *skewness* of the time series. Furthermore, the *relative speed-up*, *blockage* and *wake* effects are examined in more detail. The results of the mean flow as well as the results of the whole Bolund in the WOTAN wind tunnel study are summarized at the end of this chapter.

A pursuing statistical analysis concerning the influence of *sampling duration*, *sampling frequency* and *LDA- resampling time steps* on higher order statistical moments and velocity increments is provided in chapter 9.

Fundamentals and experimental set-up

The geometrical scaling of the geometrical Bolund model and the atmospheric boundary conditions in the Bolund in WOTAN study is 1:250. Recall that the main idea for physical simulation of fluid dynamics is to use the *scaling symmetry* of the solutions of the Navier-Stokes Equations. This was discussed in chapter 3, pp. 37. In brief, the Navier-Stokes Equations (NSE) are turned into a *dimensionless* form by the insertion of *reference* quantities which determine the flow dynamics. By the insertion of the reference quantities, the equations of motion become “non-dimensional”. Flow-characterizing numbers can be isolated, for example: The Rossby-, Froude- and Reynolds-Number. From this it follows, if and only if the *characteristic numbers* are identical as well as the *non-dimensional boundary conditions*, solutions of the modified set of equations are *identical*.⁶⁶

Recall that for practical use, the requirement is relaxed since, e.g., the *atmospheric* Reynolds number cannot be achieved in experiments with gas of the same density as air and length

⁶⁶ see “Similarity criterion as fundamental principle”, pp. 37.

scale which is smaller by the factor $1 \cdot 10^2$ (unless the characteristic velocity is larger by the factor $1 \cdot 10^2$). Hence, the Reynolds number influence on the model results *needs to be tested* in the interval of the *wind tunnel mean velocities*.

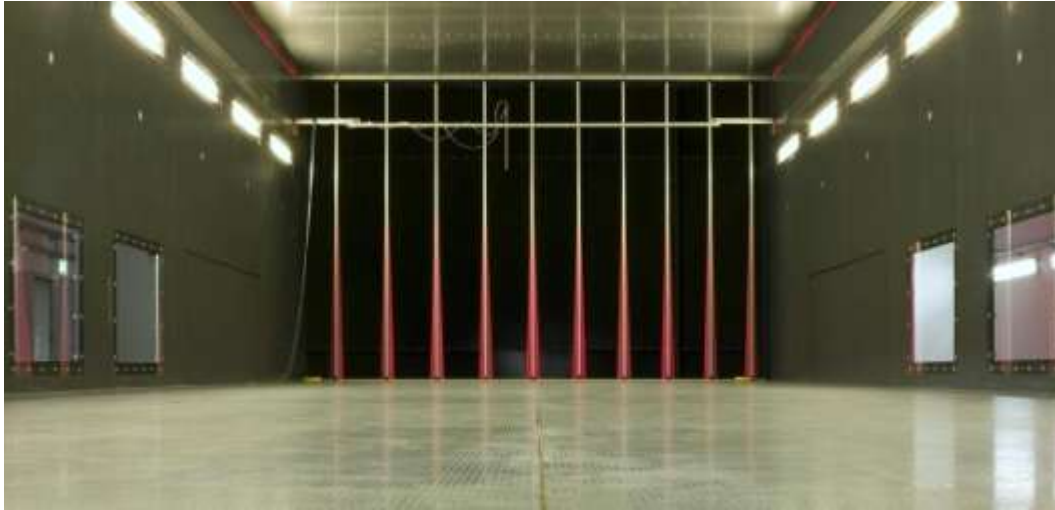


Figure 49: WOTAN wind tunnel in the Environmental Wind Tunnel Laboratory (EWTL) Hamburg with turbulence generators and base plates for the Bolund study. The Prandtl tube is between 4th and 5th spire from left. Credit: Stephan Werk

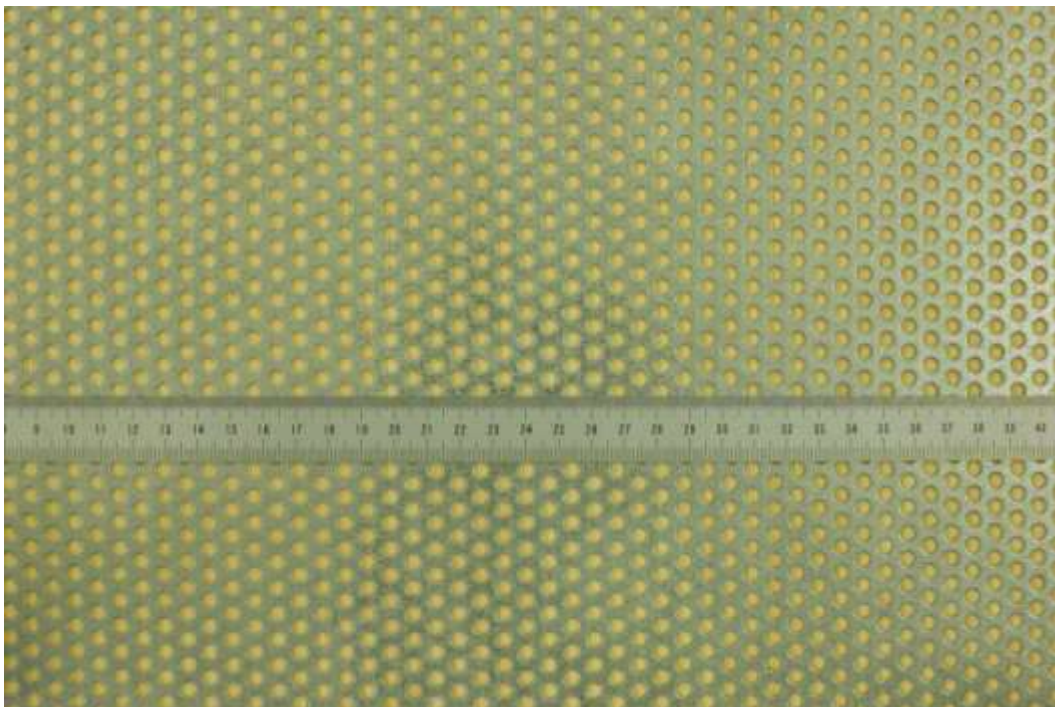


Figure 50: Base plates with low roughness for simulation of smooth Bolund alike boundary layer. Credit: Stephan Werk

If the variation of the non-dimensional results is low in the tested interval evidence is given that the flow is *fully turbulent*. Fully developed turbulence denotes the asymptotic regime “which is obtained by letting the Reynolds number tend to infinity”, [Frisch, 1980, p. 76]. This means that the statistical properties of the flow are assumed to be (nearly) independent of the Reynolds number for finite Reynolds numbers which exceed a certain (finite) critical Reynolds number.

Turbulent inflow which is consistent with the atmospheric conditions is modelled in the wind tunnel by means of *turbulence generators* at the wind tunnel intake and *roughness elements* on the ground (recall Figure 6, p. 40; for the here used set-up see Figure 49 and Figure 50, p. 169). A crucial point is to install turbulence generators and roughness elements in such a way that the *non-dimensional boundary (inflow)* conditions in the wind tunnel *match* the *desired boundary (inflow)* conditions. The *extensive documentation* of the experimental *process* to set-up the Bolund inflow conditions is given in the appendix, pp. 304, see also chapter “Adjustment of the determined inflow conditions”, pp. 184. A description of the data which is stored of the Bolund in WOTAN experiment for future analyses is given in the appendix “Description of the data structure for main Bolund in WOTAN”, pp. 327.

Wind tunnel facility WOTAN

The main wind tunnel experiment for the real Bolund hill site was conducted in the WOTAN wind tunnel in the Environmental Wind Tunnel Laboratory (ETWL) in the University of Hamburg, Figure 51. WOTAN is a large conventional type *boundary layer wind tunnel* with wind speeds between 0 and 20 m/s. It is 25 m long with an 18 m long *test section* equipped with *two turn tables* and an *adjustable ceiling*. The cross section of the tunnel measures 4 m width and between 2.75 m and 3.25 m height depending on the configuration of the ceiling. In each of the different wind tunnel projects in WOTAN, model scale and meteorological characteristics of the inflow conditions are usually different. Hence, based on the meteorological and fluid dynamical target parameters a *project-specific* set-up of *spires* and *floor roughness* is derived for each project individually. This process is further discussed in the section on the determination and adjustment of Bolund hill inflow conditions, pp. 177.

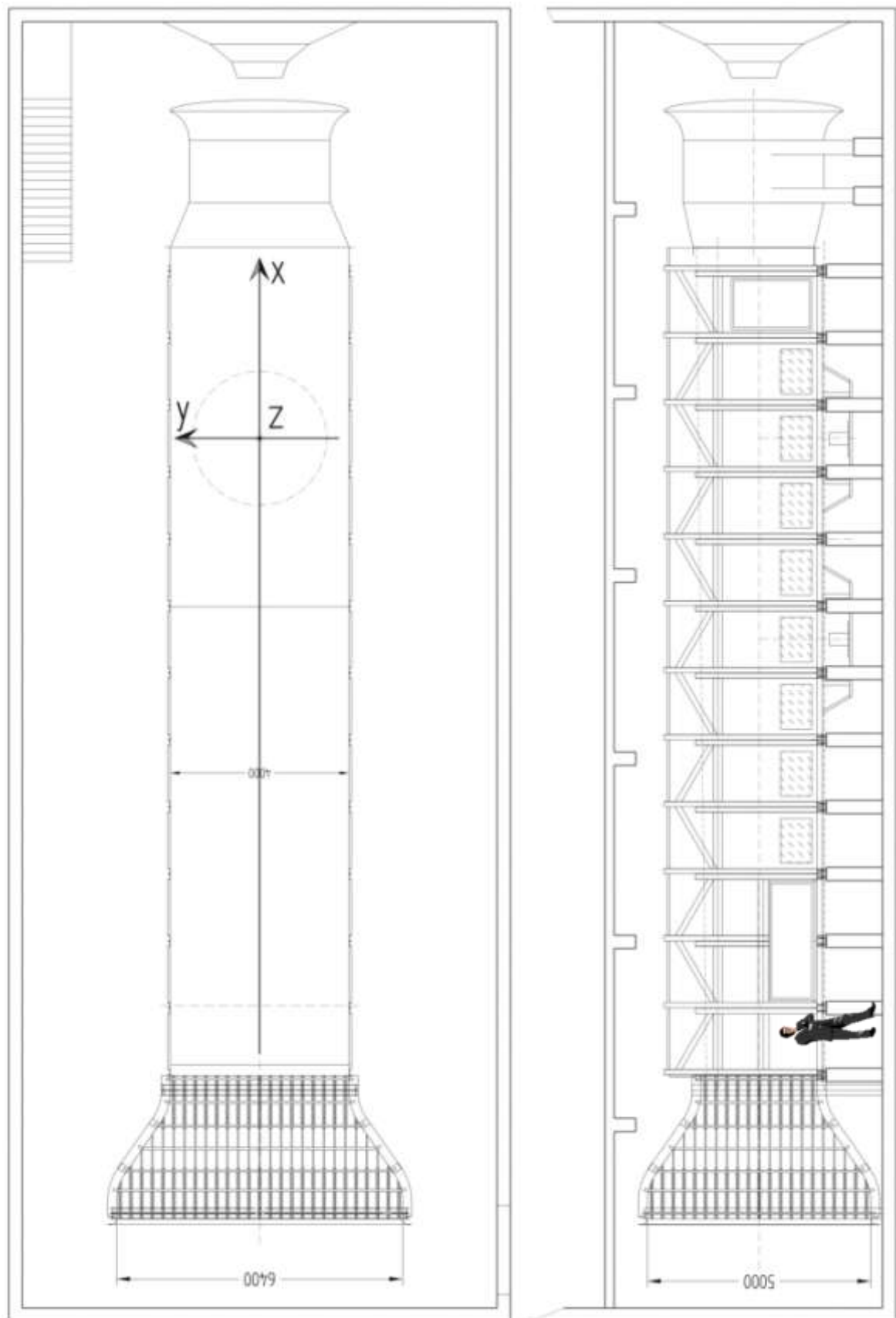


Figure 51: Technical drawing of wind tunnel WOTAN in EWTL Hamburg. Left hand side: top view/ right hand side: lateral view, z denotes the vertical component



Figure 52: Bolund study laser-doppler-anemometry (LDA) probe and empty model area. Credit: Stephan Werk

The *test section* of the tunnel is equipped with a *computer-controlled traverse system* with positioning precision uncertainty of below 0.1 mm on all three traverse directions. These information and more details on the wind tunnel facility are given in Leitl et al., [2009].

Wind tunnel instrumentation and hill model

In Figure 53, the set-up which was used for the LDA-based flow measurements in WOTAN is illustrated schematically. The technical principle of the LDA-measurements is the same as in the pilot study (pp. 136).

The *reference wind velocity* is measured at the Prandtl tube (= pneumatic probe) which monitors the free-stream approach flow velocity. The Prandtl tube is located at the wind tunnel inlet, in 320 mm longitudinal model scale distance to the plane spanned by the spires. Laterally, it is located in between of the 4th and 5th spire in order to minimize turbulence or blockage effects of the turbulence generators (Figure 49). The height of the Prandtl tube is 1740 mm in model scale above floor (435 m full scale). The wind velocities and standard deviations obtained in the model flow are divided by the *reference wind* speed measured at the Prandtl tube. The *mean of the reference wind* speed is denoted with U_{ref} .

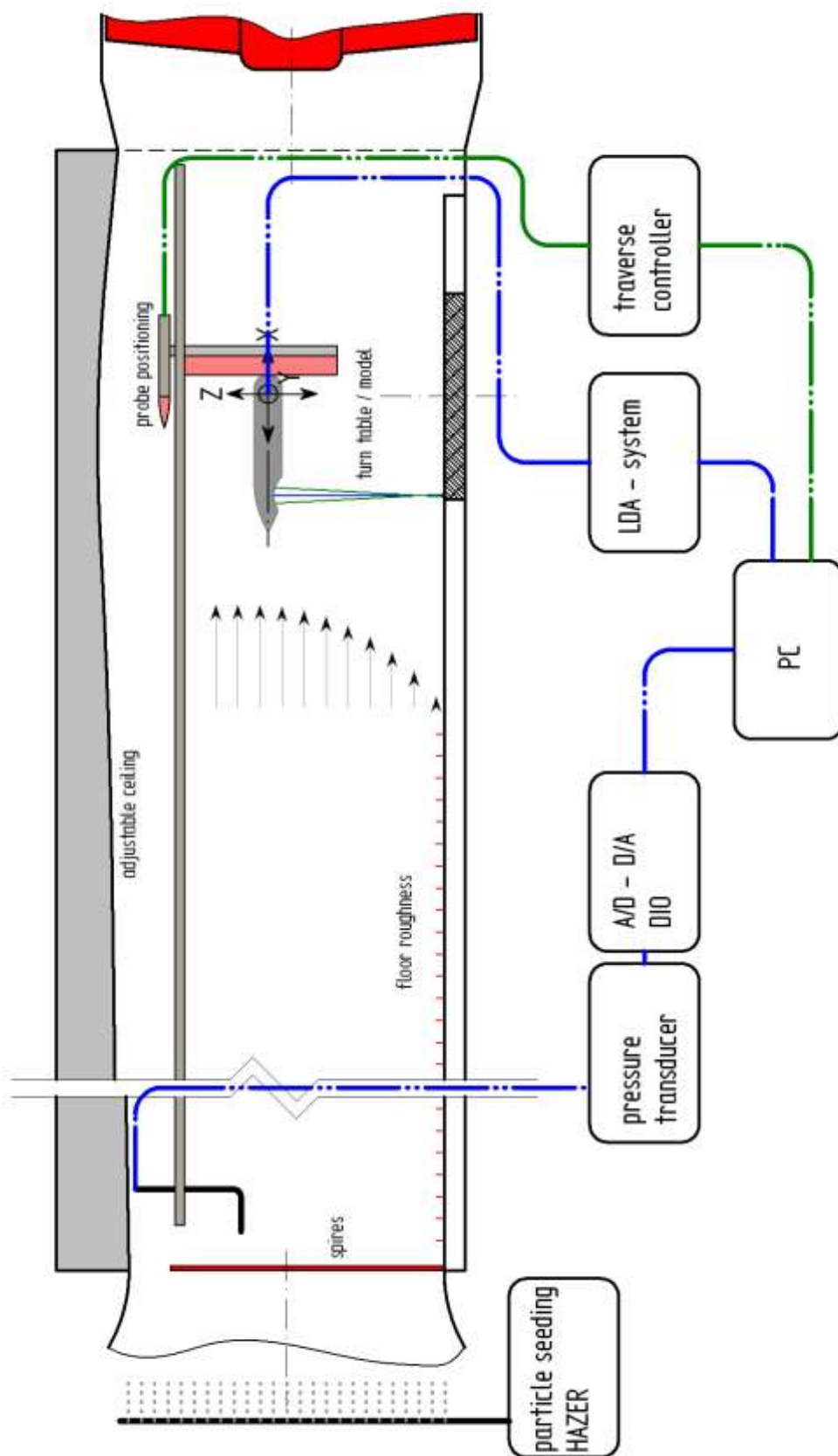


Figure 53: Scheme of the general set-up for flow measurements in WOTAN, EWTL Hamburg

The division of the velocity at a point in the flow geometry by the mean wind tunnel reference velocity can also be called “to non-dimensionalise.”⁶⁷ For data comparison, the non-dimensional wind velocities can be translated into full-scale by means of a second reference location. For example, the second reference location can be chosen in the horizontally homogenous atmospheric boundary layer inflow at height 20 m. For data comparison, the concrete reference location can be assumed at: $(X,Y,Z) = (-181 \text{ m}, -103 \text{ m}, 20 \text{ m})$ in full scale coordinates, which corresponds to the (X,Y) -position of inflow mast M0, see Figure 54. With this reference location the multiplication of all non-dimensional flow results of Bolund in WOTAN with 14 m/s yields full scale velocities reassembling field scale conditions with 10 m/s mean velocity in $z = 20 \text{ m}$ height at M0.⁶⁸

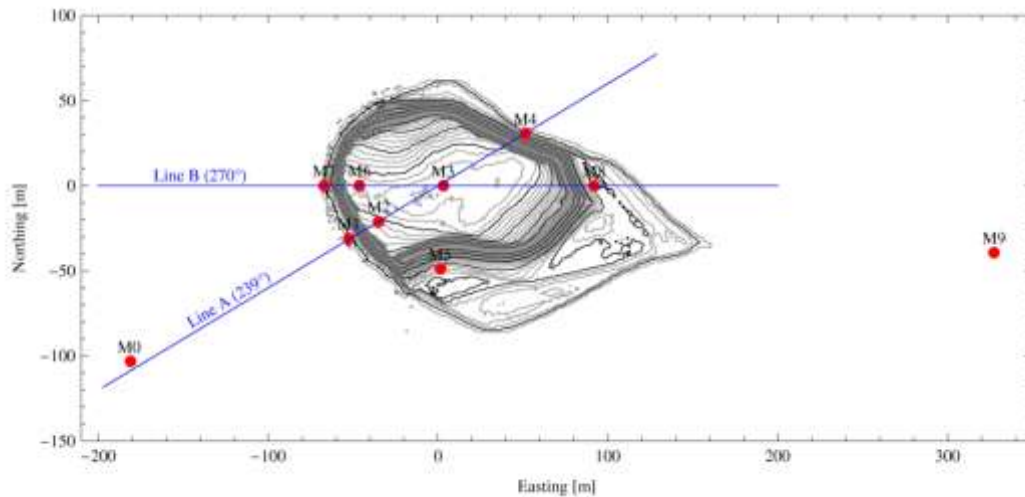


Figure 54: Bolund measurement positions of field study and corresponding wind tunnel study, with friendly permission of Bechmann et al., [2011].

The model hill was manufactured in two pieces out of styrodur 3050, in a milling machine with precision of 1 mm steps contour lines, corresponding to 25 cm geometrical resolution in full scale (Figure 55 and Figure 56).

⁶⁷ The term “dimension” refers here to the dimensions of the vector space spanned by the SI-units which are used for the treatment of the physical problem. The background is given on pp. 37.

⁶⁸ The non-dimensional velocity in the second reference location is around 0.72. The non-dimensional reference velocity at the Prandtl-tube is 1. Hence, $1/0.72 \approx 1.4$ is approximately the ratio of the Prandtl tube reference velocity and the reference velocity at the second location.



Figure 55: Bolund hill model in 1:250 and LDA probe in wind tunnel WOTAN. Credit: Stephan Werk

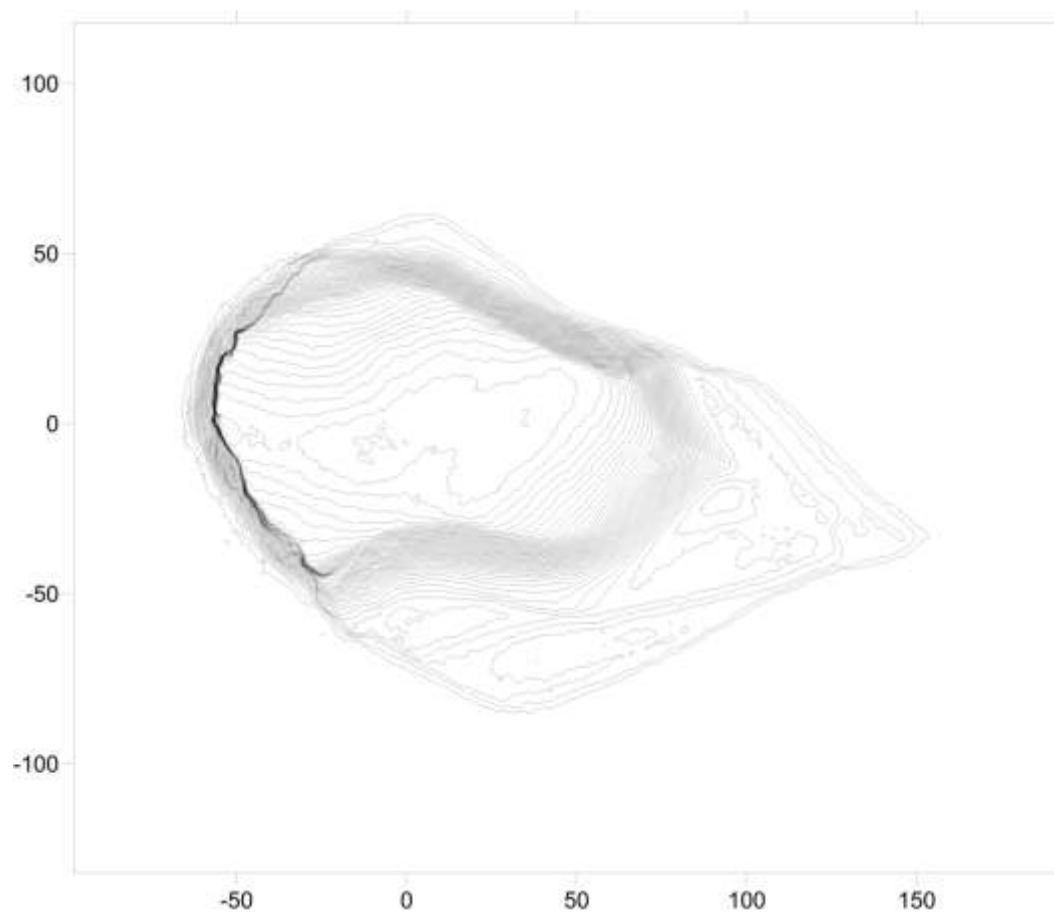


Figure 56: Bolund contour lines with 25 cm vertical resolution (full scale) and the coordinate system of the field study in meters (full scale)

As in the pilot study, the model was painted with *black, matt colour* for *minimising noise* in measurements due to reflection of LDA measurement beams. In order to enable measurements of two inflow directions, Line A and Line B (see Figure 54), the model hill was mounted on a turn table which is embedded in the floor of WOTAN, (Figure 55). The model hill was positioned with the centre point, M3, on the centre point of the turn table.

The *measurement positions* for the wind tunnel study were chosen based on those of the *field study measurement positions*. The X,Y-coordinates of the vertical profiles in the field study (and also the heights above ground level) have mostly *non-integer* values (in full scale m). This means for example that a measurement position in the field study which *appears to be* on the centre line is not perfectly located on the centre line $y = 0$, but shifted to the side by 1.4 m. However, to overcome errors due to *spatial displacement*, the *exact* field measurement positions were taken into account for the Bolund wind tunnel study in WOTAN, with resolution of 0.1 m in field scale. The access to the detailed *measurement positions* is shortly described in the following section. (This includes the access to the *time series* of the flow measurements of the Bolund experiment in WOTAN.) The table is not shown here because of its large size.

Bolund hill inflow conditions

In order to set-up plausible Bolund field *inflow conditions* in the wind tunnel, first, *consistent* and *realistic* inflow conditions and meteorological parameters have to be determined. This is substantiated in the following section. The *adjustment of plausible inflow conditions* in WOTAN is outlined in the section thereafter.

Determination of plausible inflow conditions

For the WOTAN experiment of the real Bolund hill site, the inflow area (for the significant two main inflow wind directions) is assumed to be *water surface* in *neutral* stratification. In order to determine the meteorologically *consistent* inflow conditions, *literature* is reviewed for *characteristic* parameters corresponding to the Bolund hill site. For the characteristics of atmospheric turbulence in neutral atmosphere, ESDU 85020, [2001], and VDI, [2000], is consulted⁶⁹, as well as Counihan, [1975]; Davenport, [1963] and Snyder, [1981], and the recommendations of the Bolund blind comparison, [Bechmann et al. 2009]. For an overview on the literature values of characteristics according to real Bolund inflow see Table 8, p. 180. Additionally, the original Bolund data is analysed with friendly permission of Risø DTU.

The reason for not only relying on the suggested inflow conditions by the field study are that information is missing and that the available Bolund field data shows large ambiguities (recall the analysis with the *inverse non-stationarity measure* in chapter 5, p. 95). From the perspective of this work the available data does not represent *statistically robust* and meaningful *narrow intervals* as boundary conditions for models which demand for *statistically stationary inflow conditions*. (More remarks on the Bolund field data are given on pp. 229.)

In Bechmann et al., [2009], four inflow directions are analysed. Only “case 1” and “case 3” are suggested to be modelled by *physical modellers*⁷⁰. According to this suggestion, Line A (“case 1”) and Line B (“case 3”) are modelled in the WOTAN wind tunnel. In order to extract inflow conditions, the following filter methods are applied to the Field Data, see Table 7.

⁶⁹ In the following also abbreviated with “VDI”

⁷⁰ Numerical modelers were required to model all four flow directions.

Table 7: Bolund field data filtering for Line A and B;

Measurement Instrument	location/	Filter
M0Z05S		Case 1 – (Line A)
		262° < DIR < 278°
		Case 3 – (Line B)
		231° < DIR < 247°
M0Z05S		invL < 0.004/m
		$U_{\text{mean}} > 6 \text{ m/s}$
		$4.5 < \text{TKE}/u_*^2 < 8.5$
M0Z05C		$6 \text{ m/s} < u_{\text{mean}} < 12 \text{ m/s}$
Water level		$0.35 \text{ m} < \text{water level} < 1.15 \text{ m}$

As summarized in Table 7, the sonic anemometer at mast M0 (“M0”) in five meters height (“Z05”) is chosen as *reference point* for the wind directions. This data is the 10 minutes mean wind speed computed from the 20 Hz sonic raw data (“S”). Before computing the average, the data is corrected following the guidelines of the manufacturer [Bechmann et al., 2011]. Furthermore, the horizontal, lateral and vertical wind vector is aligned with respect to the *inflow line*. Case 1 refers to *Line B*, case 3 to *Line A*. The range of wind directions is filtered for $270^\circ \pm 8^\circ$, case 1, and $239^\circ \pm 8^\circ$, case 3, see also Bechmann et al., [2011].

Nearly neutral conditions are searched for by the invers of the Monin Obukhov Length in the interval $\text{invL} \in (-0.004 \text{ m}^{-1}, 0.004 \text{ m}^{-1})$. Exclusively wind speeds larger than 6 m/s are considered. This is intersected with 10 minute averaged 5 Hz data from the cup anemometer at M0 in 5 meter height for wind speeds $u \in (6 \text{ m/s}, 12 \text{ m/s})$ [Bechmann, 2009].

Furthermore, only situations with *low turbulent kinetic energy* are considered, explicitly $\text{TKE}/u_*^2 \in (4.5, 8.5)$. *Water level* is taken into account in an interval of $\pm 0.4 \text{ m}$ around 0.75 m, which is chosen as *fixed reference level*.

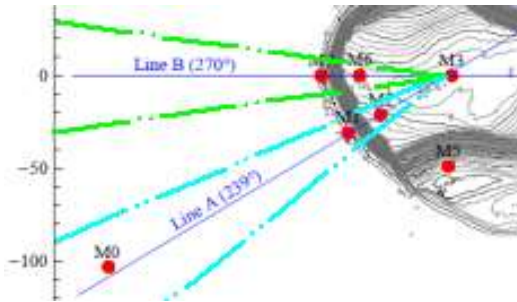


Figure 57: Illustration of Line A and Line B sectors of inflow directions

From this filtered data, the following inflow conditions are derived by Bechmann, [2009]:

Blind Comparison Inflow:
$z_0 \text{ [m]} = 3 \cdot 10^{-4}$
$u_{*0} \text{ [m/s]} = 0.4$
$\text{TKE}_0 / u_{*0}^2 = 5.8$

For the determination of plausible Bolund inflow conditions for the wind tunnel study, these values are compared with those from literature, see Table 8. It is found that the *roughness length* lies within in the intervals of literature values. However, no information on the *power law exponent*, on the *standard deviations of the velocity components*, on the *boundary layer depth*, for the *integral length scales* or *fluctuations of wind directions* are provided by Bechmann, [2009]. The power law exponent, standard deviations, boundary layer depth and integral length scales are hence based on literature (see following chapter).

The *integral length scale*, Lu_x , is a measure for the size of the *largest* eddies and is difficult to be assessed with field data (see Dias et al., [2004], for remarks on problems with existence). Estimates for *integral length scales* collected from various field measurements can be found in Counihan, [1975], see Figure 58.

Table 8: Comparison of Bolund blind test inflow and literature values

	VDI, [2000] (slightly rough)	Snyder, [1985]	Other	Bolund blind test
z_0 [m]	10^{-5} - $5 \cdot 10^{-3}$	$3 \cdot 10^{-6}$ – $5 \cdot 10^{-3}$ (1.5 m/s – 15 m/s mean wind speed at z = 10m)		$3 \cdot 10^{-4}$
α	0.08 - 0.12			X
u_{*0} [m/s]				0.4
boundary layer depth		See figure “12.” depends on G = geostrophic wind speed $G = 5$ m/s 500m $G = 10$ m/s 800 m 1) 50 -100 m 2) 80 – 160 m	Davenport, [1963]: 300 m for $z_0 = 0.03$ m Counihan, [1975]: 600 m	X
surface layer depth (10 – 20 percent of boundary layer depth)			30-60 m (Davenport) 60-120 m (Counihan)	X
TKE_0 / u_{*0}^2	$\sigma_u = 1$, $\sigma_v = 0.75$, $\sigma_w = 0.5$			5.8

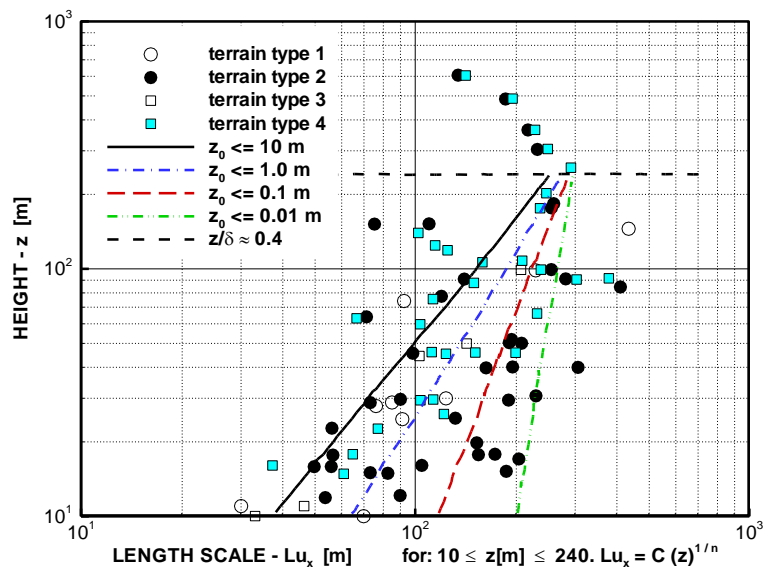


Figure 58: Adopted from [Counihan, 1975 - Figure 11 in the reference]

Furthermore, the given z_0 of the Bolund Blind Comparison is checked directly with the *Bolund field data*. For this, 10 minutes mean sonic data and cup data at M0 are used.

Explicitly, at mast M0, 10 min averages of Sonics in 5m and 12m height, for nearly neutral conditions, i.e. $|\text{invL}| < 0.002$ and wind direction Fetch $270^\circ \pm 8^\circ$, are searched for⁷¹.

For a rough estimation, 12 cases are randomly picked out of the result set. With these, z_0 , and, α , are computed with least squares log-linear fits. The same is done for 10 minute mean cup data of 2 m, 5 m, 9 m and 15 m height, see Figure 59. The plausible area of z_0 and α which is covered by VDI, [2000], or Snyder, [1985], is marked with a green boundary. Some results lie well within this area, others have a significantly lower z_0 .

The estimation of z_0 and α from just two or four sampling heights is imprecise. The variability of the results is high and is consistent with the variability of the Bolund data examined by the *influence of the filtering conditions on the sampling size* and the large *inverse non-stationarity measure* (pages 92 and 95). The only information that can be extracted from the rough estimation for, z_0 , and, α , is the following: the apparently low roughness length of $3 \cdot 10^{-4}$ m is supported by the field data or can even be assumed as being smaller.

⁷¹ As an example, the Structured Query Language (SQL) expression for searching the SQL Bolund data base for data of the sonic in 5 m height (with respect to the meteorological conditions which are named in the text) is as follows:

```
SELECT s.Name, s.Sonic_id, s.u_mean, s.windDir, ss.Name, ss.Sonic_id, ss.invL
FROM stat_nesw_metek3dcorr_10min s, stat_stability_metek3dcorr_10min ss
```

```
WHERE s.Name=ss.Name AND ss.Sonic_id='M0_S_5' AND s.Sonic_id=ss.Sonic_id AND s.windDir>262 AND
s.windDir < 278 AND ABS(ss.invL)<0.002
```

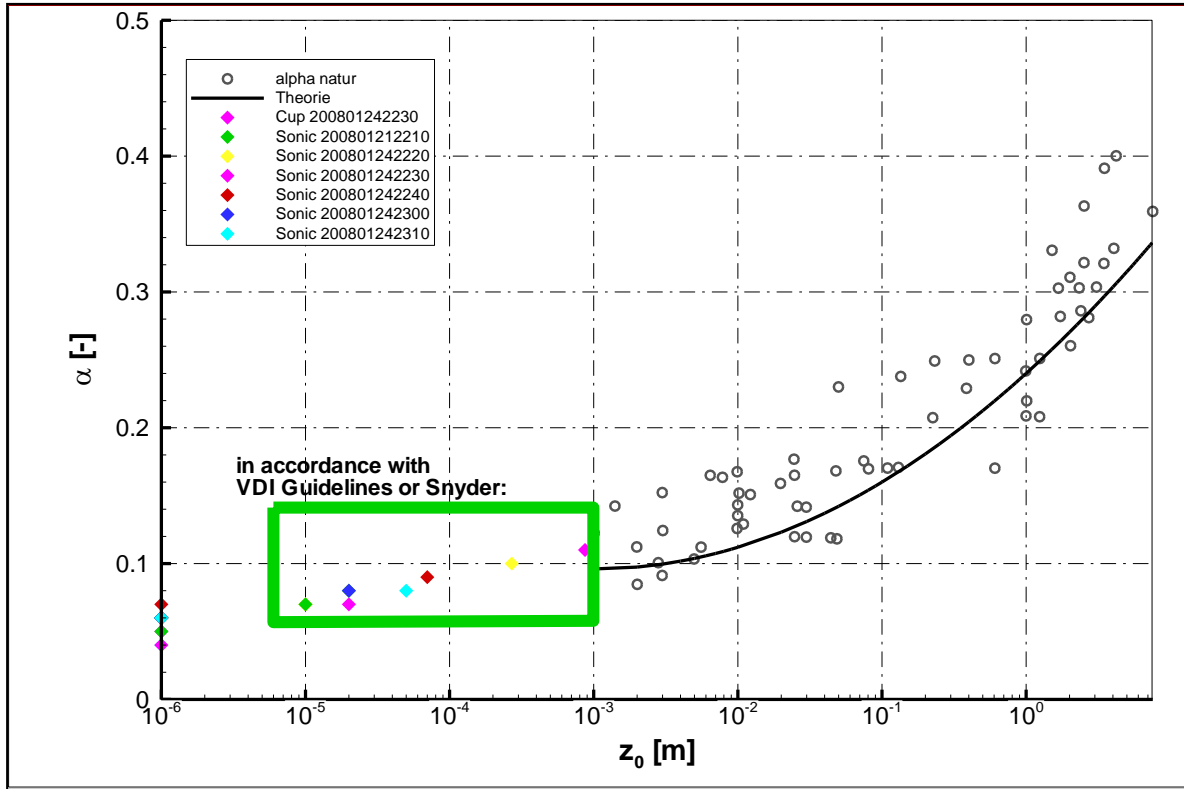


Figure 59: Relationship between roughness length and profile exponent alpha for the Bolund field data (coloured rhombuses) and other field experiments (blank circles)

Concerning the plausibility of the predefined *turbulent kinetic energy*, it has to be remarked that the reference value which was chosen in Bechmann et al., [2009], and denoted with TKE_0 , is assumed to be *constant* with height in Bechmann et al., [2009]. It is questionable whether this assumption is physically plausible. Literature values of VDI, [2000], are consulted for the determination of vertical profiles of intensities. Both references can be linked with a rough estimation:

Consider the reference values given in Bechmann et al., [2009], for turbulent kinetic energy and friction velocity;

$$TKE_0 / u_{*0}^2 = 5.8, \text{ and}$$

$$u_{*0} = 0.4 \text{ m/s},$$

This yields

$$TKE_0 = 5.8 \cdot 0.16 \approx 0.93 \text{ (m/s)}^2$$

The definition of turbulent kinetic energy used here is:

$$k = \frac{1}{2} \sum_{i=1}^3 (\overline{u_i' u_i'})$$

with a rough estimation as *lower* boundary:

$$(u_{rms})^2 = \overline{u_1' u_1'} \approx \overline{u_2' u_2'} \approx \overline{u_3' u_3'}$$

This yields

$$k \approx \frac{1}{2} \sum_{i=1}^3 3(u_{rms})^2$$

hence

$$I_u = u_{rms}/u \approx (\sqrt{2/3 k})/u$$

thus for full scale velocities, u , between 5 m/s and 15 m/s and $k = 0.93$

$$0.05 < I_u < 0.16 \quad .$$

This is a rough estimation; see chapter “Adjustment of Bolund inflow conditions”, pp. 184 for the actually used literature values. The Prandtl layer height is expected to be low in the Bolund case. Following the literature mentioned above, 50 meters height is assumed to be reasonable, see table Table 8, p.180.

It would have been desirable to examine the *fluctuations of the wind direction* as well, in order to compare the low frequency directional variations. Pascheke et. al, [2002], state that “It is often claimed that wind tunnels cannot replicate low frequency wind directional variations since the flow is ducted by solid side walls. We feel that this physical notion needs some revision”, [ibid, p. 80]. Pascheke et. al, [2002], examine the directional variations and obtain a positive results. It would have been desirable to support these results in the Bolund case with a similar analysis. However, the reference values of Pascheke et al., [2002], cannot be transferred to Bolund in WOTAN since the *urban boundary layer* in Pascheke et al., [2002], is significantly distinct from the *smooth water surface* in the Bolund case. However, this information was not accessible from the Bolund field data when the inflow was modelled⁷² and values are not found in the literature.

⁷² Now, reference values could be obtained from the raw Bolund field data. However, this would require further post processing and a thorough analysis of the data, which remains open for future work.

Adjustment of the determined inflow conditions

As stated before, the adjustment of *meteorologically consistent* boundary conditions is essential for the proper modelling of *atmospheric boundary layer* flow over any model area since the flow results depend on the boundary conditions. The *consistent combination* of all of the following parameters is checked for the Bolund wind tunnel experiment:

- Vertical mean velocity profile including
 - *vertical log law* wind profile with proper
 - *roughness length*, z_0 ,
 - *friction velocity*, u_*
 - *power law exponent*
- Turbulence profiles including
 - *vertical profiles of standard deviation (or turbulence intensities)* of all three velocity components
 - *vertical profiles of turbulence spectra*
 - *vertical profiles of integral length scales*
- Surface layer height
 - *constant shear layer* – which is assumed to be valid in the Prandtl layer
- Horizontal (lateral and longitudinal) homogeneity across the model area
 - *lateral and longitudinal profiles* of all meteorological parameters

A remark should be added: assumed that consistent inflow conditions are determined, it is *not clear*, whether or not these inflow conditions *can be* experimentally reproduced in the wind tunnel by means of the *turbulence generators* in combination with the *roughness elements*. The *process loop* of the physical adjustment of the inflow conditions for the Bolund wind tunnel study in WOTAN is illustrated in Figure 60, p. 185. It gives an example for the concrete procedure of the consistency check of above meteorological parameters in a wind tunnel. It can be emphasised that the process is usually expected to be a *loop* for the adjustment of specific ABL conditions, see also appendix, pp. 304.

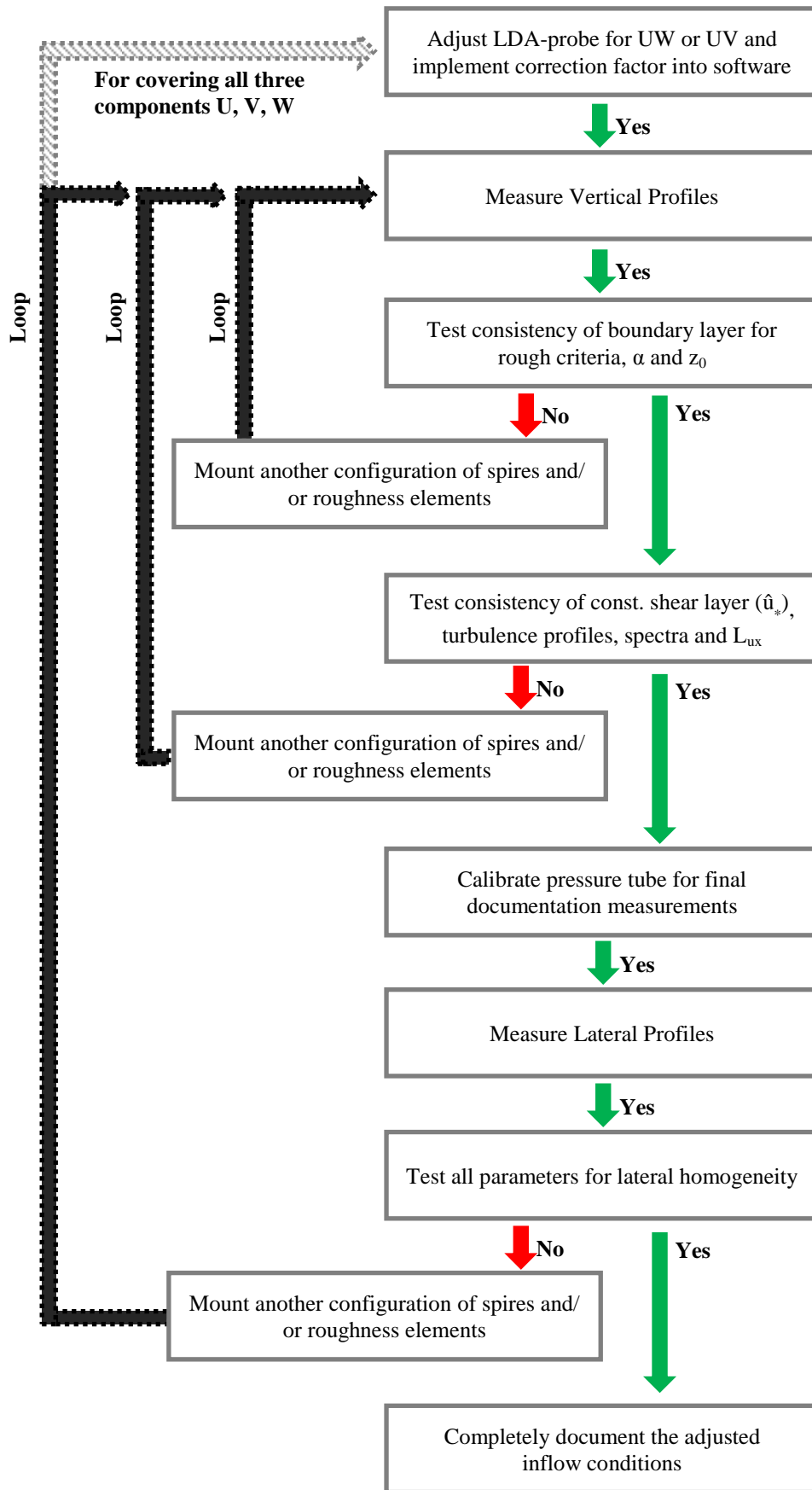


Figure 60: Wind tunnel process loop for the experimental set-up of a consistent atmospheric boundary layer as inflow conditions (previous page)

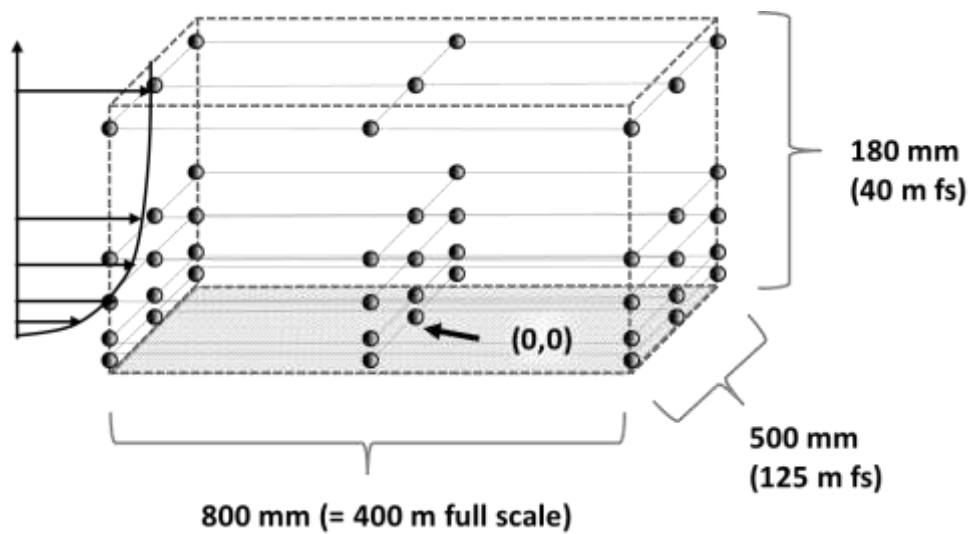


Figure 61: 3x3-measurement-grid for the check of horizontal homogeneous flow in the Bolund hill model area

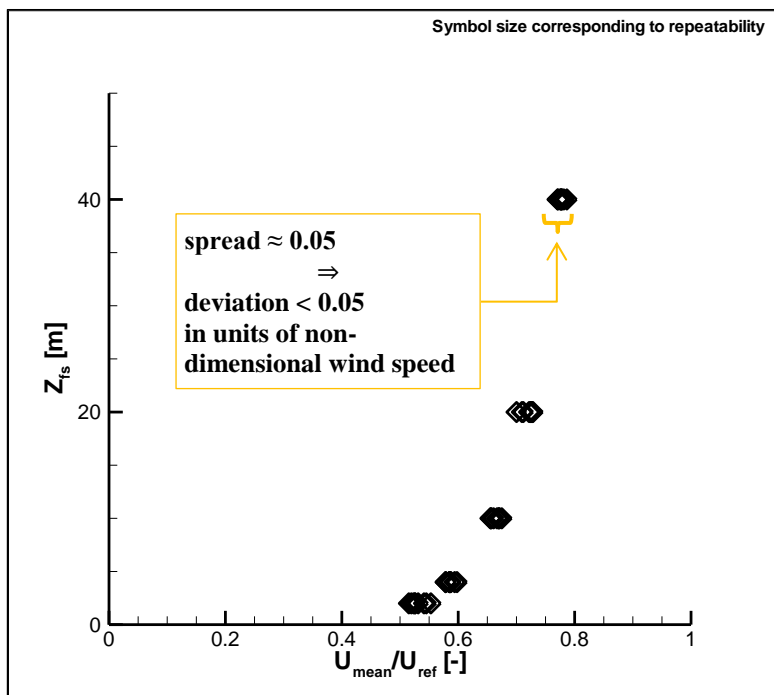


Figure 62: The black rhombuses show the spread of the vertical profiles at nine positions in the model area (along the 3x3-measurement-grid for check of horizontal homogeneous flow in model area); height is in field scale metres; symbol size corresponds to a generous (upper) estimate for the repeatability (precision). The vertical mean wind speed profile deviates from horizontal homogeneity below 0.05 in units of non-dimensional wind speed. For a free stream velocity of 10 m/s this reassembles wind velocities around 0.5 m/s in full scale.

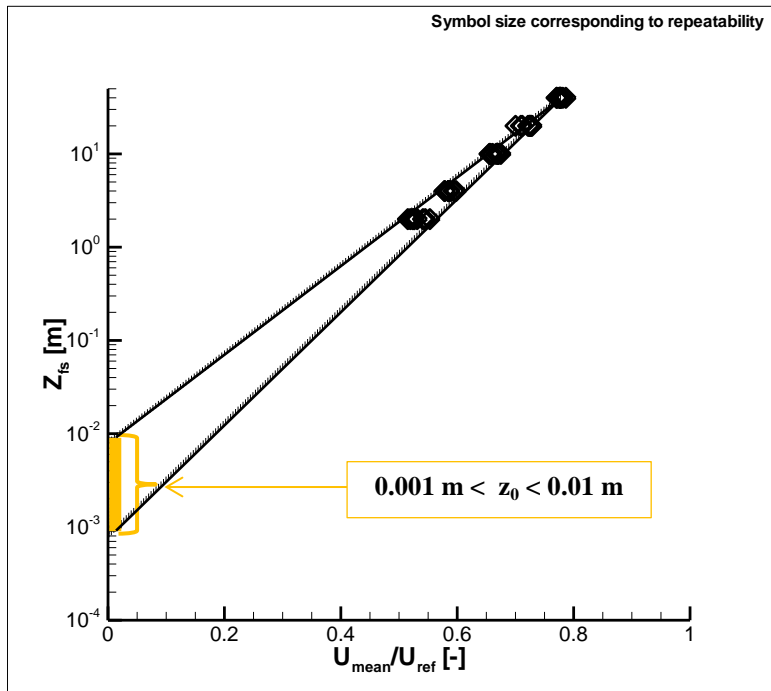


Figure 63: The black rhombuses show the homogeneity spread of the vertical profiles in log-linear axis scale. Consideration of the spread of the horizontal homogeneity of the vertical mean velocity profile in the main Bolund WOTAN study leads to an estimation of z_0 between 0.001 [m] and 0.01 [m] in full scale and hence matches the determined inflow conditions.

In order to test the *horizontal homogeneity*, the ABL conditions in the wind tunnel are measured along *horizontal slices*. Each of the slices spans a plane of ± 200 m in longitudinal direction and ± 62.5 m in lateral direction. The span indicates the length in full scale around the centre point, which is M3, or more precisely, $(X,Y)=(0,0)$, Figure 61. On each plane, a 3x3 grid is measured, see also Figure 61. All measurements of the 3x3 grid are plotted into the Figures for the visualisation of the *horizontal homogeneity*.

The *vertical mean wind profile* of the Bolund inflow in WOTANT is illustrated in Figure 62. The repeatability deviation is assumed to be 0.05 in non-dimensional wind speed (symbol size; around 0.5 m/s in field scale). This is a generous (upper) *estimation* within the spread of the repeatability deviations and around 3 times larger than the *average* value, see pp. 194. The important point here is that this estimation almost covers the *spread* of the *horizontal homogeneity test* (and hence covers almost the *inhomogeneity*.)

As illustrated in Figure 63, the vertical mean wind profiles of the Bolund inflow in WOTAN, with consideration of precision and horizontal homogeneity, lead to an estimation of a *roughness length* of $0.01 \text{ m} < z_0 < 0.001 \text{ m}$. (With best exponential fits, a power law exponent of $\alpha \approx 0.12$ can be achieved; power-law-fit is not shown here.)

Turbulence intensities, spectra, integral length scales and the *shear stress layer* are illustrated in Figure 64 to Figure 68 – and are within the boundaries of the determined inflow conditions. The *turbulence intensity*, I_u , see Figure 64, is calculated as the *standard deviation* (also: root mean square error) of the u velocity component at a certain height, z , divided by the mean wind speed at the same height, z . This distinguishes the vertical profile of the *turbulence intensity* from the vertical profile of non-dimensional *standard deviation* (*standard deviation* at height, z , divided by the *reference wind speed*.) Since both parameters are not always clearly distinguished, in literature, here, both values are computed and shown. Figure 64 illustrates that both values fit into the recommendations of VDI, [2000], for *smooth* (slightly rough) inflow.

Accordingly, in Figure 65 and Figure 66, the vertical profiles of I_v and v_{rms} , respectively I_w and w_{rms} , are plotted. As shown in Figure 65 and Figure 66, the V- and W-components of the turbulent WOTAN Bolund inflow fit into the corridor of the recommended values of VDI, [2000], for *smooth* (slightly rough) inflow. In addition, it can be noticed that the average *turbulence relations* of $u_{rms} : v_{rms} : w_{rms} = 1 : 0.73 : 0.4$ (average per height), correspond reasonably to VDI-recommendations of around $1 : 0.75 : 0.5$ for meteorologically consistent atmospheric boundary layers.

Legend:

- VDI slightly rough (lower bound)
- VDI moderately rough (lower bound)
- VDI rough (lower bound)
- VDI very rough (lower bound)
- VDI very rough (upper bound)
- ◇ Bolund WOTAN data (normalized standard deviation)
- Bolund WOTAN data (turbulence intensity)

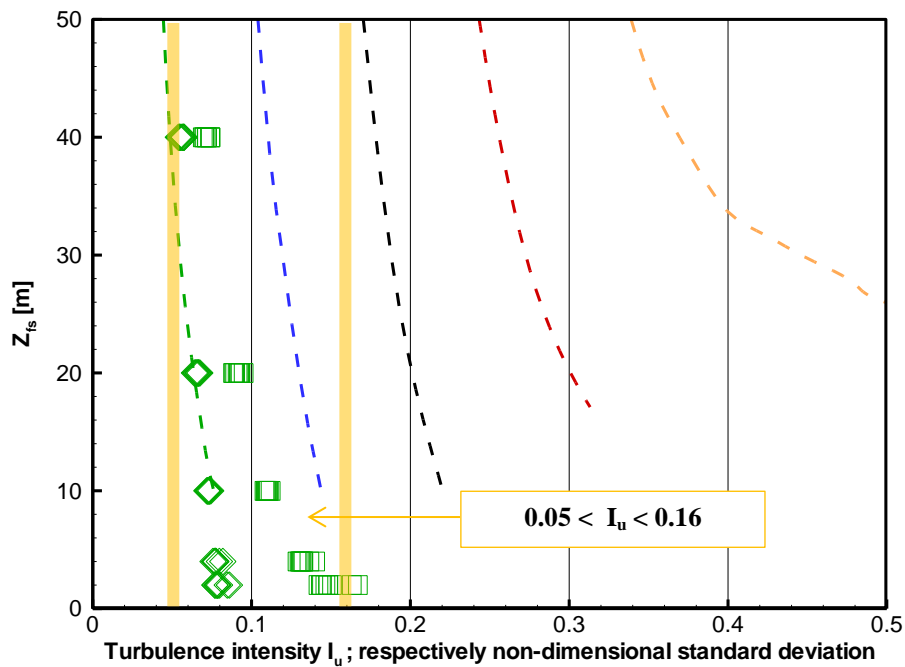


Figure 64: The x-axis illustrates turbulence intensity in U direction, the plain rhombuses show the root mean square errors of the U-component divided by the reference wind speed, the plain squares represent the root mean square errors divided by the mean wind speed at the same point (usually this is understood as turbulence intensity, but there is sometimes other use of this terms in literature.); The y-axis illustrates the height in full scale [m]. The dotted lines show the corresponding VDI ideal lines for smooth surface to rough surface from left to right. The symbol size is chosen corresponding to estimated short term repeatability. The spread of the measurements shows the horizontal homogeneity of the 9 positions in the 3x3-measurement-grid. The orange corridor shows the estimate for the Bolund field data, see p. 183.

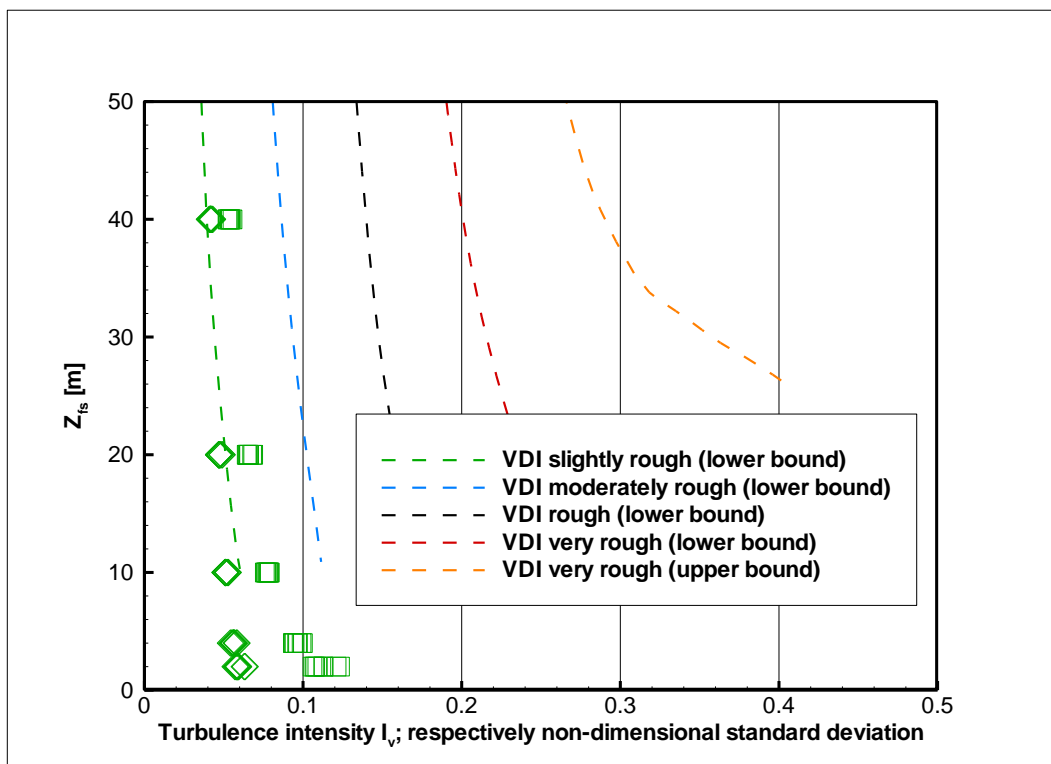


Figure 65: The x-axis illustrates turbulence intensity in V direction; the plain rhombuses show the root mean square errors of the U-component divided by the reference wind speed, the plain squares depict the root mean square errors divided by the mean wind speed at the same point; (legend see previous Figure)

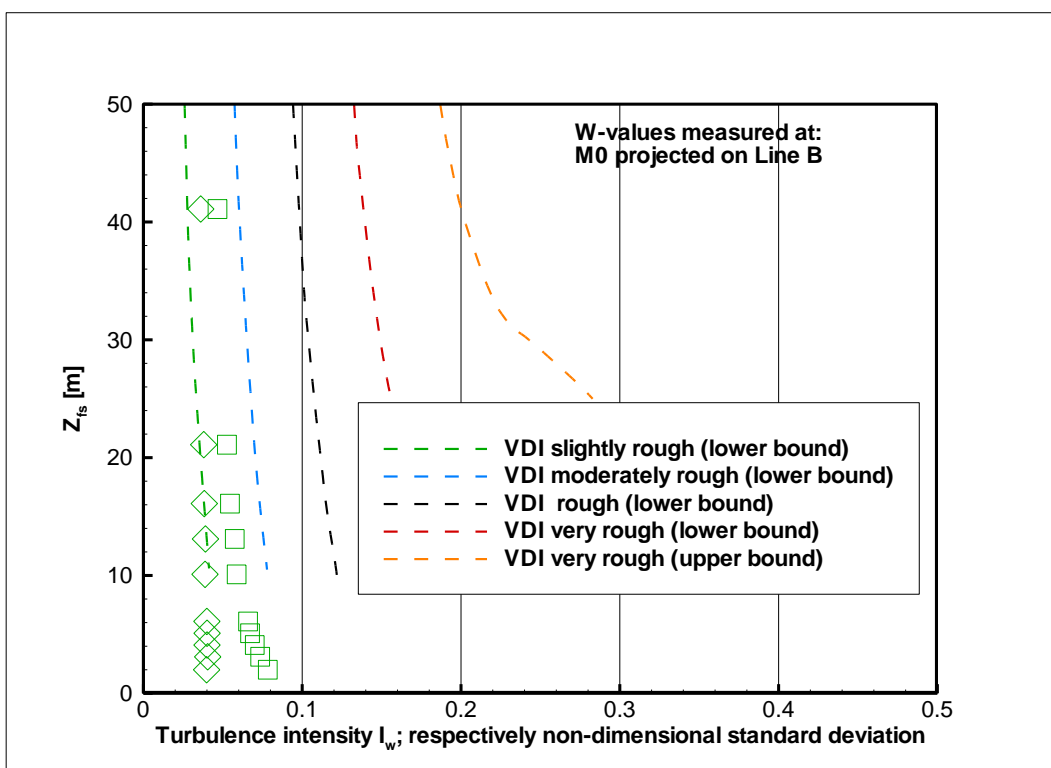


Figure 66: The x-axis illustrates turbulence intensity in W direction; the plain rhombuses show the root mean square errors of the U-component divided by the reference wind speed, the plain squares depict the root mean square errors divided by the mean wind speed at the same point; for the reference lines, see the legend.

The integral length scales of the WOTAN Bolund inflow at $z = 10$ m; 20 m; 40 m are shown in Figure 67. Details of the computation are given in Fischer, [2011]. Theoretical values are indicated by lines (see legend of the figure). As it can be seen in Figure 67, the spread of the horizontal homogeneity is around 10-25 percent and the theoretical values are not clearly matched. The reason for this can be that the turbulence spectrum is cut for *low frequencies* due to the *physical boundaries of the wind tunnel*, (recall the introduction into wind tunnel modelling, chapter 3). Recall that *geometrical scaling* of the inflow and the *size of the wind tunnel* are linked for this reason. Since WOTAN is one of the largest atmospheric boundary layer wind tunnels in Europe, the achieved values are most likely close to the optimum which can, for scaling 1 : 250, be achieved in nowadays average wind tunnel laboratories. Furthermore, Figure 67 clearly shows that the distribution of the field data partly contradicts the theoretical values.

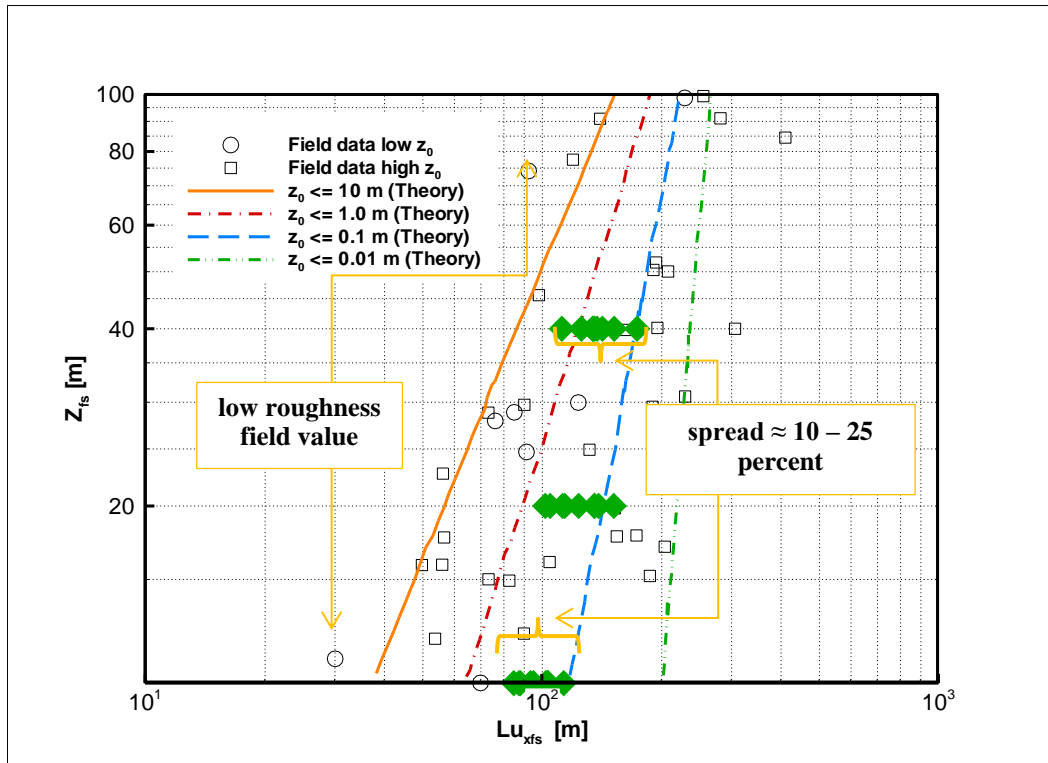


Figure 67: Green rhombuses indicate wind tunnel values for the integral length scales at the 9 measurement positions of the 3x3-measurement-grid for the check of homogeneity; plain circles show exemplary field data for low respectively high roughness length (see text) For the estimation of the spread: mind the log-scale.

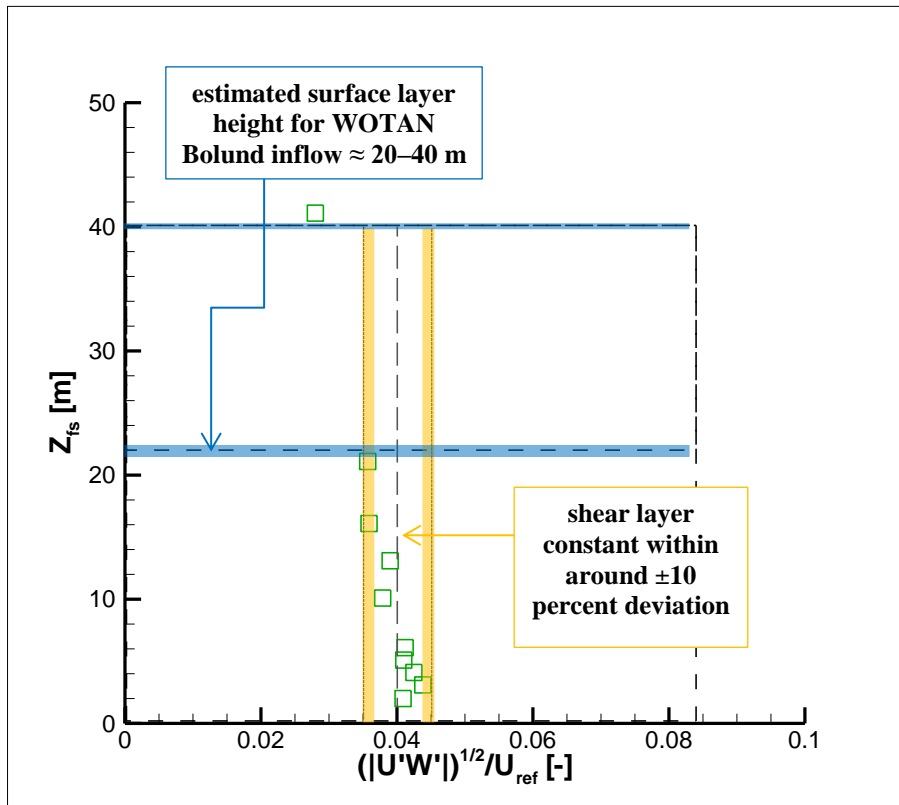


Figure 68: The green squares show the horizontal shear stress profile of WOTAN Bolund inflow with estimated repeatability (precision) of around 5-10 percent (indicated by symbol size) and an estimation of the constant shear layer yielding a 20-40 m height.

The homogeneity spread of 10-25 percent (Figure 67) for the *integral length scale* shows that this parameter is *more sensitive* on the measurement location than e.g. the mean vertical profile. In addition it is difficult to be assessed with field data, and hence only serves as a rough measure (as stated before, see Dias et al., [2004]).

The *surface layer depth* can be estimated from the *shear stress* values in Figure 68. The literature values vary between 30-160 m, depending on mean wind speed. A depth of around 20-40 m was realized as *surface layer* in the wind tunnel as indicated by Figure 68. This is at the lower boundary of the recommended values. However, the estimated WOTAN Bolund inflow *surface layer* completely covers the height of the hill (which is around 12 m field scale). It might be taken into account that the repeatability or homogeneity deviation is likely larger than ± 10 percent for the *shear stress*. Reason for this can be, on the one hand, the physical inhomogeneity of these parameters in the WOTAN inflow. Another reason can be an error imposed by *statistical convergence*. Here, this was not investigated further and

the analysis of the constant shear layer in Figure 68 was taken as an indicator for the sufficiently deep surface layer.

In Figure 69, the spectra for the WOTAN Bolund inflow are shown at *different heights*, obtained from time series measured at the *centre point* of the turn table. Details of the computation are given in Fischer, [2011]. As it is shown in Figure 69, the spectra are slightly shifted to lower frequencies with increasing height and fit up to 20 m (in field scale) into the boundaries of the recommended VDI-values. (This can be expected due to the increase of low frequency turbulence fluctuations with height.)

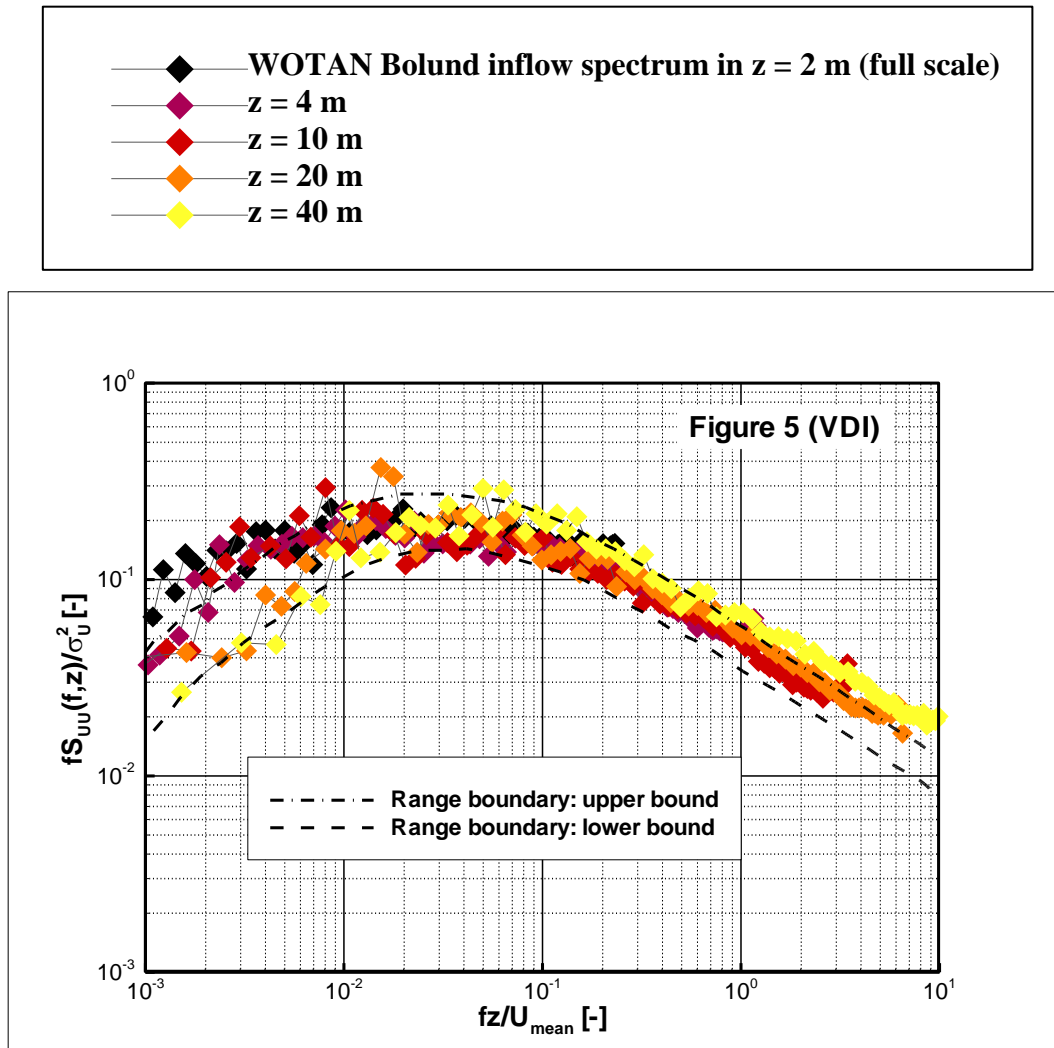


Figure 69: Spectra in the empty boundary layer at the centre point $(X,Y) = (0,0)$ in heights $z = 2$ m and 4 m (grey rhombuses) and heights $z = 10$ m, 20 m, 40 m (black rhombuses)

Analysis of precision

Recall that the “absolute error” or “accuracy” was defined as the degree of closeness of measurements of a quantity to its actual (*true*) *value*.⁷³ This is *not* a number, since the *true* value cannot be known, [JCGM 200, 2008]. The “relative error” or “repeatability” was also called “precision”. This is the degree to which *repeated measurements* under *unchanged conditions* show the *same* results⁷⁴.

Repeatability and convergence

Repeatability in the main Bolund wind tunnel experiment is defined as the deviation of repetition of measurements at the *same* measurement position with the *same* inflow conditions in the same experimental set-up (as in the pilot study). This is to give *empirical evidence* on how well the wind tunnel time series *represents* a statistical stationary stochastic process which the wind tunnel flow is assumed to be.

Deviations of the repeated measurements without variation of the Reynolds number can have different reasons. Recall that

- Any *voltage measurements* involve *basic errors*, [Bendat and Piersol, 1971].
- Measurements of a *random signal* involve a *statistical error* that depends on *sampling rate* and *measurement time*. *Convergence tests* of the time series are necessary to assure *statistical representativeness* of the results. Recall the ergodic theorem, pp. 41.
- The LDA probe used in this experiment was set-up for 2dimensional measurements. For measurements of 3dimensional wind vectors, the LDA probe has to be readjusted, i.e. rotated. The *rotation of the LDA probe* can influence the repeatability deviation of results.

⁷³ See chapter 3, p. 37, and the more extensively chapter “On error analysis”, pp. 143.

⁷⁴ Recall the distinction of the term *reproducibility*: this is the amount of repeatability of an experiment with *changed* conditions, e.g. different laboratory, different measurement technique, etc. Further on, Reynolds-number variation is included into assessment of precision, and is examined more extensively on pp. 200.

The *expected magnitude of errors* can be ordered as follows: *instrument limit of error* < *convergence error* of the time series for long enough sampling duration < *deviation for instantaneous repetition* of the measurement with same LDA adjustment < *deviation of measurements with readjusted LDA probe* and measurements taken by a *different person* with *longer time gap* between the measurements. Finally, latter is smaller than the deviation due to the *reproduction* of the experiment in another wind tunnel (also called *reproducibility*), which is not further considered at this point.

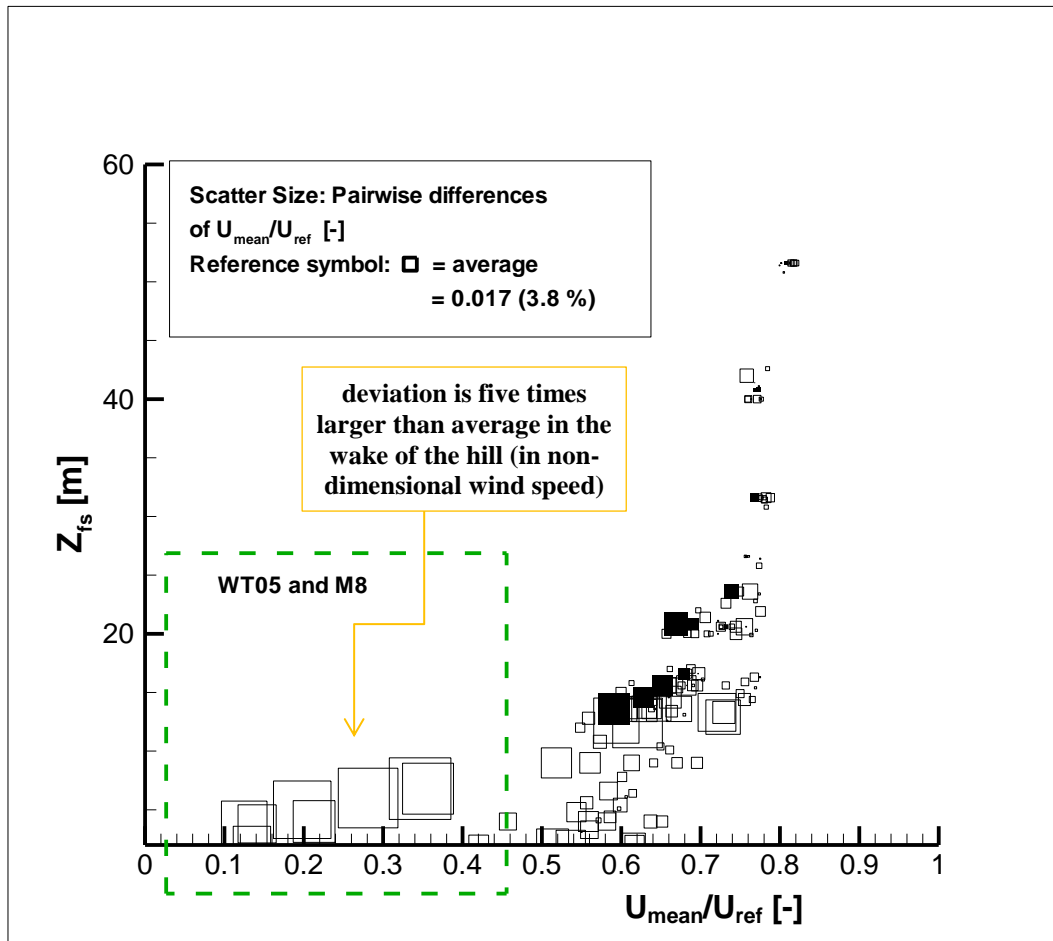


Figure 70: Repeatability of mean wind speed for the Bolund experiments in WOTAN: Scatter size symbolizes the pairwise difference of repeated measurements. The reference symbol shows the average absolute error in terms of non-dimensional mean wind speed, black squares exhibit the repeatability for the readjustment of the hill model (rotation of the turntable)

To analyse the errors, measurements at 104 characteristic locations throughout the measurement grid are *repeated*. Each of the measurements is repeated at the *same location*. The repetitions contain measurements which are repeated with *readjusted* LDA

probe. This means that one measurement contains the U,V wind vector and the other contains the U,W wind vector at the same location. Values of the U components (which are measured twice) are analysed. In Figure 70, the average absolute *pairwise differences* of the repetitions are visualized as size of the squares (see reference symbol of average deviation) and plotted against *non-dimensional mean wind speed and height*.

The computed *average absolute error* in terms of non-dimensional mean wind speed is around 0.02 and resembles an *average spread of mean wind speed* of around 4 percent. (This is e.g. an average spread of below 0.5 m/s in field scale for reference velocities of up to 20 m/s. Depending on the purpose of measurements this can be interpreted as a satisfying result.)

Figure 70 gives evidence for a significant *dependence* of the repetition error on the *mean wind speed* and the *height of measurements*. A further analysis of the data shows that the *repeatability deviation* at the points *directly behind* the hill (WT05 and M8) in terms of the non-dimensional mean wind speed is around *five times larger* (≈ 0.09) than the average error. In terms of percentage of the ensemble mean value of the average non-dimensional velocity the uncertainty is even 15-times worse (56 percent absolute spread). This can be due to the *low mean wind speed* at WT05 and M8 as it was found in the pilot study. Thus, supporting the results of the pilot study in BLASIUS, here it is found that for the interpretation of wind tunnel measurement results, the *dependence* of the measurement error on the *local flow conditions* has to be considered. In general, Figure 70 shows a *decreasing* repeatability deviation with *increasing* height of measurement location and *increasing* mean wind speed.

At last, the influence of *readjusting the hill model* (i.e. physically rotating the plate for simulating either inflow direction A or B) is considered. The average absolute *pairwise differences* of the repetitions with different inflow directions (rotation angles of the turn table) are denoted with filled squares. Figure 70 shows that the *readjustment of the hill model* does not influence the repeatability significantly since the deviations are within the spread of the general repeatability.

The results for the repeatability of the *mean velocity of the longitudinal component* are supported by the results for the repeatability of the *standard deviation of the longitudinal component*, (i.e. the 2nd order statistical moments), shown in Figure 71. The average absolute *pairwise differences* of the repetitions are visualized as size of the squares (see reference symbol of average deviation) in units of non-dimensional standard deviation and plotted against non-dimensional mean wind speed and height. The *average absolute error* in terms of the *non-dimensional standard deviation* is around 0.02 and meets an average spread of ten percent (relative to the mean standard deviation). As for the mean wind speed values, the absolute deviations of the repetitions at points such as WT05 and M8 are *significantly higher* than for the rest of measurement locations. The dependence of the repeatability of the standard deviation on local flow features is even larger than for mean values which can be estimated by the spread of the *size of the squares*.

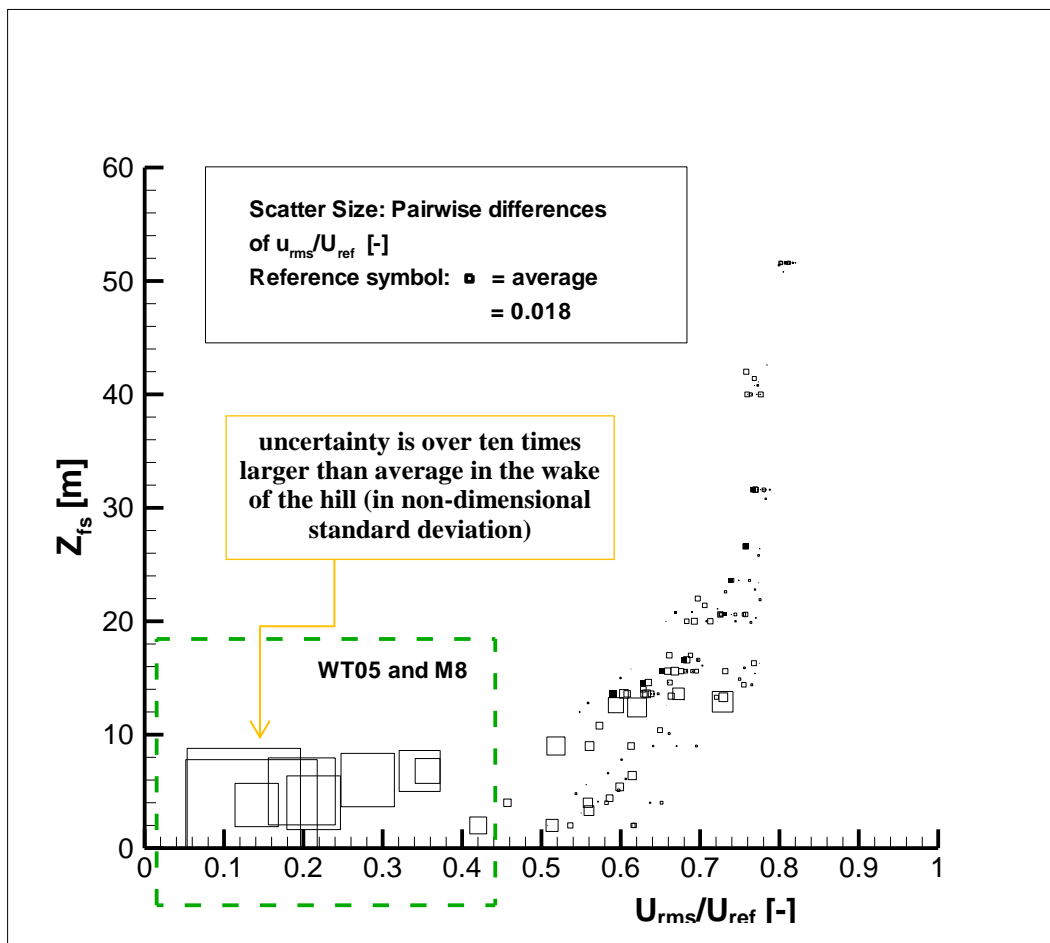


Figure 71: Repeatability of standard deviation for the Bolund experiments in WOTAN: Scatter size symbolizes the pairwise difference of repeated measurements. The reference symbol shows the average absolute error in terms of non-dimensional standard deviation.

The influence of the *local flow features* on the spread of the repeatability can be *minimized* by an increase of the *measurement duration* if the uncertainty is for statistical reasons (due to the finiteness of the sampling duration). The dependence of the results on the sampling duration is analysed here at a point that is found to be “difficult” in terms of *convergence* (this was assessed in the pilot-study on the idealized Bolund hill, see p.154). The point M6 is located right *at the front edge* of the hill in two meters height (= M6_S2) at full scale. Figure 72 shows the *variability* of the *empirical*⁷⁵ and *fitted* probability density functions (PDFs) of the wind speed fluctuations at M6_S2 for the inflow direction Line B and three exemplary subset samples with size 1000.

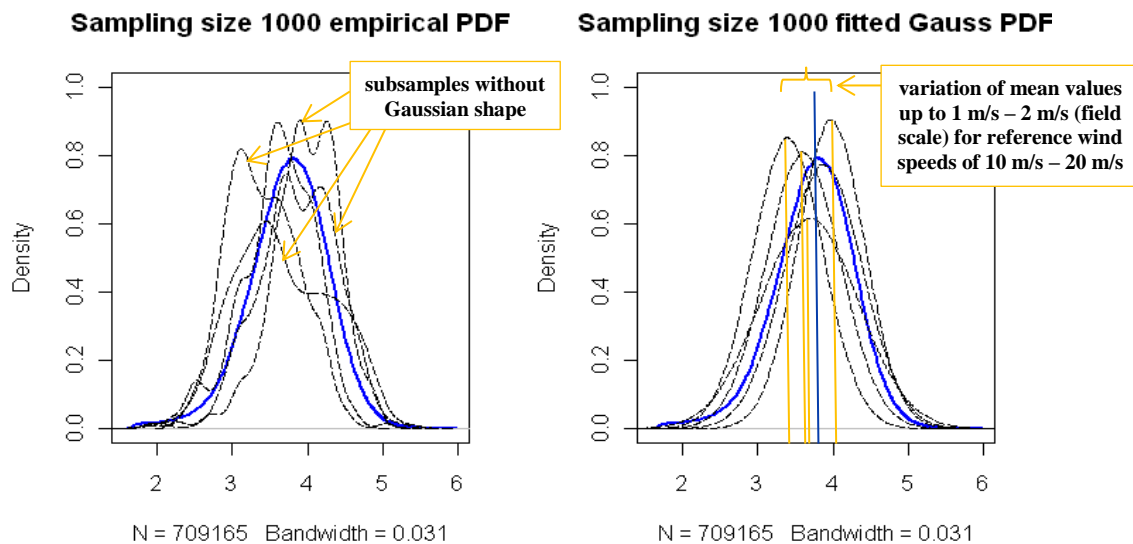


Figure 72: Left: Exemplary empirical distributions of wind speed fluctuations at M6_S2 for inflow direction Line B are shown, the subset samples have a size of 1000 (dashed lines); The empirical distribution of wind speed fluctuations at the same point for the whole sampling size $N=709165$ is shown as reference (blue line).

Right: Estimated Gauss distributions for the left hand side empirical distributions (dashed) are shown and the empirical distribution of wind speed fluctuations at the same point for the whole sampling size (over 700000); (blue line). The values at the x-axes denote in both cases the wind speed (= can be interpreted as full scale wind speeds in m/s for a free stream reference velocity of 5 m/s).

Figure 73 exhibits the status of *convergence* of the wind time series with sampling size ≈ 50000 (60 s measurement interval) towards the *empirical* density distribution of the full

⁷⁵ In this context, *empirical* probability density functions (PDF) are the actually computed probability densities of the measurement data – whereas *fitted* PDFs are estimated Gaussian distributions based on the measurement data – fitted with the open source program “R”.

time series (size over 700000, 12 minutes measurement time in wind tunnel scale.) *In contrast* to the recommendations of the LDA software handbook, a time series with sample size of 1000 is obviously *not* enough for robust statistical analysis, see Figure 72. Summarising these results, the *convergence* depends on the *measurement frequency* and the *sampling duration* and *intrinsic statistical features* of the analysed time series.

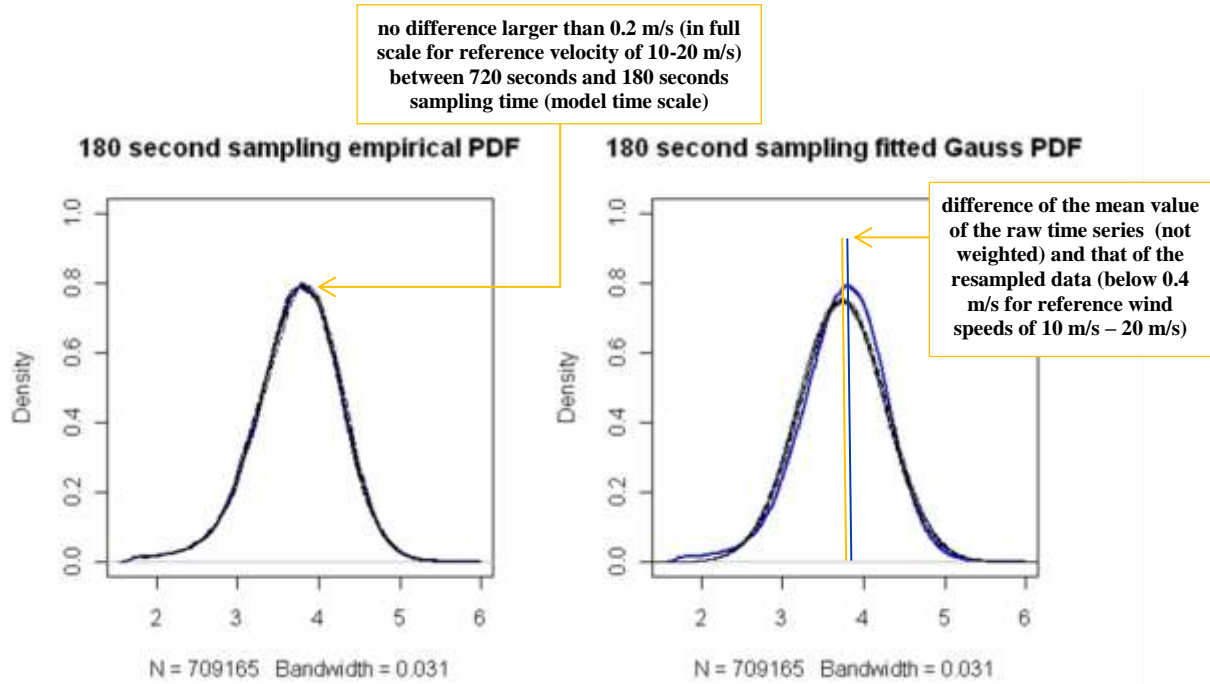


Figure 73: Left: Five exemplary empirical distributions of wind speed fluctuations at M6_S2 inflow direction Line B are shown; The subset samples have a measurement duration of 180 seconds (wind tunnel scale); The empirical distribution of wind speed fluctuations at the same point for the whole sampling size $N=709165$ is shown as reference (blue line) and lies within the subset distributions.

Right: Estimated Gauss distributions for the left hand side empirical distributions (dashed) are shown and the empirical distribution of wind speed fluctuations at the same point for the whole sampling size raw time series. The values at the x-axes denote in both cases the experimental wind speed (can be interpreted as full scale wind speeds in m/s for free stream reference velocity of 5 m/s).

In addition: As aforementioned, LDA measurements are *not* conducted in *equidistant* time steps and need to be *resampled* to obtain equidistant values. Here, *zero order sample-and-hold* resampling is chosen. Details of the method can be found in Fischer, [2011], and an analysis is given in chapter 9. The mean value of a full time series with 720 seconds (wind tunnel scale) of sampling duration was assumed as reference value to check statistical convergence. This means that the mean value of the 720 seconds (wind tunnel) record empirically replaced the mathematical (not assessable) limit value for measurement

duration $t \rightarrow \infty$. It is shown in pp. 246 that for 180 second (wind tunnel) sampling duration the relative *statistical convergence* error reduces to below two percent of the reference value. This is within the boundaries of the *experimental repeatability* error of around four percent assessed in the previous analysis. Thus, the sampling duration of 180 seconds (wind tunnel scale) was assumed to be *sufficient* for obtaining *statistically representative* data for mean wind speed and standard deviation of Bolund in WOTAN. (More details on the statistical analysis and the sampling rate are given in pp. 244)

Summarising the *analysis of repeatability deviation* and *convergence* of measurements, an average spread of around four percent can be expected as an *intrinsic* measurements deviation of the mean wind velocity results for the here used sampling frequency and 180 s sampling duration for Bolund in WOTAN. The computed *immediate repeatability* of the measurements at the same points with the same two orthogonal velocity components (UW respectively UV) is even below 1.5 percent spread.

Reynolds number tests

Reynolds number effects on the measurement results are analysed in the *range* of the operationally feasible mean wind tunnel reference velocities.

In Cermak and Ayra, [1970, p. 55], it is stated: “If the topographical features are fairly sharp, however, mean flow patterns are independent of the Reynolds number provided that it exceeds a lower limit which will depend on the sharpness of the topographical features.” On the Reynolds number dependence of flow around bluff bodies and bridges see also Larose and D’Auteuil, [2006], and Irwin, [2008]. Here, the Reynolds number effects on *local flow features* around Bolund are analysed at six *characteristic* measurement positions, namely at M2 (Line A), M6 and M8 (Line B), with heights of 2 m and 5 m in full scale above ground level. M2 and M6 are located at the front edge of the hill, M8 at the lee slope (see Figure 54 on p. 174). Emphasis on this flow area was taken due to the pilot study, in which the Re-test was negative at this position.

In order to examine the Reynolds number effects here the differences of the measurement results for different Reynolds numbers are compared to the *bounds of error of repeatability*.

Furthermore, since Reynolds number tests are conducted with *short time gap* between the measurements, not the *overall* repeatability of the experimental results is significant but the *instantaneous* repeatability, which is assumed to give a *smaller* error interval than the overall repeatability (and hence is more difficult to achieve). This was also discussed in the pilot study, pp. 146. The author is aware of the fact that for an increase of the consistency of the analysis, the immediate repeatability would need to be examined for *each* reference wind speed *separately*. This point is skipped here. Instead, the repeatability for the *largest* reference wind speed is taken into account and taken as an *upper bound*. The *measurement locations* are indicated schematically in the rectangle at the upper right-hand corner of each figure. In Figure 74 - Figure 76, the Reynolds number effects on the mean U component and the mean UW direction of the velocity vector are shown. The *mean U component* is plotted against the *reference wind speed*. The *reference intervals* of the *immediate repeatability* at that point are indicated by *dotted lines*. The *UW direction of the mean velocity vectors* is simply given by the directions of the plotted vectors. For example, Figure 74 exhibits the non-dimensional wind velocities ($U_{\text{mean}}/U_{\text{ref}}$) and the UW-directions (direction of the vector) measured in the wind tunnel at M2 in the height of 2 m (M2_S2) and 5 m (M2_S5) in full scale above ground level at the front edge. (The length of the vectors is chosen to be uniform for best visual representation.)

As shown in Figure 74, the deviation of $U_{\text{mean}}/U_{\text{ref}}$ for $6\text{ m/s} < U_{\text{ref}} < 9\text{ m/s}$ is smaller than 0.01 in units of non-dimensional wind velocity (< 1 percent of non-dimensional wind velocity for $U_{\text{ref}} = 9\text{ m/s}$); hence, the deviation due to variation of U_{ref} is *within the bounds* of the deviation of the *immediate repeatability* and hence this interval can be regarded as *Re-independent*. (This means translated to full scale with reference velocity 9 m/s that the Re-deviation is below 1 m/s at M2_S2 and M2_S5.)

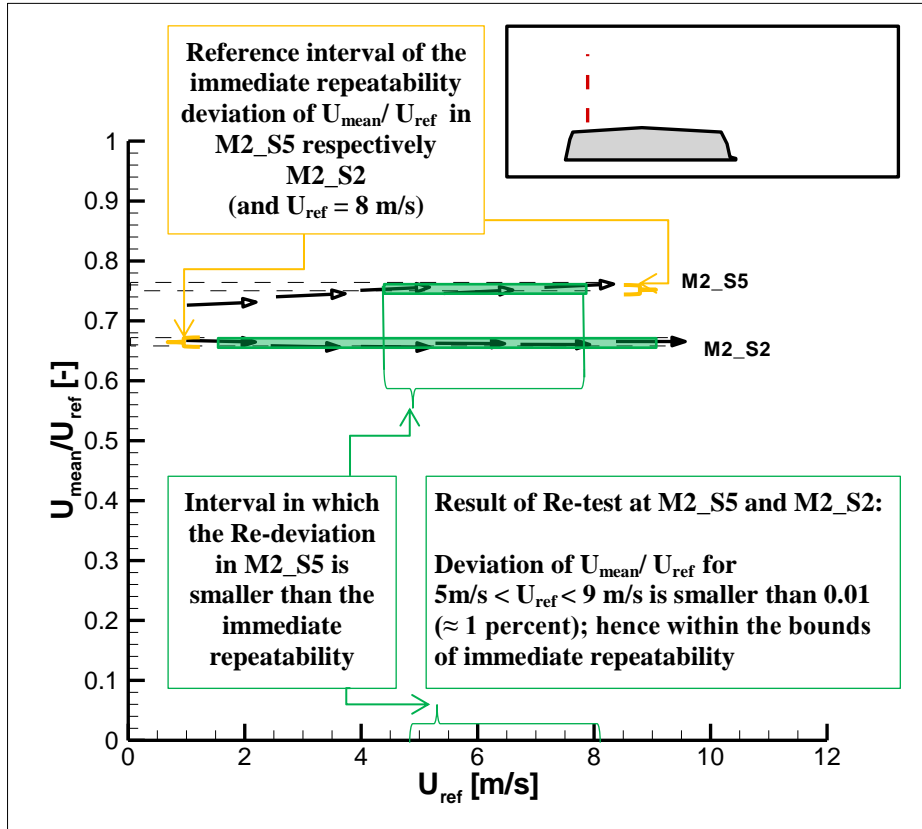


Figure 74: Reynolds test for (real) Bolund in WOTAN at M2, Inflow direction Line A. The UW-vectors of the measurements are shown. The centre of the vectors depicture the non-dimensional velocity of the vector given by the vertical axis ($U_{\text{mean}}/U_{\text{ref}}$); the directions of the vectors illustrate the UW-direction of the measurement; the corridor of instantaneous deviation (of immediate repeatability) is given by the dotted lines, see remark in the orange box on the picture; the green area indicates interval of empirical Re-independence relative to the immediate repeatability

Figure 75 and Figure 76 show that the *Reynolds number effects* on the U mean component are also not larger than the *immediate repeatability deviation* for reference velocities $7 \text{ m/s} < U_{\text{ref}} < 9 \text{ m/s}$ in the measurement positions M6 and M8 in 2 m and 5 m (in field scale) above ground level. In this interval, also the UW directions are robust. This holds for the flow *above the front edge* (Figure 74 and Figure 75) as well as for the *area at the lee slope*.

Since M8 shows the *largest dependence* on U_{ref} for low U_{ref} , this area is analysed further by means of the *standard deviations*. In Figure 77, the *non-dimensional standard deviation* of the U -component in dependence on U_{ref} is plotted. At M8 in height $z_{\text{agl}} = 5 \text{ m}$ full scale above ground level, the deviation of $u_{\text{ms}}/U_{\text{ref}}$ *converges below the immediate repeatability deviation* in the interval of $8 \text{ m/s} < U_{\text{ref}} < 10 \text{ m/s}$.

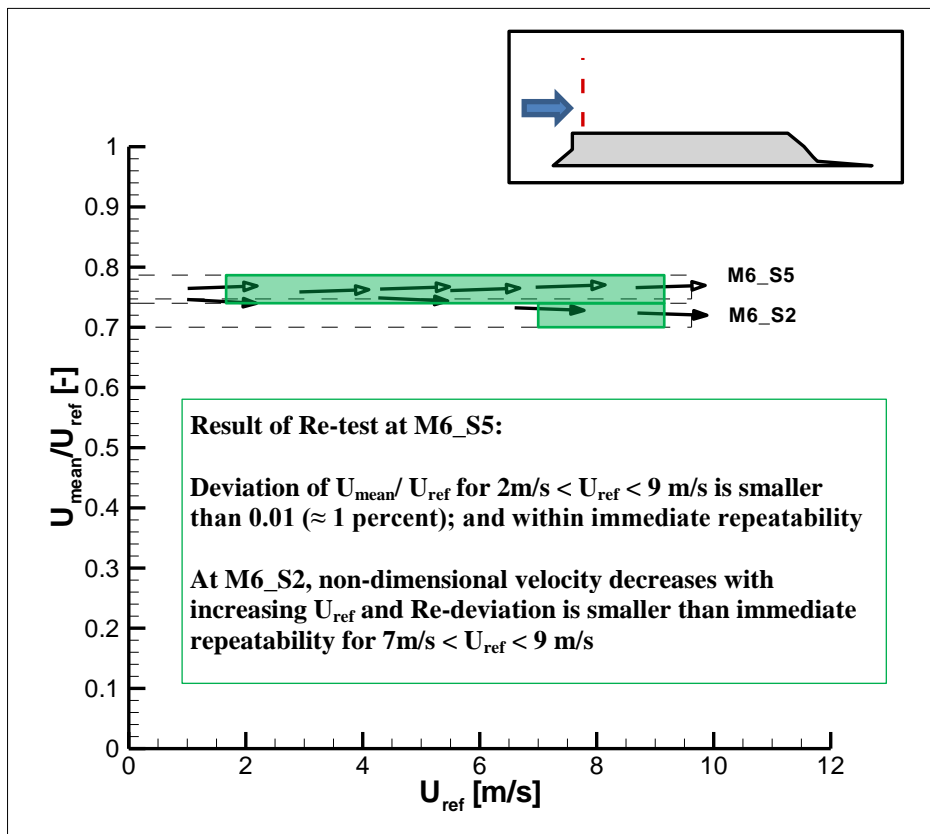


Figure 75: Reynolds test at M6, Inflow direction Line B

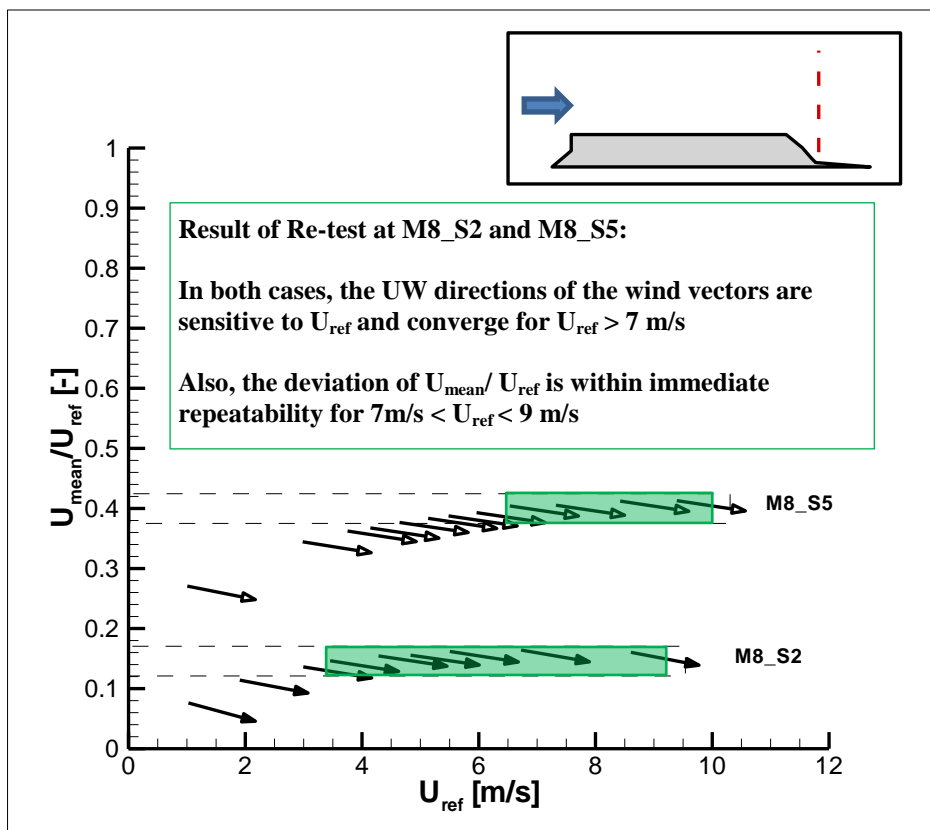


Figure 76: Reynolds test at M8, Inflow direction Line B

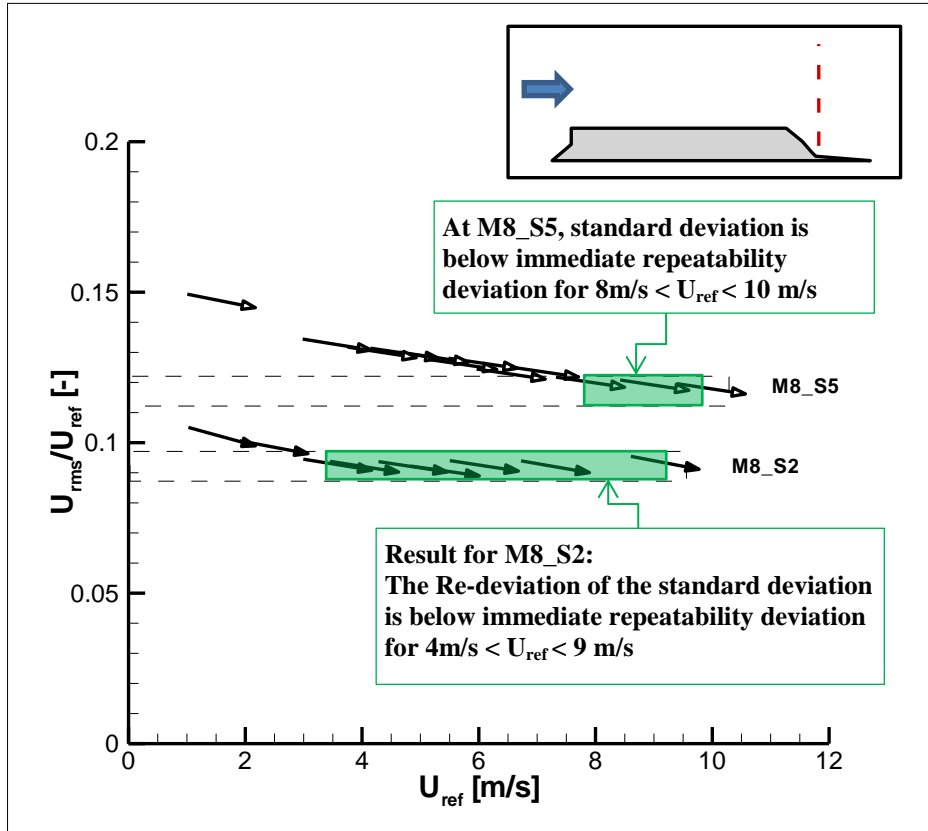


Figure 77: Reynolds test for the standard deviation of the U component at M8, Inflow direction Line B, the direction of the vectors shows the relationship of u_{rms} and w_{rms} (direction of the vector sum)

In summary, the key result of this section is that Reynolds number effects of the *non-dimensional mean U-component* as well as the UW-mean direction is *smaller* than the *immediate repeatability deviation* in the Reynolds number interval for $7\text{ m/s} < U_{\text{ref}} < 9\text{ m/s}$. Further investigation of Re-influence for the lateral and vertical component as well as for the standard deviations of all components (and higher order statistics) is skipped here and recommended for future work. However, this result is positive in comparison to the Re-tests of the pilot study which can be for example due to the distinct inflow conditions or different hill shape or distinct sampling configuration.

Mean flow results for Bolund in WOTAN

In Figure 78 - Figure 89, the *mean flow characteristics* are shown. The figures are vertically stretched by factor five for *visual* reasons. The *level lines* show the areas of value intervals, defined in the legend of each figure. Areas are computed by *triangulation*. This means that the measurement grid is triangulated and *original values are preserved*⁷⁶. For all figures, the mean wind speed direction is from the left.

Mean velocity around the hill

Figure 78 and Figure 79 show the *mean flow characteristics* for the U component at inflow directions A and B, the measurement positions (mid-point of the black arrows) and the UW mean velocity direction (direction of the black arrows).

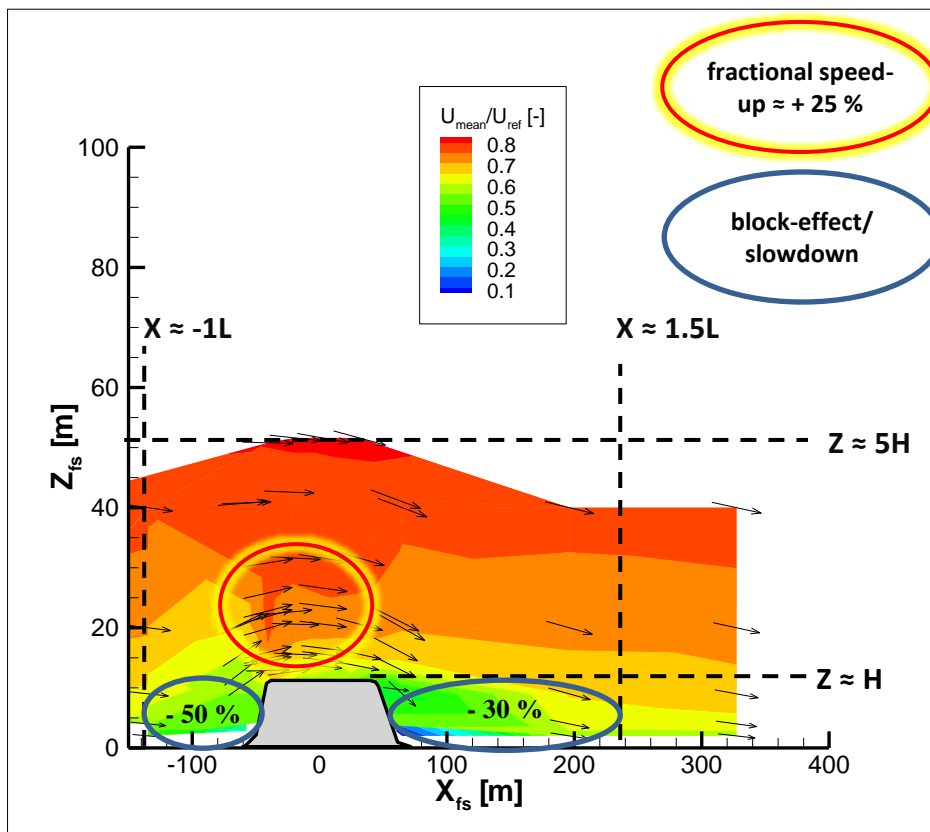


Figure 78: Mean U component for inflow direction A for (real) Bolund in WOTAN; the arrows show measurement positions and UW-directions of mean values (length of vectors is uniform for visual reasons); dotted lines show characteristic lengths (see text); the blockage area in front of the hill and the deceleration area behind the hill is marked with a blue ellipse; the speed-up area of p to 20-30 percent fractional speed-up is indicated with a red ellipse (highlighted with yellow for visual reasons)

⁷⁶ Thus, sharp edges in the contour lines are artefacts and due to the triangulation of the data. This method is preferred over other methods since in triangulation the original data is preserved.

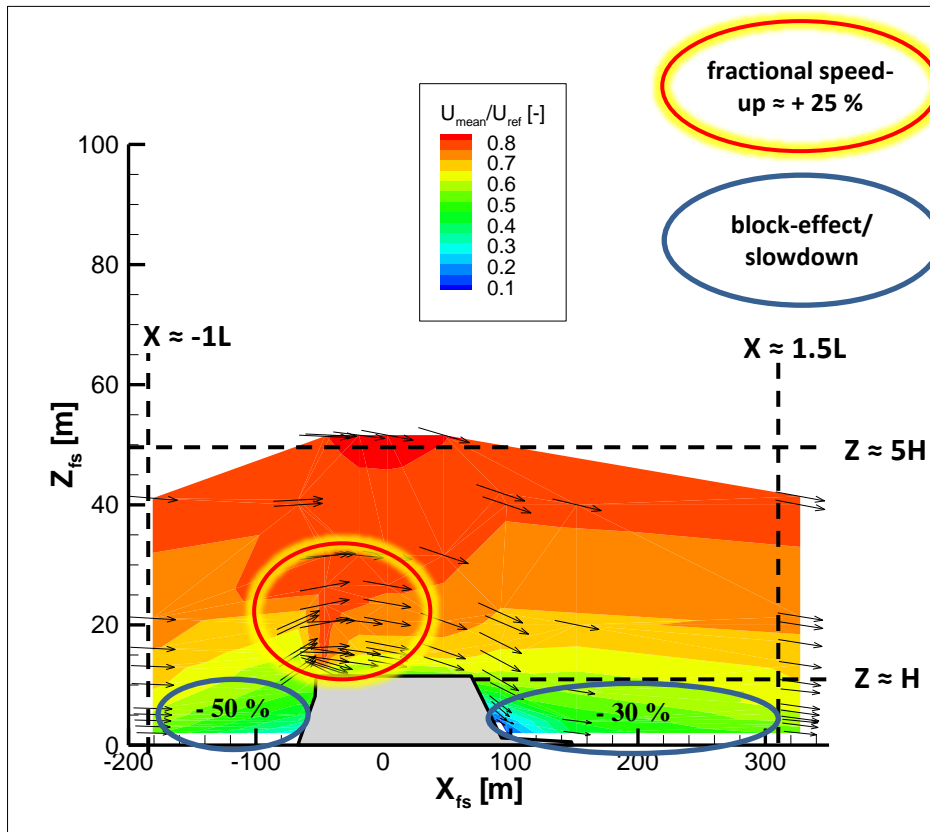


Figure 79: Mean U component level lines for inflow direction B; description of the legend as in the previous figure.

As shown in Figure 78 and Figure 79, the atmospheric boundary layer flow is *distorted* (at least) up to a height of $5H$ (H = hill height) for *both inflow directions*. Also, for both inflow directions the influence of the hill on the mean U component for $z < H$ starts around $1L$ in front of the hill (L = hill length for the corresponding wind direction).

In the *blockage area* in front of the hill, the mean flow *decelerates* down to around $0.2 - 0.4 U_{\text{mean}}/U_{\text{ref}}$. This is around 40 – 60 percent deceleration relative to the undisturbed flow ($\approx 0.6 U_{\text{mean}}/U_{\text{ref}}$ in the same height), see Figure 78 and Figure 79. The mean flow is still influenced $1.5L$ behind the hill for heights up to H (see black dotted lines in Figure 78 and Figure 79). The slowdown of the U-component is around 30 percent in this area. At the *bottom* behind the hill, the mean flow *decelerates* down to $0.1 U_{\text{mean}}/U_{\text{ref}}$. This will be analysed further in the section on the “deceleration areas around the hill”.

For both inflow directions, the mean flow *accelerates above the front edge*. Here, at around $z = 0.5H$ above ground level, the velocity is around 20 – 30 percent larger than in the same

height above ground level (agl) in the undisturbed flow. (The acceleration is in $z = 0.5H$ agl from around $0.5 - 0.6 U_{\text{mean}}/U_{\text{ref}}$ to $0.7 - 0.8 U_{\text{mean}}/U_{\text{ref}}$). This will be analysed further in the section on the “speed-up effect above front edge”.

Furthermore, in Figure 78 and Figure 79 the influence of the hill on the W-component of the mean flow is shown. Around $1L$ in front of the hill, the mean flow is approximately *horizontal*, (see $X = -150$ m in Figure 78 and $X = -200$ m in Figure 79). In front of the hill and in the speed-up area, the W-component increases relative to the U-component and the mean flow *points upwards*. This means that the W-component is *positive*. Along the hill, the W-component *changes its sign*. The mean flow *reverses* its UW deflection and, in the lee of the hill, *points downwards*. Hence, the mean flow approximately *follows the shape of the hill* as it is expected for the explanation of the speed-up effect (see Bernoulli equation, pp. 116).

Mean standard deviations around the hill

In Figure 80 - Figure 82, the influence of the hill on the mean *turbulence characteristics* of the atmospheric boundary layer flow (for Bolund in WOTAN) is shown for inflow direction A. The mean turbulence characteristics are displayed as the standard deviations of the U,V and W-component of the flow. The values of the *level lines* are indicated in the legends and chosen for each figure separately (for visual reasons). For all three components, a strong influence is shown *at the front edge* and in the *wake of the hill*.

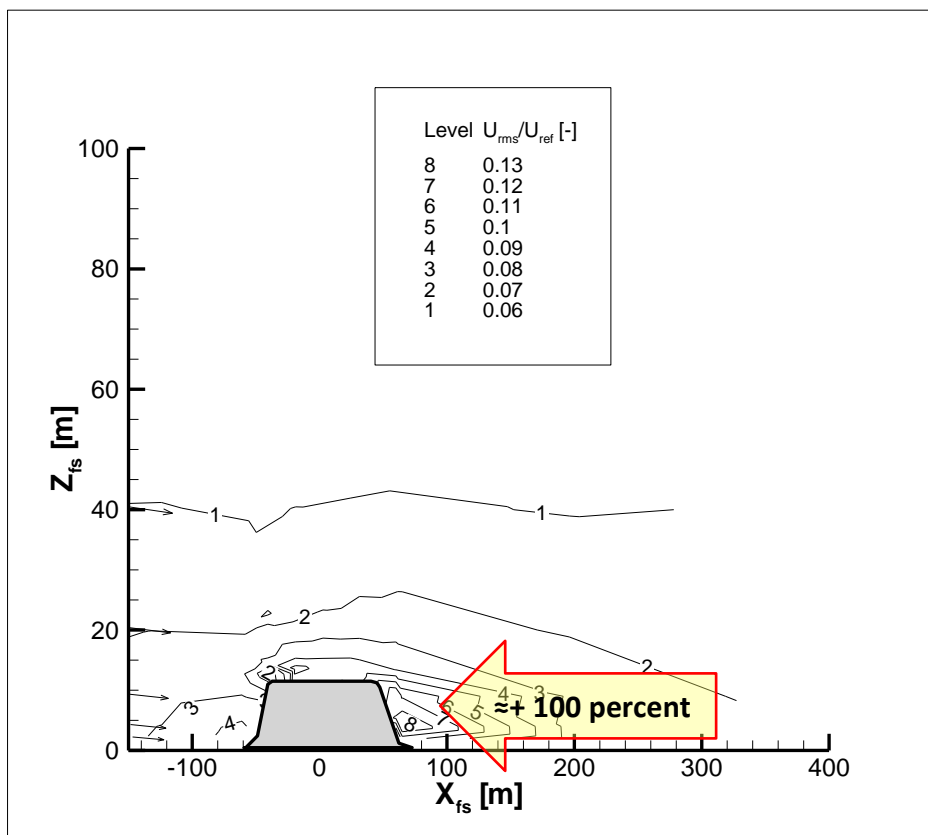


Figure 80: U component standard deviation for inflow Line A for (real) Bolund in WOTAN. The contour lines are chosen in each figure separately for the best visual representation. The figure shows that u_{rms}/U_{ref} almost doubles in the lee of the hill at around $z = 0.5H$ relative to u_{rms}/U_{ref} in the undisturbed flow at around the same height. (This is indicated by the text in the large arrow.) Sharp edges in the contour lines can occur as artefacts due to the triangulation of the data

Figure 80 shows that the non-dimensional standard deviation of the U-component, u_{rms}/U_{ref} , in height $z \approx 0.5H$ in the *wake of the hill*, is around 0.13 in units of u_{rms}/U_{ref} (level line 8) whereas u_{rms}/U_{ref} in the same height in the *undisturbed flow* (in front or behind the hill) is around 0.06 - 0.07 in units of u_{rms}/U_{ref} . Hence, in consideration of a *precision estimation* of around 10 percent, the increase of u_{rms}/U_{ref} in the wake of the hill is around 100 percent. It

can be noticed that the *influence of the hill* on u_{rms}/U_{ref} *above the front edge* is smaller than the influence on the mean wind speed. (This means that the *relative increase* of u_{rms}/U_{ref} above the front edge is around 10 percent and below the relative speed-up effect.)

Figure 81 exhibits the influence of the Bolund hill in WOTAN on the *standard deviation of the V-component*. As for the U-component, the largest influence is shown at the front edge and in the wake of the hill. In consideration of a *precision estimation* of around 10 percent, the increase of v_{rms}/U_{ref} in the *wake of the hill* is around 80 - 100 percent. (The increase is from around 0.6 in units of v_{rms}/U_{ref} to around 1 in units of non-dimensional v_{rms}/U_{ref} .) Here, in contrast to Figure 80, the maximum of the increase is slightly shifted to the bottom and is located towards heights $z < 0.5H$.

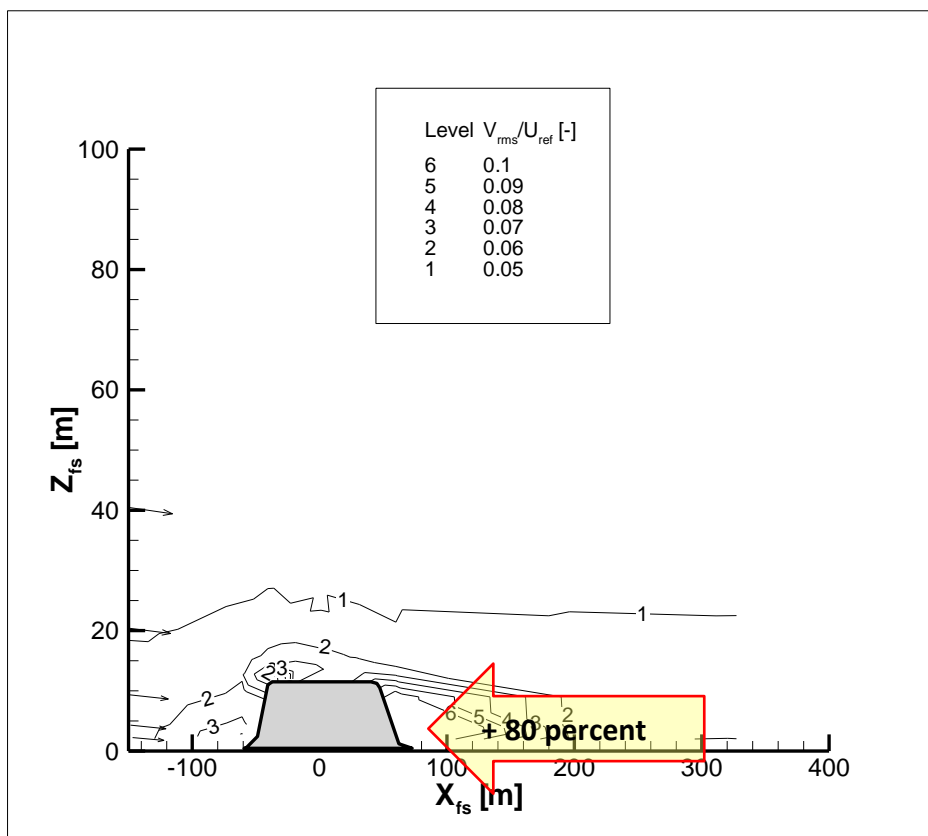


Figure 81: V component standard deviation for inflow Line A (see text). Sharp edges in the contour lines can occur as artefacts due to the triangulation of the data

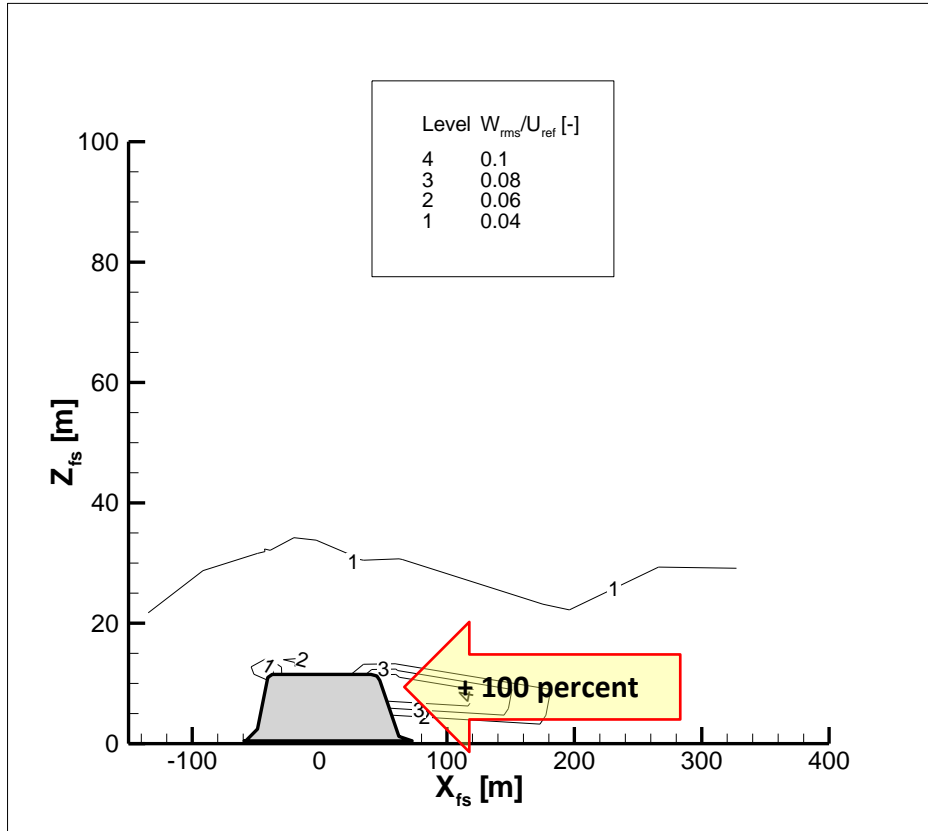


Figure 82: W component standard deviation for Line A (see text). Sharp edges in the contour lines can occur as artefacts due to the triangulation of the data.

In Figure 82, the influence of the Bolund hill in WOTAN on the *standard deviation of the W-component* is shown. As for the U- and the V-components, the largest influence of the hill on the standard deviation of the W-component is shown *at the front edge and in the wake of the hill*. In contrast to the U- and V-component, the standard deviation of the W-component decreases *at the front edge*. The decrease is from around 0.06 in non-dimensional w_{rms}/U_{ref} to 0.04 in non-dimensional w_{rms}/U_{ref} . In consideration of a *precision estimation* of around 10 percent, this is a decrease of around 30 percent. In the *wake of the hill*, the standard deviation of the vertical component *nearly doubles* (from around 0.06 in units of w_{rms}/U_{ref} to around 1 in units of w_{rms}/U_{ref}). In contrast to the location of the maximum increase of the standard deviations of the U- and the V-component, the location of the maximum of w_{rms}/U_{ref} is shifted upwards and is found at heights $z > 0.5$, see Figure 82.

In Figure 83 - Figure 85, the influence of the Bolund hill on the mean *turbulence characteristics* of the atmospheric boundary layer flow (for Bolund in WOTAN) is shown for

inflow direction B (recall Figure 24 in which the corresponding Bolund profile is shown from the south; recall Figure 25 in which the inflow directions are shown). As before, the mean turbulence characteristics are displayed as the standard deviations of the U-, V- and W-component of the flow. The values of the *level lines* are indicated in the legends and chosen for each figure separately (for visual reasons). As for inflow direction A, the strongest influence of the hill on the standard deviations is shown *at the front edge* and in the *wake of the hill* for all three components.

For the inflow direction B, Figure 83 shows that u_{rms}/U_{ref} is around 0.12 in non-dimensional u_{rms}/U_{ref} (level line 4) in height $z \approx 0.5H$ in the *wake of the hill*. Taking precision errors of around 10 percent into account, the increase is from around 0.8 (level line 2) to around 0.12 (level line 4) and hence approximately 50 percent. The comparison of both inflow directions in WOTAN shows that the influence of the Bolund hill on u_{rms}/U_{ref} is *larger at the front edge* for inflow direction B (Figure 83) than for inflow direction A (Figure 80). The reason for this can be that the front edge of the Bolund profile for inflow line B is *sharper* than for inflow direction A. The other way around, the influence on u_{rms}/U_{ref} is *less in the wake* for inflow direction B (Figure 83) than for inflow direction A (Figure 80). The reason for this can be that the lee slope of Bolund for inflow direction B is *less steep* than for inflow direction A.

Figure 84 exhibits the influence of the Bolund hill in WOTAN on the *standard deviation of the V-component*. As for inflow direction A (Figure 81) and the U-component of inflow direction B (Figure 83), the largest influence is shown *at the front edge* and *in the wake of the hill*.

In consideration of a *precision estimation* of around 10 percent, the increase of v_{rms}/U_{ref} in the *wake of the hill* is around 50 percent (Figure 84). As for inflow line A (Figure 81) the location of the maximum increase of v_{rms}/U_{ref} is slightly *shifted to the bottom* of the wake of the hill, in heights $z < 0.5H$. As for the standard deviation of the U-component (Figure 80 and Figure 83), the influence on v_{rms}/U_{ref} is less for direction B (Figure 84) than for direction A (Figure 81).

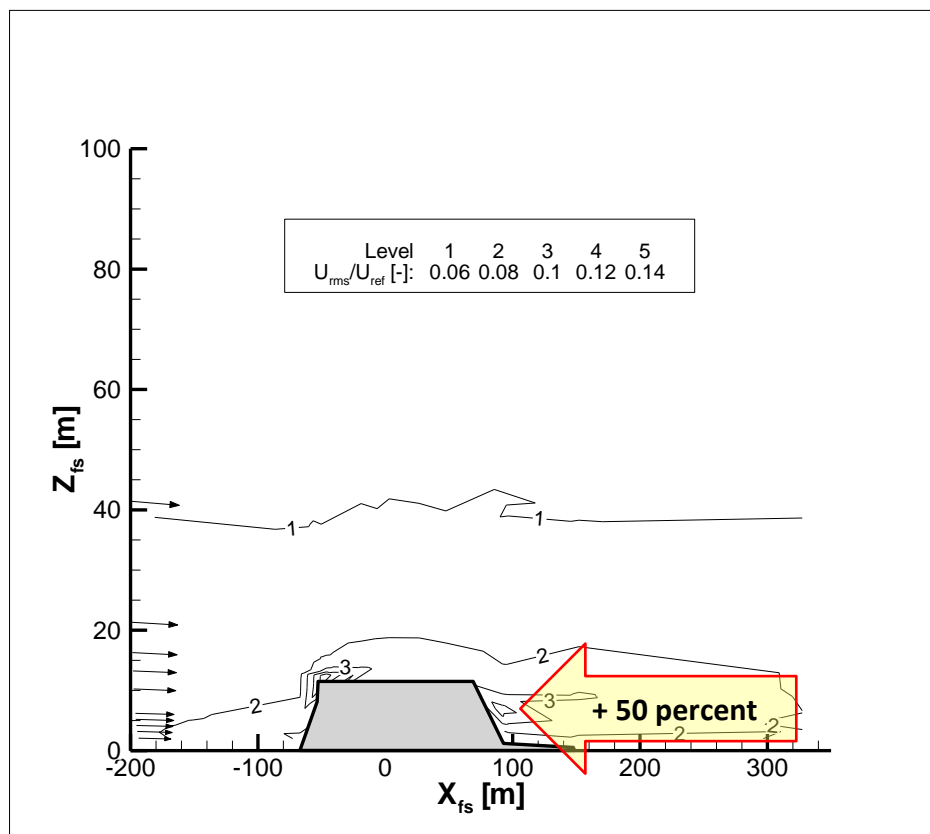


Figure 83: U component standard deviation for Line B (see text). Sharp edges in the contour lines can occur as artefacts due to the triangulation of the data.

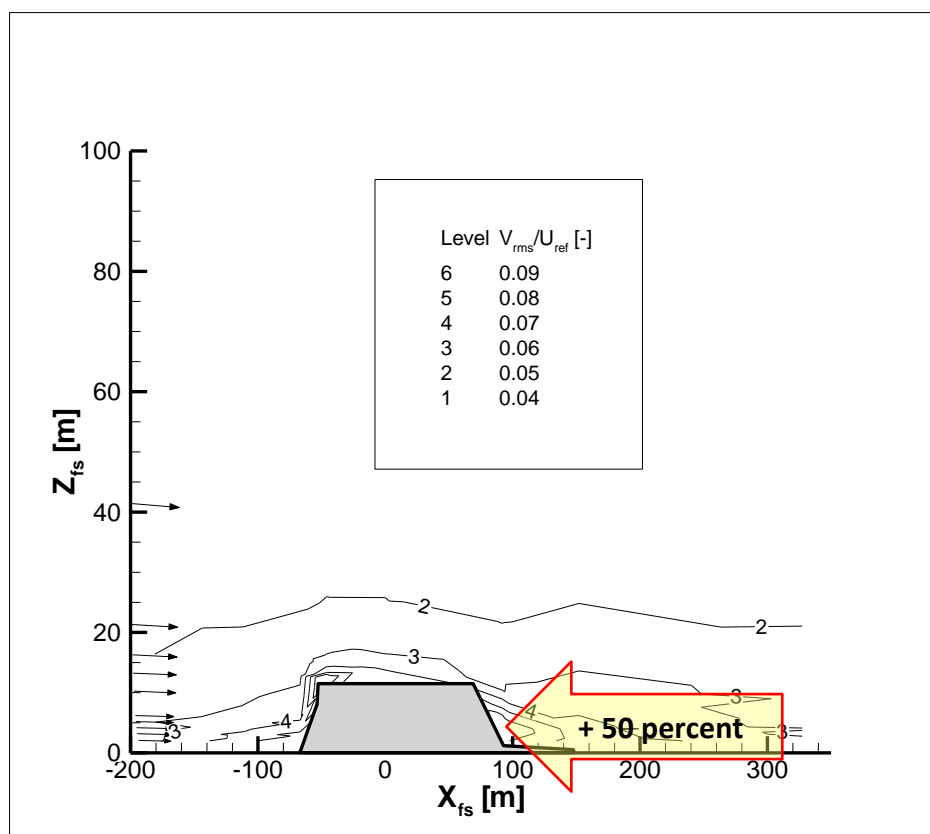


Figure 84: V component standard deviation for Line B (see text). Sharp edges in the contour lines can occur as artefacts due to the triangulation of the data.

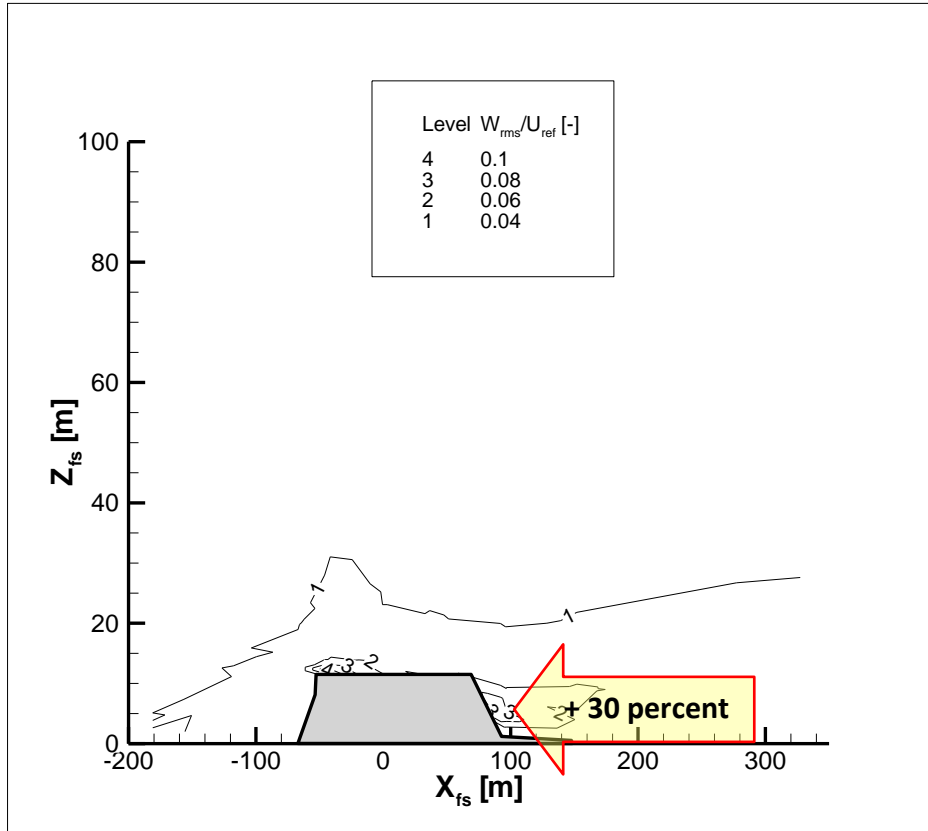


Figure 85: W component standard deviation for Line B (see text). Sharp edges in the contour lines can occur as artefacts due to the triangulation of the data.

In Figure 85, the influence of the Bolund hill in WOTAN on the *standard deviation of the W -component* is shown. As for the U - and the V -components, the largest influence of the hill on the standard deviation of the W -component is shown *at the front edge and in the wake of the hill*. In consideration of a *precision estimation* of around 10 percent, the standard deviation of the vertical component *increases* by around 30 percent relative to the value in undisturbed flow at the same height (from around 0.06 in units of w_{rms}/U_{ref} to around 0.08 in units of w_{rms}/U_{ref}).

Recall that the *location of the maximum increase* of w_{rms}/U_{ref} for inflow direction A was found in heights $z > 0.5H$ in the wake of the hill (Figure 82). This is not found for line B. Here, the maximum increase is in heights around $z \approx 0.5H$ (Figure 85). Furthermore, the *area of influence* on w_{rms}/U_{ref} is *smaller* for inflow direction B (Figure 85) than for inflow direction A (Figure 82). In addition, the *relative increase is smaller* for inflow direction B (≈ 30 percent) than for inflow direction A (≈ 100 percent). Reason for this can be that the lee slope of

Bolund is *less steep* for the inflow direction B than for the inflow direction A, as mentioned before.

For the inflow direction B, the non-dimensional standard deviation of the W-component *increases* by around 60 percent (from 0.06 to 1 in units of w_{rms}/U_{ref}) above the *front edge*. This is in contrast to the result for inflow direction A. For inflow direction A, w_{rms}/U_{ref} was found to *decrease at the front edge* (Figure 82). This can be an indication that the vertical standard deviation is *more sensitive on the sharpness of the front edge* than the standard deviation of the U- and the V-component.

Skewness and shear stress around the hill

The hill has also an influence on the *shear stress* around the hill. Figure 86 exhibits the *non-dimensional mean shear stress* for Bolund in WOTAN for the inflow direction A. It shows that the absolute value *increases by five times* above the front edge and at the lee slope of the hill around hill height. The same is found for the inflow direction B. This is shown in Figure 87. Here, the *non-dimensional mean shear stress* for Bolund in WOTAN for the inflow direction B is exhibited. Furthermore, the influence of the Bolund hill in WOTAN on the *skewness* of the velocities is examined. Figure 88 exhibits exemplarily the influence of the hill on the *skewness* of the U-component in the flow around the hill for inflow direction A.

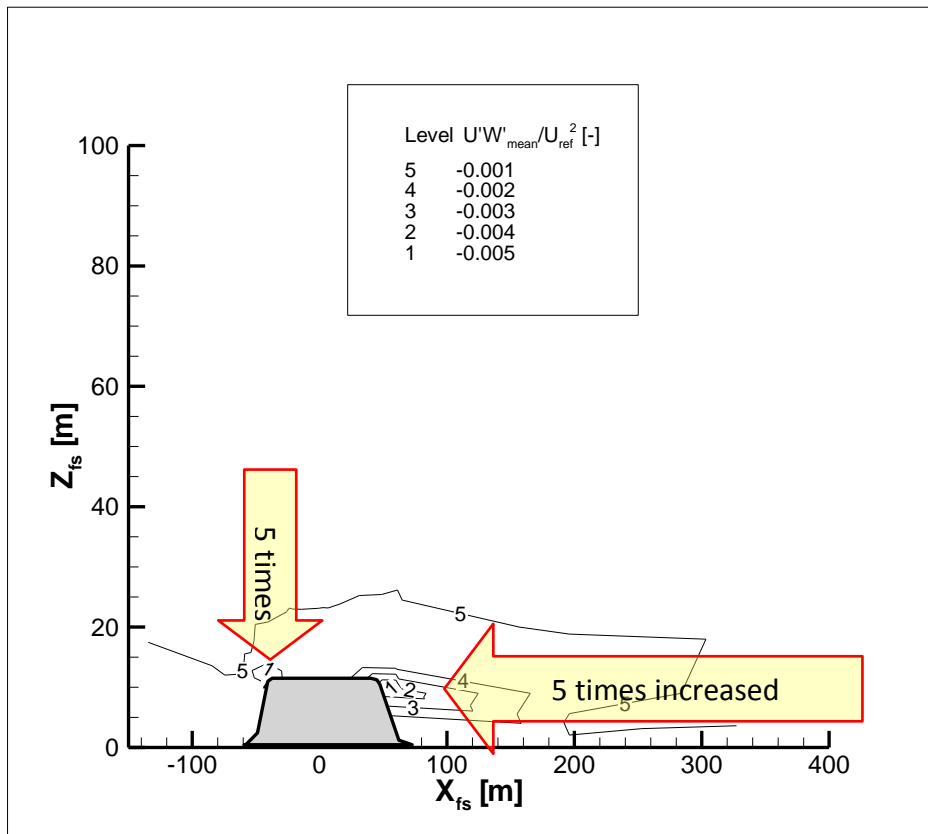


Figure 86: Shear stress for Line A for (real) Bolund in WOTAN. The contour lines are chosen in each figure separately for the best visual representation. The figure shows that the absolute values of $u'w'/(U_{\text{ref}})^2$ increases by around 5 times at the front edge and in the lee of the hill at around $z = H$ relative to $u'w'/(U_{\text{ref}})^2$ in the undisturbed flow at around the same height. (This is indicated by the text in the large arrows.)

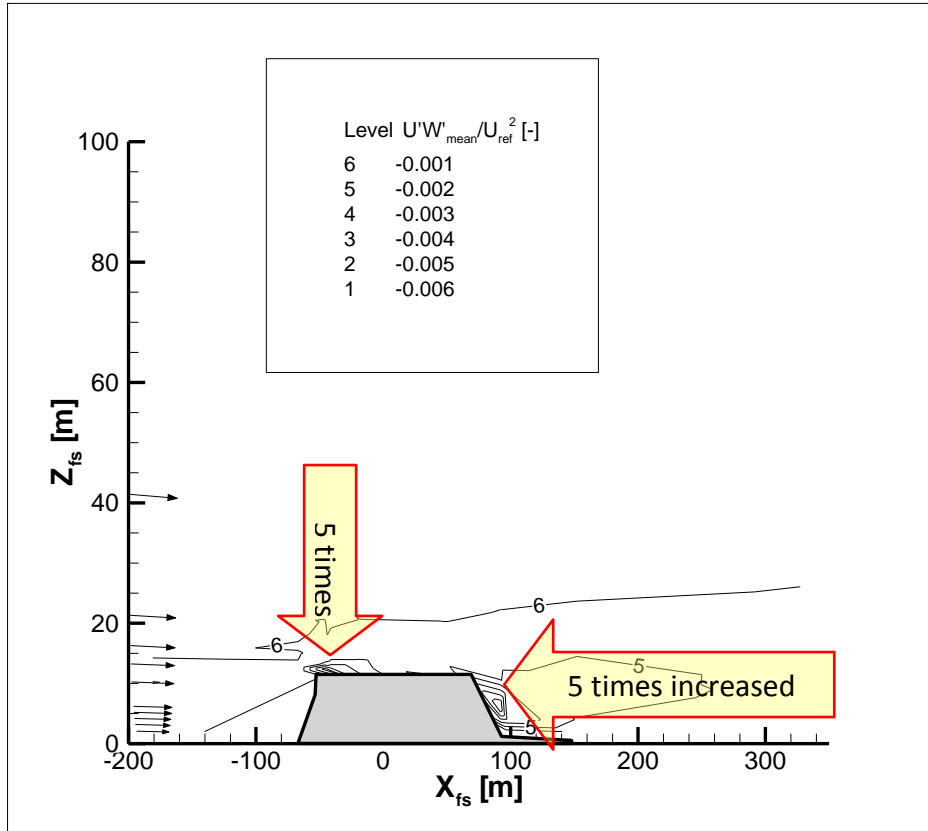


Figure 87: Shear stress for inflow Line B (real) Bolund in WOTAN; text in the large arrows indicates increase of the absolute values of $u'w'/(U_{ref})^2$

As shown in Figure 88, the skewness is *negative* for free stream flow and *turns positive* close to the ground in the blockage area and in the wake of the hill. In contrast, at the top of the luv slope of the hill, skewness *increases* in its *negative* value by around *five times*. The same effect of the hill on the skewness of the U-component in the flow is shown in Figure 89 for Bolund in WOTAN (inflow direction B). This indicates that the hill has a *significant influence on the shape of the velocity distribution of the turbulent small scale fluctuations*⁷⁷.

⁷⁷ Symmetric distributions (such as the Gaussian distribution) have zero skewness; A positive skewness indicates a “longer” tail to the right; negative skewness indicates a “longer” tail to the left.

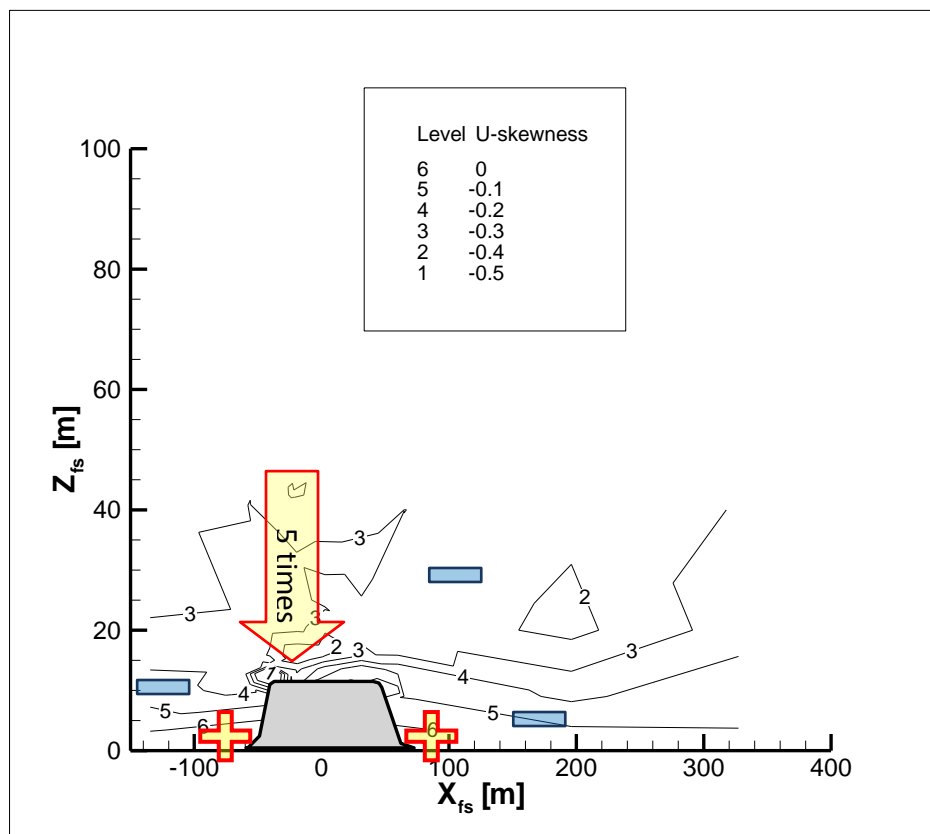


Figure 88: U component skewness for Bolund in WOTAN inflow Line A, the large yellow "+" and blue "-" show the sign of the skewness in this area, the text in the large yellow arrow indicates that the absolute value of the skewness increases by 5 times at the front edge of the hill.

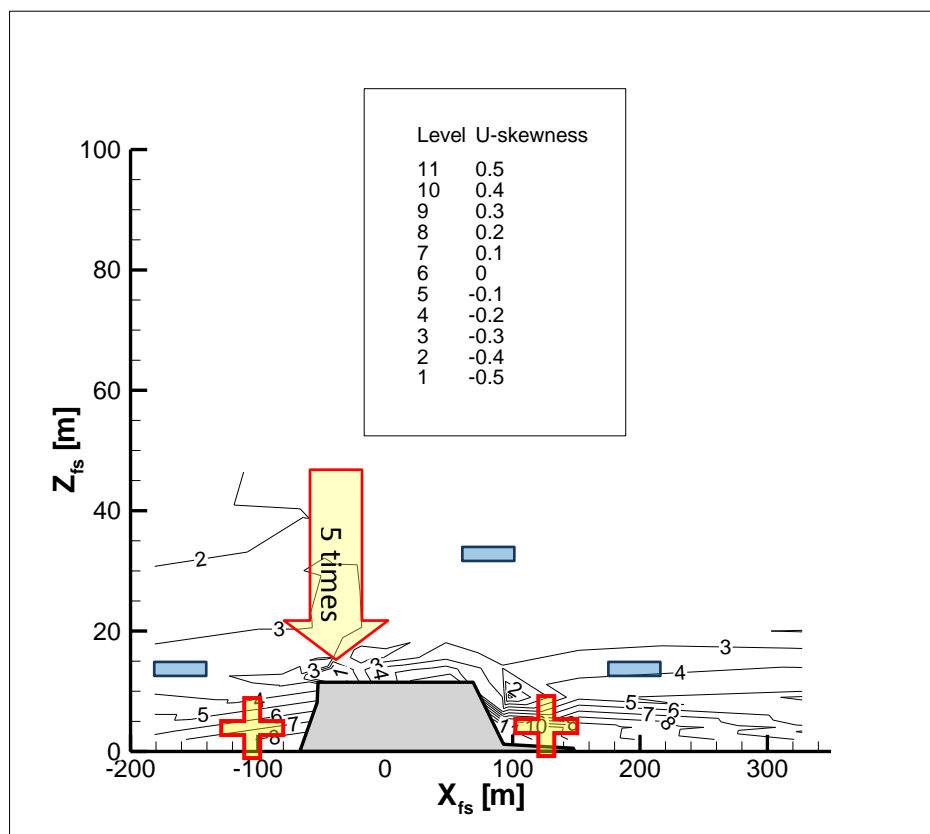


Figure 89: U component skewness for Line B, description as in the previous figure

The flow results will be summarized at the end of this chapter. At this point it can be remarked: To obtain more reliable results for the above parameters, it would be necessary to conduct further Re-tests and further convergence-analyses for *all of these quantities*. This is skipped here. For the following more detailed analyses of the flow around Bolund in WOTAN, it is focused on the mean U-component for which the extensive precision analysis was conducted (section “Analysis of precision”, pp. 194).

Speed-up effect above the front edge

As stated before, the mean flow *speeds-up over the front edge* due to the Bernoulli effect. Since the speed-up is a *derived quantity*, the propagation of uncertainty is here analysed further. The *speed-up* can be defined as speed-up ratio:

$$\Delta s(x,z) := (u_{xz} - u_{0z})/u_{0z}$$

with

$$u_{xz} := u(x, 0, z_{agl}),$$

and u_0 measured at M0 for same z_{agl} , for illustration see Figure 5, p. 36.

For Δs , the *propagation of uncertainty* can be considered in the following way:

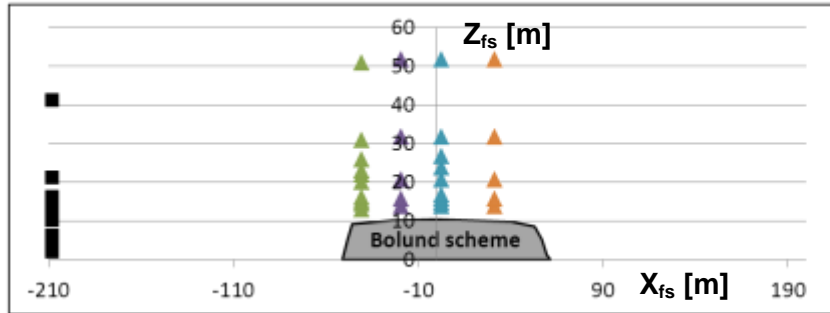
Let $e(u_{xz})$, $e(u_{0z})$ denote the *random error* of u_{xz} , respectively u_{0z} , assessed by the *repeatability measurements* in the previous section. The measurements are conducted at different moments in time and space. Hence, the random errors are assumed as being *non-correlated*. Then the propagation of uncertainty is computed as:

$$\begin{aligned} e(\Delta s) &= |\partial \Delta s / \partial u_{xz}| e(u_{xz}) + |\partial \Delta s / \partial u_{0z}| e(u_{0z}). \\ \Rightarrow e(\Delta s) &= |u_{0z} / (u_{0z})^2| e(u_{xz}) + |-u_{xz} / (u_{0z})^2| e(u_{0z}). \end{aligned}$$

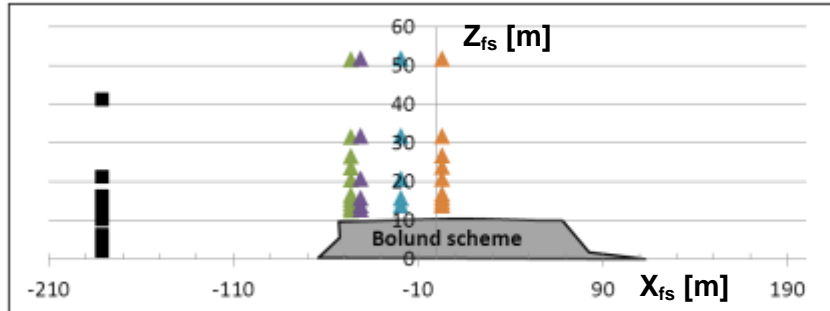
It can be assumed that $e(u_{xz}) \approx e(u_{0z})$ and $u_{xz} \approx u_{0z}$. This leads to $e(\Delta s) \approx 2e(u_{xz})/|u_{xz}|$. This means that the relative error can easily be *doubled*. In other words, for its property as derived quantity, the empirically assessed fractional speed-up ratio can easily have twice the

precision deviation of the measured velocity values. This can be a crucial factor with respect to the uncertainties of field measurements⁷⁸. For the wind tunnel measurements of Bolund in WOTAN this might be less relevant. Recall that the precision deviation in the speed-up location M2_S5 (5 m in field scale above ground level at the front edge for inflow direction A) was around 0.01 in terms of $U_{\text{mean}}/U_{\text{ref}}$ including the deviation assessed by the Re-tests (Figure 74, p. 202). Hence, with the assumption of $e(u_{xz}) \approx e(u_{0z}) \approx 0.01$ and $u_{xz} \approx u_{0z} \approx 0.75$, the random error of the speed-up yields $e(\Delta s) \approx 0.03$. This yields a precision deviation of below 0.5 m/s in field scale with a reference velocity of around 10 m/s.

Measurement positions, Line A:



Measurement positions, Line B:



X and Z coordinates in full scale meters

Figure 90: Measurement positions for calculation of fractional speed-up ratio (relative speed-up) for both inflow directions, Line A (on top) and Line B (below)

⁷⁸ This is especially a challenge for application in wind energy since the mean kinetic energy of the wind flow is proportional to the square of the mean velocity; furthermore, the power production is proportional to the third power of the mean velocity (within a certain interval of operational wind speeds of the wind turbine).

Line A, relative speed-up:

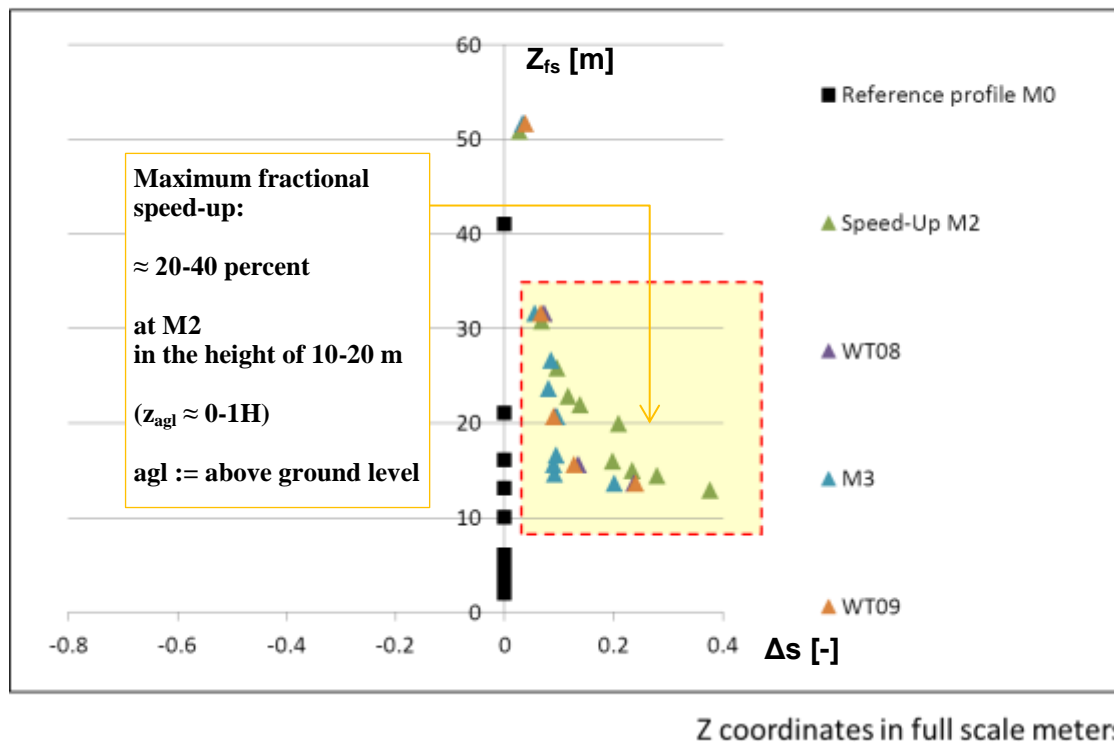


Figure 91: Relative speed-up for Bolund in WOTAN, inflow direction A; the x-axis denotes relative differences of non-dimensional wind-speeds (difference of profile and reference profile); the y-axis denotes the height in full-scale meters; the names of the vertical profiles are given in the legend; the exact measurement positions of the speed-up profiles (triangles) as well as the reference profile (black circles) are shown in the previous figure; symbol size is an estimate for precision

Figure 90 - Figure 92 illustrate the *fractional speed-up ratios* for the vertical profiles in the speed-up areas above the Bolund hill in WOTAN (for inflow directions A and B). This analysis is an addition to the overview on the mean velocity flow field around the hill, as presented in the section “Mean velocity around the hill”, pp. 205. Figure 90 exhibits the *measurement positions* for the computations of the *fractional speed-up ratios*. The computed values are shown in Figure 91 and Figure 92.

Figure 91 shows that the *maximum speed-up* for inflow direction A is found at the measurement position M2, above the front edge of the hill at around $0.2H < z_{agl} < 0.5H$ ($2 \text{ m} < z_{agl} < 5 \text{ m}$ in full scale). Here, the fractional speed-up ratio is around $0.2 - 0.4$. This means that the mean velocity of the U-component increases of around $20 - 40$ percent *relative* to the velocity in the undisturbed boundary layer flow in front of the hill *in the same*

height above ground level. Figure 91 also shows that Δs decreases significantly along the hill. At WT08, M3 and WT09 the speed-up ratio is only half (or less of) the speed-up ratio above the front edge, see Figure 91. Hence the *maximum speed-up ratio* is sensitive on the location and largest above the front edge of Bolund in WOTAN for Line A.

Line B, relative speed-up:

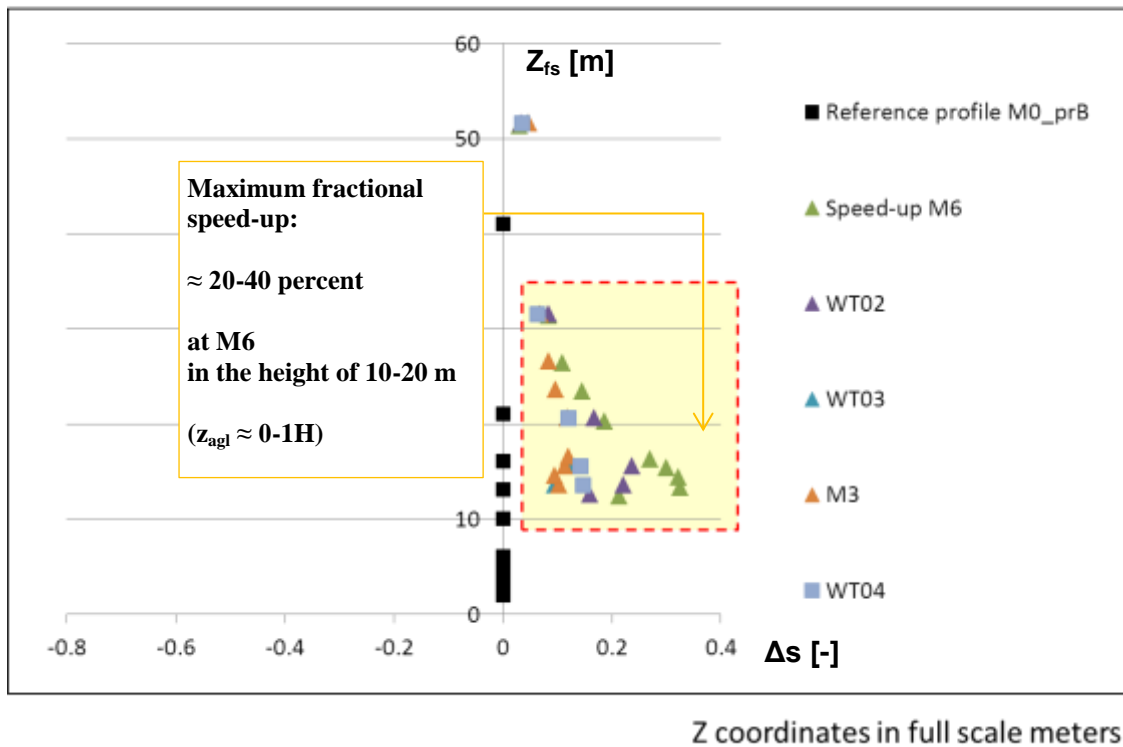


Figure 92: Relative speed-up for Bolund in WOTAN, inflow direction B; the x-axis denotes relative differences of non-dimensional wind-speeds (difference of profile and reference profile); the y-axis denotes the height in full-scale meters; the names of the vertical profiles are given in the legend; the exact measurement positions of the speed-up profiles (triangles) as well as the reference profile (black circles) are indicated in Figure 90.

As shown in Figure 92, the *maximum speed-up* for inflow direction B of real Bolund in WOTAN is also found above the front edge of the hill (at measurement position M6) at around $0.2H < z_{agl} < 0.5H$ ($2 \text{ m} < z_{agl} < 5 \text{ m}$ in full scale). Furthermore, the speed-up ratio decreases from around 35 percent at M6 (above the front edge) to around 20 percent at WT02. The measurement location WT02 is located around $0.5H$ (5 m in full scale) downstream from M6. As for line A, this indicates the sensitivity of the *maximum speed-up ratio* on the location and maximum speed-up occurs above the front edge of the hill.

Around $0.5H$ downstream of the front edge, the relative speed-up of the mean U-component along the Bolund hill is still around 10 percent (at heights of around $0.2H - 2H$ above ground level, shown for both inflow directions in Figure 91 and Figure 92.)⁷⁹

Deceleration areas around the hill

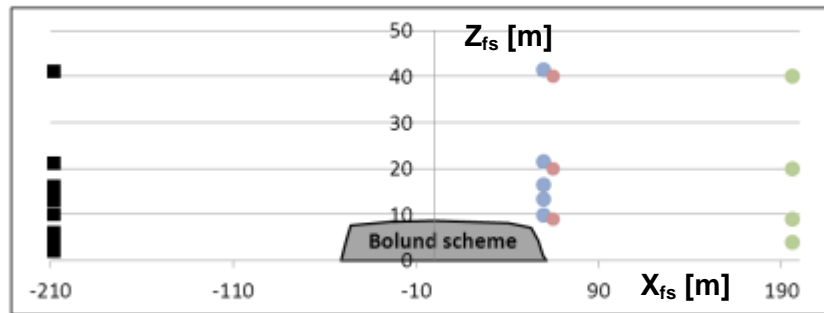
In addition to the *speed-up effect* over the hill top, the flow over hills is characterized by *deceleration* in front of the hill and at the *lee slope*. In the following, the *wake deceleration* behind and the *deceleration effect* in front of Bolund in WOTAN for specific vertical profiles of the mean U-component are computed similarly to the calculation of the fractional speed-up ratio (for inflow directions A and B). This is in addition to the overview on the mean velocity flow field around the hill, as presented in the section “Mean velocity around the hill”, pp. 205.

In Figure 93, the *measurement positions* for the computations of the *wake deceleration* are exhibited. The computed values are shown in Figure 94 and Figure 95. The measurement positions for the *relative blockage effect* are shown in Figure 97. The relative blockage effect is exhibited in Figure 98. As shown in Figure 93 and Figure 94, the *relative deceleration* in hill height *above the lee slope* of Bolund in WOTAN for inflow direction A is around 40 percent⁸⁰. In around $1.5H$ above ground level, the mean flow is *not influenced by the hill*. Furthermore, the full vertical profile has *recovered* around $1.5L$ downstream (behind) the hill, (see Figure 94; the measurement position M11 is indicated with green circles.)

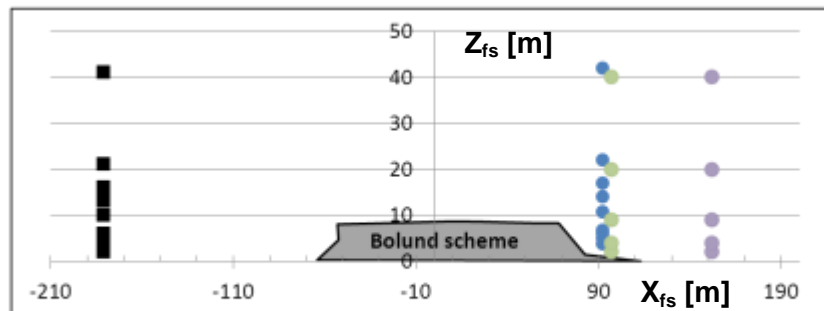
⁷⁹ This can be interesting for wind energy applications with respect to hills with around $H = 40 - 50$ m and which have approximately Bolund shape (for wind turbines with around $80 - 100$ m hub height).

⁸⁰ At M04 and WT10, measurements for heights below H were not feasible due to the UW-set-up of the probe. In general, this can be achieved with UV-set-up of the probe, as done for inflow line B. In the experimental design, this was left to line B since exact rotation of the turntable and new set-up of the LDA probe is time consuming. This remains a recommendation for future work with focus on the wake effects around Bolund.

Measurement positions, Line A:



Measurement positions, Line B:



X and Z coordinates in full scale meters

Figure 93: Measurement positions for calculation of wake deceleration for both inflow directions, Line A (on top) and Line B (below)

Line A, relative wake deceleration around Bolund:

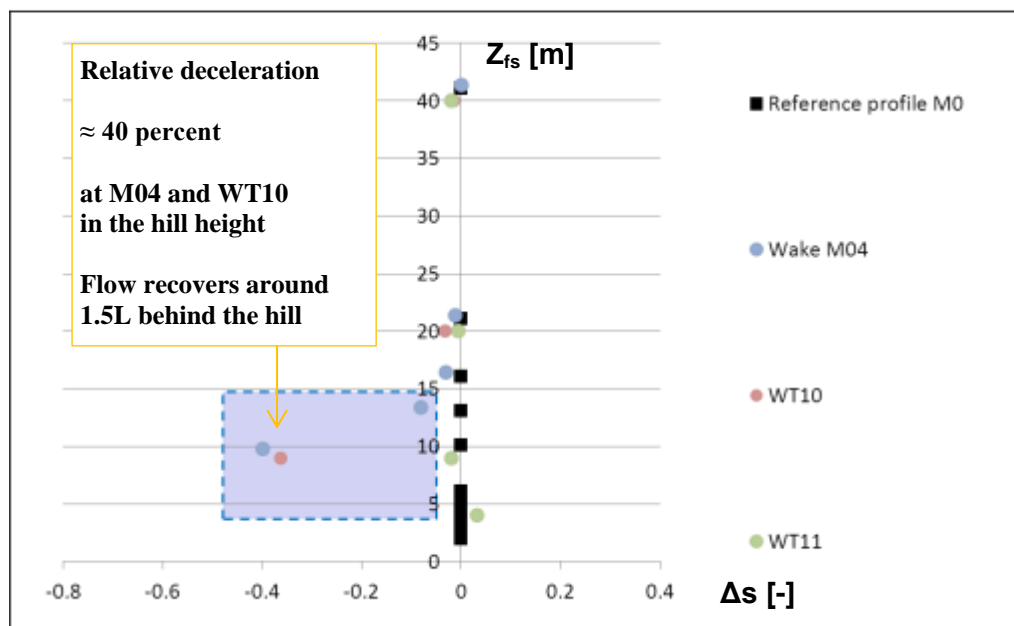


Figure 94: Relative wake deceleration in the lee of Bolund in WOTAN, inflow direction A; the x-axis denotes relative differences of non-dimensional wind-speeds (difference of profile and reference profile); the y-axis denotes the height in full-scale meters; the names of the the vertical profiles are given in the legend; the exact measurement positions of the wake profiles (circles) and the reference profile are indicated in Figure 90

Line B, relative wake deceleration around Bolund:

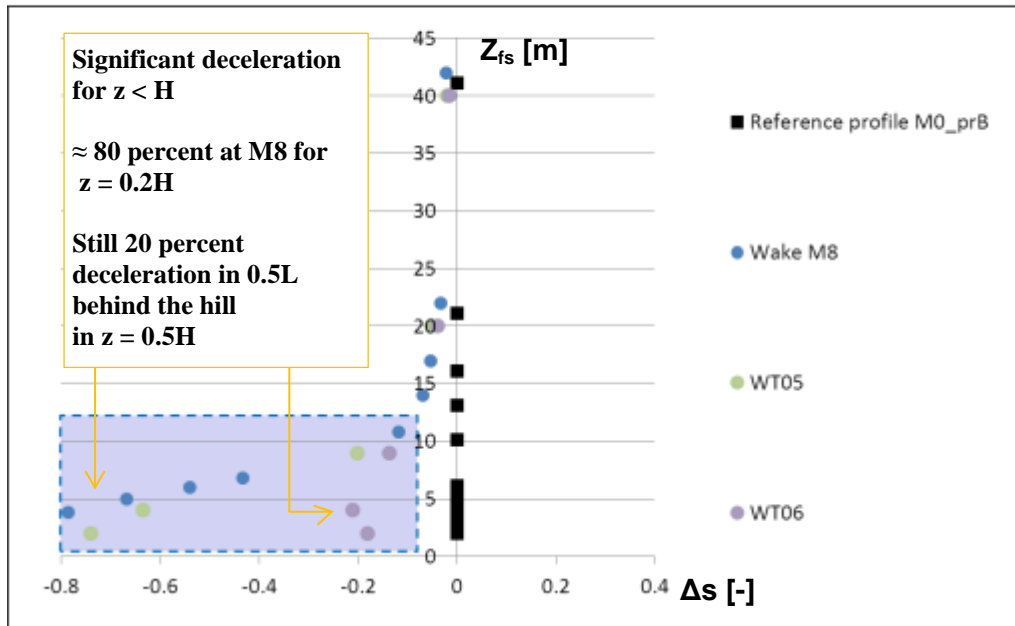


Figure 95: Relative wake deceleration in the lee of Bolund in WOTAN, inflow direction B; indication of the axes as before; the exact measurement positions of the wake profiles are given in Figure 90

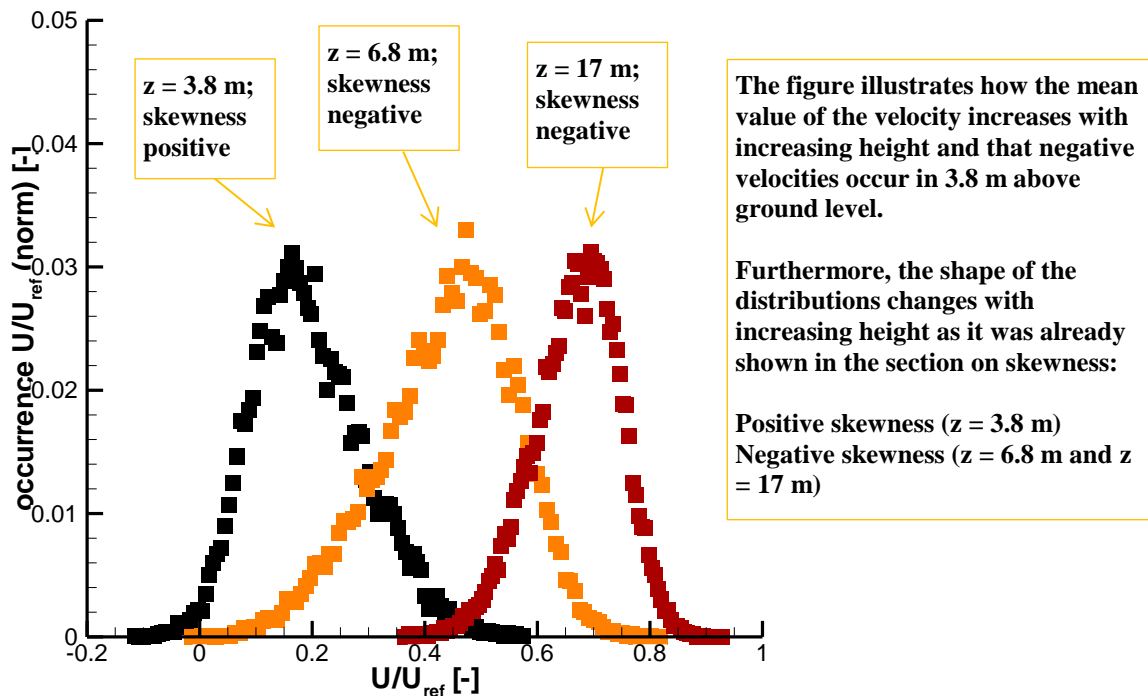
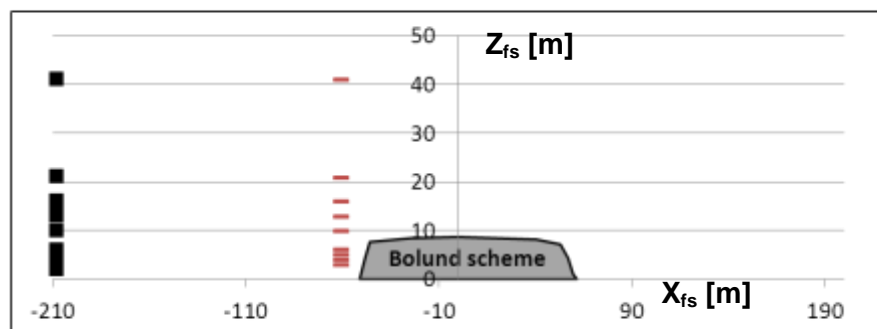


Figure 96: Distribution of instantaneous non-dimensional velocities in the wake of Bolund (at M8 inflow Line B) with increasing height (3.8 m, 6.8 m and 17 m in full scale above ground level); the occurrence of the velocities is normalized (non-dimensional velocities: x-axis; normalized occurrence: y-axis); non-integer measurement heights in full scale metres are due to the non-integer values of the field study.

Figure 95 illustrates the *relative deceleration in the wake* of Bolund in WOTAN for the inflow direction B. For $z < H$, the flow decelerates significantly. At M8 (right behind the hill), flow *decelerates* by around 80 percent in 2 m full scale height ($z \approx 0.2H$). The flow decelerates of around 40 percent in 7 m full scale height ($z \approx 0.6H$). The *deceleration effect* is still found in around $0.5L$ downstream behind the hill (WT06). More precisely, around 60 m in full scale ($0.5L$) behind the lee slope, the *relative deceleration in half of the hill height* is still around 20 percent. In the *hill height* and around 60 m full scale ($0.5L$) downstream behind the hill the deviation from the reference profile is still around 10 percent. Directly behind the hill, in M8, negative instantaneous values of the U component occur and indicate the presence of small eddies (*flow separation*). This is accompanied by a change of the shape of the distribution of the velocity time series, Figure 96.

Equivalent to the analysis of the *wake of the hill*, the measurement positions for the *relative blockage in front of Bolund* in WOTAN for inflow direction A are shown in Figure 97. The calculated values are exhibited in Figure 98. It is found that the deceleration at M1 in front of the hill is around 40 percent in half of the hill height. For $z \approx H$, the deceleration of the mean U-component is around 20 percent. The effect of the hill *decreases with height*. In $z \approx 4H$, the mean flow is not measurably influenced by the hill. The results are summarized in the following section.

Measurement positions, Line A:



X and Z coordinates in full scale meters

Figure 97: Measurement positions for the calculation of the relative blockage in front of the Bolund hill, for inflow direction A

Line A, relative blockage in front of Bolund:

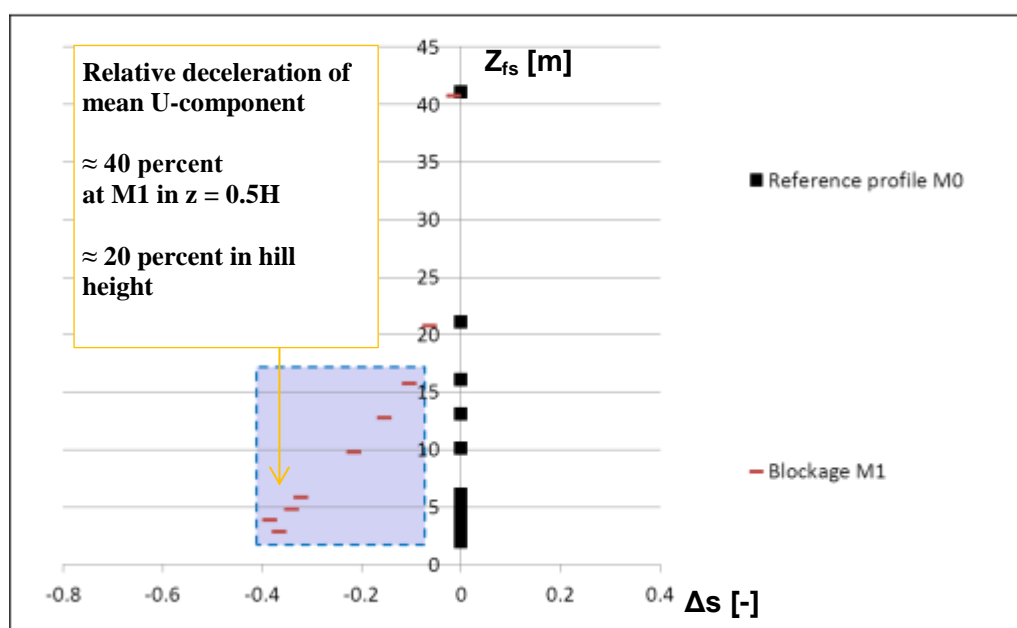


Figure 98: Relative blockage in front of Bolund in WOTAN, inflow direction A; the x-axis denotes relative differences of non-dimensional wind-speeds (difference of profile and reference profile); the y-axis denotes the height in full-scale meters; the names of the vertical profiles are given in the legend; the exact measurement positions of the blockage profile is indicated in Figure 97

Summary of the flow results

For both inflow directions, the *influence of the hill* on the mean U component for $z < H$ starts around $1L$ horizontally in front of the hill. Also, the atmospheric boundary layer flow is *distorted* up to a height of $5H$ (H = hill height) for both inflow directions. The mean flow is still *influenced* up to a distance of $1.5L$ behind the hill for heights up to H (see black dotted lines in Figure 78 and Figure 79)

The W-component is *positive* in front of the hill, turns *negative* along the hill and is *maximally negative* in the lee of the hill. This indicates that the mean flow approximately *follows* the shape of the hill.

The standard deviation *almost doubles* behind the hill at height around $z_{agl} = 0.5H$ for all three components at both inflow directions, Figure 80 - Figure 85. The maximum v_{rms} is slightly shifted to the ground, the maximum w_{rms} to the upper hill edge.

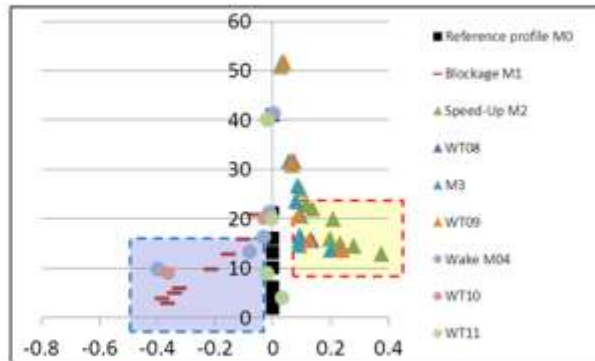
The *shear stress* is negative around the hill and increases (in absolute value) by around *five times* at the *front edge* and *behind the hill*, Figure 86 and Figure 87. The *skewness* is *negative* for free stream flow and *turns positive* close to the *ground* in the *blockage area* and in the *wake of the hill*. In contrast, at the top *luv edge* of the hill, skewness *increases* in its *negative* value by around *five times*.

Negative instantaneous values of the U component indicate *flow separation*. This is according to values in the literature. For 2dimensional hills, 0.31 (≈ 17 degree) are assumed to be the critical slope for flow separation, and 0.63 (≈ 32 degree) in 3dimensional case [Wood, 1995]. To obtain more reliable results for the statistics of the V- and W-component it would be necessary to conduct further Re-tests and further convergence-analyses for *all of these quantities*.

Line A, relative speed-up, wake deceleration and blockage around Bolund:

Results:

- Speed-up in 2-5 m agl is around 20-40 %
- It is largest above front edge in M2
- Blockage in front of the hill is up to 40% at half hill height
- Wake deceleration is up to 40% in hill height
- Reference profile $u_0(\Delta z)$ = vertical profile in M0

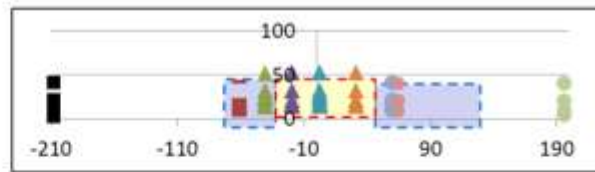


Notation:

- X-axis

$$\Delta s := \frac{u_0(\Delta z) - \Delta \hat{u}(x, \Delta z)}{u_0(\Delta z)}$$
- Y-axis
 Δz := height in full scale meters

Measurement positions:

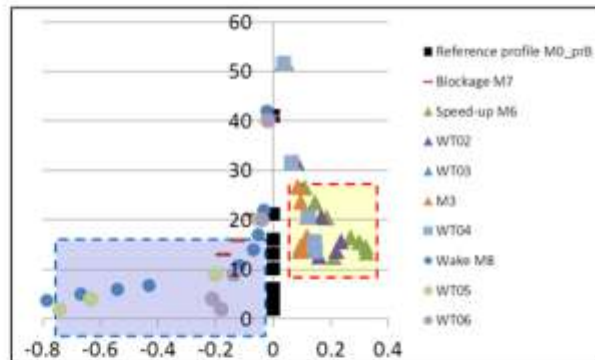


X and Z coordinates in full scale meters

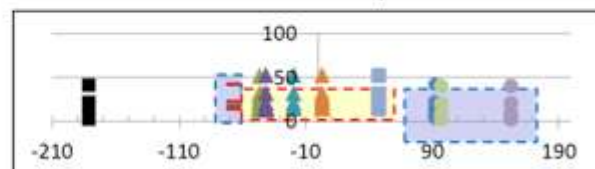
Line B, relative speed-up, wake deceleration and blockage around Bolund:

Results:

- Speed-up in 2-5 m agl is around 20-30 %
- It is largest above front edge in M6
- Blockage in front of the hill is up to 20% at hill height
- Wake deceleration is up to 80%
- Reference profile $u_0(\Delta z)$ = vertical profile in M0_prB



Measurement positions:



X and Z coordinates in full scale meters

Figure 99: Summary of the hill impact on the mean U-component, Line A and Line B

Also, Figure 90 - Figure 98 can be summarized (the *relative speed-up ratio*, the *relative deceleration in the wake* and the *relative deceleration in the blockage area* of Bolund in WOTAN). This is exhibited in Figure 99 for both inflow directions.

Finally, in comparison of both inflow directions (*different hill profiles* of Bolund) the *maximum speed-up ratio* is found to be *larger* for inflow direction A in WT11 than for inflow direction B in M6. Hence, for steady state inflow conditions (as in WOTAN) the speed-up ratio is sensitive on slight variations of the front shape. This supports the results of the pilot study in chapter 7.

Remarks on the Bolund field data

In this section, insights into the Bolund field data are given. Then conclusions are drawn with regard to the results of the Bolund in WOTAN wind tunnel study. The *filtering method* for obtaining field time series with *meteorologically nearly constant boundary conditions* is based on the filtering method which was applied by Bechmann et al., [2011]. It has to be emphasised that Bechmann et al., [2011], used *ensemble averaged statistics* in order to determine inflow conditions for the atmospheric micro-scale flow models. The *ensemble averaged* values are also used for the comparison of the model results in Bechmann et al., [2011]. The analysis which is carried out in this section goes beyond ensemble averaged statistics and tries to figure out in how far the *ensemble averaged properties of different* time periods are statistically representative for the ensemble and can lead to meaningful results in the comparison of models. Three main theses are derived from the analysis of the Bolund field data and are substantiated in the following:

1. The *Taylor hypothesis* is *not* valid along the hill. (This is according to the expectations.)
2. The Bolund inflow is *not statistically stationary*.
3. The Bolund field data shows *deviations* from the *Reynolds number independency*.

For this purpose, Sonic 20 Hz time series from the Bolund MySQL data base veadata-01.risoe.dk at measurement positions M0S5, M3S2, M3S5, M6S2, M6S5, M7S2, M7S5 and

M9S5 are analysed for inflow direction B. Details on the instrumentation and the data is provided in Bechmann et al., [2011], and Berg et al., [2011]. For the analysis in this work, the wind data is aligned with the North-East-South-West-coordinate system and filtered for 10-minutes mean wind directions (262° - 278°) and neutral atmospheric conditions (absolute inverse Obukhov-length below 0.002) at free-stream mast M0. The time interval Z2 is a 1.17-hour connected measurement time interval that is covered by all measurement positions M0, M9, M3, M6 and M7. It consists of data which is recorded from 7:40 to 8:50 a.m. on the 27th of January in 2008. The time interval Z3 is a 2.17-hours connected measurement time interval which is covered by all masts M0, M9, M3, M6 and M7. It contains records from 8:00 to 10:10 p.m. on the 30th of January of the same year. Z2 and Z3 are chosen in this analysis since they are comparable in the sampling duration and the time gap between the samplings is only three days; (Z4 and Z5 could have been used for these reasons as well). More details on the field data are given in appendix, pp. 307.

The *Taylor hypothesis* states that “if the mean wind speed were high enough, the turbulence would not have time to change as it was being convected past a point” [Lumley and Panofsky, 1964]. This assumption is also called “*frozen turbulence*” and builds the basis for the assessment of statistical errors with respect to the *sampling duration* for field data e.g. in Wyngaard, [1973], (see also chapter 9). It is also the foundation of *rapid distortion theory* which was discussed in the section on Linear Theory in part II, pp. 119.

In this section, cross correlations of the Bolund field data base are computed for two data record time periods. Figure 100 shows that the time series of the *horizontal longitudinal velocity component* in 5 m above ground level (in field scale) at the reference locations south-west (in front of) the hill and south-east (behind the) hill are *correlated*. The correlation is *larger* for the time period Z3 than for Z2. Furthermore, the cross correlation for the time period Z3 exhibits a *peak* at a *time lag* of around 1-2 minutes. This corresponds to the *travel time* of an air parcel at around 6 m/s mean velocity from M0 to M9 (around 0.5 km *longitudinal* distance). Furthermore, M0 and M9 have a *lateral* distance of around 80 m. Hence, Figure 100 substantiates the assumptions of a *physically existing* integral length scale at least as large as 80 m *in lateral direction*. (Here the integral length scale is called

“physically existing” since in the next step it will be argued that the overall flow is not statistically stationary and hence the integral length does not exist in the strict mathematical sense).

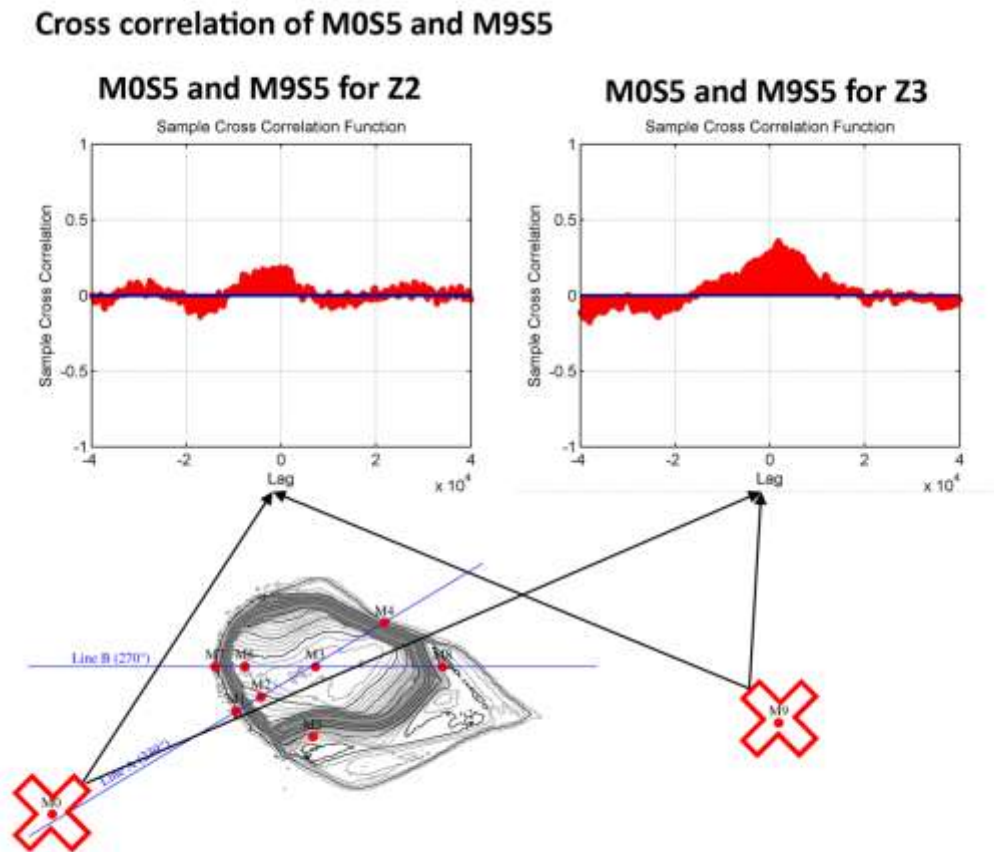


Figure 100: The red crosses on the map show the measurement location (the exact location is given by the red circle in the cross); the plots show cross correlations of the horizontal longitudinal (west-east) velocity component of Bolund field data; The x-axis denotes the time lag in units of 0.05 seconds in field scale time according to the sampling frequency of the 20 Hz sonic anemometers; The cross correlation of M0 and M9 for Z3 exhibits correlation and indicates the existence of a lateral integral length scale.

For the same time periods, Z2 and Z3, Figure 101 exhibits the cross correlations of the reference location, M0, with the centre point on the hill, M3, in two different heights. As before the correlation is *larger* for the time period Z3 than for Z2. The *travel time lag* is again visible for the time period Z3. Furthermore, the correlation between the centre point and the inflow is *larger* in 5 m height above ground level than in 2 m height above ground level. Figure 102 exhibits the cross correlations of the longitudinal velocity component at the reference position, M0, with the location at the front edge of the hill, M6, in 2 m above

ground level and 5 m above ground level. As before the correlation is *larger* for the time period Z3 than for Z2 in 5 m height. In contrast to the correlation between the inflow and the *centre point*, the correlation pattern for the time period Z3 “breaks down” in 2 m above ground level *at the front edge*. In the time period Z2, new frequencies arise. As Figure 100 and Figure 101, also Figure 102 exhibits *different characteristics of the cross correlations* at the same measurement positions for the *different time periods*, Z2 and Z3,.

In summary the flow of the real Bolund hill shows *spatial correlations* which are larger for Z3 than for Z2. The cross correlations are strongly influenced by the hill. In conclusion the *Taylor hypothesis* does *not* hold for the overall flow. This supports the results of Berg et al., [2011], who analysed the field data of the *turbulence intensities* along the hill and concluded that the Taylor hypothesis is violated and that linear models “may provide no insight” in the Bolund case since the effects are non-linear. Yet another conclusion can be drawn: theories which rely on the validity of the *Taylor hypothesis* for the estimation of *statistical errors* of moments of velocity and fluctuations may lead to false results. It is also shown that the spatial cross correlations of the velocity time series of the Bolund field data *are different* for *different periods* of data record which are in the same *ensemble of data* (according to the filter which is used here). The differences of the cross correlations are linked to the thesis that the interpretation of the time series for the time periods Z2 and Z3 as *realisations of one and the same statistically stationary stochastic process* is not necessarily meaningful. This is substantiated in the following.

No “frozen turbulence” along the hill: Cross correlation M0 and M3

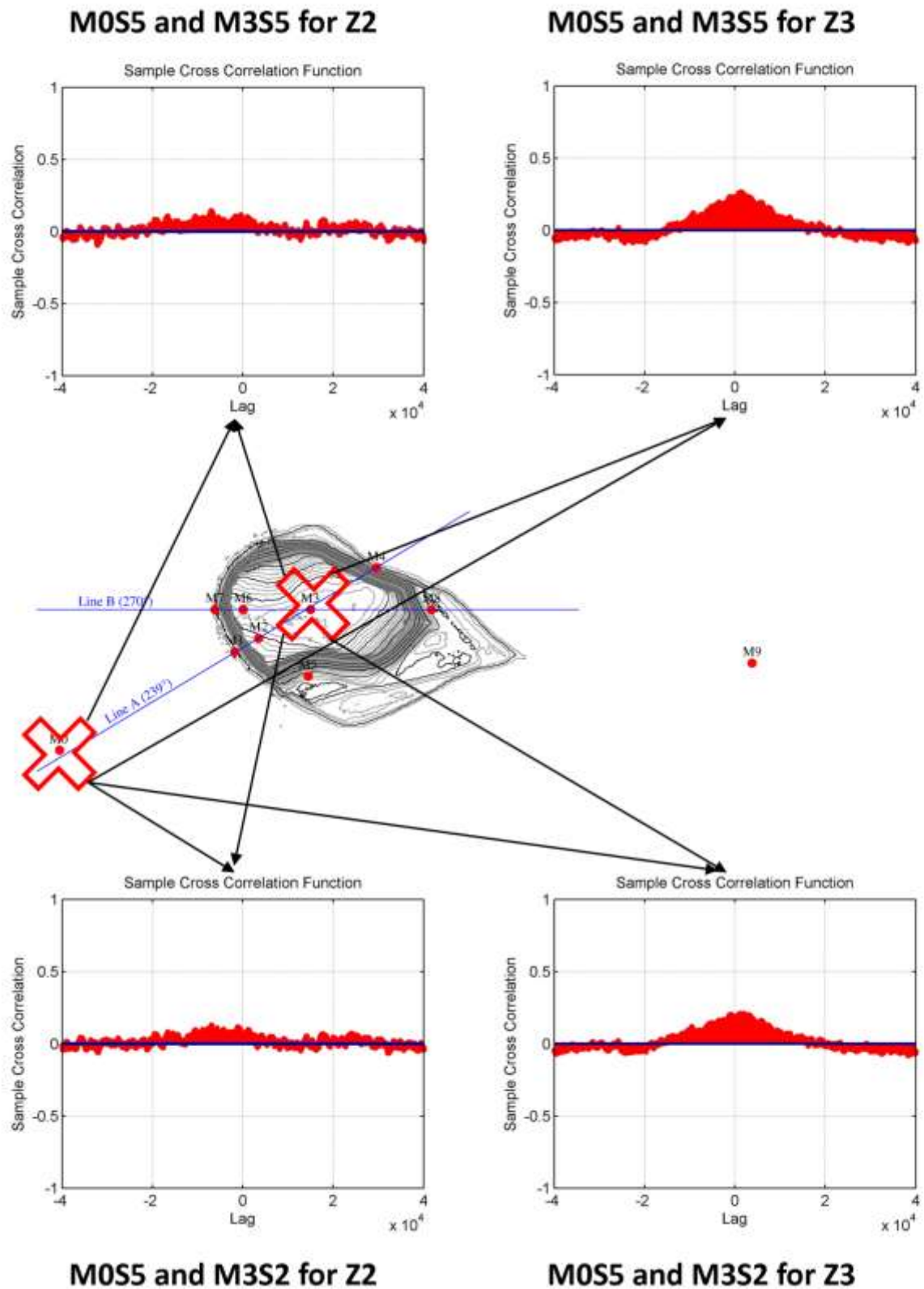


Figure 101: Cross correlations of the longitudinal velocity component of Bolund field data; the x-axis denotes the time lag in units of 0.05 seconds in field scale time.

No “frozen turbulence” along the hill and destruction of large scale structures at the front edge: Cross correlation of M0 and M6

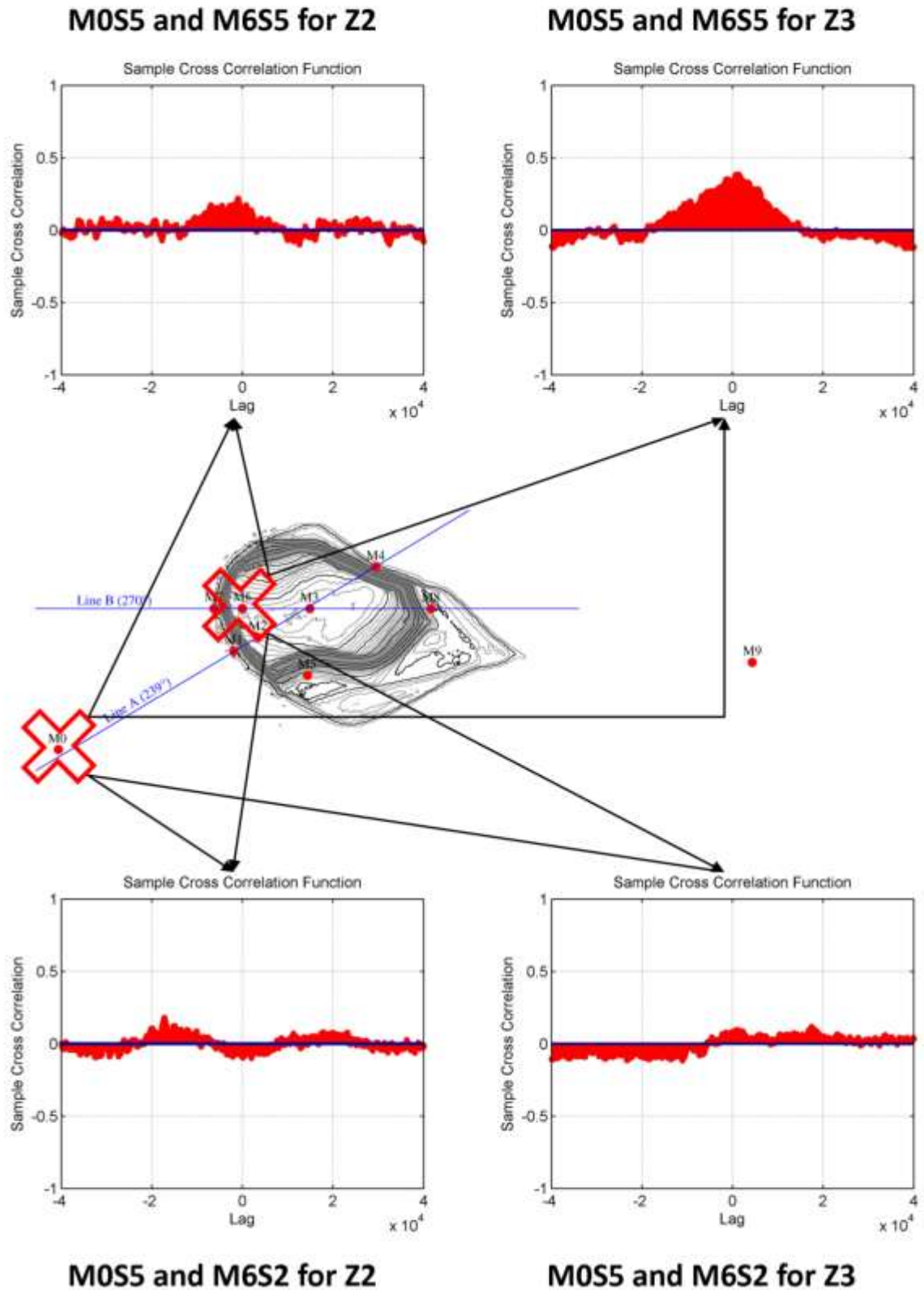


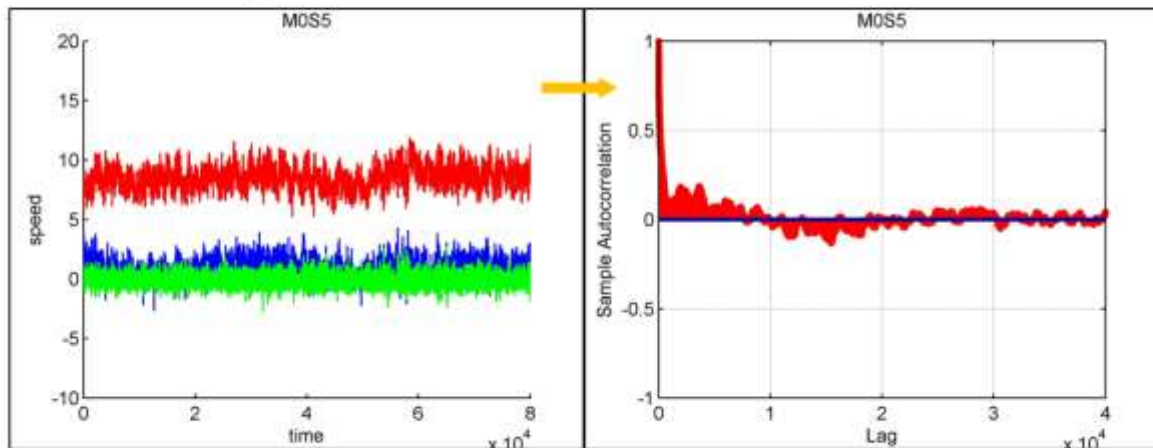
Figure 102: Description as in the previous figure; further interpretation of the figure is given in the text.

Not only the *cross correlations* between different points are not similar for *different time periods*. Also the *autocorrelation functions* along the hill are different. Here it is focused on the examination of the *autocorrelation functions* in M0 and M9. (More corresponding figures are shown in the appendix, pp. 307.) The time series and autocorrelation functions of M0 in 5 m height above ground level for the time periods Z2 and Z3 are presented in Figure 108. Figure 108 illustrates that the *mean wind velocity* is slightly *larger* for Z2 (around 8 m/s in full scale) than for Z3 (around 6 m/s in full scale). The *standard deviations* and the *shape of trends* seem to be comparable. Further statistical differences of the two time series cannot be clearly detected or excluded from a rough visual analysis. The different statistical characteristics are more adequately visible in the *autocorrelation functions*. The *autocorrelation function* of the reference mast in M0 for the time period Z2 shows a *steep declination* within 2-3 minutes and exhibits *frequencies with smaller periods* (around 5 to 10 minutes) superimposed on larger ones (cycle of around half an hour). The superposition of the small periods (around 5 to 10 minutes) is also exhibited in the autocorrelation function for the time period Z3. However, for Z3 the *decrease of the autocorrelation* is *less steep* than that for Z2. The cause is not only the *mean velocity* which is *slower* in the latter case. The difference is too large. The question is whether this difference has a significant meaning for the physics of the atmospheric flow. From the visual comparison of *the integrals of the positive parts* of the two autocorrelation functions up to the first zero of the function the *estimated integral length scale* in longitudinal direction is more than *twice* for Z3 than for Z2. This is supported by the examination of the autocorrelation functions at another *reference position* (M9) for the same time periods Z2 and Z3, shown in Figure 104. Furthermore, from a visual assessment *a trend* can be detected in the second half of the time period Z3, in Figure 104. The trend of the time series is also visible in the *slow decay* of the autocorrelation.

In summary, the *autocorrelation functions* of the reference positions show *differences* for the *different time periods*. This leads to a significant ambiguity in the derivation of *physical properties* of the flow (e.g. an uncertainty of 50 – 100 percent for the estimated value of the “physical” integral length scale.) Hence, the conclusion in this work is that the time series for Z2 and Z3 should not be interpreted as realisations of *one and the same* statistically stationary stochastic process unless large uncertainties are taken into account.

Time series and autocorrelation at M0: the autocorrelation functions are different for different time periods in the undisturbed ABL flow hence the ensemble of field data is not statistically stationary

Time period Z2



Time period Z3

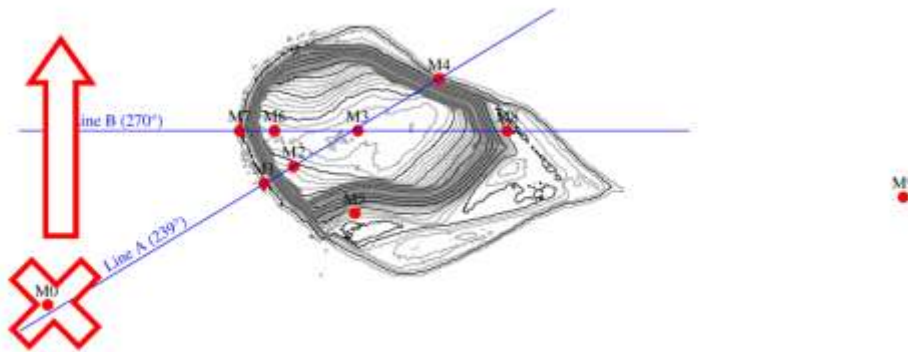
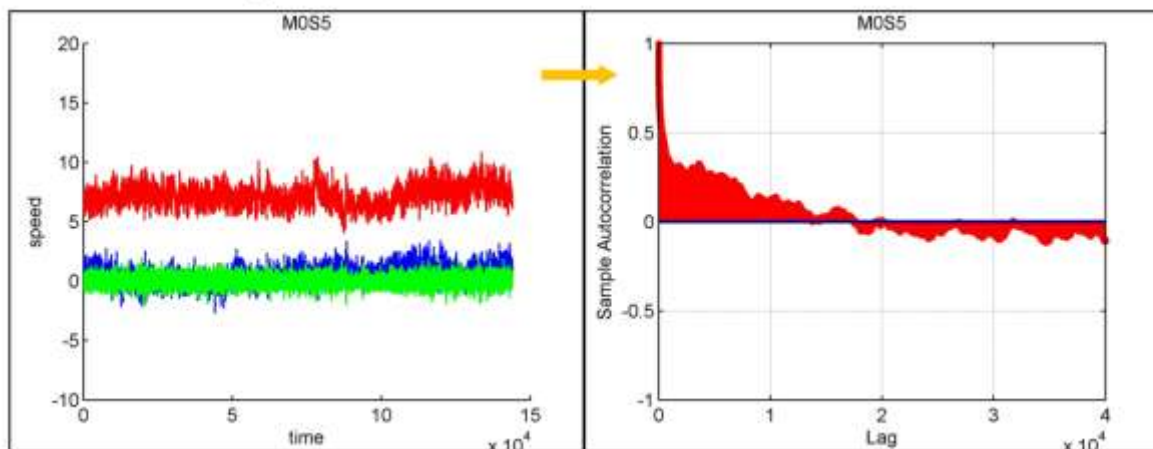


Figure 103: The red time series exhibits the U-component of the velocity (in direction of Line B); The lateral component is shown in blue and the vertical component in green; The y-axes of the time series plots (left) denote velocity in m/s (field scale), the x-axes of the time series and autocorrelation plots show the time steps in 0.05 s (field scale) which corresponds to 20Hz Sonic data.

Time series and autocorrelation at M9: the autocorrelation functions are different for different time periods in the undisturbed ABL flow

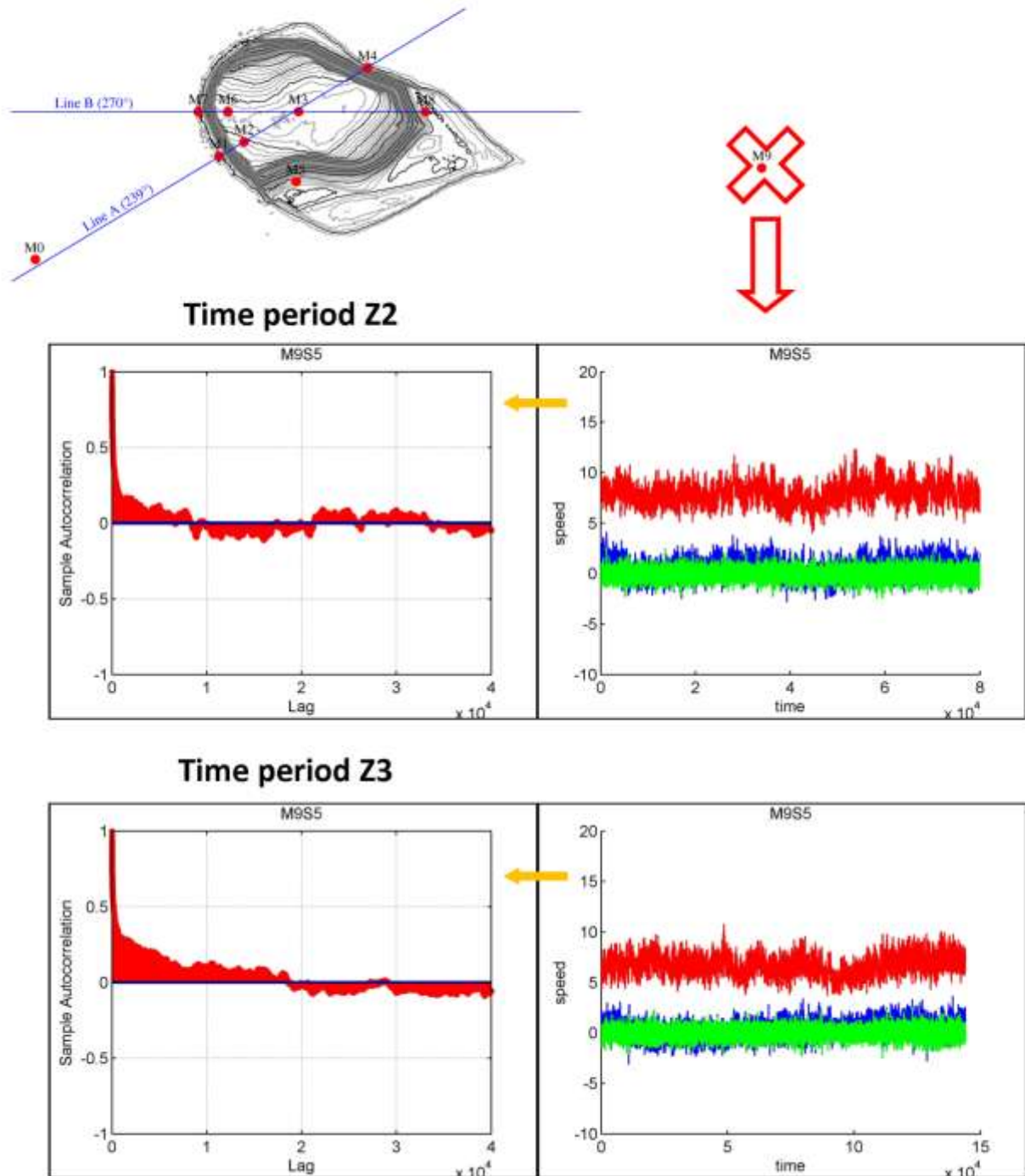


Figure 104: As in the previous figure the red time series exhibits the U-component of the velocity (in direction of Line B); The lateral component is shown in blue and the vertical component in green; The y-axes of the time series plots (left) denote velocity in m/s (field scale), the x-axes of the time series and autocorrelation plots show the time steps in 0.05 s (field scale) which corresponds to 20Hz Sonic data.

The third thesis claims that the Bolund field data shows deviations from the *Reynolds number independency*. This is already substantiated in the section on *field data* in the chapter on *models as mediators in wind assessment* in part II of this work, pp. 91. It was shown that the spread of ten minutes mean values is around 20 to 60 percent (up to 9 m/s in field scale) for different locations along the hill. The spread is worst at the front edge in 2 m height above ground level (± 50 percent) and in the lee of the hill (± 35 percent). The reason can be that the *variability of the atmosphere* leads to changes in the inflow conditions which are intensified at the measurement positions along the hill due to the *effects of the topography*. In the field study, slight changes of the *shape of the front edge* are indirectly present due to slight changes of the *mean inflow direction* and the *asymmetric shape of the hill*. It is already shown in the pilot study on the idealized Bolund hill in BLASIUS that the flow properties are sensitive on slight changes of the *shape of the front edge* even for the laboratory inflow conditions (pp. 159).

Furthermore it can be remarked that the *Reynolds number* is not uniquely defined for flow over *asymmetric shapes*. It is plausible that the *characteristic velocity* approaches zero in the flow areas around the hill. Here, the mean flow is strongly disturbed by the hill (e.g. due to strong deceleration in the blockage area). Furthermore, at certain points along the hill the *characteristic length* is rather a local *geometrical feature* (e.g. the height of the hill). Here, the fetch of the inflow or the height of the boundary layer is rather not a characteristic length for the local flow. It is even plausible that the Reynolds number falls below the critical Reynolds number for certain areas around the Bolund hill⁸¹.

Another reason for the large spread at the front edge in relation to other measurement positions can be that the *statistical properties of the turbulence* are distorted *due to the effect of the topography*. The (assumedly) underlying stochastic process can change such that the convergence of the statistical properties at 10-minutes averaging time in flow area *at the front edge* is much worse than the convergence at 10-minutes averaging time *in the undisturbed flow*.

In conclusion, the aforementioned *variability of the atmosphere* and the *drop of the Reynolds number* in *local flow areas* as well as the *dependence of the (statistical)*

⁸¹ It is remarkable that the flow area at the front edge yields the largest deviations from the Reynolds number independence in both the pilot study on idealized Bolund in BLASIUS and in the data of the field study.

convergence properties of the flow due to the effects of the topography are suggested as three *different possible causes* for the *symptom* of deviations from the *Reynolds number independence* which was found in the Bolund field data (p. 96).

In summary, in this section the relationship of the Bolund *field data* with the *theories* on “frozen turbulence”, statistically stationary properties and fully developed turbulence was examined. Three main theses were derived: it was argued that the *Taylor hypothesis* is not valid along the hill, that the Bolund inflow is *not statistically stationary* and that the Bolund field data shows *deviations from the Reynolds number independency*, especially at the front edge. The conclusion is that the use of *ensemble averaged statistics* as in Bechmann et al., [2011], should be accompanied by an analysis on the *homogeneity of the statistical properties* within the *ensemble*. Otherwise the use of the *ensemble averages* for model comparison can lead to wrong values with respect to the *theories* which are implemented in the models. The range of the uncertainty of the conclusions which are drawn from field data is also mentioned in Bechmann et al, [2011] and Berg et al., [2012], however, their analyses are only based on *ensemble averaged statistics*.

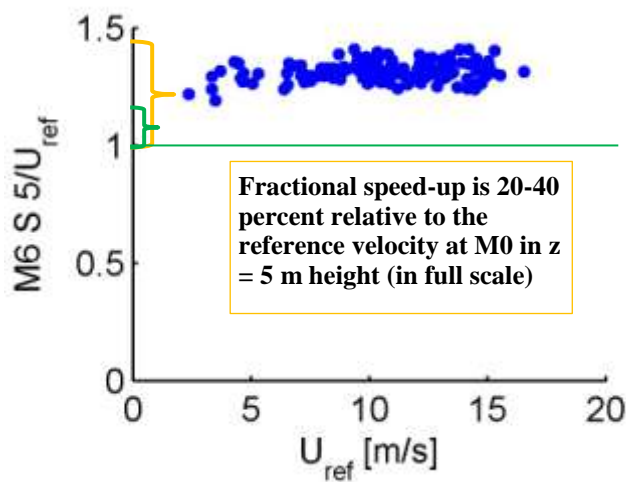


Figure 105: Bolund field data as in p. 96

For future research it would be interesting to compare the mean flow results of the wind tunnel study of Bolund in WOTAN with results of other models or field data.

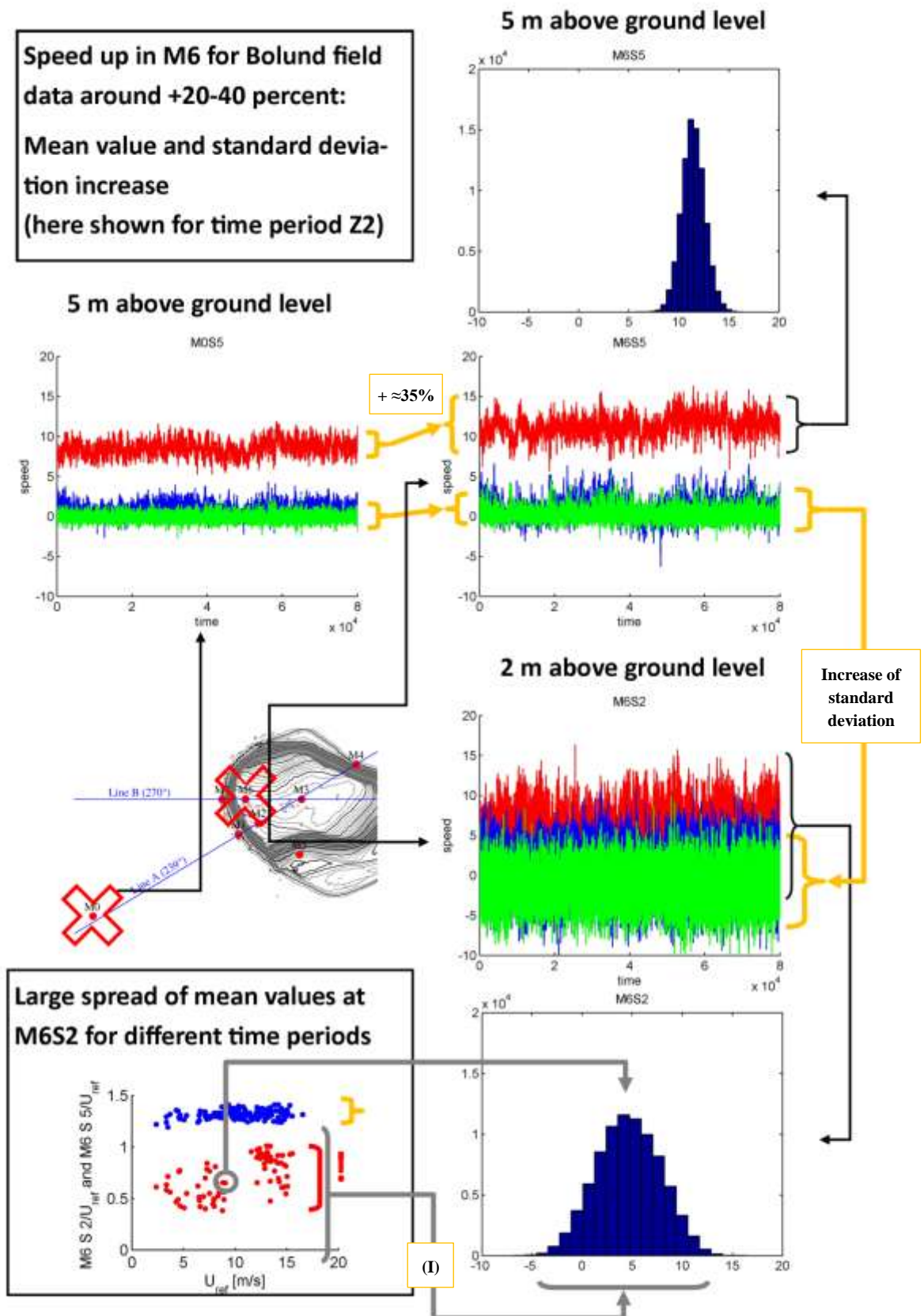


Figure 106: The reference velocity is measured at M0 in 5 m height above ground level (full scale); the grey line (I) at the bottom illustrates that the spread of the instantaneous velocities in the analysed time series is larger than the spread of the time averages within the ensemble of all time series.

Influence of the Bolund hill on the shape of the probability density functions for time period Z2 (x-axis denotes wind speed in full scale m/s)

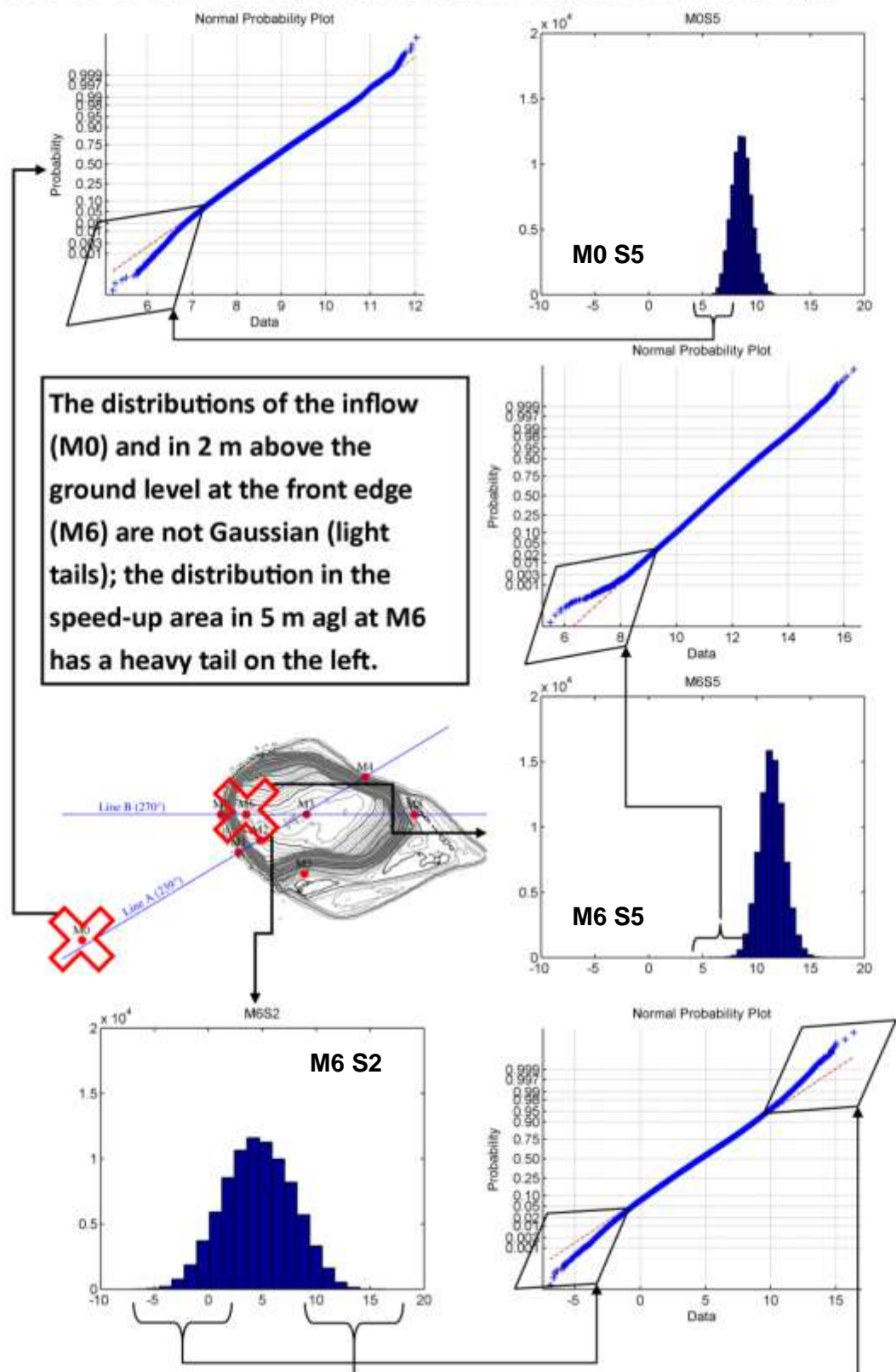


Figure 107: See explanation in the text.

A start for an extended analysis of the Bolund field results is given in the following. Figure 105 to Figure 107 illustrates the *speed-up effect* and *properties of the exemplary probability density distribution*. The fractional speed-up of 20-40 percent in 5 m above ground level (in field scale) at the front edge (at M6) shows good agreement with the 20 – 40 percent estimation for the Bolund in WOTAN wind tunnel results. (This is also according to Bechmann et al., [2011], which give a value of 30 percent. However, the incomplete information of the Bolund field inflow conditions has to be considered.) Figure 106 also shows the *increase of the amplitude of the fluctuations* in 2 m above the front edge (M6S2). Furthermore, the hill has an influence on the shape of the velocity distribution for the here analysed time period. This is illustrated more explicitly in Figure 107 in comparison of the distributions with reference Gaussian distribution. Figure 107 shows the *light-tailed distribution* at the front edge in 2 m height and the *occurrence of instantaneous “negative” velocities* which gives evidence for flow separation. Also, whereas the inflow at M0 in 5 m above ground level is *light-tailed* the flow in the speed-up area is *heavy-tailed* to the left. For a further comparison of the Bolund in WOTAN wind tunnel results with the Bolund field study the analysis of the Bolund field data needs to be extended.

It would be interesting to extend the analysis which was carried out here to the *cross correlations* and the *autocorrelations* with respectively of the *lateral* and *vertical* velocity components. Also, an extension of the analysis to further time periods (e.g. Z1, Z4, Z5 and Z6) would be meaningful in order to assess the *spread* of the statistical properties *within the ensemble*. Furthermore, the surrounding *meteorological conditions* (weather) can be analysed further. The result may be that filtering methods different from those which were used here (based on Bechmann et al., [2011]) are more appropriate for obtaining an ensemble of time series with nearly constant (statistically stationary) meteorological boundary conditions. Furthermore, a sensitivity study on the *influence of the filtering methods* on the ensemble of the time series and its *averaged ensemble statistics* could be meaningful. Also, a sensitivity study on the influence of the *averaging time* on the results would be useful in order to assess the *statistical convergence* with respect to the *sampling duration*.

Summary of Bolund in WOTAN

The purpose of the *main Bolund hill wind tunnel experiment* was to increase the knowledge how and how well the Bolund hill can physically be modelled in the *large atmospheric boundary layer wind tunnel* WOTAN of the University of Hamburg. *Precision* and *accuracy* were defined as the *measures of the quality of the experiment* (= validity of the model, recall p. 167). The main results of the quality assessment are summarized as follows:

Smooth atmospheric boundary layer flow over Bolund (a steep hill in Denmark) is modelled with satisfying repeatability (precision) in the large boundary layer wind tunnel. It is found that the *precision uncertainty* can be significantly (e.g. five times) larger in characteristic flow areas around the hill than in the undisturbed flow⁸². This is supported by the pilot study on *idealized hill shapes*. Hence, (depending on the purpose of modelling) a careful assessment of the *precision* with respect to the *local topographical features* and *flow areas* is an important factor for the interpretation of the results of physically modelled atmospheric boundary layer flow over hills .

For Bolund in WOTAN, the precision deviation for the mean U-component (including Reynolds number tests) in terms of full scale wind speeds (with reference wind speed of 10 m/s) was *in average* around 0.2 m/s. (This value was assessed by repeatability tests, convergence test and Reynolds tests.) The *precision assessment* is of utmost importance if the Bolund in WOTAN data is used for the *validation of numerical models* which use the same *inflow conditions* as the wind tunnel model.

For the maximisation of *accuracy* emphasis was put on the *maximisation of the geometrical similarity* between the model and the full scale Bolund hill. For Bolund in WOTAN, a geometrical resolution of 1 mm in model scale was achieved (0.25 m in field scale). Based on the Re-tests and the results of the pilot study the model was assumed to be *sufficiently aerodynamically rough*.

⁸² For example, the precision deviation in the wake of the hill can be around 1 m/s in full scale wind speeds (with reference wind speed of 10 m/s). This can be significant with respect to the low wind speeds in this area. "Significance" is part of the interpretation of the results and depends on the purpose of the experiment.

Further on, for the maximisation of *accuracy*, special diligence was put on the determination and physical adjustment of the *meteorologically consistent* boundary layer with respect to the Bolund field conditions. For the adjustment in WOTAN the following properties were analysed: the vertical mean velocity profile (vertical log law wind profile with proper roughness length, z_0 , friction velocity, u_* , power law exponent), turbulence profiles (vertical profiles of standard deviation and turbulence intensities of all three velocity components, vertical profiles of turbulence spectra, vertical profiles of integral length scales), surface layer height (constant shear layer – which is assumed to be valid in the Prandtl layer) and the lateral and longitudinal homogeneity of the model area in the wind tunnel (lateral and longitudinal profiles of all meteorological parameters). The available values of the Bolund blind comparison and Bolund raw data were supplemented with literature values *for smooth atmospheric boundary layer flow*.

The main model results are that the *area of influence* of the hill on the mean flow extends to one hill-length in horizontal distance *in front of the hill*, up to five hill-heights in the *vertical direction above ground level* and to the horizontal distance of 1.5 hill-lengths *behind the hill*. The *maximum speed-up* around Bolund in WOTAN occurs *above the front edge of the hill*; the mean velocity increases of up to 40 percent in 2 – 5 m in field scale above ground level (relative to the mean velocity in the same height in the boundary layer flow without topography). Furthermore, it is found that the *turbulent flow statistics* are sensitive on the flow geometry: The *standard deviation almost doubles* behind the hill at half hill-height for all three velocity components; The *shear stress* is *negative* around the hill and *increases* (in absolute value) by around *five times* at the front edge and behind the hill; The *skewness* is *negative* for the free stream flow and *turns positive* close to the ground in the blockage area and in the wake of the hill. In contrast, at the top luv edge of the hill, skewness *increases* in its *negative* value by around *five times*.

With respect to the Bolund field study further analysis of the field data is necessary if the *purpose* is to compare the model results with the field data. Only if the statistical properties of the field data are clear then field data can serve for *increasing, maintaining or decreasing the belief* into the *accuracy* of the model. A *sensitivity study on the influence of the filtering*

methods on the ensemble of the time series and its averaged ensemble statistics is suggested for future work. Also, a *sensitivity study on the influence of the averaging time* on the field data is pointed out as interesting question in order to assess the statistical convergence of the field data with respect to the sampling duration – given that for difficult measurement positions in the flow the established theories which are based on “frozen turbulence” fail (e.g. at the front edge of the hill).

The *statistical convergence* of Bolund in WOTAN *wind tunnel measurements* at the front edge of the hill is analysed in more detail in the following chapter.

9. Statistical analysis of the influence of resampling configurations on higher order statistics at the luv edge

“An experiment is a question which science poses to nature, and a measurement is the recording of nature's answer. But before an experiment can be performed, it must be planned – the question to nature must be formulated before being posed. Before the result of a measurement can be used, it must be interpreted - nature's answer must be understood properly.”

– Max Planck, 1949 [Planck, 1949, p. 325]

In this chapter, the *statistical representativeness* of measurements of Bolund in WOTAN at the front edge of the hill is analysed in more detail. (This is a “difficult” location with regard to the *precision* in the pilot study and difficult with respect to the ambiguity of the field data, as well. However, here is the focus on the wind tunnel data). This chapter is to be understood as an extension of the *precision assessment* of the main wind tunnel study Bolund in WOTAN. The motivation is to gain insights into the statistical properties of *small scale turbulence* of atmospheric boundary layer flow over topography and to *be prepared* for using laboratory data to give insights for theories which try to explain *small scale turbulence*. For this purpose, the *statistical properties* of a long wind tunnel velocity time series (corresponding to around 40 hours of sampling time in full scale) are directly computed from the *time series* and compared to *subsets* (intervals) of the same time series with *shorter* sampling durations and variations of re-sampling configurations.

Much literature exists on “how long is long enough when measuring turbulence statistics” and on the estimation of *statistical errors of moments of velocity and fluctuations* in the atmospheric surface layer, for example by Lenschow et al., [1994], Lenschow and Stankov, [1986], Screenivasan et al., [1978], Lumley and Panofsky, [1964], Wyngaard, [1973] and Liepmann, [1952]. However, the research so far is concentrated on turbulence statistics in the atmospheric boundary layer *over flat terrain* and not for flow which is disturbed by topography. Screenivasan et al., [1978], for example investigate velocity measurements in 5 m (field scale) height above water obtained at the ESSO-BHP natural gas platform about 80 km off the Gipssland coast of Vicotria, Australia. Lenschow and Stankov, [1986], analyse data

obtained by aircraft flights in the convective boundary layer in heights between 680 m and 1900 m above ground level. The theories which are established go back to Lumley and Panofsky, [1964], Wyngaard, [1973] and Liepmann, [1952] and rely on more or less strict assumptions for the underlying stochastic process based on the physics of the atmospheric boundary layer over *flat terrain*. The most important assumptions are that of *flow over horizontally homogeneous flat terrain* and the validity of “*frozen turbulence*” [Wyngaard, 1973], hence the *existence of the integral time scale* [Wyngaard, 1973, Lumley and Panofsky, 1964, p.36, Liepmann, 1952, p. 324] or an *exponentially decaying autocorrelation function*, [Lenschow et al., 1994].

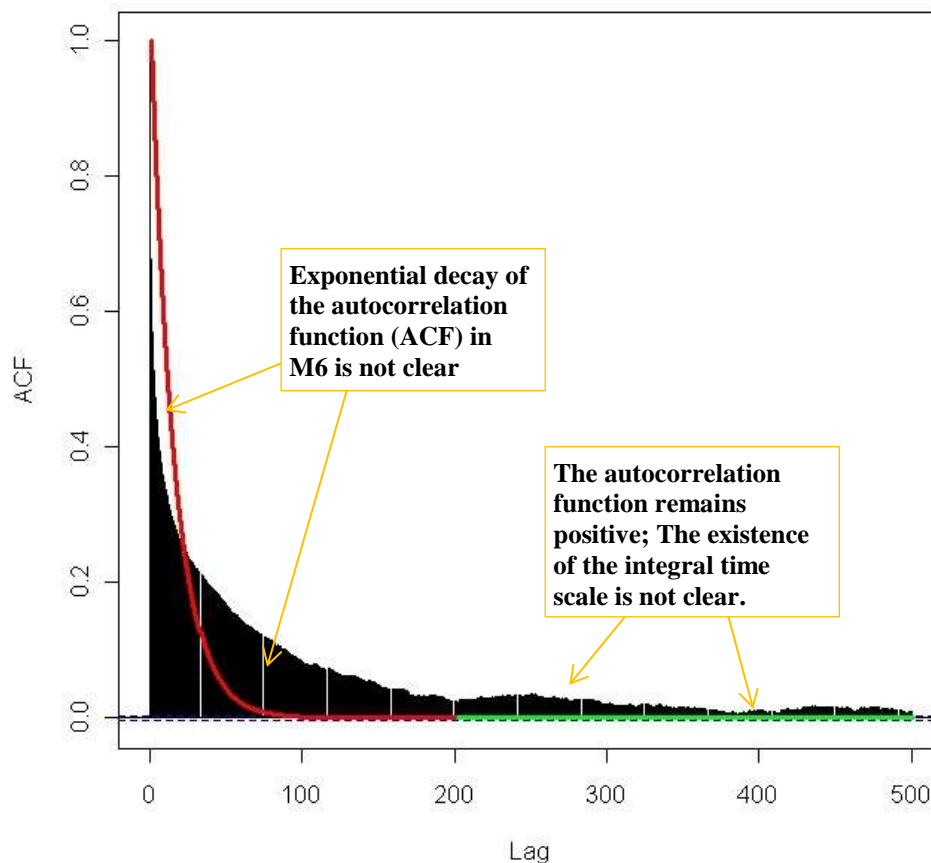


Figure 108: Here, the autocorrelation function for the investigated time series of Bolund in WOTAN at the measurement position above the front edge in 2 m height above ground level (M6_S2) is shown (black bars). The best exponential fit is shown for the interval up to time-lag 200 (red line) respectively up to time lag 500 (green line). The unit of the time-lag is the sampling frequency, $3 \cdot 10^{-3}$ seconds (in model time scale), corresponding to 95 percent q-resampling (this will be explained further below in the text).

The author of this work regards it as being dangerous to transfer these assumptions to *any point* in the flow over *steep topography* since the turbulence properties are completely different, here. For example, the assumption of *homogeneous flat terrain* is violated. Also, (as it was argued in the previous chapter) the assumption of “frozen turbulence” is not valid and it is not evident that the dynamical system is such that an *integral time scale* exists. Figure 108 indicates that the assumptions are also not satisfied for the here analysed wind tunnel time series at the measurement position in 2 m (full scale) above ground level above the front edge of the hill (M6_S2).

Furthermore, an issue for laser-doppler-anemometry (LDA) measurements in the wind tunnel is that the raw data does *not* have *equidistant* time steps. A crucial point is that the sampling interval is *not independent* of the measured velocity. This means that a measurable offset e.g. of the mean value or the standard deviation of the *raw data* compared to that of the *resampled time series* can occur. (This is illustrated later in the text. It is common knowledge and usually remarked in the user guides of LDA software, such as Dantec User’s Guide, [2006].) However, the crucial point for the analysis in this text is that the statistical properties of the “true” time series *cannot be known* and that the “absolute” *distorting effects* of the *resampling-method* are unclear.

Due to the new type of question (topography and not flat terrain) which is not covered by established theories on sampling durations for atmospheric turbulence, in this work, an analysis was chosen which relies on as little *physical assumption* as necessary for estimating the effects of the process-oriented parameters on the finally used time series. For the *measurement process* and *data-post-processing* of wind tunnel experiments with LDA, the choice of the *sampling frequency* and the *sampling duration* as well as the *resampling method* is crucial. Hence, in this work it is decided to conduct an inter-comparison of time series with variations of *sampling frequency*, *sampling duration* and *resampling* and to analyse the respective effects on the statistical representativeness of the time series *within* this set of different outcomes of the same raw-data. (This means that a “relative” analysis is conducted since the “absolute” *distorting effects* of the *resampling-method* are unknown.) The analysis is mainly addressed to wind tunnel modellers and those who are interested into the process of wind tunnel experiments. Hence wind tunnel time scaling and velocities are used in this section (unless it is clearly indicated that full scale examples are given.)

Statistical representativeness

The resampling procedure is important for the *statistical representativeness* of LDA-data since it leads to the *data rate* of the *final* time series. Usually these questions are dealt with in the measurement equipment handbooks, e.g. Dantec User's Guide, [2006]. The User's Guide considers as a "large" number of samples preferably "10000 or more". Furthermore, *sample-and-hold* or *exponential interpolation* are suggested as resampling methods and *sample-and-hold* is *recommended* for being most wide spread and easy to implement [Dantec, 2006]. *Sample-and-hold* means that the velocity is kept *constant* until a next measurement value indicates that the velocity has changed. That is: let $u_{\text{resamp}}(t)$ be the resampled time-series and $u(t_i)$ be the raw-time series. Then the sample-and-hold method is:

$$u_{\text{resamp}}(t) = u(t_i), \quad t_i < t < t_{i+1}, \quad i \in \mathbb{N}.$$

However, it is not stated why this should be sufficient. For *higher order* statistics and application of *extreme value analysis*, as far as the author knows, the *statistical representativeness* of wind tunnel time series has not yet been examined for atmospheric boundary layer flow over hills. Denotations for *higher order statistics* are as follows:

Definition: n^{th} order (statistical) moment

Let $u : \Omega \rightarrow \mathbb{R}$ be a *random variable* with *probability density function* p (p. 42). The n^{th} order (statistical) moment of u can be defined as:

$$\langle u^n \rangle := \int_{\mathbb{R}} x^n p(x) dx, \quad n \in \mathbb{N}.$$

—/

The 1^{st} order moment is the *mean value*; the 2^{nd} order moment is the *variance*; the 3^{rd} order moment is also called *skewness* and the 4^{th} order moment *kurtosis*. For *discrete* time series, above integral is computed as a discrete sum.

Definition: n^{th} order structure function

Let $u_\tau(t)$ denote the *velocity increments* of the time series $u(t)$, that is:

$$u_\tau(t) := u(t+\tau) - u(t)$$

The *structure function of order n* of $u(t)$ is defined as n^{th} order (statistical) moment of $u_\tau(t)$ as function of τ :

$$s_u(\tau)^n := \langle u_\tau^n \rangle$$

For example, the structure function of order one with $\tau = 0$ (namely $s_u(0)^1$) is the *mean value of the differences*. Another example: The *standard deviation of the differences* is the *mean value of the autocorrelation function of the differences with zero time step*, denoted with $s_u(0)^2$. Yet another example: $s_u(1)^2$ is the mean value of the autocorrelation function of the differences with time step one. (The unit of the time step depends on the sampling rate.)

The important *objective* for the use of structure functions is to translate the *non-stationary* field data into *stationary* data. An extended motivation for the use of structure functions is also given in the appendix of this work, “*Structure function – what is this for?*” pp. 341.

Description of methodology

The main Bolund measurements in WOTAN are analysed along three dimensions: *data rate, sampling duration and time steps* for zero order sample-and-hold resampling.

A measurement position is chosen which is found to be sensitive on slight changes in the *idealized* Bolund hill pre-study. This is M6_S2, right above the front edge of the hill, corresponding to 2 m above ground level in full scale. Each of the three test dimensions is divided into three cases, leading to 27 model output time series. The original raw time series (not equidistant time steps) is added to the evaluation set. The set is evaluated for the n^{th} order statistical moments, $n=1,2,3,4$. Also, the structure functions are computed. A background on *structure functions and statistical features of velocity increments* in turbulence is given in Böttcher et al., [2003, 2006].

Data resampling is divided into three choices of time steps selected via the *quantile* of the empirical probability density function (PDF) of the *measurement increments*, see Figure 109. Chosen quantiles are the 88 percent, 95 percent and 99 percent quantile leading to around 2, 3 and 5 milliseconds of *resampling time steps*. The influence of the sampling frequency on the statistical moments is tested by taking the *full*, *half* and a *quarter* of the resampled time series, assuming that lowering the data rate at data record leads to *nearly* comparable results for *time series analysis of the statistical moments* as lowering the data rate after data record .

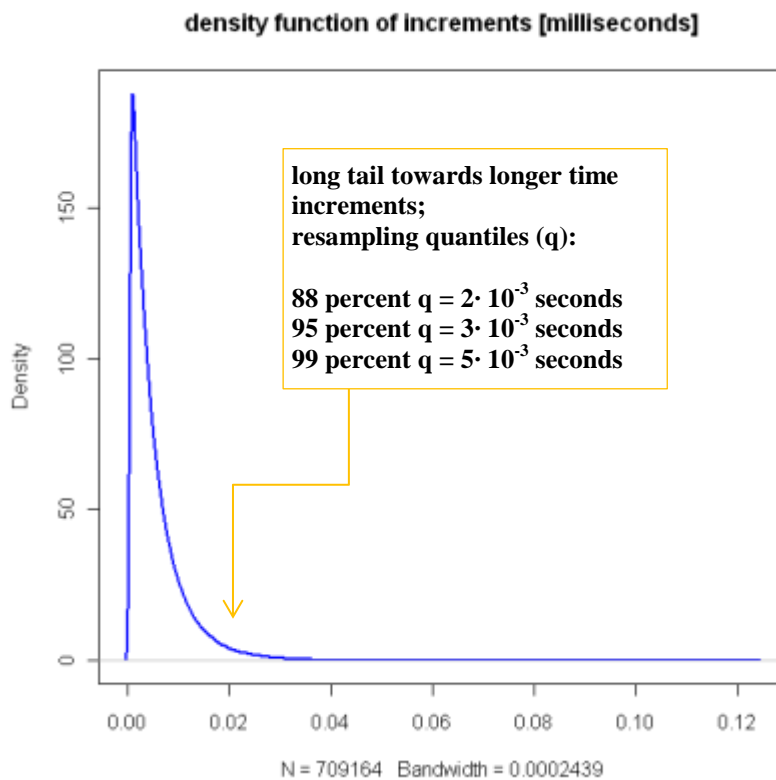


Figure 109: Estimated empiric PDF of LDA measurement increments for Bolund in WOTAN; the x-axis exhibits measurement increments in the unit of 10^{-3} second wind tunnel time, the y-axis shows relative density of occurrence

The evaluation ensemble at this step contains 9 configurations: 120 Hz, 240 Hz and 480 Hz with 88 percent-quantile resampling (88 percent-q resampling); 80 Hz, 160 Hz and 320 Hz with 95 percent-q resampling and 50 Hz, 100 Hz and 200 Hz with 99 percent-q resampling. The influence of *sampling duration* on the empirically obtained n^{th} order statistical

moments, $n=1,2,3,4$, is analysed by the *distribution of the statistical moments* for 1000 *randomly selected sub-samples* of the full time series (720 seconds). The *sampling duration* of the sub-samples is 60 s, 120 s and 180 s.

Results of the statistical analysis

Almost no sensitivity on the calculated PDFs is found for all *combinations* of sampling frequency and resampling quantile for the 720 second full time measurements⁸³, see Figure 110. However, a clear deviation from both the *Gaussian distribution* and the distribution of the *raw data* is found (Figure 110).

For the analysis of the dependence of n^{th} order moments, $n=1,2,3,4$, on the *sampling duration*, subsets of 60 s, 120 s and 180 s are *randomly selected*⁸⁴ from each of the 9 configurations with full sampling duration. Convergence is tested relative to the full time series record which is only four times larger than the largest sub-sample. This means that the subsets are *not pairwise independent* (they can *intersect* each other). For this the full time series would need to be more than 1000 times longer than the subset samples. This means that *convergence* towards the 720 seconds full time value is to be *expected*. (*Absolute convergence* is not directly computable due to the finiteness of the time series). However, relatively, the *convergence dynamics* in dependence on the sampling duration can be examined within the evaluation set. The *distributions* of the *mean values* and *standard deviations* for exemplary configurations are shown in Figure 111: - Figure 114. The 95 percent-q resampled 320 Hz full time record is chosen as *reference time series*. *Dashed lines* denote one percent deviation of the corresponding *moment* of the *reference time series*. *Distribution of skewness* and *kurtosis* are shown in Figure 115- Figure 118. As above, dashed lines denote one percent deviation of the *reference value*. The three percent deviation level is additionally marked with *dotted lines*. Not all figures of all 27 configurations are shown here.

⁸³ In field scale (with geometrical scaling 1:250 and free stream velocity of 5 m/s), this corresponds to 38 hours

⁸⁴ i.e. by the “random selection” of the open source statistics program “R”. The author is aware of the fact that a “random” selection based on a computer program is not necessarily “random” in a pure sense.

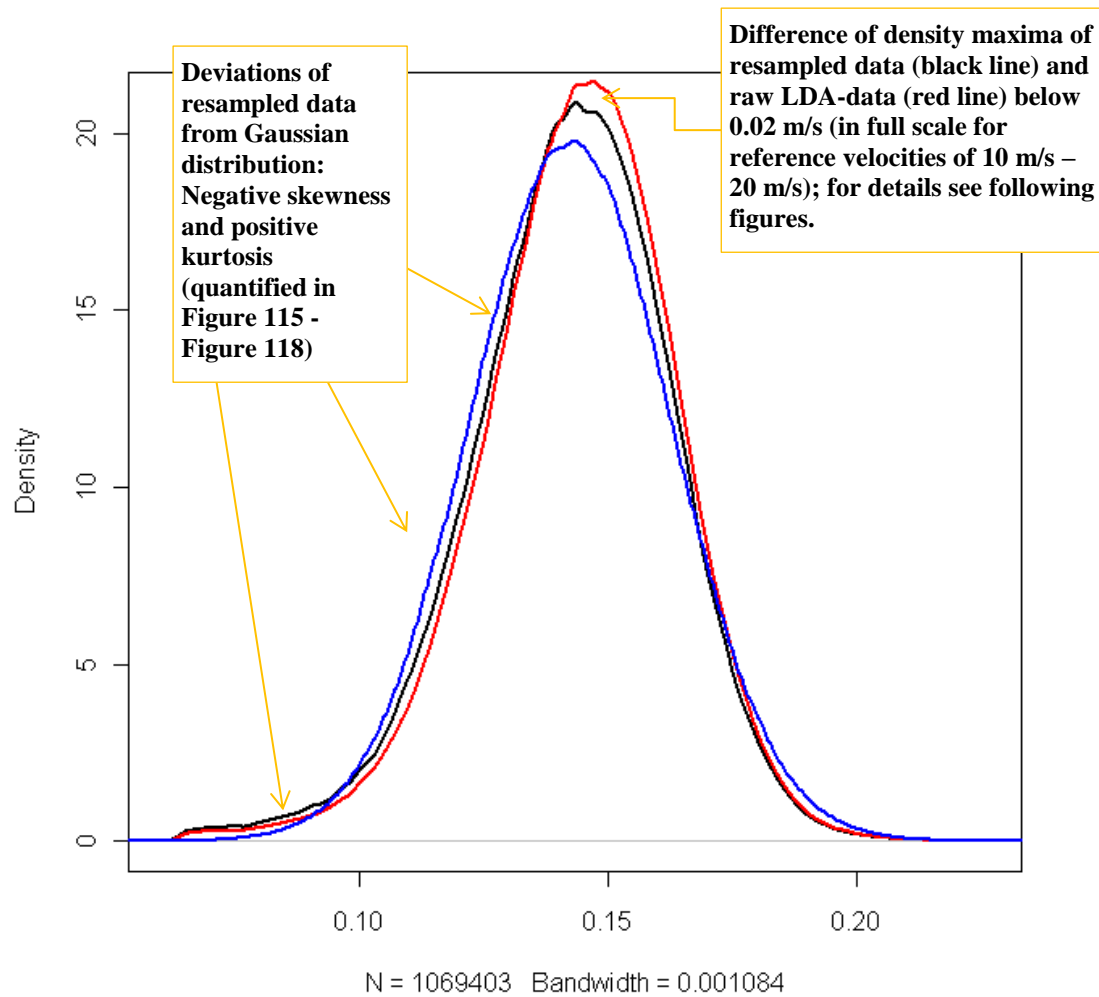


Figure 110: Estimated probability density functions of resampled data (black line) of Bolund in WOTAN at measurement position M6, estimated Gauss for 95 percent-q resampling full frequency (blue line) and empirical PDF of raw LDA data (red line); the x-axis denotes non-dimensional wind speeds (this is low due to the measurement location in the blockage area in front of the hill); y-axis denotes density; the properties of the resampled data (black line) and the density distribution of the raw LDA data (red line) is detailed in the following figures.

It turns out, that the *dynamics of convergence* in the dependence on the sampling duration is quite similar for *all* configurations and all *moments* of order 1,2,3,4. For all here tested configurations of data collection and resampling, 1st and 2nd order moments converge to below one percent deviation of the reference value at 180 seconds sampling duration. *Skewness* shows over 10 percent deviation at the same time. 4th order moments converge to below 5 percent deviation.

It has to be emphasised that the convergence is rapidly *decreasing* for 3rd and 4th order moments in comparison to the *mean value* and the *standard deviation*, as it is expected

especially for field data, see [Dias et al., 2004]. *Skewness* is statistically less representative in 180 s sampling duration than *kurtosis*.

The 1st and 2nd order moments of the *raw time* series are over 1 percent *off* the reference value, *underestimating* standard deviation and *overestimating* the mean value. For *skewness* and *kurtosis*, the *raw* LDA time series does not deviate more from the reference value than all configurations of the resampled time series.

The patterns that are shown in the scatter plots are quite *stable* for *random selection* of the 1000 subsets (the *variation of random selection* not shown here.) To which extend the *patterns* are meaningful with respect to *local flow characteristics* at the front edge of the model hill remains an open question at this point.

The *structure functions* of order one to ten of 88 percent q-resampling at 480 Hz, 99 percent q-resampling at 50 Hz, raw LDA data and reference value 95 percent q-resampling at 320 Hz are shown in Figure 119. The *structure function* of the *raw time series* is of higher gradient and visibly shifted *downwards* relative to the resampled time series. This can be expected since the *raw time* series has nearly 980 Hz average sampling frequency, thus is shifted horizontally. This is also the case for the structure functions of 95 percent-q resampling with 320 Hz, 160 Hz and 80 Hz as computed in Figure 120. Besides that, here, no anomalies are visible for the lower frequent time series.

Definition: intercept and coefficient of log-lin fit for $s_u(\tau)^n$

The *intercept* is the y-axis intercept of the linear fit to $s_u(\tau)^n$ in logarithmic representation. The *coefficient* is the gradient.

—/

Intercepts and coefficients of log-linear fits of structure functions (increasing order from top to bottom) for the three 95 percent-q resampled configurations are plotted in Figure 121. Deviations of Figure 120 are better visible in Figure 121.

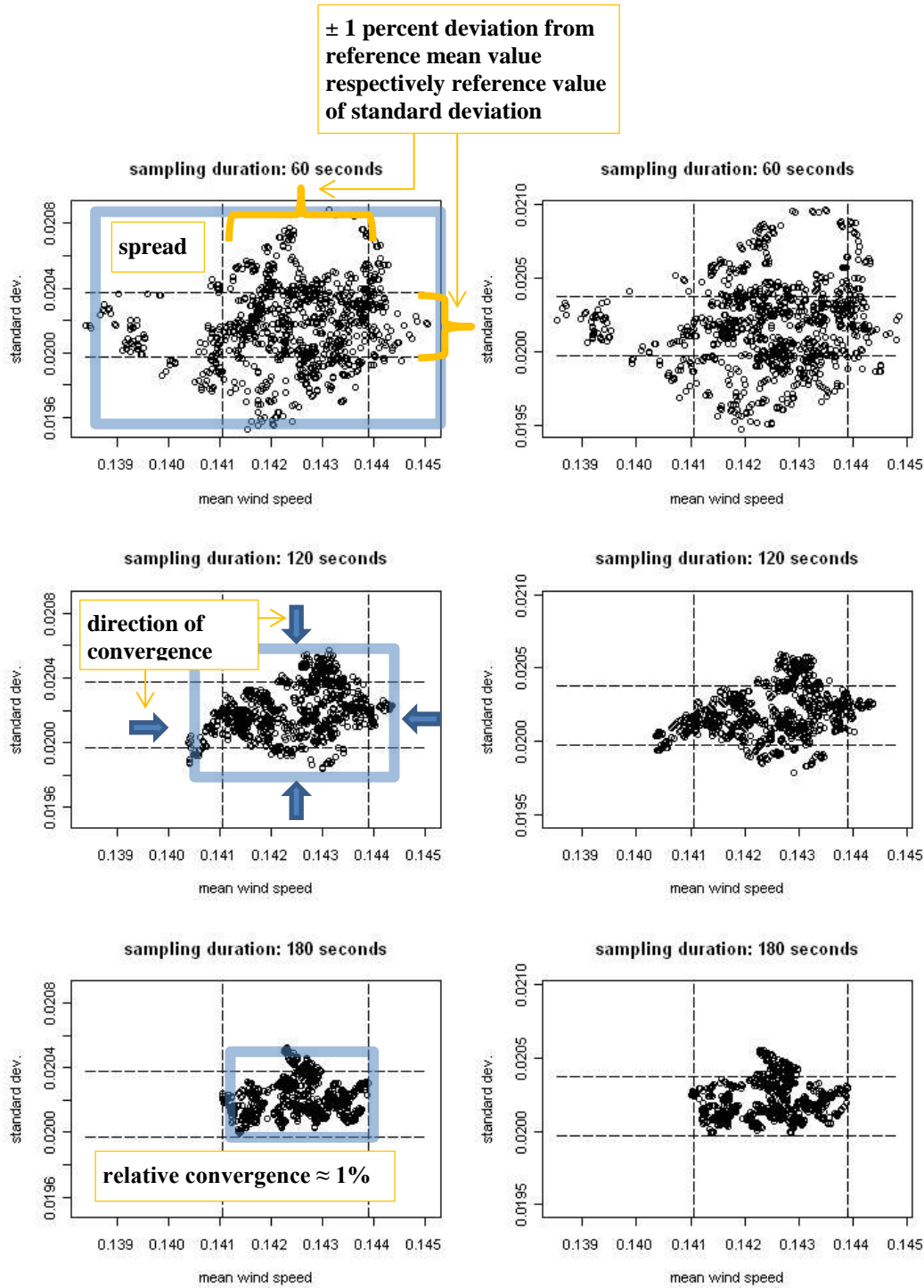


Figure 111: The following figures show the density distributions of mean values correlated to the standard deviations (plain circles) for 1000 randomly chosen subsamples from the full time series; the three plots in row (from top to bottom) show the convergence dynamics for increasing sampling duration (60 s, 120 s, 180 s) in wind tunnel time scale; the x-axes and y-axes denote non-dimensional wind speeds; the patterns of distribution were not significantly dependent with the (random) choice of 1000 subsamples (not shown here);

Figure 112: 95 percent quantile resampling (320 Hz)

The distribution shown here is for the 88 percent quantile resampling (480 Hz); dashed lines denote ± 1 percent deviation of reference value (95 percent-q resampling full frequency full time series)

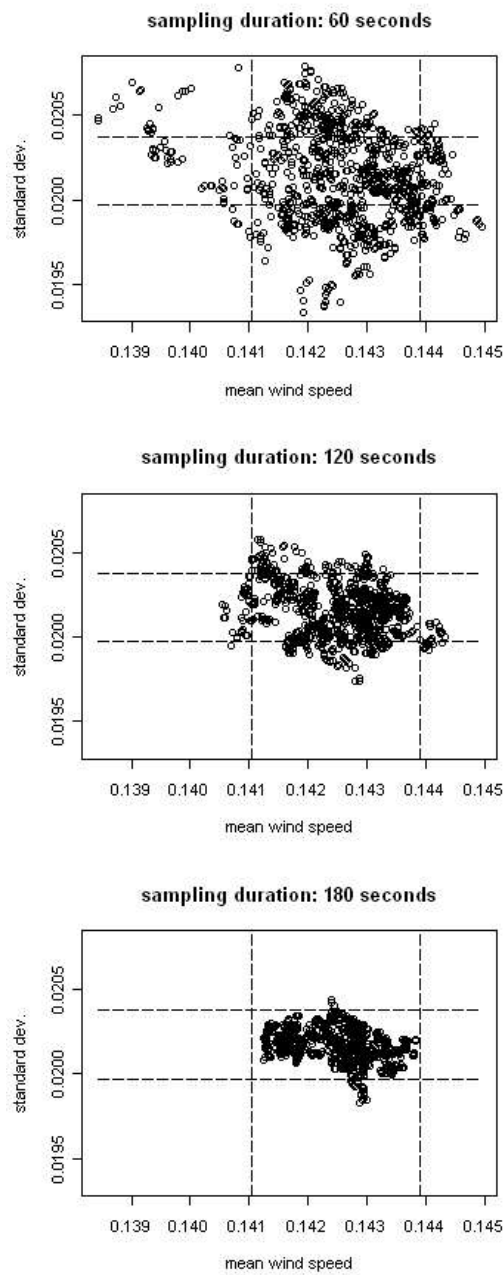


Figure 113: 99 percent-q resampling at 50 Hz

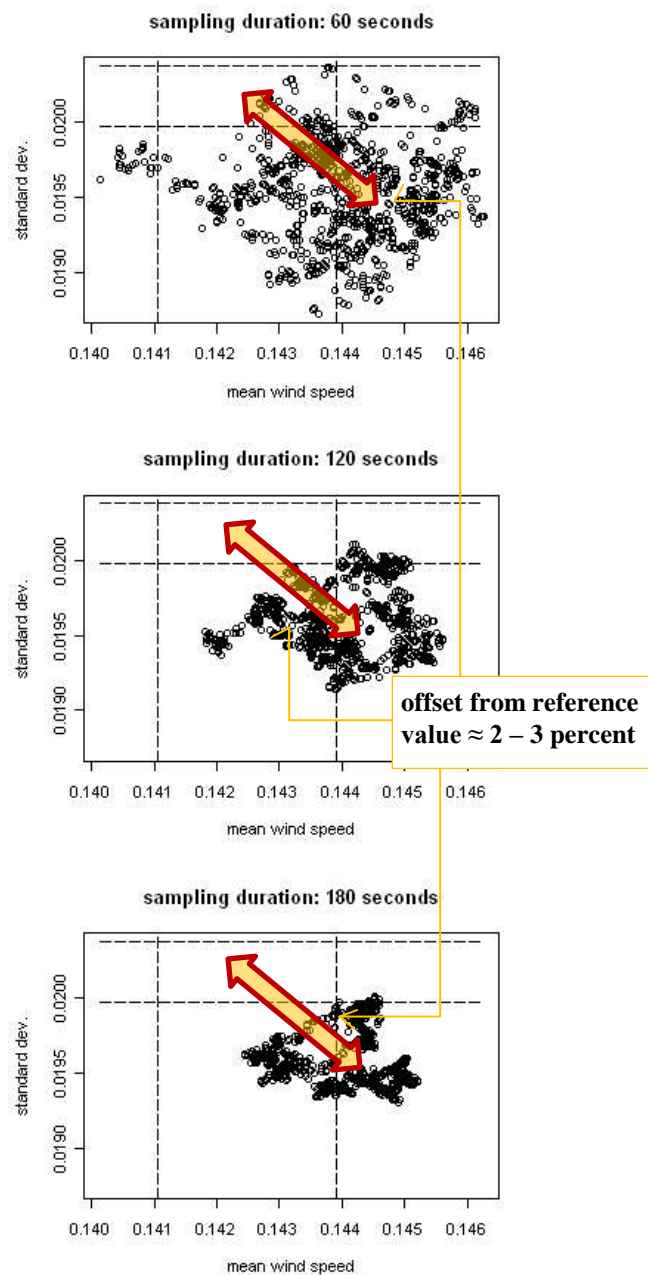


Figure 114: LDA raw time series

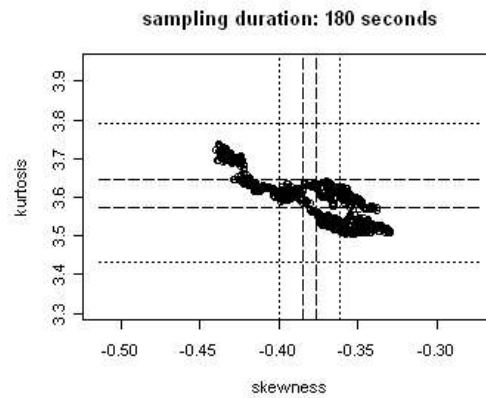
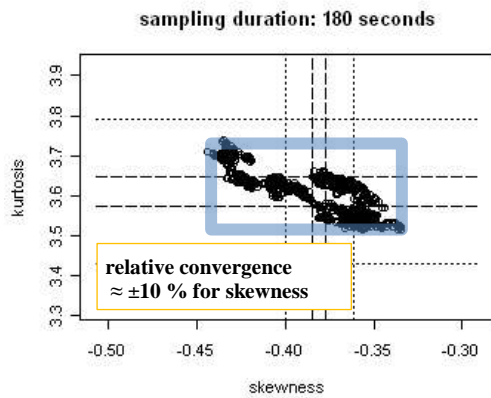
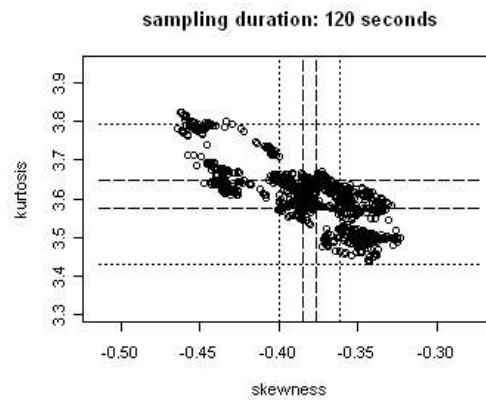
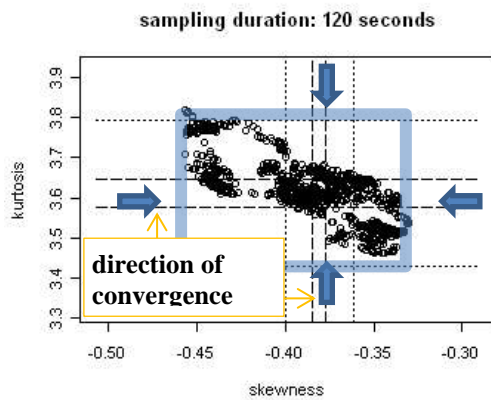
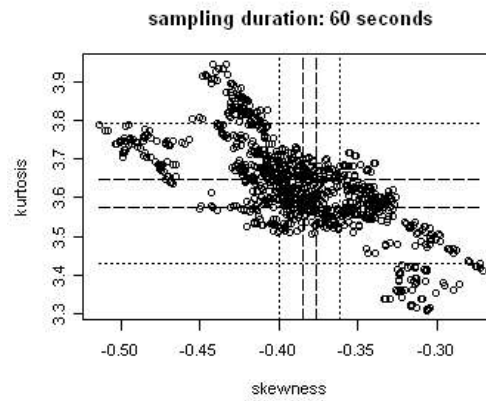
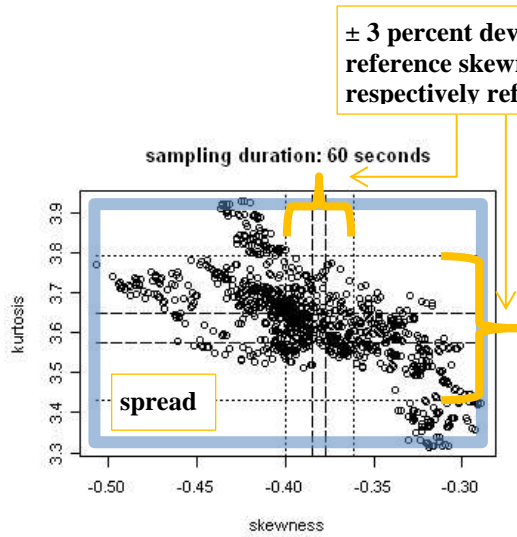


Figure 115: 88 percent-q resampling (480 Hz); dashed lines: 1 percent deviation of reference value dotted lines: 3 percent deviation of reference value

Figure 116: 95 percent-q resampling (320 Hz)

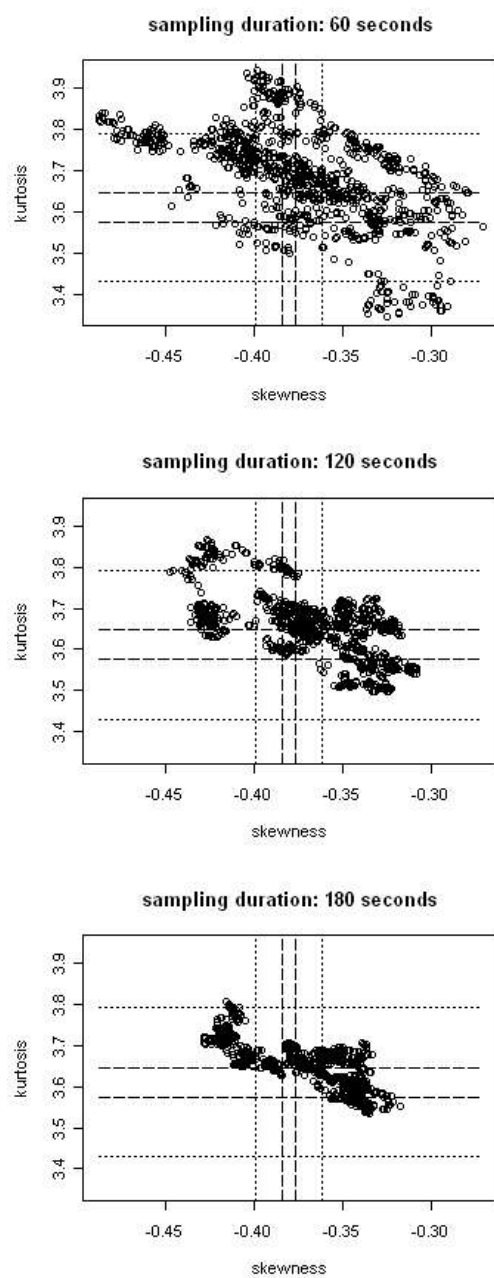


Figure 117: 99 percent-q resampling (50 Hz)

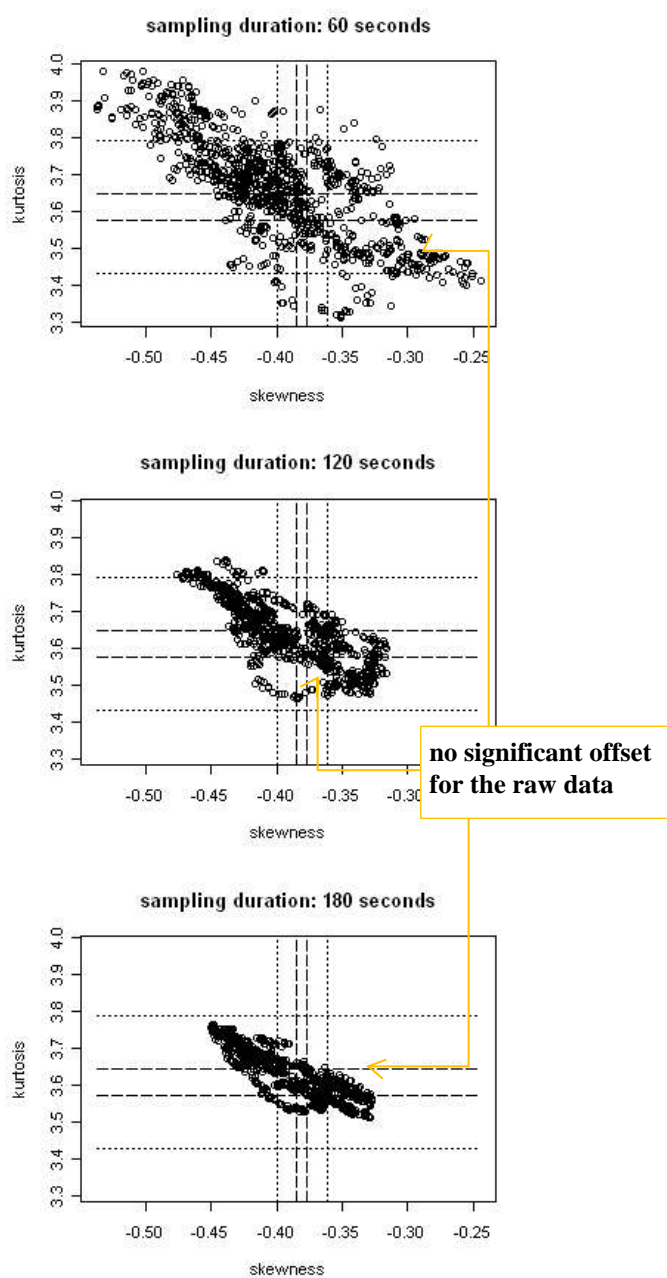


Figure 118: LDA raw

For the local flow characteristics close to the hill surface, Kolmogorov scaling is not to be expected since the turbulence is most likely not in equilibrium. Positive $s_u(\tau)^3$ indicates positive skewness, i.e. *asymmetry* in the *probability density function* of the *velocity increments* such that the *tail* is *longer* to the *positive* velocity increments, and the *bulk* of velocity increments is on the *left* side of the *mean*. Positive $s_u(\tau)^4$ indicates heavier tails than in the Gaussian distribution. The increment step τ is such that τ in 80 Hz is the same as 2τ in 160 Hz or 4τ in 320 Hz. Thus larger values for 320 Hz resampling than 160 Hz or 80 Hz for the same τ indicate larger values for larger increments, as in Figure 119 and Figure 120.

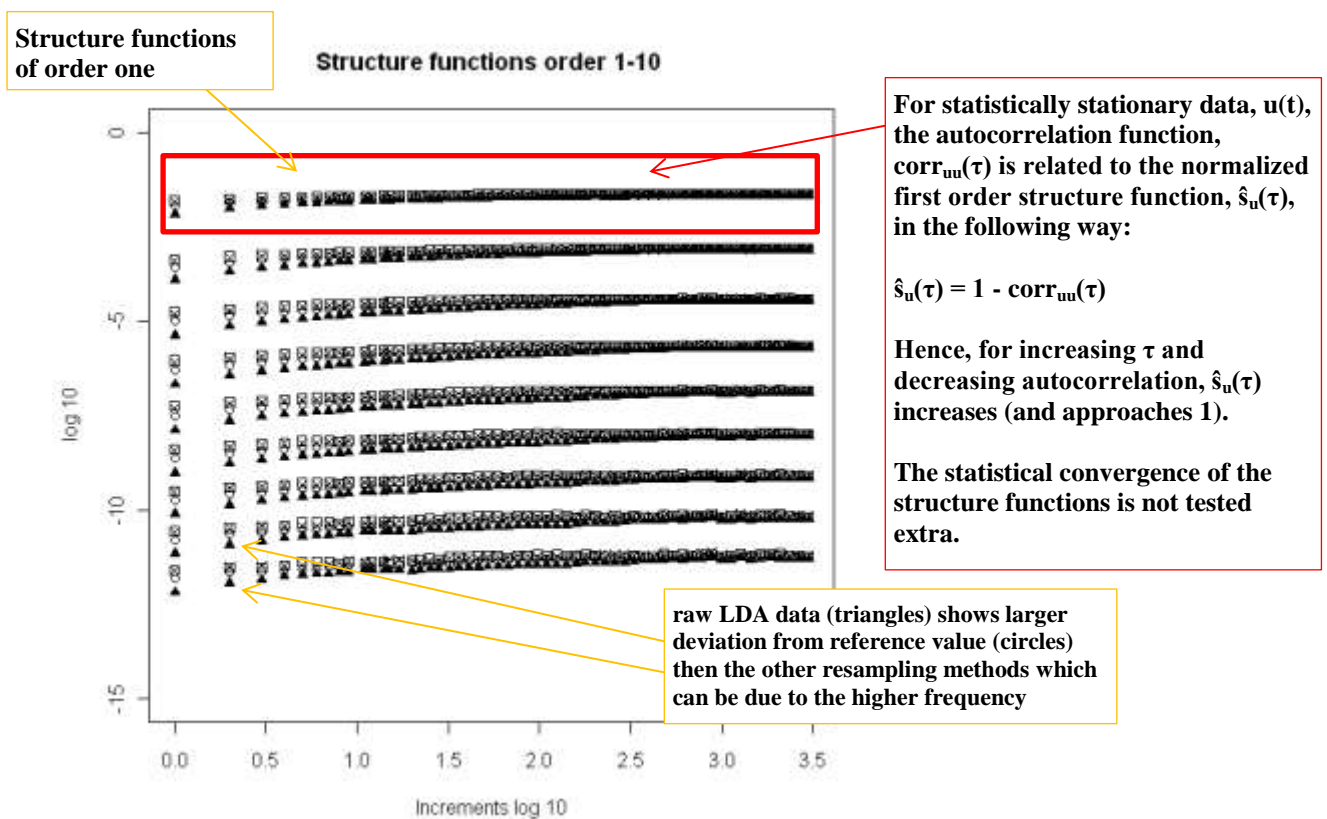


Figure 119: The structure functions are the n th order statistical moments of the velocity increments and hence characterise the probability density functions of the differences of the time series. Here, the structure functions are normalized. This means that the autocorrelation functions are divided by the appropriate power of the standard deviations. The result is that all values are smaller than one.

Here shown: the structure functions of order 1-10 (top to bottom) of 88 percent quantile-resampling at 480 Hz (crosses), 99 percent q-resampling at 50 Hz (squares), raw LDA data (triangles) and reference value 95 percent q-resampling at 320 Hz (circles); structure function of order two are the autocorrelations of the velocity increments as function of the increments; the x-axis denotes increments in logarithmic scale to the basis of 10 (depending on the sampling frequency); the y-axis shows the non-dimensional and normalized values of the structure functions

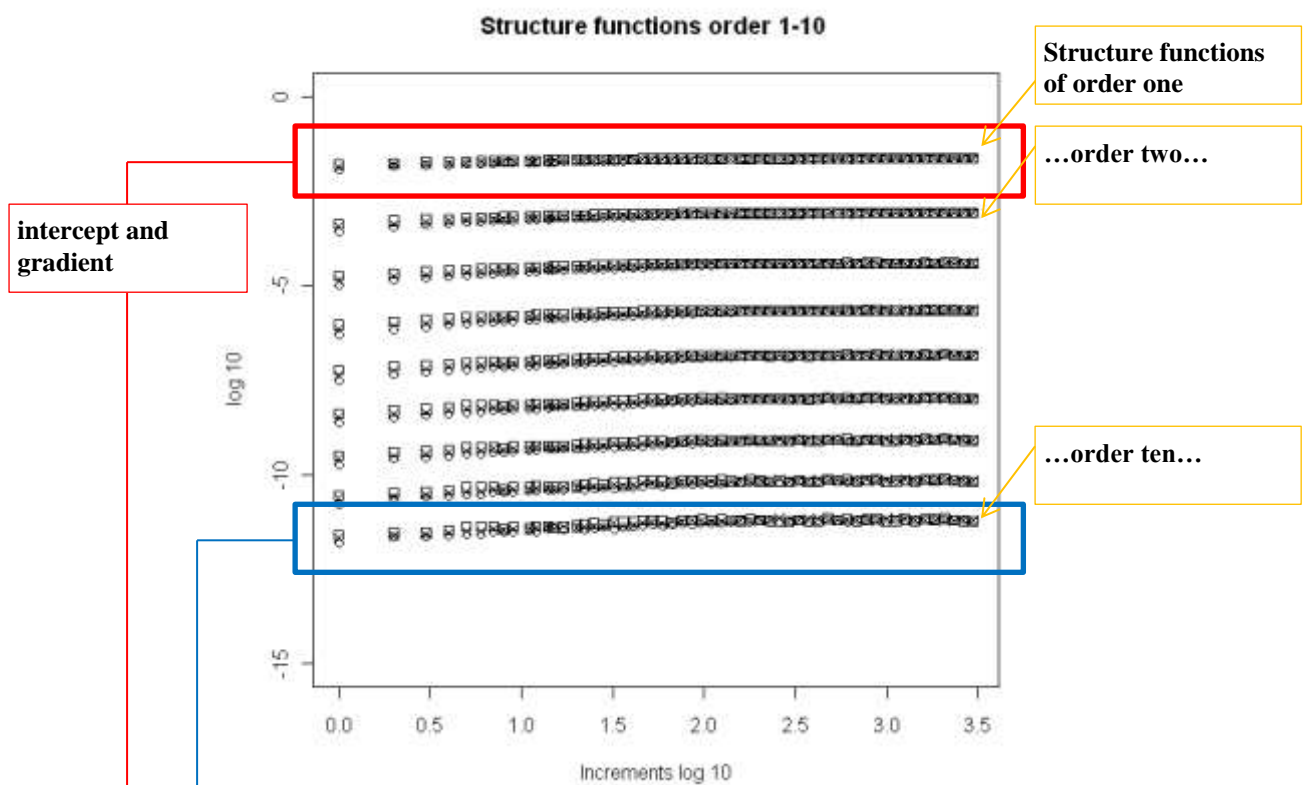


Figure 120: Structure functions of order 1-10 (top to bottom) of 95 percent quantile resampling with 320 Hz (circles), 160 Hz (crosses) and 80 Hz (squares)

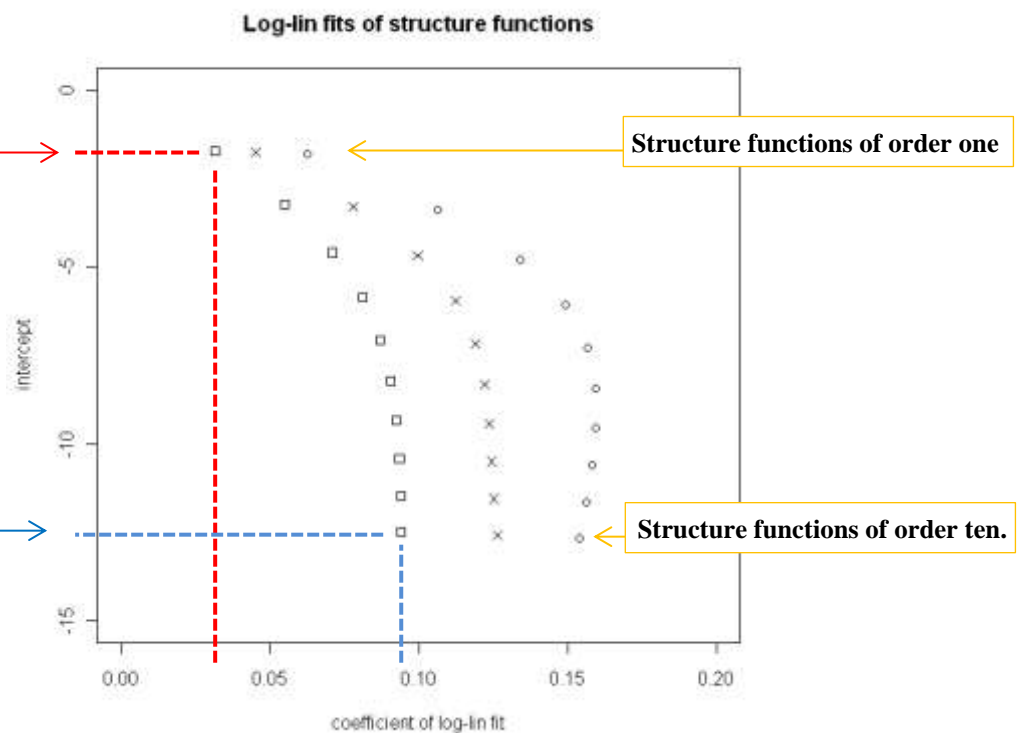


Figure 121 coefficients (gradient) and intercepts (intercept of the structure function with the y-axis in the previous figure) of linear fit to the logarithmic structure functions for order 1-10 (top to bottom); interpretation see also text

Discussion of the statistical analysis

In order to determine the *best experimental practice*, quality and time economy needs to be considered for each wind tunnel study separately. This means that the details of the *experimental process* and the *data post-processing* need to be determined with regard to the *purpose of modelling*.

For example, in this case the 88 percent-q resampling maintains almost half of the *average data rate of the raw time series*. In contrast to this, the 99 percent-q resampling maintains only 25 percent. However, 88 percent-q resampling leads to more data distortion than 99 percent-q resampling. This is because in 88 percent-q resampling, time steps are smaller and lead in more cases to a *false* sample-and-hold than the larger time steps derived for the 99 percent-q resampling.

Also, sampling duration of 60 seconds is more time economic than 180 seconds for wind tunnel studies with *many measurement positions*. However, the *higher order statistical representativeness* of the measurement results improves *significantly* for 180 second measurements, as shown above. It can further be analysed whether the *local flow features* have an effect on the *statistical representativeness* of higher order statistics. The influence can be assessed by comparison of time series at different *measurement locations*.

In this case, 95 percent-q resampling and 180 seconds of sampling duration are found to be a *good compromise* for *data rate* and *sampling duration* with regard to obtain representative experimental results for *higher order* statistics.

Conclusion of the statistical analysis

In this chapter, an *inter-comparison of time series* with different configurations of *sampling frequency*, *sampling duration* and *resampling time steps* was conducted. The aim was to assess the relative effects of the different configurations on the statistical representativeness of the time series. The main conclusions can be summarized as follows:

- A variation of the *sampling duration* between 60 s and 180 s has a stronger influence on the statistical results than the here tested *resampling configurations* between 88 percent q-resampling and 99 percent q-resampling.
- The deviations of the 3^{rd} and 4^{th} order statistical moments are *significantly larger* than the deviations of the 1^{st} and 2^{nd} order moments (according to the theoretical expectations.)
 - Statistical errors of up to 5 - 10 percent for the higher order moments of the wind tunnel data with data rate 200 – 500 Hz and sampling duration 180 are found here.
 - This can be interpreted as a *lower estimate* for statistical errors of *field scale hill measurements* with 13 hours sampling duration, (statistically stationary) neutral conditions, free stream velocity of 5 m /s and a data rate of 1 - 2 Hz.
- Here, 95 percent-q resampling of LDA data with an average sampling frequency of 980 Hz (yielding effectively an equidistant time series with 320 Hz data rate) and 180 seconds of sampling duration were found as a good compromise for obtaining representative experimental model results with respect to the alternative resampling methods which were tested here.
- For future application of LDA data for *more advanced statistical methods of turbulence research* (e.g. extreme value analysis or tests of theories on turbulence scaling laws), the results of this chapter indicate that *sensitivity studies* of the *advanced statistical parameters* on the data *sampling duration* and *resampling method* might be useful.
- For linking *statistical properties of velocity increments* to *practicable meteorological parameters* (e.g. for the determination of inflow conditions for models) further research on velocity increments of field data (e.g. the Bolund field data) could be interesting (see also appendix “Structure function – what is this for?”, pp. 341).

- The analysis which was carried out in this chapter can be extended to *different flow areas around the Bolund in WOTAN hill*, especially in the wake region.

Acknowledgement (III)

For the experimental part, G.P. acknowledges Frank Harms and Stephan Werk for extraordinary help with the measurements and photography, Andreas Bechmann from Risø DTU for help all around the Bolund field study, Denise Hertwig, for the BLASIUS boundary layer inflow, figures and advice, Brad Cochran from CPP Wind for helpful hints and the WAUDIT Marie Curie program for being a platform for research on ABL flow over complex terrain with regard to wind energy assessment. Most thanks belong to Prof. B. Leitl for the overall guidance and sophisticated and inexhaustible knowledge in wind tunnel modelling.

Also, G.P. acknowledges Uniol, FORWIND, Michael Hölling, for discussion on R-codes for computation of structure functions and Prof. H. Drees, University of Hamburg for discussing resampling of LDA data.

Part IV: Conclusions and future work

10. Final summary and conclusions

“EXACT SCIENCE - what wealth of connotation these two words have! [...] There must be something wrong somewhere!”⁸⁵

– Max Planck [Planck, 1949, p. 319]

In the following chapter, the main results of the experimental and fundamental parts are summarized. Also, *practical* suggestions for future wind tunnel experiments of atmospheric boundary layer flow over hills are given (basically the EWTL guidelines for proper wind tunnel modelling transferred to the modelling of atmospheric boundary layer flow over hills). Finally, pursuing remarks on this topic as well as suggestions for future research are pointed out.

Summary of the main results

Here, a short summary of the main results of the *fundamental* and the *experimental* part is given:

Fundamental part:

An atmospheric boundary layer wind tunnel (e.g. WOTAN in the University of Hamburg) can be interpreted as *mediator between theories* (e.g. fluid dynamics and meteorology) and *reality* (the real atmospheric boundary layer). Concerning theories, the *Navier-Stokes Equations* can be interpreted as a *specialisation of the Euler Equations* (introducing *viscosity* of fluids) and as the *core* of modern *fluid dynamics* (*core and specialisation* are terms of *structuralism*, which is a framework for the analysis of theories in philosophy of science). The analyses of fluid dynamics in the two *technical meta-frameworks* structuralism and

⁸⁵ Longer excerpt of the quotation: “EXACT SCIENCE - what wealth of connotation these two words have! They conjure up a vision of a lofty structure, of imperishable slabs of stone firmly joined together, treasure house of all wisdom, symbol and promise of the coveted goal for a human race thirsting for knowledge, longing for the final revelation of truth. [...]”

There must be something wrong somewhere! And in fact, if we take a closer look and scrutinize the edifice of exact science more intently, we must very soon become aware of the fact that it has a dangerously weak point – namely, its very foundation.” [Planck, *ibid.*]

conceptual spaces yield a similar result: the set-theoretical (structuralist) and geometrical (spatial) reconstructions are *merged* in the differential geometric objects (manifolds) which (possibly) solve the Navier-Stokes Equations.

Models bridge the gap between *theories* and *observational data* and create a new sort of experience by combining theories, model output and field data in an amount which goes far beyond the capacity of the human brain. The conception of models as mediators between theories *and reality* by means of data comparison can be used as a foundation for the establishment of a *methodological framework* concerning quality assessment for wind prognosis tools. The *comparison of models* needs to be accompanied by a *qualitative* (structural) analysis and *comparison of the theories* which are involved. A comparison of “numbers” is insufficient since the *accuracy* of models is *not quantifiable*. (*Accuracy and precision* can be strictly distinguished for the *validation* of models.) Data for model *validation* needs to be *adequate* with respect to the specific model. It is shown that field data might *not* provide satisfyingly narrow “precision” translated to the theories which are implemented in the model. The fundamental findings are supported by concrete wind tunnel experiments (of which the summary is given in the following paragraph).

Experimental part:

Smooth atmospheric boundary layer flow over Bolund (a steep hill in Denmark) was modelled for two inflow directions with special emphasis on accuracy and precision-assessment in the atmospheric boundary wind tunnel WOTAN at the University of Hamburg. It is found that the mean flow is influenced already one hill-length in horizontal distance *in front of the hill*. The *area of influence* extends up to five hill-heights in the *vertical direction above ground level* and within a horizontal distance of 1.5 hill-lengths *behind the hill*.

The *maximum speed-up* around Bolund in WOTAN occurs *above the front edge of the hill*; the mean velocity increases of up to 40 percent in 2 – 5 m in field scale above ground level (relative to the mean velocity in the same height in the boundary layer flow without topography). Furthermore, it is found that the *turbulent flow statistics* are sensitive on the flow geometry: The *standard deviation almost doubles* behind the hill at half hill-height for all three velocity components; The *shear stress is negative* around the hill and *increases* (in

absolute value) by around *five times* at the front edge and behind the hill; The *skewness* is *negative* for the free stream flow and *turns positive* close to the ground in the blockage area and in the wake of the hill. In contrast, at the top luv edge of the hill, skewness *increases* in its *negative* value by around *five times*.

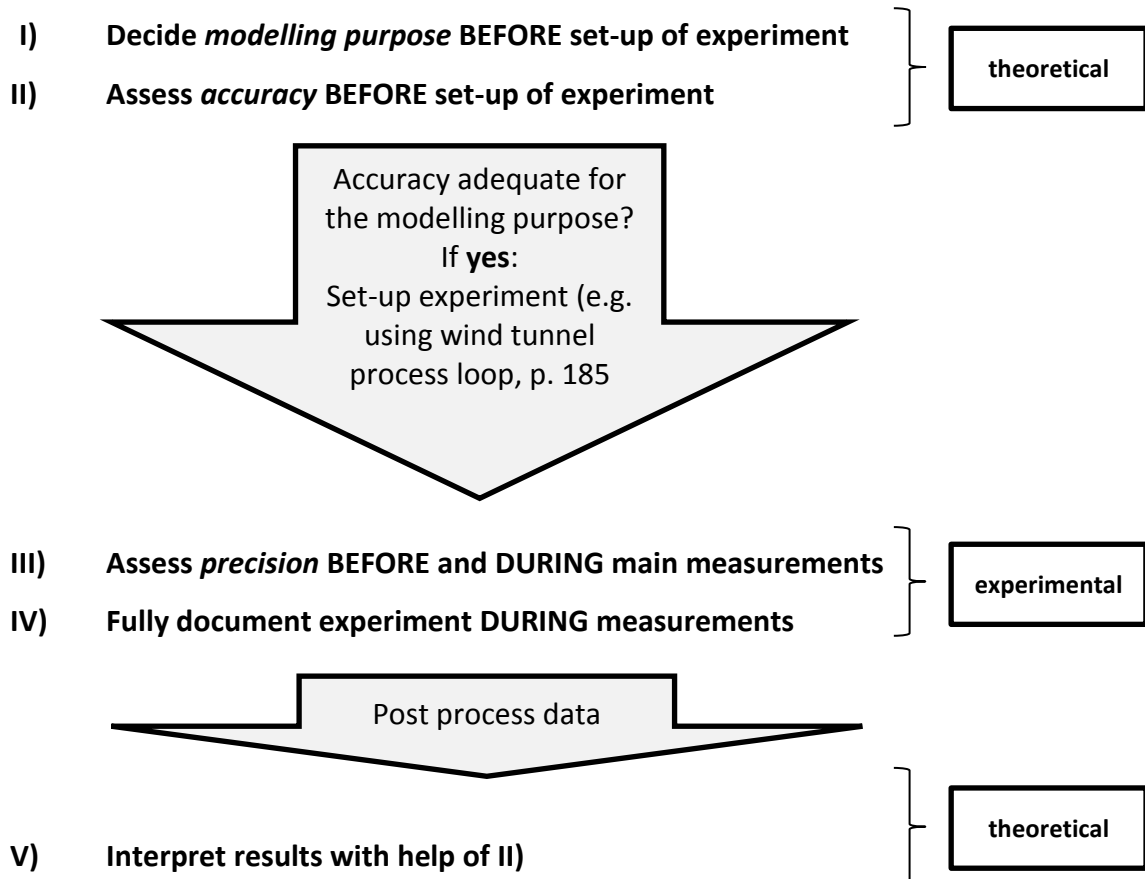
It is found that the *precision* of the measurements depends strongly on the local flow properties. Explicitly, the *repetition spread* increases by *7 times* for different *locations*. In the pilot study it is found that the flow is sensitive to the *geometrical resolution* of the model. A *separation vortex* above the front edge is found at a spatial resolution of 2.5 m in field scale. The vortex *disappeared* for modelling *smooth contours*. (Here, in non-dimensional numbers for hill height, H , and hill length, L , 2.5 m field resolution reassembles around $0.1H$ respectively $0.01L$). The *location and size* of the speed-up area as well as the wake region is influenced by modelling the slopes with a spatial resolution of 1.5 m in field scale ($0.05H$ respectively $0.01L$ high steps). Also, it is shown that the *statistical convergence of higher order statistical moments* (order 1-4) at a characteristic location above the front edge of the hill depends more on the *sampling duration* than on the *resampling frequency* (within the here tested resampling configurations).

Finally, open questions were pointed out, e.g. how to treat *field data* for comparison with *statistically stationary model data*; How to post-process wind tunnel LDA data for *advanced statistical analyses including velocity increments, structure functions or extreme value statistics*; Can a Bayesian ansatz help for the interpretation of *model results* considering that the *model accuracy*, in general, is not quantifiable?

In the next section, *practical suggestions* for the *planning and conduction* of future wind tunnel modelling of hills in an atmospheric boundary layer flow are given.

Summary: Suggestions for wind tunnel modelling of ABL flow over hills

This summary is based on the theoretical analyses in chapter 1-6 and the detailed data analysis in chapter 7-9. In the following, three main rules for *a priori preparation* are summarized. Altogether, five key points can be formulated as guidance for future wind tunnel experiments for ABL flow over hills:



This can be outlined in more detail. The following list contains the author's suggestions and is not exhaustive. The first and second level is general and can be applied to *general* wind tunnel experiments. The third level is formulated with respect to the modelling of *atmospheric flow over hills*.

I) Modelling purpose

The *modelling purpose* can be classified into one of the following categories:

- a. Comparison of models
- b. Comparison of model with data
- c. Comparison of model with theories (“academic” test case)

II) Accuracy assessment

After the classification of the *model purpose*, the *accuracy* of the experiment can be assessed.

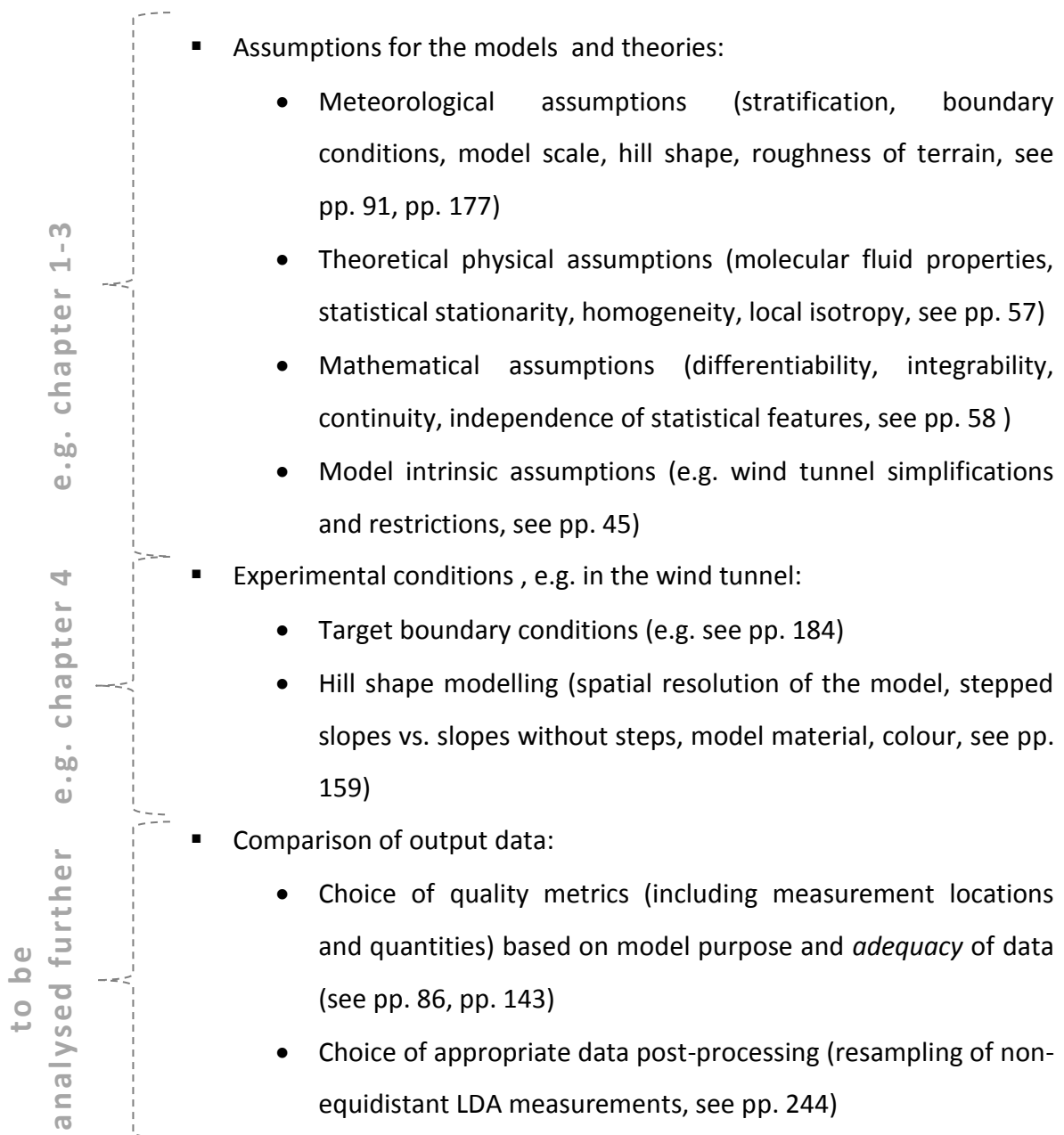
Case distinction:

- a. **For comparison of models⁸⁶, examine:**

e.g. chapter 1-3

- Relation between models and theories
 - Implementation of theories into the model, i.e. for wind tunnel models: similarity criterion and dimensional analysis see pp. 37; for numerical models: implementation of the mathematical model into a computer
 - Structure of the theories (e.g. with conceptual spaces or structuralism, see pp. 53)
 - Recursive learning processes between models and theories (are the models based on theories which are based on the model output? Are the models based on fitting empirical data? See p. 39 “Is the *similarity criterion* usable as a basic law for wind tunnel modelling? “, pp. 86, pp.97)

⁸⁶ See also pp. 86.



b. For comparison of models with data:

- Assess the *model* behind the data and proceed as in a.; for field data, assess the *assumptions* made for the use of the field measurement equipment and apply e.g. the *inverse non-stationarity measure* in order to assess the *adequacy* of data, pp.95

c. For comparison of models with theories:

- Proceed as in a., only replace “comparison with output data” with “comparison of output data with *theoretically predicted values*”. However, quantitative comparison is not feasible if the theory is not quantitative

III) Precision assessment

As *precision assessment*, *repeatability* tests for the wind time series are suggested. *Repeatability* needs to be assessed for all *quantities* which will be used for *interpretation*. Furthermore, repeatability depends on the level of *statistical convergence* of time series and Reynolds number.

It is suggested that physical flow modellers divide the flow around the hill into areas of characteristic flow geometry. The *areas of interest*, which are determined for the model purpose, can set the basis. Furthermore, it is suggested that physical flow modellers conduct a mix of *convergence*, *Reynolds* and *repeatability tests*.

For *convergence analyses*, record time series with

- long sampling duration
- high data rate
- characteristic location in the flow geometry around the hill,

and assess the statistical convergence of *all* relevant quantities (see pp. 244). Derive an *adequate data rate* and *sampling duration* for the following repeatability tests and main measurements.

For *Reynolds* tests, record time series with

- adequate sampling duration and data rate
- full range of mean wind tunnel reference velocities (variation of Reynolds number)
- characteristic locations in the flow geometry around the hill.

Reynolds tests can be combined with *convergence* tests. The adequate mean wind tunnel reference velocity per characteristic area can be derived from the Reynolds tests and model purpose (time economy vs. high data rate and long sampling duration).

For *repeatability tests*, record *sufficiently many* time series with

- adequate sampling duration and data rate
- adequate mean wind tunnel reference velocity
- location at characteristic points in the flow geometry around the hill
- [possibly: differently long time shifts between the measurements]

for assessment of *precision* with respect to local flow characteristics. Also consider *propagation of errors* for derived quantities.

For more concrete hints on precision assessment, see also the section “Lessons learnt from the pilot study”, pp. 165.

IV) Experimental documentation

For *reproducibility* and *repeatability* of wind tunnel experiments, a full documentation is necessary (see chapter 8). This is also crucial for the interpretation of the wind tunnel results with respect to field data or results of other models. Literature review shows that this needs improvement for experiments on *flow over hills*, see pp. 111.

Here, the suggestion is that an appropriate *documentation* of wind tunnel modelling of atmospheric boundary layer flow over hills contains at least the following information:

- Wind tunnel *type* and *size* and *measurement equipment*
- Hill *shape* and hill shape *modelling*
- Full documentation of *inflow conditions* (including measurement location, roughness length(s), turbulence intensities...)

- Results of Reynolds number tests (including measurement location)
- Reynolds number of main measurements (or mean wind tunnel reference velocity and reference location)
- Results of *convergence* and *repeatability measurements* (= *precision*)
- Results of the main measurements with assignment of *precision* (e.g. *error bars*)

IV) Interpretation of results

The *interpretation* of the model results is driven by the *purpose of the model*. Here, it is claimed that appropriate interpretation of model output consists of presentation of data results against the background of the *validity of the model*. That is, the proper assessment of *accuracy* and *precision* in step II) and III) is the *basis* for appropriate interpretation of results. Recall that the *validity* is the combination of *accuracy* and *precision* of a model - and accuracy is determined to be only *qualitatively*, and *not quantitatively*, assessable (see p. 37).

Remarks

- **Variability of (field scale time) 10-minute-mean wind tunnel data:** The *variability* of 10-minute time series of *field data* can be compared to the variability of *wind tunnel data* corresponding to 10-minute field scale time. In the already mentioned Bachelor thesis „Analyse von Strömungsmessungen an idealisierten Hügelstrukturen in einem Grenzschichtwindkanal“ by Gillmeier, [2011], the wind tunnel flow measurements of the different *idealized Bolund hill* shapes were analysed for 10-minute *mean values* corresponding to full scale time.

The average *spread* of the 10-minute *mean values* in the wind tunnel was around 0.1 in units of non-dimensional wind speed. According to the *similarity criterion*, this can correspond to a *deviation* in *full scale* wind speed of order $1 \cdot 10^0$ m/s. In addition to the spread of the *mean values*, large differences in the properties of the *probability distribution* occur for subsamples of ten minutes length. Figure 122 (p. 275) exhibits

the statistical properties of the *subsamples of ten minute length* at the front edge in 5 m height above ground level (in full scale) [figures re-edited based on Gillmeier, 2011]. The vertical profile on the left at the bottom shows the *10-minutes averages vertical profile* at the front edge for hill model A2 (sharp edges, with steps). In 10 mm height (5 m full scale) the spread of the wind tunnel 10-minute averages is larger than the average spread in the other measurement positions of this vertical profile. The details of the *empirical probability distributions* of single ten minute subsamples are shown in the small histograms in the centre of Figure 122. Here, the red line in each plot denotes the Gaussian fitted probability density distribution as reference value.

Furthermore in Figure 122, the deviations of the empirical probability density distribution of four examples of the ensemble of the 10-minutes subsamples are more clearly visualized in *normal probability plots*. The red line exhibits the *Gaussian reference value*. The blue crosses show the *empirical distribution* of the 10-minute time series. The deviations from the normal distribution are visible *in the tails*. As shown in the figure, the deviations are *not similar* for different subsamples. This emphasises the fact that *larger ensemble sizes* are necessary for *field data* in order to obtain statistically representative *ensemble average statistical properties*. Recall that in the Bolund field study despite of months of field measurements only eight 10-minutes time series were available for wind direction $270^\circ \pm 8^\circ$ and $|\text{invL}| < 0.002$ and wind speeds 4-6 m/s. In the wind tunnel, this problem can be overcome by simply increasing the sampling duration since the inflow conditions can be controlled.

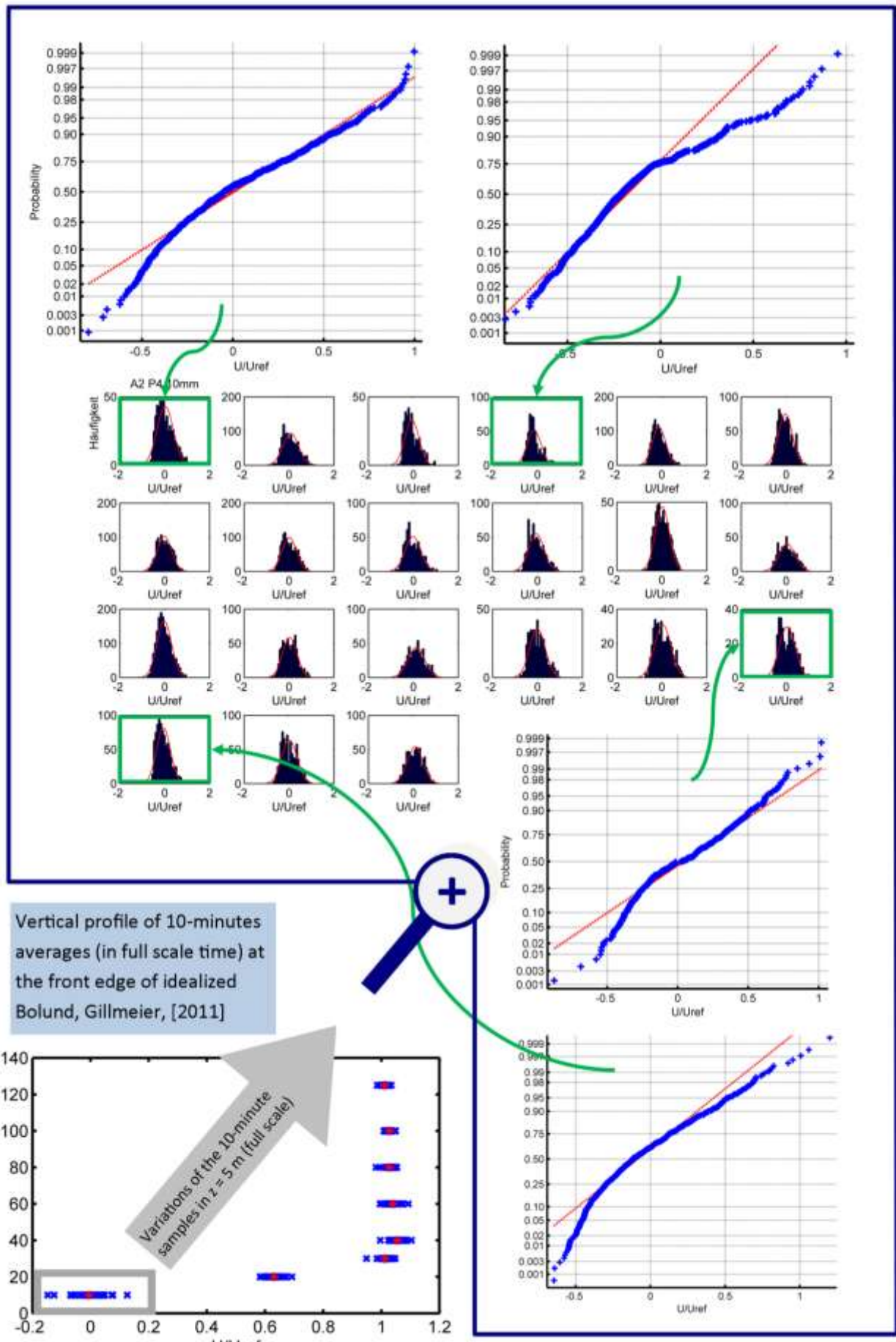


Figure 122 shows the variability of 10-minute wind tunnel time series (10-minutes in full scale time)

In the appendix, further brief remarks by the author on this work are given (see pp. 342). The key points are as follows:

- Model as model AND reality
- Incompatibility of flow scales
- Distinction of flow over hills and flow in urban canopies
- Logical pitfall of stationarity tests
- Mathematical modelling of small scale turbulence as a stochastic process
- Extreme value analysis and stationarity
- Extreme value statistics and self-similarity of wind tunnel data (with ETH Zürich)
- Geomorphological dynamics

Future work

In this section, remaining open questions and propositions for future work are presented including the suggestion for an assessment of the utilities of models by modelling based reasoning in the light of Bayesian interference.

Open questions

Questions that emerged or remained open during this work are amongst others:

- **Impossibility of absolute model validation:** Absolute quantification of model validity is not possible. With regard to the improvement of model quality in spite of this condition, one may ask: how do models *improve* or *specify our knowledge* of the world? What is the alternative to having *absolute certainty* of validation?

Validation of models is necessary in order to *interpret the results*. A first step forward is the insight that modelling helps us to analyse phenomena and is a *mediator* between *theories* and *reality* (or the true value). This can also be interpreted in Cartwrights' idea, as a step forward in the level of *preparedness of description*. A

second step forward is to admit *relative certainty*. Modelling can be interpreted as an attempt to *increase the degree of belief*. The *increase of belief* can be quantified by means of *Bayesianism* (Bayesian interference). This is detailed further in the outlook on “Modelling based reasoning in the light of Bayesian interference”.

- **De-trending of non-stationary data:** It is not clear how to de-trend field data in order to treat it as being statistically stationary. The only recommendation to avoid inappropriate data manipulation is to collect larger field data samples with inverse non-stationarity measures below e.g. 0.1 deviation in units of non-dimensional wind speed. This data could be used for extending analysis in the manner of chapter 9 or *extreme value analysis*.
- **Resampling of LDA data:** Extension of chapter 9 and *extreme value analysis* would also be interesting for wind tunnel LDA data. To do so, sensitivity of LDA data on *resampling methods* needs to be examined. The assessment of a best practice resampling method which *appropriately* represents the *actual* wind speed time series underlying the *measured signal* contains following *conceptual challenge*: the *measured signal* is *not independent* of the measurement *time steps*. This means that a *slower* particle needs *more time* to cross the LASER measurement volume. While this particle is in the measurement volume, no faster particle can be measured. This influences the *number of particles* whose velocity is recorded during a fixed time interval as well as the *sampling time steps* in between the particles.
- **Development of theories for flow over complex terrain:** No simple and *adequate* theory for modelling flow over hills is available at this time. Instead of Navier-Stokes-analysis, a systematic data analysis could be helpful. The establishment of a *wind data base* with *statistically representative long term wind data over complex terrain* could be helpful for linking the wind data to *geomorphological parameters*. The aim could be to build an empirical *statistical theory for atmospheric boundary layer flow over hills* and use this for understanding of the flow dynamics and for Navier-Stokes analysis.

- Wind tunnel data for theory development:** A characteristic *hill shape transformation matrix* for the flow geometry could be derived from statistically stationary wind tunnel measurements. This means that for development of an *empirical statistical theory on topographic effects*, the idealized Bolund *sensitivity study on hill shape effects* (conducted in this work) could be extended, namely: hill shapes could be classified with *geomorphometric* parameters which are chosen based on geomorphometric statistics of occurrence in e.g. Germany or Europe. Based on *systematic variation of the geomorphometric parameters*, 10-20 hill shapes could be incorporated into two or three different wind tunnel inflows (smooth, slightly rough and rough) to set the basis for a data base. Fluid dynamical parameters could be extracted from this data base, e.g. the *vertical mean wind profile, turbulence intensities, skewness and kurtosis of time series, speed-up along hill elevation, blockage in front of the hill and hill wake behaviour* – could statistically be extracted.
- Improvement of wind assessment:** From the author's point of view, the most promising opportunity for a quick and reliable improvement of wind energy prediction is to consider the *right models* for the *right purpose* – and to establish model *quality assurance procedures* and *data output-interpretation theories* to embed the scientific work into society as a basis for decision. For improvement of *wind energy assessment*, the author supports the view on *dispersion modelling* of COST 732, [2010]:

“Nevertheless, these models are used in the preparation of decisions with profound economic and political consequences. The reason that most of the models lack quality assurance is not due to insufficient efforts made by the model developers. It is mainly caused by

 - a lack of a commonly accepted quality assurance procedures for such models, and
 - a lack of data sets that are quality checked and commonly accepted as a standard for model validation purposes.” [COST 732, 2010]

From the author's point of view, this holds equivalently for the models in wind energy assessment.

- **Models and causality/ models and politics:** Strongly linked to the impossibility of absolute model validation is the question for appropriate *use of model results as a basis for decisions* in *socio-economical and -political* contexts. A simple thought experiment illustrates the danger of modelling-based reasoning: Assume that a sufficiently *precise* model shows satisfying results when *quantitatively compared* with *representative field data*. This is *not* a *sufficient condition* for the model to be *valid*, as was already pointed out. Models are *not unique* (i.e. different models can lead to the same data). This means that a satisfying model-data output does *not* give *logical power* to assume that the *model causality* can be transferred to *reality*. In other words, argumentation such as “if we increase x then y will decrease” – based on model results – is only valid based on the *model assumptions*.

Modelling based reasoning in the light of Bayesian interference

As pointed out, from the author's point of view, an interesting question is how models *improve the knowledge* about the world and how model results can be used as a *decision basis* in a *socio-economical and -political* context. This paragraph continues the analysis of *models as mediators* and the fact that absolute validation is not possible. *Bayesian theory* is used.

In the modelling practice, *uncertainties* of results are induced by uncertainties of *precision* and *accuracy*. Since an absolute quantification of the *accuracy* is not possible, the assignment of *probabilities for alternative outcomes* concerning the accuracy is the crucial point. For *precision*, it can be formulated positively: *uncertainties are the probabilities for alternative outcomes* for the model results. Hence, it can be stated that any appropriate *interpretation* of model results is based on probabilities of alternative outcomes and that the use of *model results* in argumentation and reasoning is *non-deductive*.

This can be quantified in a *Bayesian theory*. “[...] a Bayesian theory is any theory of non-deductive reasoning that uses the mathematical theory of probability to formulate its rules” [Weisberg, 2012, p.3]. The *mathematical machinery* of probability theory can be used while the *meaning of the machinery* might be yet another point for discussion⁸⁷. In the appendix, pp. 341, the fundamental concepts of Bayesianism are reviewed according to Weisberg, [2012]. For a mathematical introduction into probability theory the interested reader is referred to Dehling and Haupt, [2004].

Epistemic utility of models

In the *Bayesian framework*, a central aspect is *inductive inference* and how probabilities *change over time* if *new evidence* arises. The term of *conditionalization* can be used to point out the meaning of *conditional probability* in the following sense:

- When *new evidence*, *E*, is acquired, the *new probability* of any proposition *F* should be the *previous conditional probability* of *F* given *E*.

There are numerous thoughts of *ambiguity* in *conditionalization* and further developments of this framework such as “Jeffrey Conditionalization”, see Weisberg, [2012]. The crucial point here is: *change of beliefs* with acquisition of new evidence is exactly the case if scientists build and run a model, e.g. models for wind (energy) prediction. This means that the impact of a model could be measured in differences of *degrees of belief*. The impact of the model is the *difference of the degree of belief* before and after *building* and *running* the model (and interpreting the model results).

As a concrete example, consider a rough modelling task, e.g. a *prediction* for wind speeds in a certain area. Consider that this task *has already been conducted* for a few points, *x*, by some model. Each of the predictions consists of a wind speed interval *[a,b]*. Each of the

⁸⁷ In philosophy, it is on-going discussion on the question *what* probabilities *are* and which *probabilistic rules* are the *right ones*.

predictions has an *uncertainty* of X percent. Let us restrict the analysis to one interval of wind directions and a certain range of meteorological conditions.

Now, by *building* and *running* a *new* model, concrete insights can be obtained along different dimensions:

1. We can increase the number of locations, e.g. measure or compute a grid of wind speeds consisting of x' measurement locations.
2. We can decrease the level of uncertainty, X' percent, or narrow down the interval of expected wind speeds $[a', b']$ for the same uncertainty X percent.

Ad 1.: This will add *outcome spaces* and *enrich* the sigma-algebras of the outcome space. This means that the knowledge is increased in the sense that a *broader set of cases* is considered. Also, in general the number of *possible outcomes* will increase.

Ad 2.: This will determine the *argumentative power* for the reasoning based on the model results. This interpretational output is *required* to be provided by *the modeller* in addition to the pure data values. As stated in the chapter on *models as mediators*, a suggestion is to qualitatively and systematically analyse the relation between the *model*, *theories* and *reality*.

Here, it is suggested that a model is a *beneficiary tool* for *increasing knowledge* if it can be ensured that

$$\{x' - x > 0\} \text{ and } \{\{X - X' > 0\} \text{ or } \{a - b - (a' - b') > 0\}\}.$$

The first part might be violated – however, the author thinks that the second part is a necessary condition. It illustrates why *quality assessment* and *estimation of uncertainties* are crucial points in the practice of modelling. The *benefit* of good scientific mode is in *reducing* uncertainties and increasing the clarity on the appropriate use of the model results.

This fits well into the established theories of *belief and acceptance* within the *Bayesian framework*. The basic idea of the *theory of belief and acceptance* can be summarized as follows: belief if doing so *maximizes epistemic* or *cognitive utility* [Weisberg, 2012]. This

means that belief can be translated into a *decision problem* in the context of *cognitive utility*: we want answers to be *true* as *often* as *possible* – and *information* contained in the answers to be *as much* and *specific* as possible. In other words, *epistemic utility* has the currency of *truth* and *informativeness*. Following Levi, *simplicity* and *explanatory power* can be added to these fundamentals [Levi, 1980]. The benefit of using models, in this case for *wind prediction*, can thus be translated into epistemic utility: *reduction* of *uncertainties* and *increase* of *considered cases*. E.g., increase of prediction points, namely $\{x' - x > 0\}$, with for the same level of uncertainty as before, increases informativeness and hence is *epistemically util*. The *truth* of the model is modified by the *boundaries of uncertainty* which are assigned to the model (*quantitatively* in case of *precision* and *qualitatively* in case of *accuracy*).

Reducing uncertainties

In order to *decrease uncertainty* or *narrow down* the *interval of expected prediction values*, for example for wind speeds, the use of models can be interpreted as *mapping* between *probability density functions* – or even as mapping between *probability spaces* (also transforming Ω).

Let Ω be an outcome space and $\mathcal{F}(\Omega)$ the set of *probability density functions* $f: \Omega \rightarrow \mathbb{R}$ such that $\int_{\Omega} f(x) = 1$ and $\int_A f(x) = P(A)$.

In the case that f is not integrable, presuppose $\sum_{\Omega} f(x) = 1$ and $\sum_A f(x) = P(A)$. The decrease of uncertainty by use of models can be understood as the mapping:

$$\begin{aligned} &*: \mathcal{F}(\Omega) \rightarrow \mathcal{F}(\Omega). \\ &\text{such that } \int_A f \leq \int_A *(f). \end{aligned}$$

For convenience, it can be written: $f^* := *(f)$, for $f \in \mathcal{F}(\Omega)$, and $\int_A f^*$ can be understood as $P(A|*)$, thus model utility means $\int_A f \leq \int_A f^*$ respectively $P(A) \leq P(A|*)$. For illustration see Figure 123.

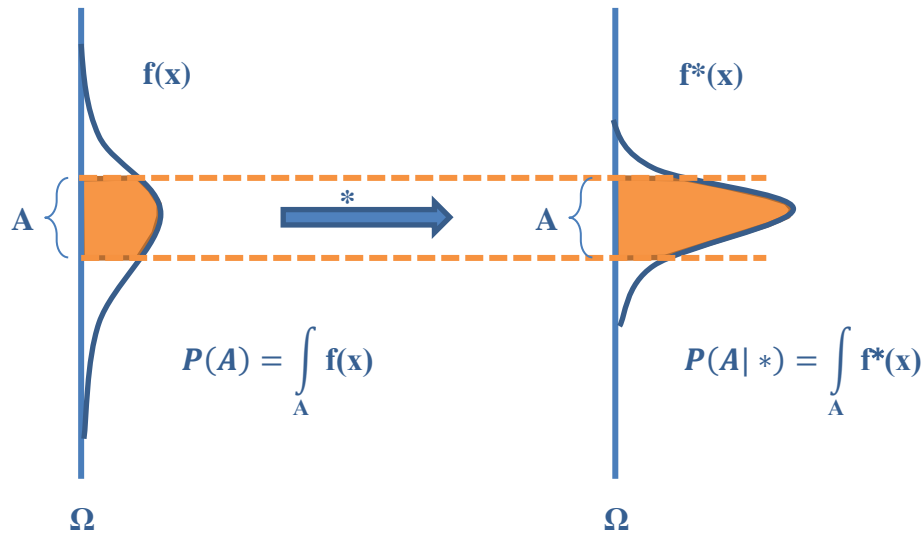


Figure 123: Modelling as mapping between probability density functions

As an example, consider the *speed-up effect* of atmospheric boundary layer flow over a hill. This can be estimated with a *rule of thumb*.⁸⁸ According to the rule of thumb the maximum relative speed up of wind flow over hill top (not exceeding one hill height above ground level) is expected to be $1.6 h/\hat{L}$ for a hill with height H and characteristic length \hat{L} ⁸⁹, [Kaimal and Finnigan, 1994].

Let us consider $10 \text{ m} < H < 12 \text{ m}$ and, as *characteristic length* of the asymmetric hill for the wind inflow from a certain range of wind directions, $50 \text{ m} < \hat{L} < 60 \text{ m}$.

With the rule of thumb, this leads to an estimation of the maximum speed up of 26-38 percent in the vertical profile above the hill top *somewhere* below 12 m above ground level. This holds for the range of wind directions for which approximately $50 \text{ m} < \hat{L} < 60 \text{ m}$ and *specific but non-quantified* meteorological boundary conditions (such as: “neutral stratification and moderate wind speeds”). Since the rule of thumb tends to over-predict,

⁸⁸ The rule of thumb itself is not on the level of *unprepared description*. It is – so to say – an empirical model derived as best fit to field studies that have been conducted.

⁸⁹ Here, the point is skipped that \hat{L} is not necessarily well defined since the hill might strongly deviate from rotational symmetric shape. Also H is not necessarily well defined since it does not need to be clear where the hill elevation starts. Also the hill might have two hill tops. On top, the rule of thumb does not specify in which height z above ground level the speed-up occurs.

[Lubitz and White, 2007], as an example, assume that we only believe with 40 percent of confidence that this is correct.

Assume that this situation has been modelled for the same range of wind directions as in the consideration above in a wind tunnel. Then, speed-up-ratios can be assigned for measurement locations with high spatial resolution from wind tunnel data.

Assume that the *error and error propagation analysis on precision of results* yield an assessment of speed-up for $z = 5$ m height above ground level such that the *mean fractional speed-up* is around 15 percent and *Gaussian distributed*. Consider further that the 95 percent confidence interval (of the distribution) yields a fractional speed-up of 13-18 percent (for the *specific* meteorological boundary conditions assumed for the model in the wind tunnel). Notice that this is approximately the result for the Bolund wind tunnel measurements at the defined hill top, M3, inflow direction Line B. What is the *model utility* in this case? The utility of the use of the *model* over the use of the rule of thumb can be formulated as follows:

- First of all, the *probability space* was adjusted and specified. This means that the *location* of the speed-up assignment was narrowed down from *somewhere* to a spatial *precision* of 0.5 m in full scale (namely an exemplary *spatial precision* of wind tunnel measurements).
- Furthermore, the certainty about the value of fractional speed-up was increased, i.e. the fractional speed-up interval was *specified*.
- Our *degree of belief* increased from 40 percent to 95 percent for specification of the assumptions for the result.

Of course, 95 percent is still *not* the *absolute certainty*. The important fact here is that the *model utility* is judged *relative* to *alternative* models, or *alternative* sources of information and prediction. The *difference* of exactness of the prediction statements is the crucial point.

This means that for both the rule of thumb as well as for the wind tunnel study, an *uncertainty concerning influence of meteorological boundary conditions* needs to be added. However, if this uncertainty is the same for both models, a *benefit* from using the model instead of the rule of thumb can still occur.

To conclude, this *perception of relative model results* fits into the trend amongst modellers to think in terms of probabilities. For example, the COST action ES1006, [COST ES1006, 2012] examines *evaluation, improvement and guidance* for the use of local-scale *emergency prediction and response tools* for airborne hazards⁹⁰ in built environments. Response models for airborne hazards are based on the *prediction of wind speeds* since concentration of hazardous substances strongly depends on the atmospheric flow. COST action ES1006 actively seeks *methodologies to assess uncertainties of the model results*. For example, *future needs* for model development are stated as: “Methodologies should be developed to assess the (bounds of) uncertainties in model predictions. These might be presented as a range of concentration values with respective probabilities, or as confidence estimates that prescribed concentrations will not be exceeded outside of the predicted hazard zones”, [COST ES1006, 2012, p. 52]. This perception fits with the understanding of a *quality measure* for the *epistemic utility* of model results in this thesis.

The author hopes that his analyses on wind tunnel modelling of atmospheric boundary layer flow over hills in the previous chapters have provided *guidance for proper physical modelling of atmospheric flow over hills*, as it was the scope of this work. In addition, from a more general perspective, the author hopes to have illustrated the challenges of *modelling based-reasoning*, emphasised the *importance of quality assessment of models* and, thus, paved the way for future work.

Finally, decision makers in science and politics hopefully become ever more aware of the fact that the aim of a good model should be to *specify the uncertainties of the model results*. Determination of *uncertainties* and the scientific and real world's *complexity increases* the

⁹⁰ Hazardous releases can be caused by natural emissions such as volcanic eruptions, forest fires. Harmful atmospheric releases can also be caused by accidents or terrorist attacks.

degree of belief and is the basis for the *utility* of the model. Model development is necessarily linked to the development of the *methodological framework* in which the model output can be interpreted. Hence, model development includes the *specification* of the *uncertainties* and the analysis of the scientific and real world's *complexity* in which the models are embedded. Concretely, this includes an analysis of the *theories* which are used in the models and the relationship between the *models*, *theories* and *reality*. Furthermore, it includes the analyses of the context of production, the use of the model results and the preparedness for public perception. This closes the loop to the considerations in the preface.

Fin

References

Alcalde, Jorge Gabriel Flematti: Reconstrucción lógica de teorías empíricas, el caso de la hidrodinámica de flúidos ideales. Tesis en la Universidad Nacional Autónoma de México, 1984

Arya, S.P.: Micrometeorology. International Geophysics Series, Volume 79, Academic Press, 2001

Athanassiadou, M. and Castro, I. P.: Neutral flow over a series of rough hills: A laboratory experiment. *Boundary Layer Meteorology*, 101:1–30, 2001.

Ayotte, K. W. and Hughes, D. E.: Observations of boundary-layer wind tunnel flow over isolated ridges of varying steepness and roughness. *Boundary-Layer Meteorology*, 112:525–556, 2004.

Baker, C.J.: The determination of topographical exposure factors for railway embankments. *Journal of Wind Engineering and Industrial Aerodynamics*, Volume 21, Issue 1, August 1985, Pages 89-99, 1985

Balzer, W., Pearce, D. A., and Schmidt, H.-J.: *Reduction in science: Structure, examples, philosophical problems*. Dordrecht: Reidel, 1984

Balzer, W., Moulines, C. U., and Sneed, J. D.: *An architectonic for science: The structuralist program*. Dordrecht: Reidel, 1987

Barndorff-Nielsen, O. E., P. ; Blaesild, and J. Schmiegel: A parsimonious and universal description of turbulent velocity increments. *The European Physical Journal B - Condensed Matter and Complex Systems* 41, 345{363, (2004).

Batchelor, G.: An Introduction to Fluid Dynamics. Cambridge University Press, 1970

Batchelor, G.K and Proudman, I.: The effect of rapid distortion of a fluid in turbulent motion. Quarterly Jnl. of Mechanics & App. Maths., Volume 7, Issue 1, pp. 83-103, 1954

Bechmann A., Berg J., Courtney M., Jørgensen H., Mann J. and N., Sørensen: The Bolund experiment: overview and background. Risø DTU report Risø-R1658(EN), 2009

Bechmann, A., Sørensen, N. N., Berg, J., Mann, J. and Réthoré, P.-E.: The Bolund Experiment, Part II: Blind Comparison of Microscale Flow Models, Boundary Layer Meteorology. DOI 10.1007/s10546-011-9637-x, 2011

Belcher, S.E., Newleyt, M.J. and Hunt, J.C.R.: The drag on an undulating surface induced by the flow of a turbulent boundary layer. J. Fluid Mech, vol. 249, pp. 557-596, 1993

Belcher, S. E. and Hunt, J.C.R.: Turbulent shear flow over slowly moving waves. J. Fluid Mech, vol. 251, pp. 109-148, 1993

Belcher, S.E. and Hunt, J.C.R: Turbulent flow over hills and waves. Ann. Rev. Fluid Mech. 30, 1998

Beljaars, A. C. M. and Taylor, P. A.: On the inner-layer scale height of boundary-layer flow over low hills Boundary-Layer Meteorology. Springer Netherlands, 49, 433-438, 1989

Berg, J., Mann, J., Bechmann, A., Courtney, M.S., Jorgensen, H.E.: The Bolund Experiment, Part I: Flow Over a Steep, Three-Dimensional Hill. Boundary-Layer Meteorol., 141:219–243, DOI 10.1007/s10546-011-9636-y, 2011

Bendat, J. and Piersol, A.: Random Data: Analysis and Measurement Procedures. Wiley Interscience, 1971

Berkhuizen JC, de Vries ET, Slob AFL.: Siting procedure for large wind energy projects. *J Wind Eng Ind Aerodyn*, 27:191–8, 1988

Boisvert, R.E., Ames, W.F. and Srivastava, U.N.: Group properties and new solutions of Navier-Stokes equations. *Journal of Engineering Math.* 17, 203-221, 1983

Böttcher, F., Renner Ch., Waldl H.-P. and Peinke, J.: On the statistics of wind gusts. *Boundary-Layer Meteorology*, 108: 163-173, 2003

Böttcher, F., Barth, St. and Peinke, J.: Small and large scale fluctuations in atmospheric wind speeds. *Stoch Environ Res Ris Assess*, 21: 299-308, 2006

Bradley, E. F.: An experimental study of the profiles of wind speed, shearing stress and turbulence at the crest of a large hill. *Quart. J. Roy. Meteorol. Soc.*, 106:101–124, 1980.

Britter, R.E., Hunt, J.C.R. and Richards, K.J.: Air flow over a two-dimensional hill: studies of velocity speed-up, roughness effects and turbulence. *Quart. J. R. Met. Soc.*, 107 (451):91–110, 1981.

Buckingham, E.: On physically similar systems; illustrations of the use of dimensional equations. *Physical Review* 4 (4): 345–376, 1914

Carpenter, P. and Locke, N.: Investigation of wind speeds over multiple two-dimensional hills. *Journal of Wind Engineering and Industrial Aerodynamics*, Volume 83, Issues 1–3, November 1999, Pages 109-120, 1999

Cartwright, N.: *How the Laws of Physics Lie*. Oxford University Press, 1983

Castaing, B., Gagne, Y. and Hopfinger, E. J.: Velocity probability density functions of high Reynolds number turbulence. *Phys D*, 46(2):177–200, 1990

Castro, F. A., Palma, J. and Lopes, A. S.: Simulation of the Askervein flow. Part 1: Reynolds averaged Navier–Stokes Equations. *Boundary Layer Meteorology*, 107, 501-530, 2003

Cao, S. and T. Tamura: Experimental study on roughness effects on turbulent boundary layer flow over a two-dimensional steep hill. *Journal of Wind Engineering and Industrial Aerodynamics*, 94:119, 2006.

Cao, S. and T. Tamura: Effects of roughness blocks on atmospheric boundary layer flow over a two-dimensional low hill with/without sudden roughness change. *Journal of Wind Engineering and Industrial Aerodynamics*, 95:679–695, 2007.

Cermak, J. E.: Physical modelling of flow and dispersion over complex terrain. *Boundary Layer Meteorology*, Vol. 30, 261-292, 1984.

Cermak, J., Arya, S.: Problems of atmospheric shear flows and their laboratory simulation. *Boundary Layer Meteorology*, 1, 40-60, 1970

Cheng, J., Lubitz, D. and White, B. R.: Wind tunnel prediction of wind power production in complex terrain. American Institute of Aeronautics and Astronautics, AIAA/ASME Wind Energy Symposium 2004, 2004

Claussen, M.: On the inner-layer scale height of boundary layer flow over low hills. *Boundary Layer Meteorology*, 44, 411-413, 1988

Coppin, P., Bradley, E. and Finnigan, J.: Measurements of flow over an elongated ridge and its thermal stability dependence: the mean field. *Boundary Layer Meteorology*, 69, 173-199, 1994

Corby, G. A.: The Airflow over Mountains – A Review of the State of Current Knowledge. *Quart. J. Roy. Meteorol. Soc.* 80, 491–521, 1954

COST ES1006 – Background and Justification Document, COST Action ES1006, May 2012

COST 732 – Quality Assurance and Improvement of Microscale Meteorological Models. edited by Schatzmann, M., Olesen, H. and Franke, J.: COST Action 732 Technical Report, 2010

Counihan, J.: Adiabatic Atmospheric Boundary Layers: A Review and Analysis of Data. Atmospheric Environment, 9, 1975

Dantec Dynamics A/S: BSA Flow Software Version 4.10 Installation and User's Guide. 2006, Publication number 9040U5734, 2006

Davenport, A.: The relationship of wind structure to wind loading. Paper 2, Symposium 16, Int. Conf. on Wind effects on Buildings and Structures at NPL, H.M.S.O., London, 1963

Darrigol, O.: Worlds of Flow—A History of Hydrodynamics from the Bernoulli to Prandtl. Oxford, UK: Oxford University Press, 2005

Davidson et al.: A Voyage through turbulence. Cambridge University Press, 2011

Dehling, H. and Haupt, B.: Einführung in die Wahrscheinlichkeitstheorie und Statistik. Springer, ISBN: 978-3-540-20380-3, 2004

Deng, Yongxin: New trends in digital terrain analysis: landform definition, representation, and classification. Progress in Physical Geography 31: 405, DOI: 10.1177/0309133307081291, 2007

Dias, N. L., Chamecki, M., Kan, A. and Okawa, C. M. P.: A Study of Spectra, Structure and Correlation Functions and Their Implications for the Stationarity of Surface-Layer Turbulence. Boundary-Layer Meteorology, Springer Netherlands, 110, 165-189, 2004

Einstein, A.: Über die von der molekularkinetischen Theorie der Wärme geforderte Bewegung von in ruhenden Flüssigkeiten suspendierten Teilchen. *Annalen der Physik* 17: 549–560, 1905

Erdős, László: Lecture Notes on Quantum Brownian Motion. Institute of Mathematics, University of Munich, Sep 4, 2010

ESDU 85020: Characteristics of atmospheric turbulence near the ground. Part II: single point data for strong winds (neutral atmosphere), ISBN: 978 0 85679 526 8, 2008

Ferreira, A.D., A.M.G. Lopes, D.X. Viegas, and A.C.M. Sousa: Experimental and numerical simulation of flow around two-dimensional hills. *Journal of Wind Engineering and Industrial Aerodynamics*, 54/55:173–181, 1995.

Fischer, R.: Entwicklung eines problemorientierten Software-Pakets zur automatisierten Aufbereitung, Analyse und Dokumentation von im Windkanal produzierten Daten zur LES-Validierung. Dissertation, 2011

Frisch, U.: Turbulence - The legacy of A.N. Kolmogorov. Cambridge University Press, 2004

Frisch, U: Fully developed turbulence and intermittency, *Annals of the New York Academy of Sciences*, Blackwell Publishing Ltd, 357, 359-367, 1980

Gähde, U.: Holism, underdetermination, and the dynamics of empirical theories. *Synthese*, 130, 69–90. 2002

Gärdenfors, P.: Conceptual spaces: The geometry of thought. Cambridge, MA: The MIT Press, 2000

Gärdenfors, P., and Zenker, F: Using conceptual spaces to model the dynamics of empirical theories. In E. J. Olsson and S. Enqvist (Eds.), *Belief revision meets philosophy of science* (pp. 137–153). Berlin: Springer, 2011

Gillmeier, Stefanie: Analyse von Strömungsmessungen an idealisierten Hügelstrukturen in einem Grenzschichtwindkanal. Bachelor thesis, University of Hamburg, 2011

Gluhovsky, A. and Agee, E.: A Definitive Approach to Turbulence Statistical Studies in Planetary Boundary Layers. *J. Atmos. Sci.* 51, 1682–1690, 1994

Gong, W. and Ibbetson, A.: A Wind Tunnel Study of Turbulent Flow over Model Hills. *Boundary Layer Meteorology*, 49, 113-148, 1989

Harms, F.: Systematische Windkanaluntersuchungen zur Charakterisierung instationärer Ausbreitungsprozesse einzelner Gaswolken in urbanen Rauigkeitsstrukturen. Dissertation, 2010

Hänel, Dieter: Molekulare Gasdynamik. ISBN 3-540-44247-2, Springer, Berlin / Heidelberg / New York 2004,

Hertwig, R., Benz, B., and Krauss, B. S.: The conjunction fallacy and the many meanings of and. *Cognition*, 108, 740–753, 2008

Hunt, J.C.R.: A theory of turbulent flow round two-dimensional bluff bodies. *Journal of Fluid Mechanics*, 61 , pp 625-706 doi:10.1017/S0022112073000893, 1973

Hunt, J.C.R. and Carruthers, D.J.: Rapid distortion theory and the ‘problems ’ of turbulence. *Journal of Fluid Mechanics*, vol. 212, pp . 497-532, 1990

Hunt JCR, Leibovich S, Richards KJ.: Turbulent shear flows over low hills. *Q. J. R. Meteorol., Soc.* 114:1435–70, 1988

Heisenberg: Physics and Philosophy: The Revolution in Modern Science. (1958) Lectures delivered at University of St. Andrews, Scotland, Winter 1955-56

Hirschfelder, J.O., Curtiss, C.F. and Bird, R.B.: Molecular Theory of Gases and Liquids. John Wiley and Sons, 1964

Irwin, P. A.: Bluff body aerodynamics in wind engineering. Journal of Wind Engineering and Industrial Aerodynamics, 2008, 96, 701-712

Ishihara, T., K. Hibi, and S. Oikawa. A wind tunnel study of turbulent flow over a three-dimensional steep hill. Journal of Wind Engineering and Industrial Aerodynamics, 83:95 – 107, 1999.

Jackson, P.S. and Hunt, J.C.R.: Turbulent wind flow over a low hill. Quart. J. R. Met. Soc., 101:929–955, 1975

JCGM 200: International vocabulary of metrology — Basic and general concepts and associated terms (VIM), 2008

Jenkins, G. J., Mason, P. J., Moores, W. H. and Sykes, R. I: Measurements of the flow structure around Ailsa Craig, a steep, three-dimensional, isolated hill. Q.J.R. Meteorol. Soc., 107: 833–851. doi: 10.1002/qj.49710745406, 1981

Kaimal JC and Finnigan JJ: Atmospheric Boundary Layer Flows: Their Structure and Measurement. New York: Oxford University Press, 1994

Kaltschmitt M., Wiese A.: Erneuerbare Energien, Systemtechnik, Wirtschaftlichkeit, Umweltaspekte. Springer Verlag, Berlin, Heidelberg, New York, 1995

Kevlahan, N.K.-R.: Rapid distortion of turbulent structures. Applied Scientific Research, 51:411–415, 1993.

Kim, Hyun Goo, Choung Mook Lee, H.C. Lim, N.H. Kyong: An experimental and numerical study on the flow over two-dimensional hills. *Journal of Wind Engineering and Industrial Aerodynamics*, Volume 66, Issue 1, January 1997, Pages 17-33, 1997

Kim, Jongkil: Heavy tails and Self Similarity of wind turbulence data. Master Thesis, ETH Zurich, Department of Mathematics, Submission Date: November 5th 2011

Kitabayashi, K: Wind tunnel and field studies of stagnant flow upstream of a ridge. *Meteorological Society of Japan, Journal*. Vol. 55, pp. 193-204. Apr. 1977

Larose, G. and D'Auteuil, A.: On the Reynolds number sensitivity of the aerodynamics of bluff bodies with sharp edges. *Journal of Wind Engineering and Industrial Aerodynamics*, 2006, 94

Leitl, B.: Quality assurance of urban flow and dispersion models - new challenges and data requirements. *Journal of Wind and Engineering*, vol 5, no. 2, pp. 60-73, 2008

Leitl, B., Pascheke, F. and Schatzmann, M.: Generation of Wind Tunnel Data Sets in Support of the Joint Urban 2003 Atmospheric Dispersion Study - Final Report, Phase I. Meteorological Institute, University of Hamburg, Germany, 2003

Leitl, B. and Schatzmann, M.: Generation of Wind Tunnel Data Sets in Support of the Joint Urban 2003 Atmospheric Dispersion Study - Final Report, Phase II. Meteorological Institute, University of Hamburg, Germany, 2005

Leitl, B., Schatzmann, M. and Harms, F.: Benchmark for Computational Modeling of Urban Flows, Final Report, Meteorological Institute, University of Hamburg, Germany, 2009

Lenschow, D., J. Mann, and L. Kristensen: How long is long enough when measuring fluxes and other turbulence statistics? *J Atmos Ocean Tech*, 11 (3), 661-673, 1994

Lenschow, D. and B. Stankov: Length scales in the convective boundary layer. *J Atmos Sci*, 43 (12), 1198-1209, 1986

Levi, Isaac: *The Enterprise of Knowledge: An Essay on Knowledge. Credal Probability, and Chance.* The MIT Press, 1980

Liepmann, H.: Aspects of the turbulence problem. *Z Angew Math Phys*, 3 (5), 321-342, 1952

Long, R. R.: *Some Aspects of the Flow of Stratified Fluids: I. A Theoretical Investigation.* Tellus, Blackwell Publishing Ltd, 5, 42-58. 1953

Long, R. R.: *Some Aspects of the Flow of Stratified Fluids: II. Experiments with a Two-Fluid System.* Tellus, Blackwell Publishing Ltd, 6, 97-115, 1954

Long, R. R.: *Some Aspects of the Flow of Stratified Fluids.* Tellus, Blackwell Publishing Ltd, 7, 341-357, 1955

Lopes, A. S., Palma, J. and Castro, F.: Simulation of the Askervein flow. Part 2: Large-eddy simulations. *Boundary Layer Meteorology*, 125, 85-108, 2007

Lopes, A. Silva, Palma. J.M.L.K., and Castro, F.A.: Simulation of the askervein flow. part 2: Large-eddy simulations. *Boundary Layer Meteorology*, 125:85–108, 2007.

Lubitz, W.D. and B.R. White: Wind tunnel and field investigation of the effect of local wind direction on speed-up over hills. *Journal of Wind Engineering and Industrial Aerodynamics*, 95:639661, 2007

Lumley, J. and H. Panofsky: *The structure of atmospheric turbulence.* Interscience, 239 pp., 1964

Magnani, L., Nersessian, N. J. and Thagard, P. (ed.): Model-based reasoning in scientific discovery. Kluwer Academic/ Plenum Publishers, 1999

Mason, P. J.: Flow over the Summit of an Isolated Hill. *Boundary-Layer Meteorology* 37, 385-405, 1986

Mason, P.J. and King, J.: Measurements and predictions of flow and turbulence over an isolated hill of moderate slope. *Quart. J. R. Met. Soc.*, 111, 617-640, 1985

Meroney, R. N.: Wind tunnel modelling of hill and vegetation influence on wind power availability task1: Literature review. Technical report, Meteorological Services U.S. Windpower, 1993

Mickle, R. E., Cook, N. J. A. M., Hoff, N. O. Jensen, J. R. Salmon, P. A. Taylor, G. Tetzlaff, and H. W. Teunissen: The askervein hill project: Vertical profiles of wind and turbulence. *Boundary Layer Meteorology*, 43:143–169, 1988.

Migliore, P. G., Obermeier, J., White, B. R.: Wind Tunnel Testing as an Aid in Site Assessment. *Proceedings of Windpower '85*, pp. 14 – 18. San Francisco, CA, USA, Aug. 27-30, 1985.

Miller, C.A. and Davenport, A.G.: Guidelines for the calculation of wind speed-ups in complex terrain. *Journal of Wind Engineering and Industrial Aerodynamics*, 74-76:189–197, 1998.

Morgan, M. S. and Morrison, M.: *Models as Mediators: Perspectives on Natural and Social Science*. Cambridge University Press, 1999

Moulines, C. U.: Introduction: Structuralism as a program for modelling theoretical science. *Synthese*, 130, 1–11., 2002

Neal, D., Stevenson, D. C. and Lindley, D.: A wind tunnel boundary-layer simulation of wind flow over complex terrain: Effect of terrain and model construction. *Boundary-Layer Meteorology*, Springer Netherlands, 21, 271-293, 1981

Neff, D. E. and Meroney, R. N.: Wind-tunnel modeling of hill and vegetation influence on wind power availability. *Journal of Wind Engineering and Industrial Aerodynamics*, 74-76, 335-343, 1998

Oberlack, M.: Symmetrie, Invarianz und Selbstähnlichkeit in der Turbulenz. Habilitation thesis. RWTH Aachen, 2000

Oberlack, M., Rosteck, A.: New statistical symmetries of the multi-point equations and its importance for turbulent scaling laws. *Discrete Contin. Dyn. Syst., Ser. S* 3, 451–471, 2010

Oreskes, N., Shrader-Frechette, K. and Belitz, K.: Verification, Validation, and Confirmation of Numerical Models in the Earth Sciences. *Science* , New Series, Vol. 263, No. 5147, pp. 641-646, Feb. 4, 1994

Pascheke, F., Leitl, B. and Schatzmann, M.: Results from Recent Observations in an Urban Boundary Layer. COST 715 Workshop on urban boundary layer parameterisations, extended abstracts, pp. 73-83, 2002

Planck, Max: The Meaning and Limits of Exact Science. *Science* (30 Sep 1949), 110, No. 2857, 1949

Petersen, G., Leitl, B. and Schatzmann, M.: On proper physical simulation of turbulent atmospheric flow over hills. EAWE proceedings, Brussels,, 2011a

Petersen, G., Leitl, B. and Schatzmann, M.: ABL flow over hills: A review on theory and critics of recent wind tunnel studies. ICWE 13, conference paper, Amsterdam, 2011b

Petersen, G., Gähde, U., Hoffman, M., Leitl, B. and Schatzmann, M.: Models in Wind Energy Assessment. PHYSMOD 2011 proceedings, 2011c

Petersen, G. and Zenker, F.: From Euler to Navier Stokes: The Conceptual Space of 19th Century Fluid Dynamics. submitted to History and Philosophy of Science, Elsevier, 2012

Pielke, R.A.: Mesoscale Meteorological Modeling. 1st Edition, Academic Press, New York, 1984

Pike, R.J.: The geometric signature: quantifying landslide-terrain types from digital elevation models. Mathematical Geology 20, 491–511, 1988

Pike, R.J.: Geomorphometry – diversity in quantitative surface analysis. Progress in Physical Geography 24,1–20, 2000

Poggi, D., Katul, G. G., Albertson, J. D. and Ridolfi, L.: An experimental investigation of turbulent flows over a hilly surface. Physics of Fluids, Volume 19, Issue 3, DOI: 10.1063/1.2565528, 2007

Pope, S.: Turbulent Flows, Cambridge University Press, 2009

Rayleigh, L.: The principle of similitude. Nature, 95, 66–68, 1915

Rehg, W.: Cogent Science in Context. Cambridge: MIT Press, 2009

Rehg, W.: Evaluating complex collaborative expertise: the case of climate change. Argumentation, 25, 385-400, 2011

Rodrigo, J. S.: State-of-the-Art of Wind Resource Assessment. CENER, 2010

Rosenblueth, A. and Wiener, N.: The Role of Models in Science. Philosophy of Science, Vol. 12, No. 4 pp. 316-321, Oct. 1945

Ross, A.N., Arnold, S., Vosper, S.B., Mobbs, S. D., Dixon, N. and Robins, A. G.: A comparison of wind-tunnel experiments and numerical simulations of neutral and stratified flow over a hill, *Boundary-Layer Meteorology*, 113, pp. 427-459, 2004

Rosteck, Andreas M., Oberlack, Martin: Lie Algebra of the Symmetries of the Multi-Point Equations in Statistical Turbulence Theory. *Journal of Nonlinear Mathematical Physics (JNMP)*, 18 (1) pp. 251-264, 2011

Rotta, J.C.: *Turbulente Strömungen*. Teubner Verlag, Stuttgart, 1972

Salmon, J. R., Teunissen, H. W., Mickle, R. E. and Taylor, P. A.: The Kettles Hill Project: Field observations, wind-tunnel simulations and numerical model predictions for flow over a low hill. *Boundary Layer Meteorology*, 43, 309-343, 1988

Sargent, Robert G.: Verification and validation of simulation models, *Proceedings of the 2009 Winter Simulation Conference*. edited by: M. D. Rossetti, R. R. Hill, B. Johansson, A. Dunkin and R. G. Ingalls, 2007

Sreenivasan, K., A. Chambers, and R. Antonia: Accuracy of moments of velocity and scalar fluctuations in the atmospheric surface layer. *Boundary-Layer Meteorol*, 14 (3), 341-359, 1978

Schatzmann, M.: *Turbulenz und Grenzschicht*. Vorlesung für Studierende der Meteorologie, University of Hamburg, 2008

Schatzmann, M. and Leitl, B.: Issues with validation of urban flow and dispersion CFD models, *Journal of Wind Engineering and Industrial Aerodynamics*. Volume 99, Issue 4, April 2011, Pages 169-186, ISSN 0167-6105, 10.1016/j.jweia.2011.01.005, 2011

Schlesinger, S.: Terminology for model credibility. *Simulation* 32 (3): 103-104, 1979

Smoluchowski, M.: Zur kinetischen Theorie der Brownschen Molekularbewegung und der Suspensionen. *Annalen der Physik* 21: 756–780, 1906

Sneed, J. D.: *The logical structure of mathematical physics*. Dordrecht: Reidel. Synthese, 1971

Snyder, W. H.: *Guideline for fluid modelling of atmospheric diffusion*. Technical report, United States Environmental Protection Agency, 1981.

Snyder, W.H.: Fluid Modelling of pollutant transport and diffusion in stably stratified flows over complex terrain. *Ann. Rev. Fluid Mech.*, 17, 239-266, 1985

Snyder, Thompson, Eskridge, Lawson, Castro, Lee, Hunt, and Ogawa: The structure of strongly stratified flow over hills: dividing-streamline concept. *J. Fluid. Mech.*, 152:249–288, 1985

Spalart, P.R.: Detached-Eddy Simulation. *Annual Review of Fluid Mechanics*, Vol. 41: 181-202, doi: 10.1146/annurev.fluid.010908.165130, 2008

Stegmüller, W.: *The structuralist view of theories*. Berlin: Springer, 1976

Stull, R.B.: *An introduction to Boundary Layer Meteorology*. Kluwer Academic Publ., 1988

Taylor, Peter A.: Turbulent boundary-layer flow over low and moderate slope hills. *Journal of Wind Engineering and Industrial Aerodynamics* 74-76, 1998

Taylor, P. A., Mickle, R. E., Salmon, J. R., and Teunissen, H. W.: *The Kettles Hill experiment - Site Description and Mean Flow Results*. Internal Report AQRB-83-002-L, Atmos. Environ. Service, Downsview, Ont, 1983

Taylor, P. A. and Teunissen, H. W.: *Askervein '82: Report on the September/October 1982*

Experiment to Study Boundary-Layer Flow Over Askervein. South Uist', Rep. MSRB-83-8, Atmospheric Environment Service, Downsview, Ontario, Canada, 1983

Taylor, P. A. and Teunissen, H. W.: The Askervein Hill Project: Report on the September/October 1983, Main Field Experiment. Rep. MSRB-84-6, Atmospheric Environment Service, Downsview, Ontario, Canada, 48 pp. plus tables and figures, 1985

Taylor, P.A. and H.W. Teunissen: The Askervein hill project: Overview and background data. *Boundary Layer Meteorology*, 39:15–39, 1987

Tennekes, H. and J. L. Lumley: *A First Course in Turbulence*. MIT Press, Cambridge, MA, 1972

Teunissen, H.W., M.E. Shokr, A.J. Bowen, C.J. Wood, and D.W.R. Green: The askervein hill project: Wind tunnel simulations at three length scales. *Boundary Layer Meteorology*, 40:1–29, 1987.

Tokaty, G.A.: *A History and Philosophy of Fluid Mechanics*. New York, NY: Dover Publications, 1971

Townsend, A. A.: Equilibrium layers and wall turbulence. *Journal of Fluid Mechanics*, 11 , pp. 97-120 doi:10.1017/S0022112061000883, 1961

Tversky, A. and Kahneman, D.: Judgments of and by representativeness. In D. Kahneman, P. Slovic and A. Tversky (Eds.), *Judgment under uncertainty: Heuristics and biases*. Cambridge, UK: Cambridge University Press, 1982

VDI-guideline 3783/Part 12, 2000: *Physical Modelling of Flow and Dispersion Processes in the Atmospheric Boundary Layer – Application of wind tunnels*. Beuth Verlag, Berlin 2000

Walmsley, John L. and Taylor, Peter A.: Boundary-layer flow over topography: Impacts of the Askervein study. *Boundary-Layer Meteorology*, Volume 78, Issue 3-4, pp. 291-320, 03/1996

Wei, S. N., Kao, T. W. and Pao, H.: Experimental study of upstream influence in the twodimensional flow of a stratified fluid over an obstacle. *Geophysical Fluid Dynamics*, 6, 315-336, 1975

Weisberg, Jonathan: *Varieties of Bayesianism*. University of Toronto – For the *Handbook of the History of Logic*, vol. 10, 2012

Wyngaard, J.C.: *Turbulence in the Atmosphere*. Cambridge University Press, 2010

Wyngaard, J.C.: On surface layer turbulence. *Workshop on Micrometeorology*, D. Haugen, Ed., *Am. Meteorol. Soc.*, 101-149, 1973

Wood, N.: The onset of separation in neutral, turbulent flow over hills. *Boundary Layer Meteorology*, 76:137–164, 1995.

Wood, N.: Wind flow over complex terrain: A historical overview and the prospect for large-eddy modelling. *Boundary Layer Meteorology*, 96:11–32, 2000.

Zeman, O., and Jensen, N. O.: Modification of Turbulence Characteristics in Flow Over Hills. *Quart. I. R. Meteorol. Sot.* 113,55-80, 1987

Appendix

Categorisation of changes in terms of conceptual spaces

Five types of changes in the toolbox of conceptual spaces are usually detailed, namely:

1. addition and deletion of special laws
2. change of scale or metric of dimensions
3. change in the importance of dimensions
4. change in the separability of dimensions
5. addition and deletion of dimensions.

In the light of these definitions, changes of fluid dynamics as analysed in chapter 4 can be categorised as follows [Petersen and Zenker, 2012]:

- The continuum hypothesis was introduced as “basis space” (fundamental assumption for development of fluid mechanics.)
- Classical mechanics was translated to fluids *adding dimensions* to the basic space (e.g. domain of force), at the same time *changing (enriching) the metric* of the space and *adding the special law* for mechanical equilibrium.
- Forces were split into body and surface forces acting on a volume fluid element respectively its surfaces (= *changing conceptual importance of force* and *adding new dimensions*). This led to the conceptual space **G**, also equipped with the dimension *pressure* derived by *adding the law* “divergence theorem”.
- Velocity was introduced as *new dimension* to **G** yielding to the conceptual space **G_{EE}** in which the Euler-Equation holds.

- The concepts (laws) of (A1) and (A2) are *added* to \mathbf{G} . This means in geometrical sense, (A1) and (A2) define a region in \mathbf{G}_{EE} that can be interpreted as conceptual space $\mathbf{G}_{EE}^* \subset \mathbf{G}_{EE}$.
- The conceptual space \mathbf{G}_{EE}^* is *extended by the dimension viscosity, μ* , based on (A1) and (A2). Also, viscosity μ is *added as new quality dimension* to the whole space \mathbf{G}_{EE} yielding to a new space \mathbf{G}_{NSE} with domains⁹¹ $(u, x, t, F, \sigma_{ij}, \rho, \mu)$.

⁹¹ From technical point of view, the boundary conditions of NSE can be added as domains to \mathbf{G}_{NSE} as well since the boundary conditions determine the solutions of NSE – in case the solutions exist. Existence and uniqueness of solutions for 3D is still an unsolved open question in pure mathematics. Pressure p can be added as quality dimension as well.

Key figures for the 18th and 19th century fluid dynamics

The key figures in the following table are a subjective selection of the author with respect to the content of chapter 4 (namely the step from Euler to Navier-Stokes)⁹²:

Year	Person	Noted for
1738	D. Bernoulli	Author of “Hydrodynamica”—known for Bernoulli’s law
1742	J. Bernoulli	Author of “Hydraulica”
1743/44	D’Alembert	Re-derived Bernoulli’s law
1752	L. Euler	Found Euler Equations using Newtonian mechanics
1781	J.L. Lagrange	Worked on the Euler Equations and, during his career, came to change his point of view on which variables are significant
1799	G.B. Venturi	Conducted experiments on viscosity
1816	P.S. Girard	Conducted experiments on flows in capillary tubes
1821	C.L.M.H. Navier	Derived the Navier-Stokes Equations (NSE), i.e., the viscosity extension of the Euler Equations
1821	H. Cauchy	Formulated a theory expressing elasticity in terms of pressures acting on a surface, introducing tangential pressures yielding the Cauchy stress tensor
1828	A. Cournot	Criticized the NSE, naming it a “hypothesis that can solely be verified by experiment
1829	S.D. Poisson	Derived NSE in a new way—inspired by Laplace’s molecular physics—mentioning neither Navier nor Cauchy
1837	A.B. de Saint-Venant	Derived the NSE again
1839	G. Hagen	Conducted experiments on pipe flows
1840	J.-L. Poiseuille	Conducted experiments on pipe flows for analysis on blood circulation
1845	G.G. Stokes	Derived the NSE in a new way, inspired by Cauchy and Saint-Venant
1859	H. Helmholtz	Derived the NSE independently and worked on viscosity (internal friction), seemingly unaware of the previous mathematical studies by Poisson, Navier, Saint-Venant and Stokes

⁹² See also Petersen and Zenker, [2012], based on Darrigol, [2005], and Tokaty, [1971].

Bolund field data analysis

For Bolund field data analysis, such as the estimation of roughness length, z_0 and α , and the following computation for autocorrelations and cross correlations, 20 Hz sonic data can be extracted from the Bolund Data Base. This data is already METEK corrected, but aligned relative to the boom direction. The boom directions are different for the different masts in the Bolund field study. The directions are given in the Bolund documentation, [Bechmann, 2009]. In the following, it is concentrated on the westerly wind, concretely in the corridor of $270^\circ \pm 8^\circ$. In order to make the wind speed comparable, the 20 Hz sonic data is aligned with 270° wind direction, it means the wind vectors are multiplied with the corresponding rotation matrix for every mast.

Furthermore, the analysis is restricted to nearly neutral conditions. Altogether this means that the Bolund data base is searched for ten minutes intervals with averaged wind direction $270^\circ \pm 8^\circ$ and $|1/L| < 0.002$ at mast M0 in 5 meters height. The selection is intersected with the corresponding measurements at the sonic anemometers in 2 and 5 meters height at masts M3, M6, M7 and M8, and the sonic at M9 in 5 meters height. From the extracted 10 minutes intervals, the maximal connected periods of times are picked. This results in following six samples of connected 10 minutes intervals covered by 20 Hz Sonic data for the desired surrounding meteorological conditions (as of date: 30/10/2012):

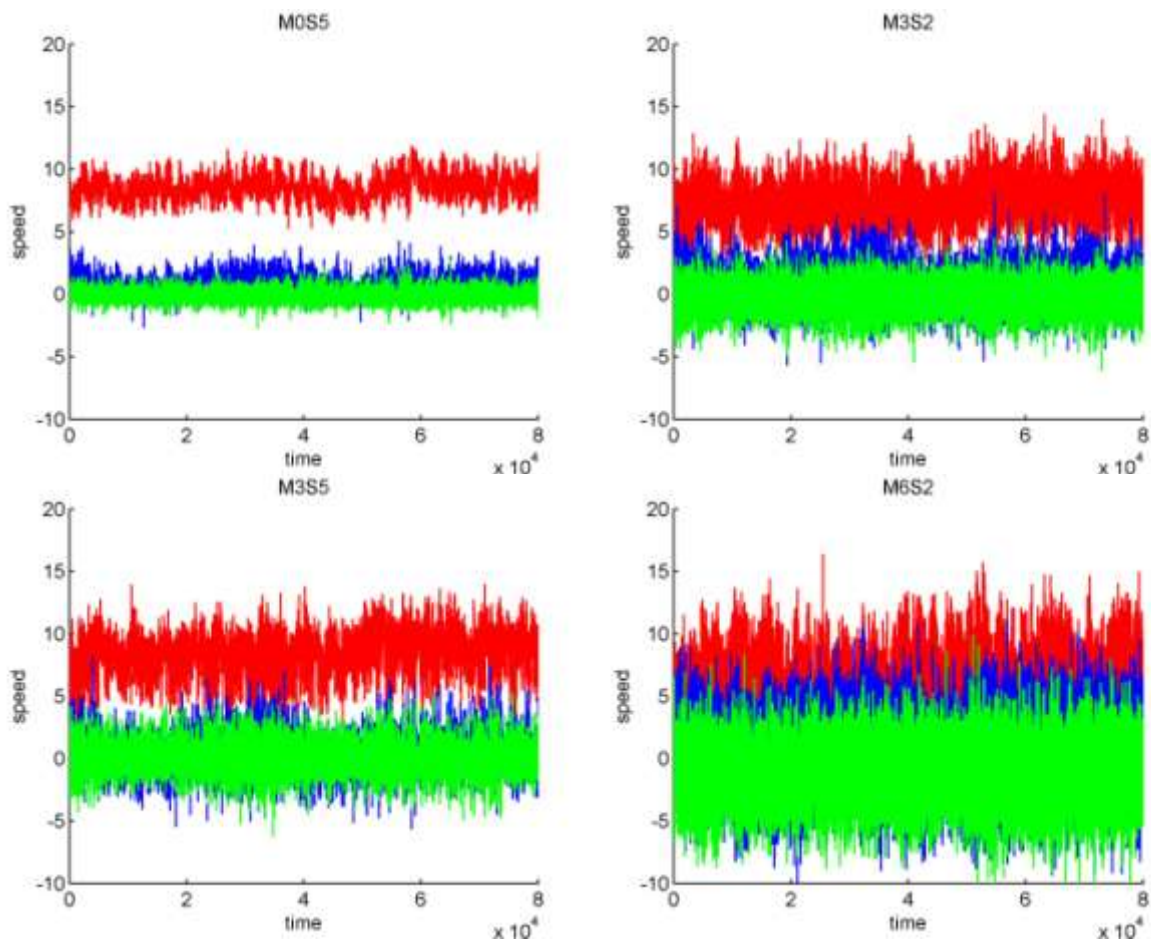
Name	Bolund Name	Date	Time	Duration
Z1	'200801212140' '200801212150' '200801212200' '200801212210'	21 Jan 2008	21:40 – 22:20	40 minutes
Z2	'200801270740' '200801270750' '200801270800' '200801270810' '200801270820' '200801270830' '200801270840'	27 Jan 2008	07:40 – 08:50	1h 10min.
Z3	'200801302000' '200801302010' '200801302020' '200801302030' '200801302040' '200801302050' '200801302100'	30 Jan 2008	20:00 – 22:10	2h 10min.

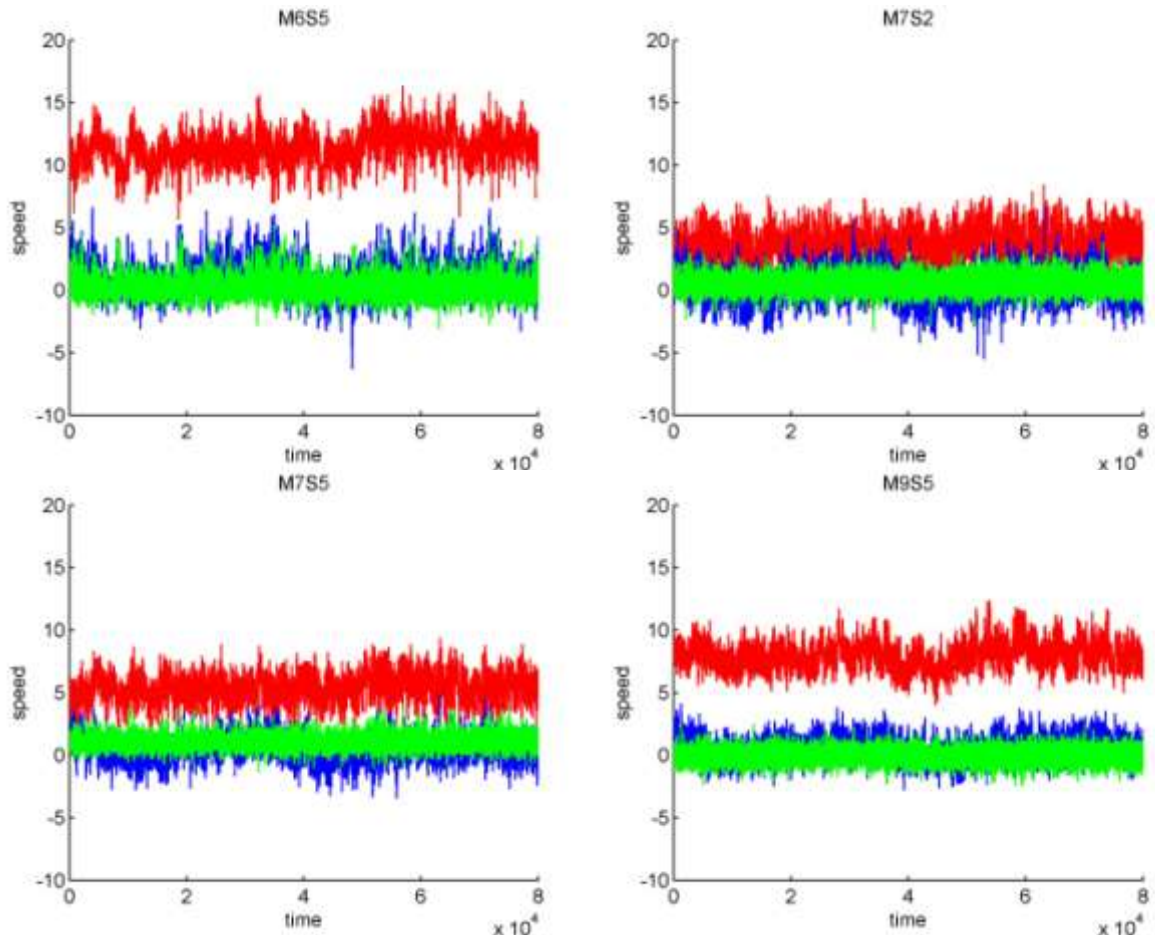
	'200801302110' '200801302120' '200801302130' '200801302140' '200801302150' '200801302200'			
Z4	'200802222200' '200802222210' '200802222220' '200802222230' '200802222240' '200802222250' '200802222300' '200802222310' '200802222320' '200802222330' '200802222340' '200802222350' '200802230000'	22 Feb 2008	22:00 – 00:10	2h 10min.
Z5	'200802230030' '200802230040' '200802230050' '200802230100' '200802230110' '200802230120' '200802230130' '200802230140' '200802230150' '200802230200'	23 Feb 2008	00:30 – 02:10	1h 40min.
Z6	'200802230240' '200802230250' '200802230300' '200802230310' '200802230320' '200802230330' '200802230340' '200802230350' '200802230400' '200802230410' '200802230420' '200802230430' '200802230440' '200802230450' '200802230500' '200802230510' '200802230520' '200802230530' '200802230540' '200802230550' '200802230600'	23 Feb 2008	02:40 – 06:10	3h 30min.

The Sonics at M0 and M9 are selected as reference values. Strictly speaking, 5 meters are low for interpretation as free stream velocity. On the other hand, the roughness length is

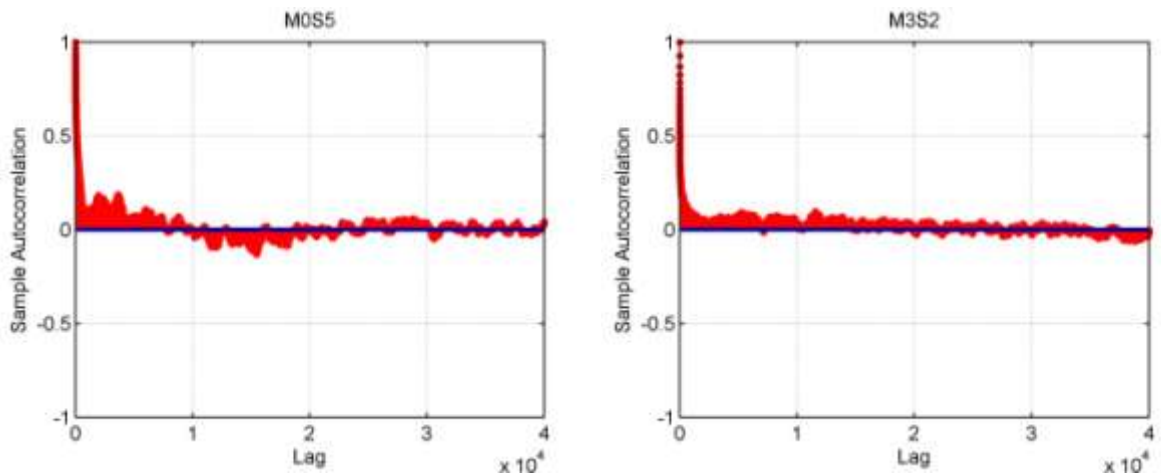
very low and no obstacles are in the inflow fetch. Thus, the measurements as M0 and M9 serve as undisturbed reference measurements. M3, M6, M7 and M8 are aligned along the 270° wind direction axis and cover representative points in front, at the front edge, in the middle and right behind the hill. The corresponding MATLAB code including the MySQL code is documented on pp. 337.

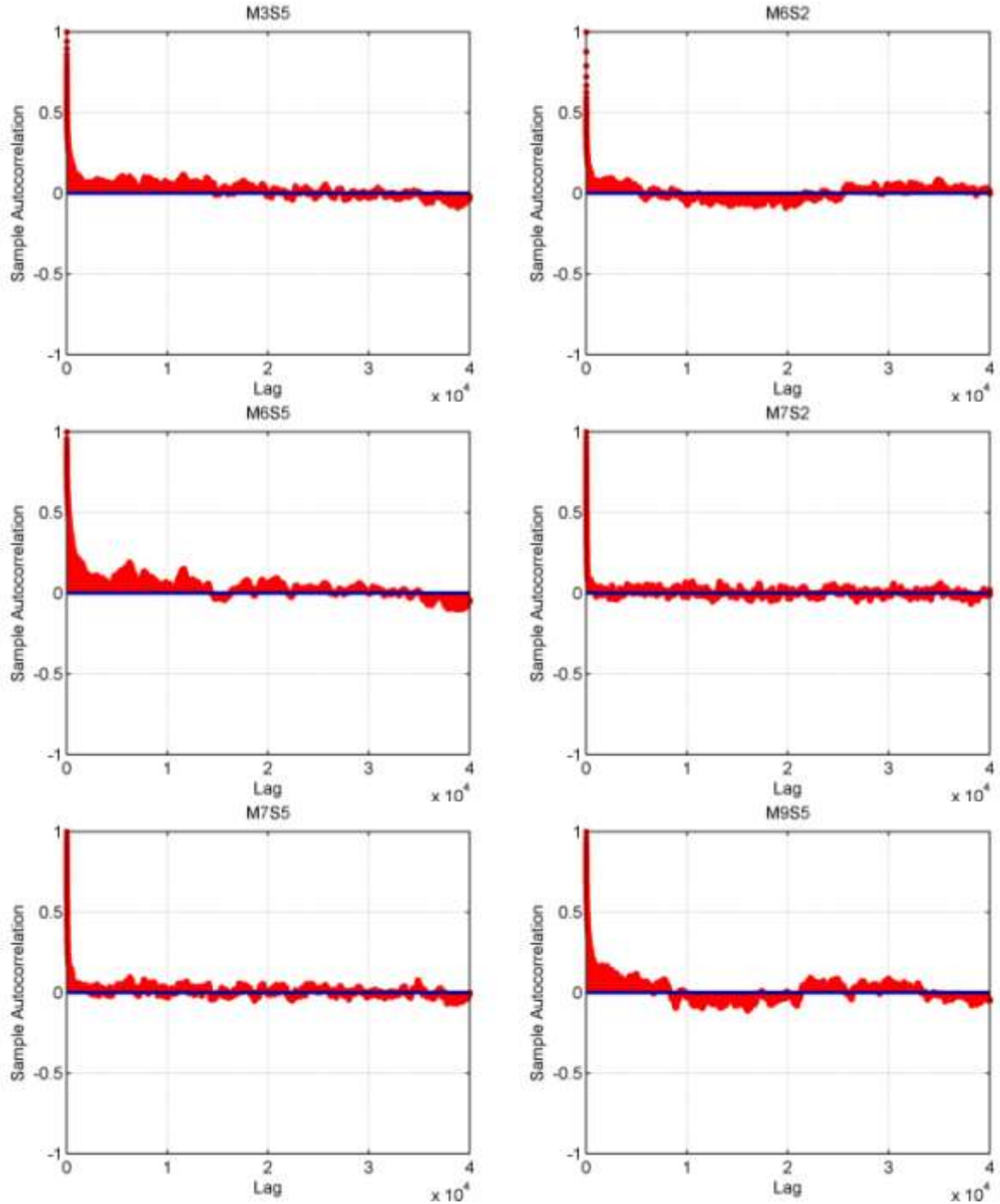
Following Figure 124: Sonic 20 Hz time series from the Bolund MySQL data base veadata-01.risoe.dk at measurement positions M0S5, M3S2, M3S5, M6S2, M6S5, M7S2, M7S5 and M9S5 in measurement time interval Z2 for inflow direction line B. Measurement positions are in above order from left to right and top down. Wind data was aligned with nesw-coordinate system and filtered for 10-minutes mean wind directions (262°-278°) and neutral atmospheric conditions (absolute inverse Obukhov-length below 0.002) at free-stream mast M0. Time interval Z2 is a 1.15-hour connected measurement time interval that is covered by all measurement positions M0, M9, M3, M6 and M7. Z2 consists of the MySQL data ensembles named: "200801270740", "200801270750", "200801270800", "200801270810", "200801270820", "200801270830", "200801270840", denoting year (yyyy), month (mm), day (dd), hour (HH) and minutes (MM) in format "yyyymmddHHMM". Red denotes wind speed in U direction, blue denotes lateral and green vertical wind fluctuations. X-axis is in units of 50 milliseconds, y-axis in units of ms^{-1} .



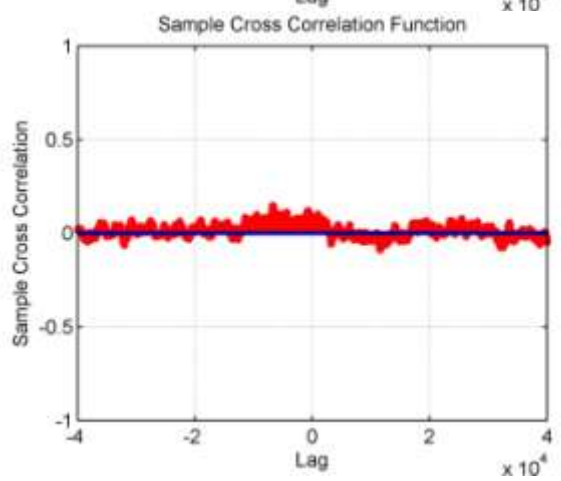
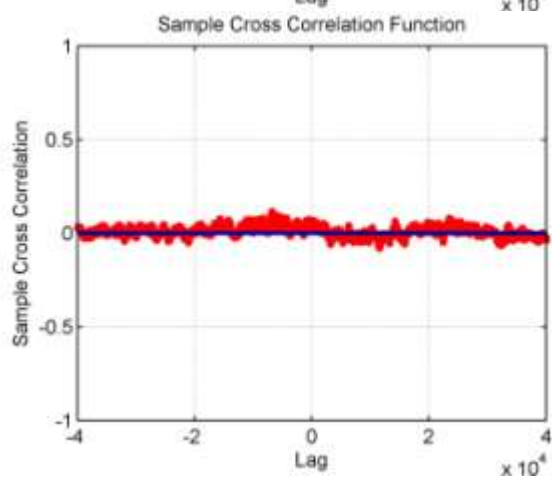
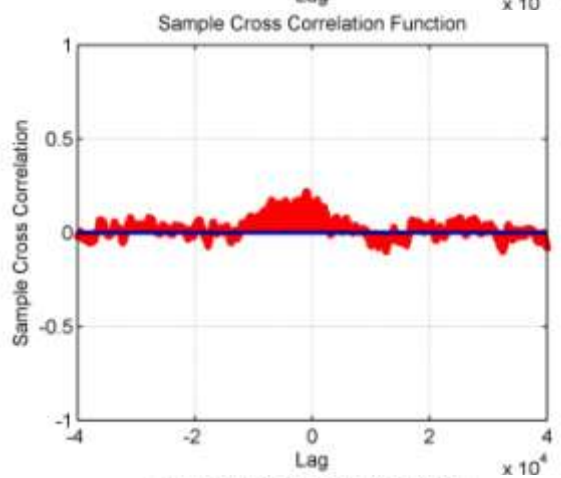
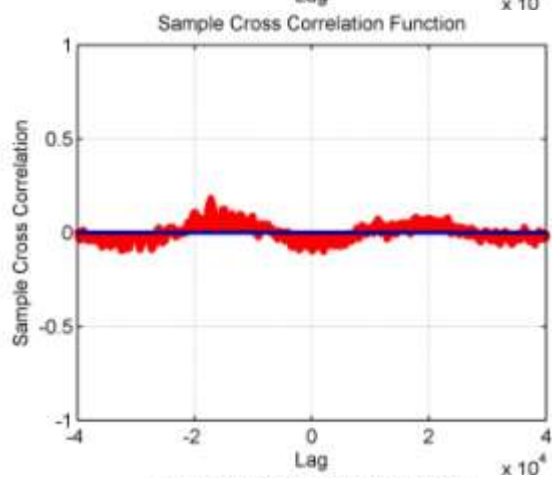
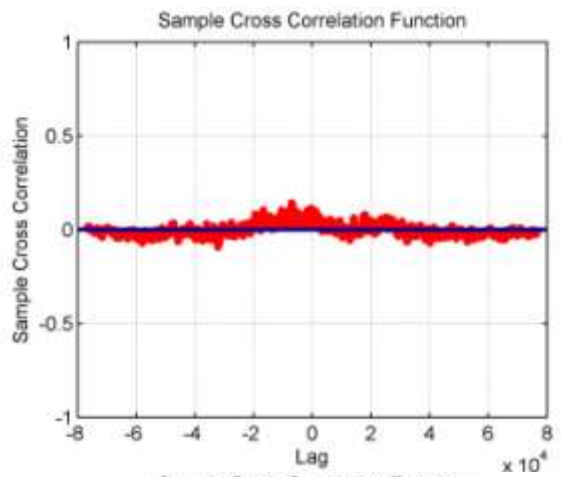
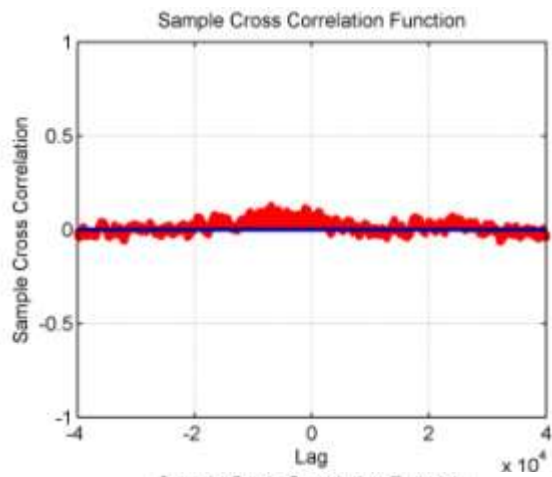


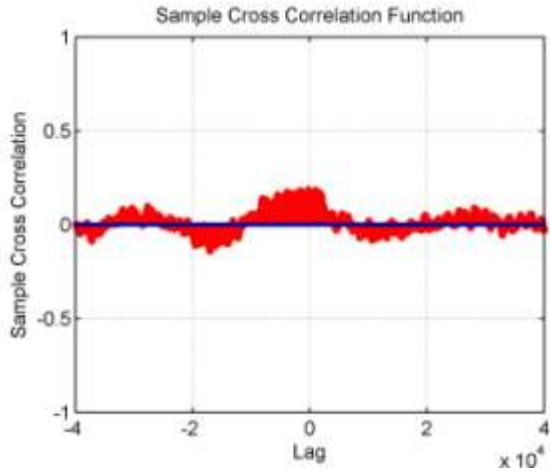
Following Figure 125: Empirical autocorrelation functions (ACF) of Sonic 20 Hz time series from the Bolund MySQL data base veadata-01.risoe.dk at measurement positions M0S5, M3S2, M3S5, M6S2, M6S5, M7S2, M7S5 and M9S5 in measurement time interval Z2 for inflow direction line B – as in figure above. Time lag is in units of 1/20 seconds. Whereas the free stream masts M0 and M9 show similar large scale frequencies, autocorrelations in front of the hill, at M7 are different. However, in front of the hill, at M, and on top of the hill, at M3, autocorrelations are similar in height 2 m and 5 m, whereas frequencies are different at different heights, whereas at the front edge of the hill, at M6, frequencies change for increasing height.



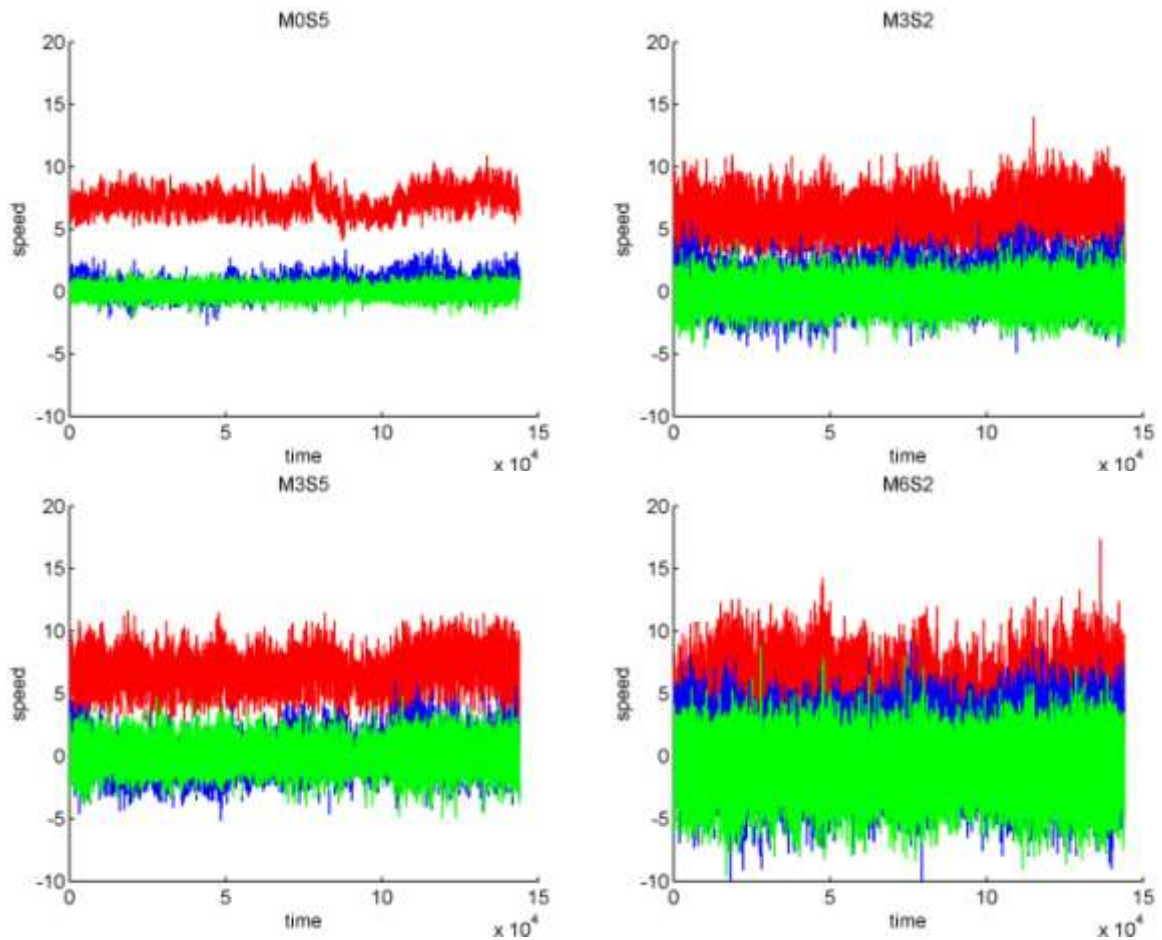


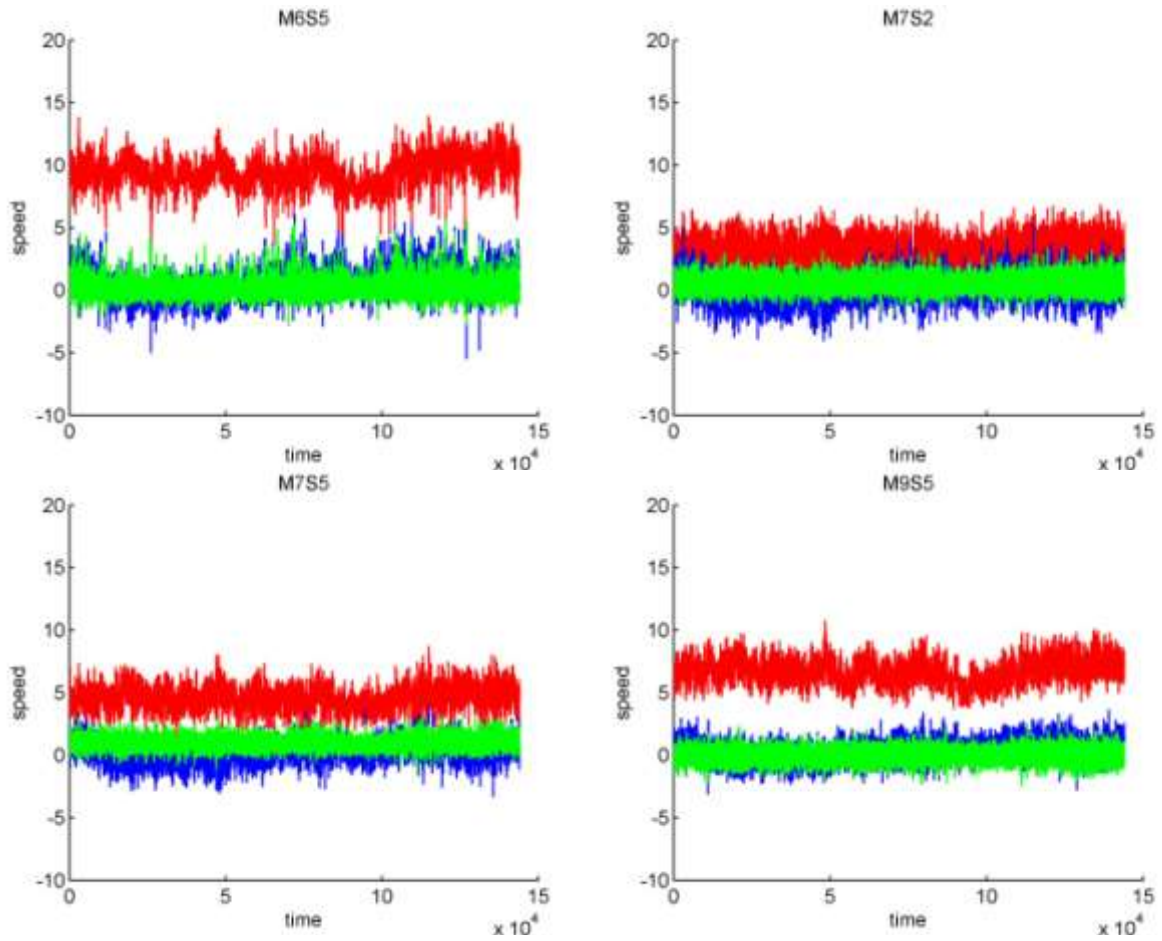
Following Figure 126: Empirical cross correlation functions of Sonic 20 Hz time series from the Bolund MySQL data base veadata-01.risoe.dk, as in Figures above, from position M0S5 with M3S2, M3S5, M6S2, M6S5, M7S2, M7S5 and M9S5. Pictures are from left to right and top down. M0 with M3 and M0 with M7 show similar patterns for both heights. M0 with M6 is inhomogeneous with height, matching expectations from the ACFs above. Between M0 and M9, a peak at time lag of around 60 seconds is to be expected, as distance between M0 and M9 is around 500 m in mean wind direction and mean wind speed is around 8 ms^{-1} in time interval Z2. Thus, the peak around zero for M0S5 and M9S5 is reasonable. This could also explain the correlation between M0S5 and M6S5. However, since the ACFs show clearly non stationarity of the data, spurious correlation have to be considered as well.



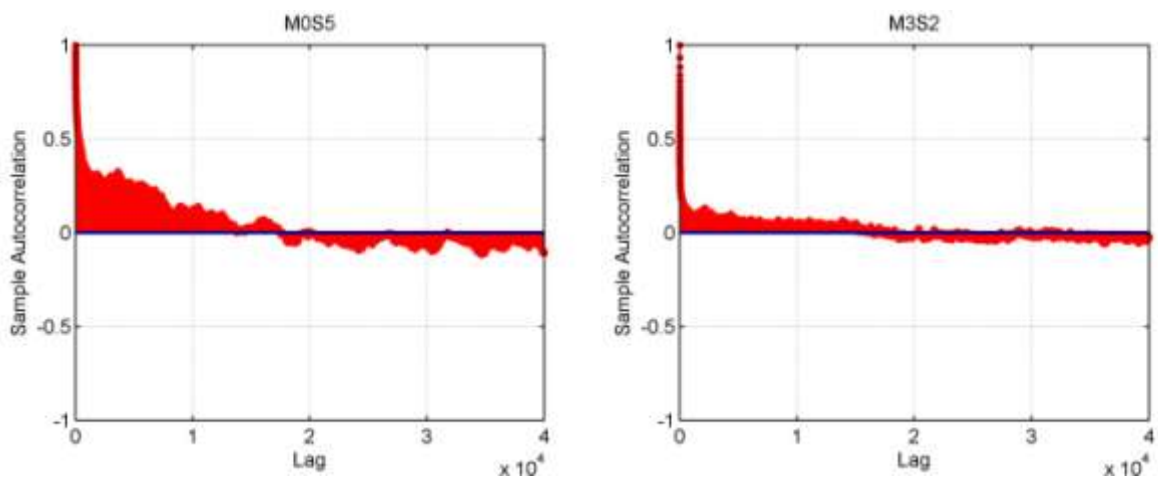


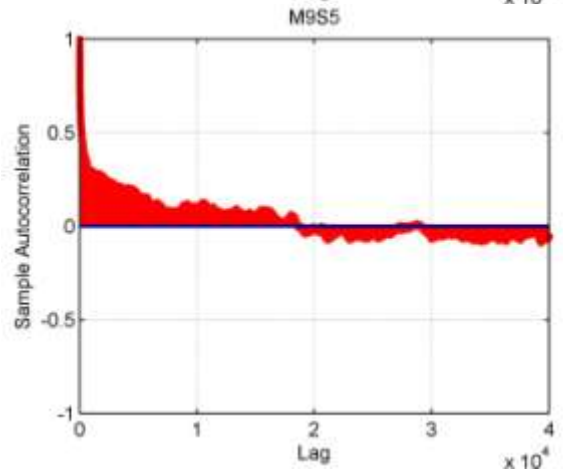
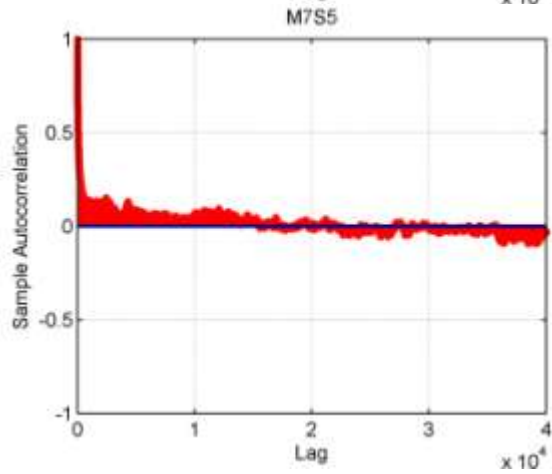
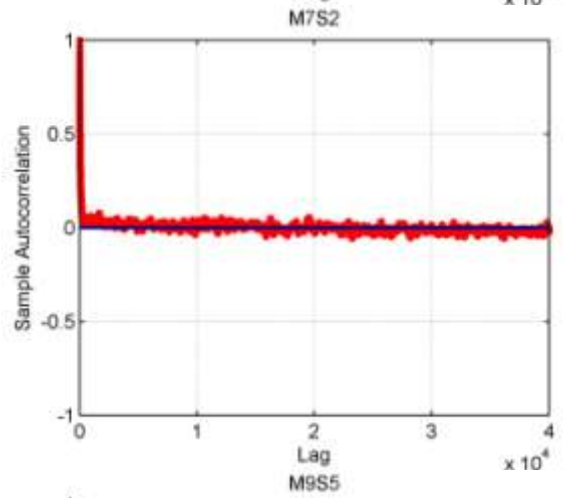
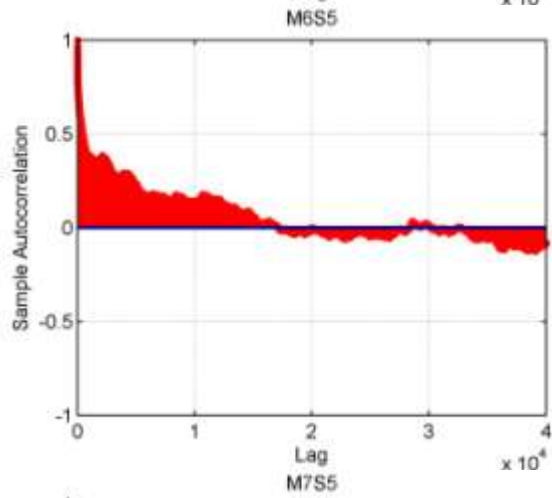
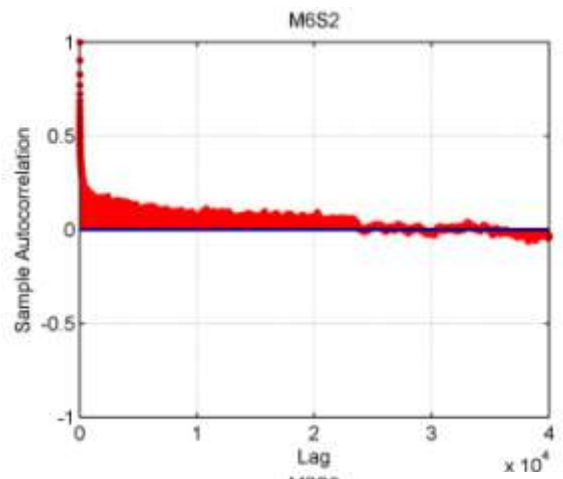
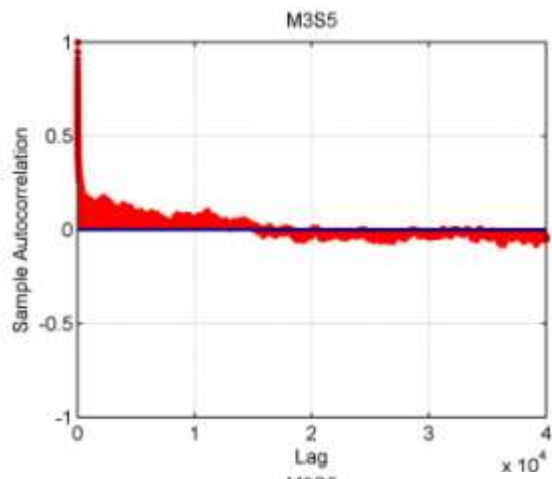
Following Figure 127: Sonic 20 Hz time series from the Bolund MySQL data base veadata-01.risoe.dk at measurement positions M0S5, M3S2, M3S5, M6S2, M6S5, M7S2, M7S5 and M9S5 in measurement time interval Z3 for inflow direction line B. Time interval Z3 is a 2-hour 10 min long connected measurement time interval that is covered by all measurement positions M0, M9, M3, M6 and M7. Red denotes wind speed in U direction, blue denotes lateral and green vertical wind fluctuations. X-axis is in units of 50 milliseconds, y-axis in units of ms^{-1} .



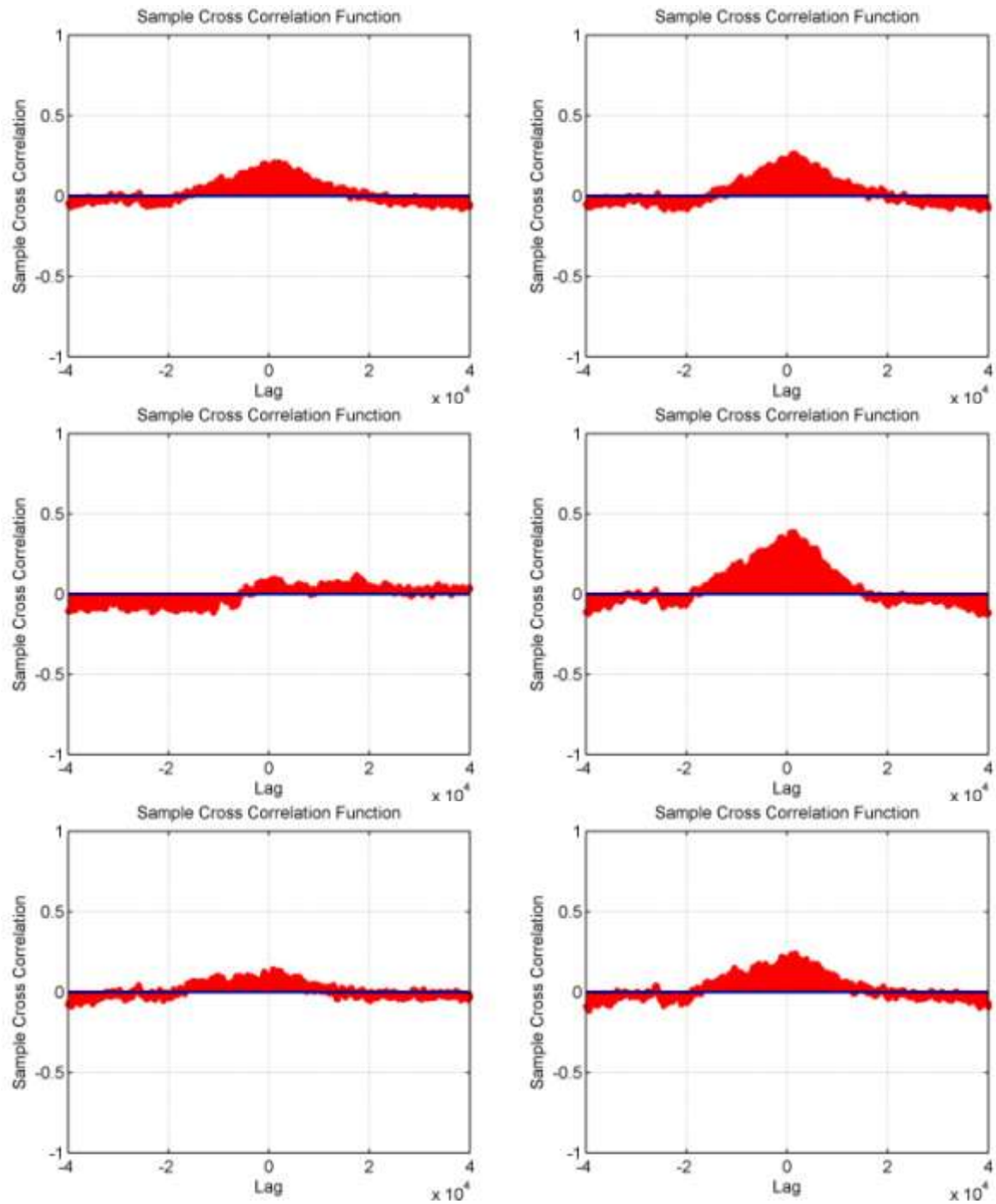


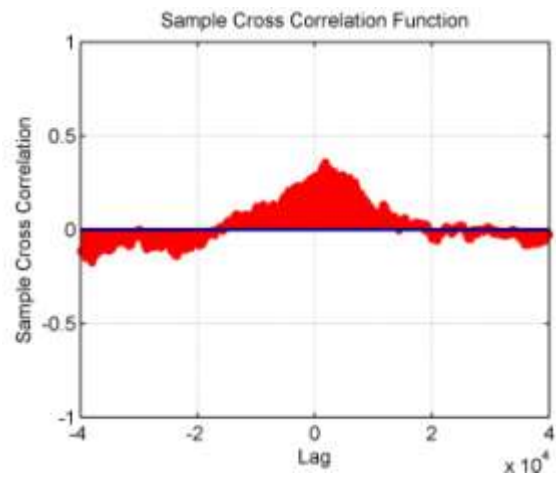
Following Figure 128: Empirical autocorrelation functions (ACF) of Sonic 20 Hz time series from the Bolund MySQL data base veadata-01.risoe.dk at measurement positions M0S5, M3S2, M3S5, M6S2, M6S5, M7S2, M7S5 and M9S5 in measurement time interval Z3 for inflow direction line B – as in figure above. Time lag is in units of 1/20 seconds.





Following Figure 129: Empirical cross correlation functions of Sonic 20 Hz time series from the Bolund MySQL data base veadata-01.risoe.dk, as in Figures above, for time period Z3 from position M0S5 with M3S2, M3S5, M6S2, M6S5, M7S2, M7S5 and M9S5. Pictures are from left to right and top down.





On basic error metrics

This is a short student's guide on three of the most often used error metrics, namely standard deviation, absolute spread and spread.

Standard Deviation

Let $x_i, i=1, \dots, N$ be a finite data set with mean value, \bar{x} . Then the *standard deviation* or *root mean square error (rms)* is defined as

$$s_N := \sqrt{\frac{1}{N} \sum_{i=1}^N (x_i - \bar{x})^2}.$$

In words: the *standard deviation* is the square root of the *average squared difference* between the *data points* and their *sample mean*.

It has to be pointed out, that use of the *standard deviation* postulates the usefulness of a *mean value* and the usefulness of *averaging deviations* from the mean. By squaring of the deviations and summing up, large deviations are going to *weight more* than, example given, if the *absolute deviation* is computed. This has to be kept in mind for the *interpretation* of deviation results.

Additionally, standard deviation is always *positive*, i.e. does not give information on the *direction* of the deviation. Also, it does not give indication on the *shape* of the deviation distribution.

Absolute Deviation

Let $x_i, i=1, \dots, N$ be a finite data set with a certain *mean value*, x_m that can be the *meridian*, the *mean value* or *another central value* of interest. Then the absolute deviation is defined as

$$D_i := |x_i - x_m|, i=1, \dots, N.$$

In words: the *absolute deviation* from a data point to a certain value x_m is its *absolute difference* from this certain value. The average from all absolute deviations from a certain

mean value is called “average absolute deviation”. The *maximum* of all *absolute deviations* is called the “maximum absolute deviation”. Obviously, the absolute deviation depends on the choice of x_m . This fact is important for the *interpretation* of deviation results. In contrast to the *standard deviation*, large deviations are *not* weighted by *square* as well as small values are *not decreased* by squaring. This means, if most of the data points are *far* from the mean, the *standard deviation* will be larger than the *average absolute deviation*. If most of the data points are *close* to the mean, the *standard deviation* will be *smaller* than the *average absolute deviation*. As the standard deviation, the *absolute deviation* is always *positive* and does not indicate the *shape* of deviation distribution. More information of *allocation* of values can be found by analysing the deviation for *each* i . The maximum absolute deviation can give a picture on the *spread* of the data set. For example, a data set with *small* standard deviation can have a *single* value with large absolute deviation. This leads to a large *maximum standard deviation* and gives no information about the deviation of the other values. In conclusion, the *absolute deviation* depends on the *choice* of the *mean value* and the absolute value of the deviation is not weighted by the square of the summands.

Spread

Let $x_i, i=1, \dots, N$ be a finite data set with maximum x_{\max} and minimum x_{\min} . Define the *spread* as $\xi = |x_{\min} - x_{\max}|$. In words: the *spread* of a data set is the *absolute difference* of its *largest* and *smallest* value. In comparison with the *absolute deviation*, the *spread* holds:

$$D \leq D_{\max} \leq \xi \leq 2D_{\max}.$$

Thus, the interval determined by *maximum absolute deviation* is the “worst case”, followed by the *spread*. As for the *maximum absolute deviation*, the spread can mislead if not used carefully. It does provide information on the *minimum* and *maximum* value of a given data set and does not give information on the *distribution* of the rest of the data.

Idealized Bolund hill test (Blasius)

The measurement positions

blue = **Repeatability test** (repeated measurement)

orange = **Reynolds test** ("Reynoldskreuz")

All Points are located on the middle line ($Y = 0$ mm), exceptions are marked red. X-Z-positions see fig. 3 and 4.

Hill	Features	Set-Up	Points X-Y-positions		
A1	slopes without steps (smooth)	UV	Name	x [mm]	y [mm]
			M1	0.0	
			M2	25.0	
			M3	100.0	
			M3.y+	100.0	50.0
			M3.y-	100.0	-50.0
			M4	300.0	
			M5	550.0	
			M6	800.0	
			M6.y+	800.0	50.0
			M6.y-	800.0	-50.0
			M7	950.0	
			M8	1100.0	
		UW	Name	x [mm]	y [mm]
			-P1	-10.0	
			P0	0.0	
			P1	25.0	
			P2	50.0	
			P3	75.0	
			P4	100.0	
			P4.y++	100.0	180.0
			P5	125.0	
			P6	150.0	
			P7	300.0	
			P8	550.0	
			P9	700.0	
P9.x+	720.0				
P9.x+-	710.0				
P10	750.0				
P11	775.0				
P11.x+	792.0				
P12	800.0				
P12.y++	800.0	150.0			

			P13 810.0 P14 820.0 P15 830.0 P15.x+ 900.0 P15.x++ 792.0 P16 1100.0
A2	Stepped slopes	UW	Name x [mm] y [mm] -P3 -100.0 -P2 -25.0 P0 0.0 P1 25.0 P2 50.0 P3 75.0 P4 100.0 P4.y++ 100.0 180.0 P5 125.0 P6 150.0 P7 300.0 P8 550.0 P9 700.0 P10 750.0 P11 775.0 P12 800.0 P12.y++ 800.0 150.0 P13 810.0 P14 820.0 P15 830.0 P15.x+ 900.0 P16 1100.0
A3	A1 with smoothed edges	UW	Name x [mm] y [mm] P0 0.0 P1 25.0 P2 50.0 P3 75.0 P4 100.0 P5 125.0 (P6) 150.0

A4	A1 with strongly smoothed edges	UW	<div>as A2 UW</div> <div>+ RKLee (Reynolds number tests at lee slope of the hill):</div> <div><table><tr><td>Name</td><td>x [mm]</td></tr><tr><td></td><td>675</td></tr><tr><td>(P9)</td><td>700</td></tr><tr><td></td><td>725</td></tr><tr><td></td><td>825</td></tr><tr><td>(P12)</td><td>800</td></tr></table></div>	Name	x [mm]		675	(P9)	700		725		825	(P12)	800
Name	x [mm]														
	675														
(P9)	700														
	725														
	825														
(P12)	800														
-	Empty Windtunnel: systematic uncertainty due to probe set-up test	UW	<div>Hill_leer_P16</div> <div>Hill_leer_-P3</div> <div>Hill_leer_P16_0Grad</div> <div>Hill_leer_-P3_0Grad</div>												

Dependence of repeatability assessment on the flow location

Here an explicit example is given on how values in percentage can distort the results if the measurement locations are not indicated.

In the repeatability analyses of idealized Bolund, pp. 147, the differences of the spreads depending on the measurement location in percentage of the mean values are > 25 percent. This means for full scale free stream wind speeds of 10-15 m/s that the *difference of spread* is between M1z10 and M1z300 is 2.5 -3.75 m/s. This can be a *significant* value for certain applications.

In contrast, the *absolute* spread amounts 0.007 in worst and 0.003 in best case in units of non-dimensional wind speeds. This leads to a difference of absolute spreads of 0.004. For a wind tunnel experiment with reference speed of 5 m/s in the wind tunnel and 5 m/s assumed to be the reference wind speed in *real conditions*, this leads to a difference of spreads of *immediate repeatability* of 0.02 m/s transferred to *real conditions* (according to the *similarity criterion*). In terms of *standard deviation*, the difference is even smaller: 0.0026 – 0.0013 = 0.0013 respectively 0.0065 m/s in the wind tunnel and real conditions at reference speed of 5 m/s.

Hence, the *difference of absolute errors* of different measurement positions can be negligible. However, the *difference of relative errors* of different measurement positions can *distort* this perspective.

Possible outcomes of this distortion can be exemplarily illustrated: according to the analysis, at high wind speeds, the spread in relation to the mean value is 0.3 percent.

The *absolute* value is 0.003, or 0.015 m/s for $U_{\text{ref}} = 5 \text{ m/s}$.

The *immediate repeatability* of the experiment at M1z10 for mean wind tunnel reference velocity of around 5 m/s could be computed as the spread in *relation to mean value in percent*. This yields 26 percent. For quality assessment, this value can be used for error assessment of other measurement positions as well, e.g. M1z300.

Assume a mean wind tunnel reference velocity of around 9 m/s and a *non-dimensional* mean velocity of 0.98. Then, the *absolute* value, with assessment of 26 percent error spread, leads to $0.98 \cdot 0.26 = 0.25$ *non-dimensional* wind speed.

For $U_{\text{ref}} = 8.8 \text{ m/s}$, this leads to $8.8 \cdot 0.25 \text{ m/s} = 2.2 \text{ m/s}$.

Consequently, the *actual* spread of 0.03 m/s (computed from the actual data) would be *overestimated* by 73 times.

The other way around an extrapolation from 0.1 percent standard deviation at M1z300, and mean wind tunnel reference velocity of around 9 m/s to low mean wind tunnel reference velocities directly at the bottom in front of the hill, M1z10, can significantly *underestimate* the *immediate repeatability* error. This exemplary consideration illustrates how the choice of the measurement position in the flow over the hill and the display of errors in percentage can distort the assignments for the measurement precision.

Influence of manual LDA-probe adjustment

Measurements of U-component with *UV-set-up* are compared with those with *UW-set-up*. In the former case, the LDA is arranged *vertically*, in the latter case *horizontally*. The change of set-up is done *by hand*. In order to measure close to the ground the adjustment of the probe is not 100 percent horizontal. It deviates of about 7 degrees. The *rotation* of the coordinate system is considered in the LDA-software and inversed by the appropriate *transformation matrix*. The *manual adjustment* and estimation of *deviation angle* which has to be implemented into the transformation matrix leads to a *systematic measurement error* (inherent in the experimental set-up).

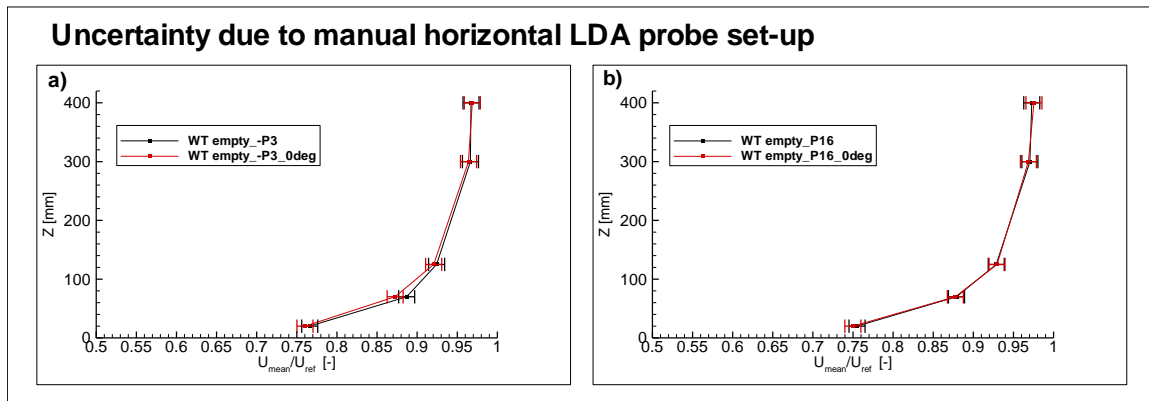


Figure 130: Influence of manual LDA-probe adjustment with error bars indicating the measurement precision. Points are connected with lines for visually emphasizing deviations.

It turns out that the error due to the LDA-arrangement *concerning the angle as isolated problem* is *small* compared to the *repeatability deviation* (Figure 130). However, this is different if the *angle estimation* is combined with the 90° rotation of the LDA probe. This is due to the asymmetry of the intersection volume of the laser beams which has an effect on the measurement results in flow areas with large velocity gradient; recall the reference to COST 732, [2010, p. 14].

Reynolds number tests of the pilot study

Reynolds tests were made for hill A1 with UV-set-up in *characteristic* measurement points around the hill. “Reynolds test” – this means that measurements are conducted with *different mean wind tunnel reference velocities* in order to estimate the *dependency* of model result on the *mean wind tunnel reference velocity*. In the plots below, the *reference* wind velocity is exhibited on the x-axis, the *non-dimensional* wind speed at the y-axis. *Error bars* of 0.01 m/s are added to the measurements due to the results of *immediate repeatability*. This means that the error bars are based on the error analysis for measurements at about 7 m/s. For *lower* reference wind speeds the precision of measurements *can be worse* and is approximated by this value.

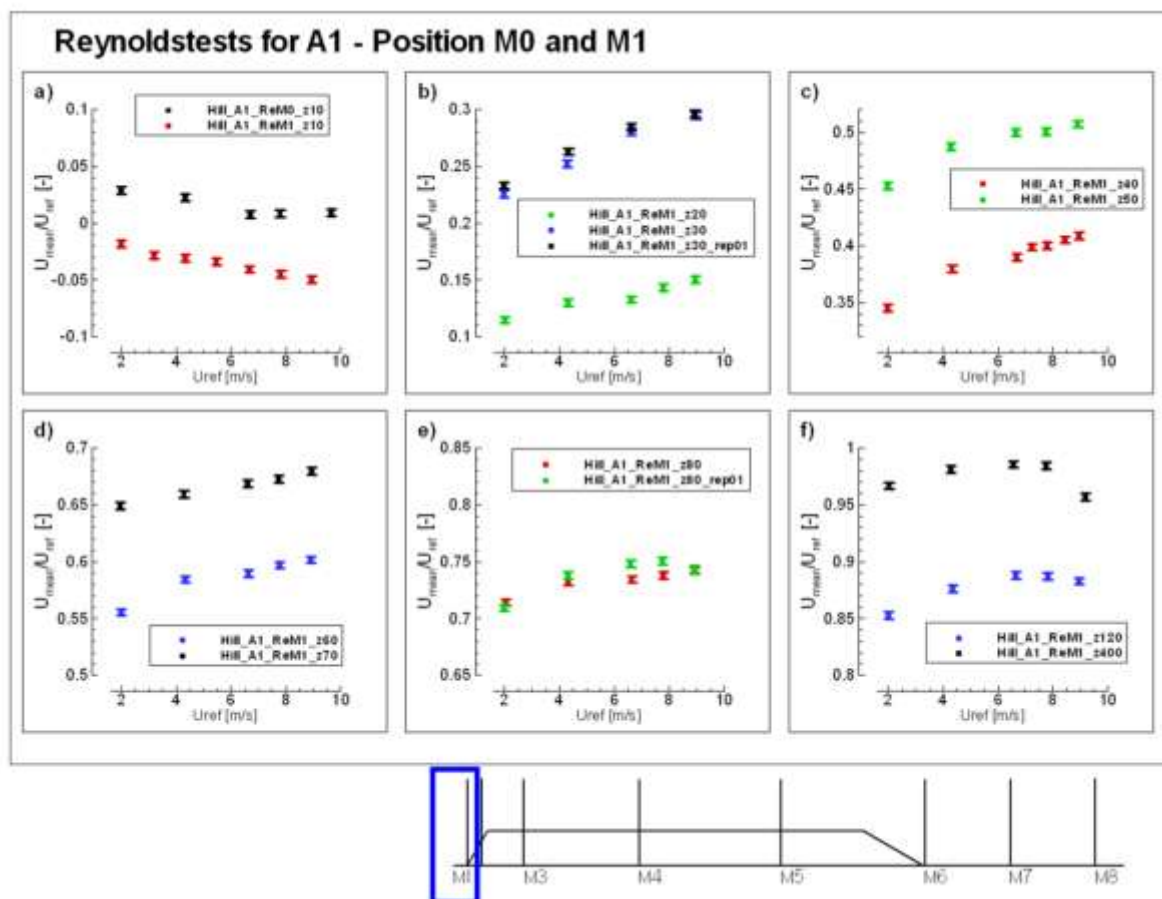


Figure 131: Re-tests in front of the hill, the x-axis denote mean reference velocity in the wind tunnel; the y-axis denotes the non-dimensional mean velocity in dependence on the reference velocity; the error bars denote precision in terms of immediate repeatability as narrow interval for the Reynolds test

In front of the hill, at M0 and M1, increasing values for increasing Reynolds numbers can be observed (“positive trend”). Exceptions are M0 and M1 with $z = 10$ mm. Both show a similar trend: Values behave *anti-proportionally* to reference wind speed, see Figure 131 a). The reason is presumably that both lie within or nearby the *blockage vortex* in front of the hill. Furthermore, the fluctuation of values at $z = 400$ m is reasonable since location is above the modelled surface layer and thus the flow is not claimed to be fully turbulent.

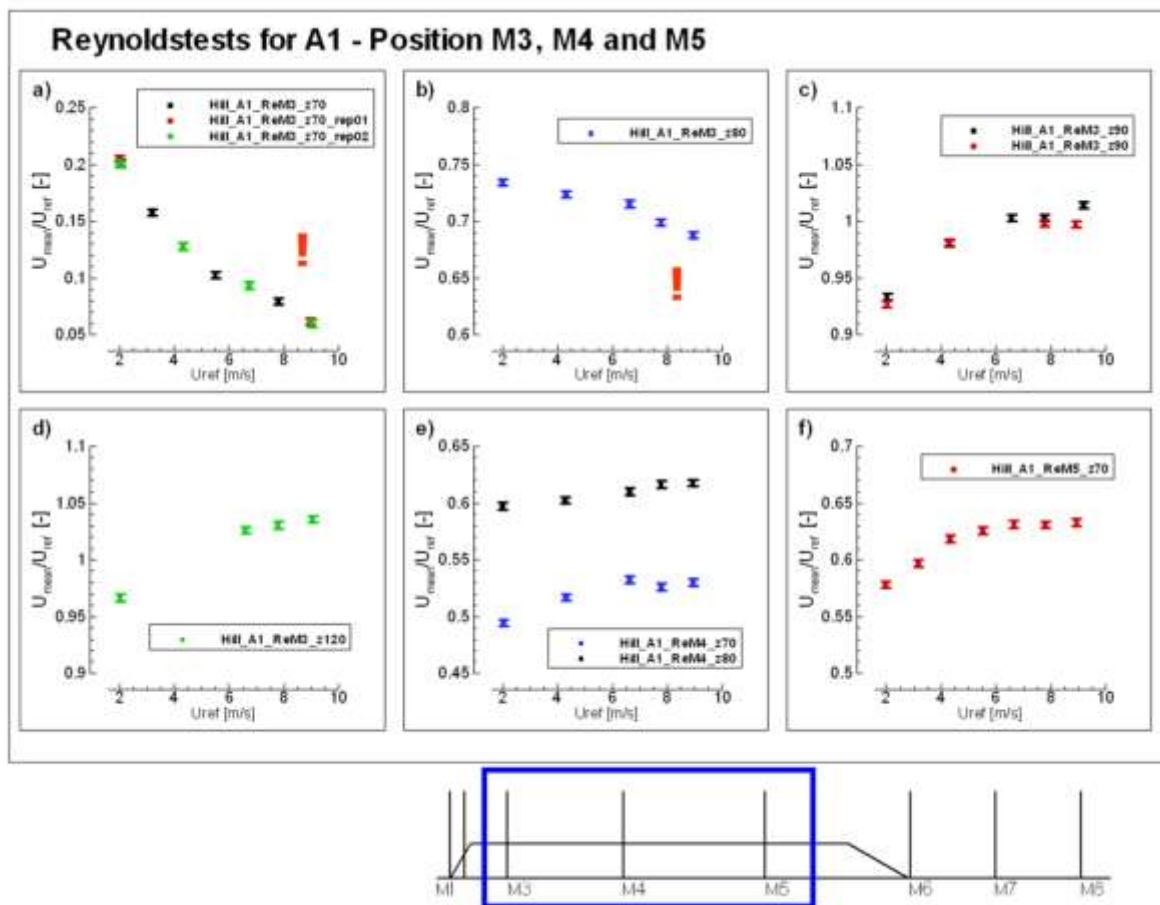


Figure 132: Re-tests along the hill

Slightly behind the *front edge* of the hill, close to the hill surface, flow separates. Point M3 at 10 mm above hill height shows a strong *anti-proportional* dependency on the reference wind speed, the anti-correlation decreases at 80 mm and reverses into a *proportional* dependency at 20 mm, see Figure 132 a)-b). At 60 mm above hill height, as well as at M4 and M5, measurements show only variation within 2 percent for reference wind speed in the range of 7 m/s and 9 m/s.

Just behind the hill, at M6, flow forms an area with *reverse* flow, Figure 133. In contrast to the *blockage area* in front of the hill and the *separation area* behind the *front edge* of the hill, this *separation vortex* is more stable for variation of Reynolds number. Measurements between 10 mm and 40 mm above ground can be defined as *Reynolds number independent* in the range between 5 m/s and 9m/s reference wind speed (variation below $1 \cdot 10^{-3}$ in units of non-dimensional wind speed.)

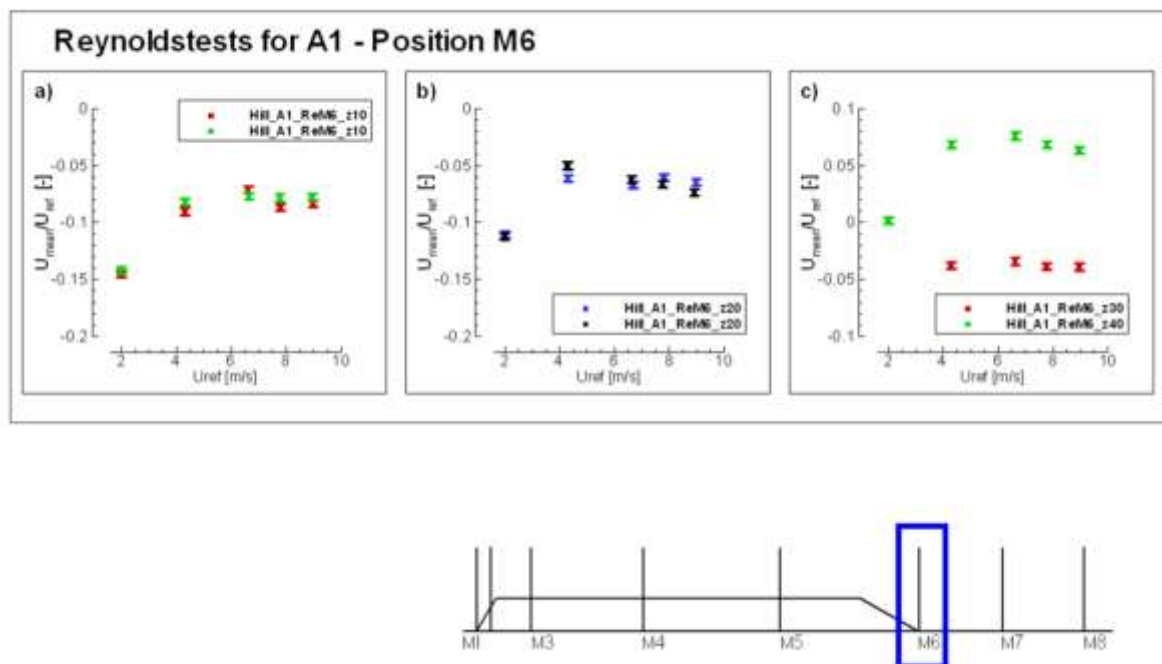


Figure 133: Re-test behind the hill

Description of the data structure for main Bolund in WOTAN

A list of all field study measurement positions can be found in

- Bechmann et al., [2009]

or in

- “Bolund 2011 Experiment Design.xls”

- in the sheet “General”, in colour code rosé, starting from line 64. In the column “Field” the field study name is inserted. “Virtual” measurement masts, i.e. in the wind tunnel study measured vertical profiles in addition to those of the field study, are coloured in orange, see for example Figure 134.

The data of the Bolund in WOTAN experiment will be stored in the archive of the server ETWL1 until final publication of this work and can be obtained via the Environmental Wind Tunnel Laboratory (EWTL) of the University of Hamburg (as of 2012/2013). Most of the wind tunnel measurement points are additionally chosen to *increase spatial resolution* of flow measurements in vertical and horizontal direction. Additional vertical profiles (“virtual wind tunnel measurement masts”) are denoted with the prefix “WT” and are counted from “WT01” to “WT11”.

The syllabus “pr” denotes the *horizontal projection*, e.g. “M0_prB” denotes the projection of the measurement position “M0” onto Line B.

For the measurement positions M3, M7 and M9, the prefix “WT” and the suffix “y+” or “y-” denotes horizontal displacement of the measurement position in “y+” or “y-” direction such that the measurement position has the same x-coordinate and is shifted aside of the hill. These horizontally shifted measurements are available in addition to the centred measurements for M3, M7 and M9 with y < 2m (nearly on the centre line).

Positions	Field	X [m]	Y [m]	Z agl [m]	Z [m]
M0_prB	M0_prB	-181.0	-103.0		
WT		-71.9	0.0	5er VP	5er VP
M7	M7_S_2	-66.9	0.0	2.0	2.8
	M7_S_5	-66.9	0.0	5.0	5.8
M6	M6_S_2	-46.1	0.2	1.9	13.3
	M6_S_5	-46.1	0.2	4.9	16.4
	M6_C_9	-46.1	0.2	8.9	20.4

Figure 134: Excerpt of “Bolund 2011 Experiment Design.xls”; the values are in field scale. This figure illustrates as an example the lateral deviation of the measurement point M6 from the centre line by 0.2 m (in field scale); it shows also the horizontal displacement of the sonic at M6 in “2 m” height which is rather located in 1.9 m above ground level.

In the sheet “measurement positions”, all *exact measurement positions* in the *wind tunnel coordinate system* and *wind tunnel scale* are listed. These coordinates could be copied into the LDA-Dantec-software provided that the coordinate system of the LDA traverse system including *zero point* and *step size* is adjusted accordingly (check carefully). Measurement positions covered by the field measurements are denoted with their *field study name*, e.g. “M3_S_2”.

For Line A, measurement positions are *rotated* from fixed *north-east-south-west coordinate system* into the wind tunnel coordinate system for the rotated model area. The *rotation matrix*, applicable for different inflow angles, can be found in

- “Bolund 2011 Experiment Design.xls” in the electronic supplementary material in sheet “Line A”, (Figure 135).

For Line B, measurement positions do not need to be rotated. Details on the measurement positions are in

- “Bolund 2011 Experiment Design.xls” in the electronic supplementary material in sheet “Line B”.

Further remarks:

- The full planning of the measurements is documented in “Bolund 2011 Experiment Design.xls” in sheet “process agenda” (in German) with action numbers per measurement task in order to clarify the *purpose of the measurement* which was decided *before the measurement*.

Line A: *all coordinates in fixed coordinatesystem (new) with CP=0°										
Positions	Field	X [m]	Y [m]	Z_agl [m]	Z [m]	Model	x [mm]	y [mm]	z_agl [mm]	z [mm]
M0	M0_C_2	-181.0	-103.0	2.0	3.1	M0_C_2	-724.0	-412.0	8.0	12.4
	M0_S_5	-181.0	-103.0	5.0	6.1	M0_S_5	-724.0	-412.0	20.0	24.4
	M0_C_9	-181.0	-103.0	9.0	10.1	M0_C_9	-724.0	-412.0	36.0	40.4
	M0_S_12	-181.0	-103.0	12.0	13.1	M0_S_12	-724.0	-412.0	48.0	52.4
	M0_C_15	-181.0	-103.0	15.0	16.1	M0_C_15	-724.0	-412.0	60.0	64.4
M1	M1_S_2	-52.4	-31.0	2.1	2.8	M1_S_2	-209.6	-124.0	8.4	11.2
	M1_S_5	-52.4	-31.0	5.1	5.8	M1_S_5	-209.6	-124.0	20.4	23.2
	M1_S_9	-52.4	-31.0	9.1	9.8	M1_S_9	-209.6	-124.0	36.4	39.2
M2	M2_S_2	-34.8	-21.0	2.1	12.9	M2_S_2	-139.2	-84.0	8.4	51.6
	M2_S_3	-34.8	-21.0	3.6	14.4	M2_S_3	-139.2	-84.0	14.4	57.6
	M2_S_5	-34.8	-21.0	5.1	15.9	M2_S_5	-139.2	-84.0	20.4	63.6
	M2_S_9	-34.8	-21.0	9.1	19.9	M2_S_9	-139.2	-84.0	36.4	79.6
	M2_C_11	-34.8	-21.0	11.1	21.9	M2_C_11	-139.2	-84.0	44.4	87.6
M3	M3_S_2	3.1	0.0	2.0	13.6	M3_S_2	12.4	0.0	8.0	54.4
	M3_S_5	3.1	0.0	5.0	16.6	M3_S_5	12.4	0.0	20.0	66.4
	M3_S_9	3.1	0.0	9.0	20.6	M3_S_9	12.4	0.0	36.0	82.4
M4	M4_S_2	51.5	30.6	1.4	2.8	M4_S_2	206.0	122.4	5.6	11.2
	M4_S_5	51.5	30.6	4.4	5.8	M4_S_5	206.0	122.4	17.6	23.2
	M4_S_9	51.5	30.6	8.4	9.8	M4_S_9	206.0	122.4	33.6	39.2
M5	M5_S_2	1.5	-48.9	2.2	4.8	M5_S_2	6.0	-195.6	8.8	19.2
	M5_S_5	1.5	-48.9	5.2	7.8	M5_S_5	6.0	-195.6	20.8	31.2
M7	M7_S_2	-66.9	0.0	2.0	2.8	M7_S_2	-267.6	0.0	8.0	11.2
	M7_S_5	-66.9	0.0	5.0	5.8	M7_S_5	-267.6	0.0	20.0	23.2
*all coordinates in fixed coordinatesystem (new) with CP=0°										
FS										
Model		x [mm]	y [mm]	z_agl [mm]	z [mm]	Z_agl [m]	Z [m]			
M0	M0_C_2	-724.0	-412.0	8.0	12.4	2	3.1			
4.4M0_WT_3		-724.0	-412.0	12.0	16.4	3	4.1			
M0_WT_4		-724.0	-412.0	16.0	29.4	4	7.35			
M0_S_5		-724.0	-412.0	20.0	24.4	5	6.1			
M0_C_9		-724.0	-412.0	36.0	40.4	9	10.1			
M0_S_12		-724.0	-412.0	48.0	52.4	12	13.1			
M0_C_15		-724.0	-412.0	60.0	64.4	15	16.1			
M0_WT_20		-724.0	-412.0	80.0	84.4	20	21.1			
*all coordinates in rotated coordinatesystem for INFLOW angle alpha										
Model		x [mm]	y [mm]	z_agl [mm]	z [mm]					
M0	M0_C_2	-832.8	19.7	8.0	12.4					
4.4M0_WT_3		-832.8	19.7	12.0	16.4					
M0_WT_4		-832.8	19.7	16.0	29.4					
M0_S_5		-832.8	19.7	20.0	24.4					
M0_C_9		-832.8	19.7	36.0	40.4					
M0_S_12		-832.8	19.7	48.0	52.4					
M0_C_15		-832.8	19.7	60.0	64.4					
M0_WT_20		-832.8	19.7	80.0	84.4					
M1	M1_S_2	-243.5	1.7	8.4	11.2					
2.8M1_WT_3		-243.5	1.7	12.4	15.2					
M1_WT_4		-243.5	1.7	16.4	19.2					
M1_S_5		-243.5	1.7	20.4	23.2					
M1_S_9		-243.5	1.7	36.0	39.2					
M1_WT_12		-243.5	1.7	48.0	51.6					
M1_WT_15		-243.5	1.7	60.0	63.6					
M1_WT_20		-243.5	1.7	80.0	83.6					
M2	M2_S_2	-162.6	-0.3	8.4	51.6					
43.2M2_S_3		-162.6	-0.3	14.4	57.6					
M2_WT_4		-162.6	-0.3	16.4	59.6					
M2_S_5		-162.6	-0.3	20.4	63.6					
M2_S_9		-162.6	-0.3	36.4	79.6					
M2_C_11		-162.6	-0.3	44.4	87.6					
M2_WT_1		-162.6	-0.3							

<

Figure 135: Exemplary excerpt of the rotation matrix for inflow Line A in “Bolund 2011 Experiment Design.xls”.

- To find the *data file* for a time series measured in the wind tunnel, open “BOLUND_WOTAN_logbook_2011.xls” and push “Control+F”. Assure in “options” that the search is activated for the full document. Type in the search field the name of the measurement location, e.g. the centre point “M3”. You find the *date*, *time* and details of *hardware* and *software* adjustments of the measurements, including *wind tunnel rotation frequency* and *measurement duration* or *problems occurred during the measurements*. Also, the *action number* (“Messplan Nr.”) is documented to track the *original purpose* of the measurements⁹³.

project file	wtref file (\$_wtref)	measurements	position	Messplan Nr.
Bo_067	Bo_wtref_067	Vertikalprofil	WT07	70
Bo_068	Bo_wtref_068	Vertikalprofil	M1	71
Bo_069	Bo_wtref_069	Vertikalprofil	M2	72
Bo_070	Bo_wtref_070	Vertikalprofil	WT08	73
Bo_071	Bo_wtref_071	Vertikalprofil	M3	74
Bo_072	Bo_wtref_072	Vertikalprofil	WT09	75

Figure 136: Excerpt of “BOLUND_WOTAN_logbook_2011.xls”.

Important is the *file name* of the measured time series. For the vertical profile at M3, the file name⁹⁴ is “Bo_071”, see Figure 136. The according time series can be found in the folder “Main flow measurements” in the subfolder “Measurements 067-080 Line A UW”⁹⁵. The time series names for different heights are “Bo_071.000001” to “Bo_071.000009”. The corresponding reference wind speed at the Prandtl tube is stored in “Bo_071_wtref”. The post-processed times series and statistics according to Fischer, [2011], can be found in the additional folders, such as “STAT”, “HIST”, etcetera. The sub-folder structure is maintained according to Fischer, [2011].

⁹³ This distinguishes between, measurements for vertical profiles, repetition measurements, Reynolds tests and measurements for convergence tests, and hence determines the required data rate and sampling duration (and components to be measured)

⁹⁴ The file name is composed of “Bo” as abbreviation for “Bolund”, an underline “_” as separator, and the number of the measurement in chronological order of the measurements “000-080”. Hence, the number of measurement can be linked to the date of the measurement.

⁹⁵ The name of the subfolder “Measurements 067-080 Line A UW” contains following information: all measurements with file number 67-80 refer to inflow direction Line A, and were conducted in UW set-up. Based on this structure, the other 3 subfolders are named “Measurements 001-026 Line B UW”; “Measurements 027-053 Line B UV”; and “Measurements 054-066 Line A UV”.

- If a time series of “some point in front of the hill for inflow Line A” is desired (without knowledge of the precise denotation of the measurement position) then an *appropriate measurement location* can be found in “Bolund 2011 Experiment Design.xls” in the sheet “General”, by help of the *sketch of the field measurement locations* therein and the *coordinates* of all measurement locations. Figure 54 (p. 174) can also serve as a first orientation. With the name of the location, proceed as before for finding the data file of the time series.

Appendix to the set-up of the inflow-conditions

Table 8 - Title: Documentation of the adjustment process for experimentally setting-up ABL inflow conditions in EWTl Wotan wind tunnel Hamburg - corresponding to the atmospheric conditions at the Bolund site in Roskilde Fjord, Denmark, for main wind directions 270 ° and 239°.

Legend in chronological order of appearance:

Meas.= Measurement number for identification;

Ceiling = 01 resp. 02 refer to different adjustments of the ceiling for minimization of the pressure gradient, 02 is the final adjustment,

Comp.= Wind speed components (Measurements in this set-up restricted to 2dimensional-measurements);

U = measurement component in main wind speed direction,

W = measurement component in vertical direction,

V = measurement component in lateral direction;

VP = Vertical Profile;

Rep = Repetition of measurement xxx;

LP = Lateral Profile;

HQ = High Quality measurements in terms of data rate;

Frieso-Set-Up = Inflow set-up of previous experiment, fully documented in internal papers

Base Plates = No roughness elements on top of the base plates.

Sharp edge [width x height] = aluminium step with sharp edges; XVI symmetric = Spire type referring to internal list with roman numbers as coding for shape and size/ “symmetric” referring to positioning of spires with regard to the centre axis

Table 9:

Meas.	Ceiling/ Comp.	Spires/ Roughness Elements	Type
001	01/ UW	<i>Frieso-Set-Up / Base Plates</i>	VP
002	01/ UW	<i>No Spires / Base Plates</i>	VP
003	01/ UW	<i>Sharp edge 150 x 6 mm at inlet / Base Plates</i>	VP
004	01/ UW	<i>Sharp edge 80 x 6 mm at inlet / Base Plates</i>	VP
005	01/ UW	<i>No Spires / Base Plates</i>	Rep 002
006	01/ UW	<i>No Spires / Base Plates</i>	LP
007	01/ UW	<i>No Spires / Base Plates</i>	LP
008	01/ UW	<i>No Spires / Base Plates</i>	LP
009	01/ UW	<i>No Spires / Base Plates</i>	LP
010	01/ UW	<i>5x XVI symmetric with distance $\Delta y = 800$ mm / Base Plates</i>	VP
011	01/ UW	<i>as meas. 010 / Base Plates</i>	VP HQ
012	01/ UW	<i>Roughness elements covering 1 m at inlet, alternately with height =40mm and 20mm and distance of 280 mm lateral and 100 mm longitudinal - for simulating the pre-island at real Bolund in 4 km</i>	VP
013	01/ UW	<i>as 012</i>	VP HQ
014	01/ UW	<i>10x XVI symmetric with distance $\Delta y = 400$ mm / Base Plates</i>	VP
015	01/ UW	<i>as 014</i>	VP HQ
016	02/ UW	<i>as 014</i>	VP
017	02/ UV	<i>as 014</i>	VP
018	02/ UV	<i>as 014</i>	LP
019	02/ UV	<i>10x XVI special configuration - see logbook / Base Plates</i>	LP
020	02/ UV	<i>as 019</i>	LP
021	02/ UV	<i>10x XVI approx. $\Delta y_{i+1} = \Delta y_i + \text{const}$ / Base Plates</i>	LP
022	02/ UV	<i>as 021</i>	VP

Table 10 - Title: Documentation of the adjustment process part II, objectives, lessons learnt and further remarks.

Legend in chronological order of appearance:

\hat{u}_* = shear stress;

w_{rms} = root mean square error of wind fluctuations in vertical direction (measure of turbulence intensity);

L_{ux} = Integral length scale in main wind speed direction;

U_{mean} = wind speed in main wind speed direction averaged over entire measurement time interval, measured with LDA-probe;

WT = Wind Tunnel;

α = power law exponent, estimated by least square error fit out of the vertical profile of the mean velocities;

z_0 [m] = roughness length in corresponding to logarithmic wind profile assumption, estimated by least square error fit out of the vertical profile of the mean velocities;

U_{ref} = reference wind speed in main wind speed direction averaged over entire measurement time interval, measured with Prandtl-tube at fixed location of the Prandtl-tube

Table 10:

Meas.	Objective	Lessons learnt	Remarks
001	<i>Test of Spires and roughness of base plates</i>	\hat{u}_* profile wrong, w_{rms} -profile wrong, no const. shear layer,	<i>No further examination necessary</i>
002	<i>Test of empty WT and roughness of base plates</i>	L_{ux} too low, spectrum wrong at certain heights maybe due to sampling frequency, repetition needed const. shear layer (\hat{u}_*) ca. 20 m in full scale	$\alpha = 0.13$; $z_0 = 0.01$ <i>(sensible for removal of points)</i>
003	<i>Influence of edge with height 160 mm</i>	const. shear layer (\hat{u}_*) as 002, no remarkable effects on L_{ux} , negative gradient of spectrum too small	$\alpha = 0.10$; $z_0 = 0.005$ <i>(sensible for removal of points)</i>
004	<i>Influence of edge with height 80 mm</i>	const. shear layer (\hat{u}_*) as 002, no remarkable effects on L_{ux} , negative gradient of spectrum too small	$\alpha = 0.12$; $z_0 = 0.005$ <i>(sensible for removal of points)</i>
005	<i>Rep of 002</i>	L_{ux} too low, negative gradient of spectrum too small but altogether a satisfactory natural grown boundary layer, const. shear layer (\hat{u}_*) and L_{ux} could be higher	$\alpha = 0.12$; $z_0 = 0.008$ <i>(sensible for removal of points)</i>
006	<i>Lateral Homogeneity at $z = 50$ mm , $U_{ref} = 7.9$ ms⁻¹</i>	S-trend in lateral profile with deviation of +- 4 percent for U_{mean} with respect to lateral averaged U_{mean} for $U_{ref} = 7.9$ ms ⁻¹ – 9.7 ms ⁻¹ S-trend increases for lower U_{ref}	
007	<i>Lateral Homogeneity at $z = 50$ mm , $U_{ref} = 9.7$ ms⁻¹</i>		

Meas.	Objective	Lessons learnt	Remarks
008	Lateral Homogeneity at $z = 50 \text{ mm}$, $U_{ref} = 3.8 \text{ ms}^{-1}$		
009	Lateral Homogeneity at $z = 50 \text{ mm}$, $U_{ref} = 1.3 \text{ ms}^{-1}$		
010	Set spires for increase of L_{ux}	Does not improve results, L_{ux} -profile does not follow a good shape above $z = 60 \text{ mm}$ ($= 12.5 \text{ m fs}$, see figure next page)	Same order as before
011	as 010 with HQ (= High quality = data rate for spectra)		
012	Set roughness for simulation of pre-island and increase of L_{ux} or cs . \dot{U}^* -height	Does not improve results, in contrary: L_{ux} worse and gradient of spectrum worse at upper level (i.e. $z=400 \text{ mm}$)	
013	as 012 with HQ		
014	Set more spires for increase of L_{ux} as 010 and a better shape of the vertical profile of L_{ux}	L_{ux} and spectra slightly better, friction velocity U^* still to small (proved with 5-10 percent rule out of Snyder and $\Delta_{min}=200\text{m}$ and $\Delta_{max}=700\text{m}$ – see excel-sheet for calculation)	
015	as 014 with HQ		
016	Adjust ceiling according to boundary layer growth for increase of u^*	\hat{u}_* slightly increased, between real-Bolund and literature-value	
017	Set-up of UV-measurements for proof whether $v'=0$, Careful calibration of Traverse steps, calibration of pressure probe and test of pressure gradient	Trend in V-component? Pressure-gradient around 2 percent of p_{inf} (at Prandtl-tube) -> very good! z_0 slightly higher than before, L_{ux} ok, I_u , I_v ok	$\alpha = 0.12$; $z_0 = 0.01$ (sensible for removal of points)
018	Lateral Homogeneity at $z = 40 \text{ mm}$, $U_{ref} = 8.4 \text{ ms}^{-1}$	S-trend along lateral profile, max deviation +- 10 percent	
019	Remove S-trend Lateral Homogeneity at $z = 40 \text{ mm}$, $U_{ref} = 8.4 \text{ ms}^{-1}$	No improvement	
020	Remove S-trend Lateral Homogeneity at $z = 40 \text{ mm}$, $U_{ref} = 8.5 \text{ ms}^{-1}$	No improvement	

Meas.	Objective	Lessons learnt	Remarks
021	Remove S-trend Lateral Homogeneity at $z = 40 \text{ mm}$, $U_{ref} = 7.6 \text{ ms}^{-1}$	Max 1.06 percent deviation for U_{mean} with respect to lateral averaged U_{mean} for $y \pm 125 \text{ mm}$ Max 1.06 percent deviation for U_{mean} with respect to lateral averaged U_{mean} for $y \pm 250 \text{ mm}$ Max 2.84 percent deviation for U_{mean} with respect to lateral averaged U_{mean} for $y \pm 500 \text{ mm}$ Max 2.84 percent deviation for U_{mean} with respect to lateral averaged U_{mean} for $y \pm 1000 \text{ mm}$	=> deviation < 3 percent, flow assumed to be nearly lateral homogeneous (S-trend minimized)
022	Influence of spire configuration 021 on vertical profile	Profile of turbulence intensities I_u , I_v better, also spectra, L_{ux} ok	

01		y- side	y+ side	middle
Element	x [mm]	Height [mm]	Height [mm]	average height
1	1500	887	885	886
2	3000	893	906	899.5
3	4500	906	907	906.5
4	6000	993	1000	996.5
5	7500	1009	1011	1010
6	9000	1014	1016	1015
7	10500	1025	1035	1030
8	12000	1045	1038	1041.5
9	13500	1060	1054	1057
10	15000	not adjustable		
11	16500	1097	1091	1094
12	18000	965	969	967

Figure 137: Ceiling "01", excerpt from "BOLUND_WOTAN_logbook_2011.xls" sheet "Deckenkonfiguration".

02		y- side	y+ side	middle
Element	x [mm]	Height [mm]	Height [mm]	average height
1	1500	887	887	887
2	3000	893	893	893
3	4500	906	906	906
4	6000	911	913	913
5	7500	920	920	920
6	9000	927	927	927
7	10500	931	934	934
8	12000	988	941	941
9	13500	952	948	948
10	15000	not adjustable		955
11	16500	965	962	962
12	18000	967	967	967

Figure 138: Ceiling "02", excerpt from "BOLUND_WOTAN_logbook_2011.xls" sheet "Deckenkonfiguration".

MATLAB program code for filtering Bolund field data

First open the file “testmysql1” in the electronic supplementary material.

Then e.g.:

```
Select M0_S_5 measurement time periods for corresponding M0_S_5 data,
filtered for wind direction and stability
M0_S_5=mysql('SELECT      s.Name      FROM      stat_nesw_metek3dcorr_10min      s,
stat_stability_metek3dcorr_10min      ss      WHERE      s.Name=ss.Name      AND
ss.Sonic_id="M0_S_5"      AND      s.Sonic_id=ss.Sonic_id      AND      s.windDir>262      AND
s.windDir < 278 AND ABS(ss.invL)<0.002');

Select M3_S_2 measurement time periods for corresponding M0_S_5 data,
filtered for wind direction and stability
M3_S_2=mysql('SELECT      s.Name      FROM      stat_nesw_metek3dcorr_10min      s      WHERE
s.Sonic_id="M3_S_2"      AND      s.Name      IN      (SELECT      s.Name      FROM
stat_nesw_metek3dcorr_10min      s,      stat_stability_metek3dcorr_10min      ss      WHERE
s.Name=ss.Name      AND      ss.Sonic_id="M0_S_5"      AND      s.Sonic_id=ss.Sonic_id      AND
s.windDir>262 AND s.windDir < 278 AND ABS(ss.invL)<0.002)');

Select M3_S_5 measurement time periods for corresponding M0_S_5 data,
filtered for wind direction and stability
M3_S_5=mysql('SELECT      s.Name      FROM      stat_nesw_metek3dcorr_10min      s      WHERE
s.Sonic_id="M3_S_5"      AND      s.Name      IN      (SELECT      s.Name      FROM
stat_nesw_metek3dcorr_10min      s,      stat_stability_metek3dcorr_10min      ss      WHERE
s.Name=ss.Name      AND      ss.Sonic_id="M0_S_5"      AND      s.Sonic_id=ss.Sonic_id      AND
s.windDir>262 AND s.windDir < 278 AND ABS(ss.invL)<0.002)');
```

Quick Bolund MySQL Query Browser manual

Alternatively, the Bolund MySQL database can be browsed with MySQL Query Browser

1. Install "MySQL Query Browser" - for example download MySQL Query Browser1.1 from <http://mysql-query-browser.soft-ware.net/download.asp> (as of 18/10/2012) Follow the installation instructions. Don't use "MySQL Workbench" since this doesn't work.
2. Start MySQL Query Browser. Type for server host: veadata-01.risoe.dk. Furthermore type your username and password see Figure 139.



Figure 139 Query Browser log-in

3. Successful log-in opens the browser window, see Figure 140.
4. Now you can browse Bolund database using structured query language (SQL), see Figure 141. For a quick start read the start guide in the browser's "help". Drag and drop function can be helpful.

More information on SQL, see e.g. <http://www.w3schools.com/sql/> (as of 18/10/2012).

Also useful, the examples given in "The Bolund Experiment: Overview and Background", pp. 40; see <http://130.226.56.153/rispubl/reports/ris-r-1658.pdf> (as of 18/10/2012)

Another query example:

Browsing sonic data, mast number 0, height 5 meter, x-direction relative to mess mast for wind direction 260-280 degree (in 10-min mean) and inverse Monin-Obukhov-length < 0.002 (in 10-min mean) – code:

```

SELECT s.Name, s.Sonic_id, m.M0_SX_5, s.windDir, ss.invL

FROM stat_nesw_metek3dcorr_10min s, metek3dcorr_1_20hz m,
stat_stability_metek3dcorr_10min ss

WHERE m.Name=s.Name AND s.Name=ss.Name AND ss.Sonic_id='M0_S_5'
AND s.Sonic_id='M0_S_5' AND s.windDir>260 AND s.windDir < 280
AND ABS(ss.invL)<0.002

```

Please contact Risø DTU before use.

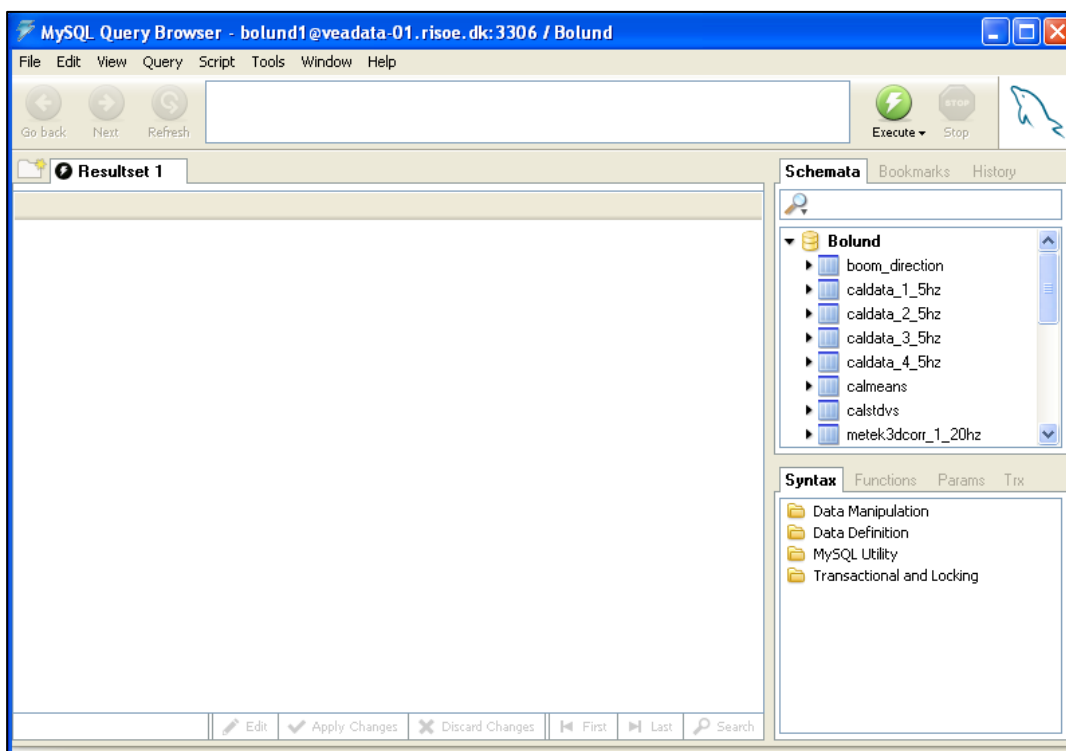


Figure 140: Browser window



Structure function – what is this for?

For the *characterization of a meteorologically atmospheric boundary layer* parameters are used such as the vertical mean wind profile, turbulence profiles and determination of a layer with constant shear stresses (see determination and adjustment of Bolund in WOTAN inflow conditions, pp. 177). These parameters involve (temporal) mean values of the *wind velocity signal* (mean wind speed) or *mean values of the autocorrelation for zero time lag* (standard deviations) or *mean values of cross-correlations* of different wind velocity components (e.g. shear stress). For field data it might not always be possible to find a reasonable averaging time⁹⁶ (for the ensemble average of the underlying stochastic process, recall “*The ergodic theorem*”, pp. 41). Also, it might not be possible to assess integral length scales. The reason for this is the *non-stationarity* of the data. A solution can be to analyse the *differences* (velocity increments) instead. Non-stationary data can have *stationary differences*. (By taking differences, the trends are removed from the time series and it is more likely that the differences are statistically stationary.) Hence, the examination of *differences of turbulent velocity data* can be a solution to the non-stationarity problem of field data.

Dias et al., [2004], state: “Non-stationarity in the atmospheric boundary layer, however, is not very well studied, and only recently has been receiving more attention” [ibid p. 166]. As far as the author sees, the interest into the examination of small scale turbulence and differences of field data increases (e.g. University of Oldenburg). Also, examination exists for *laboratory turbulence*, e.g. by Castaing et al., [1990]. From the author’s point of view, further work could be useful to clearly relate the *abstract statistical properties* of differences (e.g. structure functions) to *empirically observable* and *meteorologically meaningful properties* of the boundary layer (such as the integral length scale). This could fundamentally help in the *determination of turbulent features of field data* (and hence in the determination of *inflow conditions* for future *advanced flow modelling*).

⁹⁶ This is also supported by Gluhovsky and Agee, [1994]: “In the atmosphere, integral scales are relatively large (in comparison with other areas of turbulence research), which results in the problem of obtaining records of adequate length. Furthermore, stationarity is no and then questionable, so averages can sometimes be statistically unreliable”, [ibid p. 1682]. Gluhovsky and Agee, [1994], provide a comprehensive framework on turbulence statistical studies in planetary boundary layers and examine the “averaging problem.”

Remarks on the work carried out

Here, further remarks on the work carried out on wind tunnel modelling by the author are given:

- **Model as model AND reality:** In the case of wind tunnel modelling, the *model* itself becomes a *reality*. The wind tunnel flow prior to the measurements turns into the *true value* for a *numerical modeller*, who models the wind tunnel flow. Hence, *validation* in terms of COST 732, with combination of wind tunnel and field data can *increase the belief* (in terms of Bayesian interference, see outlook, pp. 279) into the numerical model.
- **Incompatibility of flow scales:** Atmospheric flow over hills is a good example of a flow geometry in which the *incompatibility of flow scales* imposes a challenging task for the modeller: the molecular friction processes induced by the orography are not well resolved in the microscale CFD models (above molecular level). This *small scale error* can be passed through to *mesoscale* and *regional weather models*.
- **Distinction of flow over hills and flow in urban canopies:** Modelling atmospheric boundary layer flow over topography is significantly different from modelling urban canopies concerning the *heterogeneity of the geometries*. Urban geometries are usually a compound of sharp-edged buildings. In contrast, hill shapes are usually not box-shaped or sharp-edged which can cause problems with the aerodynamical roughness in wind tunnel modelling. This was not a pitfall for the main Bolund WOTAN wind tunnel study. However, correct hill shape modelling is crucial; over-roughening of the hill model surface can lead to distortion of flow geometry. Sensitivity on the *sharpness of the front edge* of the hill model was shown in the idealized Bolund study. The author of this work does currently not see a theoretical law as an alternative to the empirical sensitivity studies, in this case.

- **Logical pitfall of stationarity tests:** A problem for field data (and also wind tunnel data) is: A method for testing time series for *statistical stationarity* without *assuming* by application of the test that *the time series was stationary* – does not yet exist.
- **Mathematical modelling of small scale turbulence as a stochastic process:** One could examine the correct modelling of *small scale time resolution* of turbulence in the wind tunnel with an a posteriori analysis of the *fluctuations* of wind tunnel time series in comparison with field data with advanced statistics. However, there are two major problems: First, the *limitations* and *strong assumptions* of the *mathematical* statistical models have to be taken into account. For example, the popular ARMA-models (Autoregressive Moving Averages) tend to be *over-fitted* and thus epistemically meaningless. Also, ARMA-models lack of *physical interpretation* for small scale turbulence. This means that a well-fitted ARMA model can produce time series which are physically meaningless (this was tried and is not shown, here).
- **Extreme value analysis and stationarity:** *Extreme value analysis* can also be considered for comparison of wind tunnel with field inflow data, e.g. for consideration of correct modelling of *block maxima*. However, extreme value analysis depends on *the statistical stationarity of data*. Field data is useless without strong manipulation of data (e.g. trend removal), and it is unclear how to assess the *impact of the manipulation*. The same holds for advanced statistics of *resampled wind tunnel data*. For non-equidistant time steps, the *influence of the resampling method* on the small scale statistics of the time series would have to be assessed.
- **Extreme value statistics and self-similarity of wind tunnel data:** In collaboration with the Seminar für Statistik in ETH Zurich, Prof. Hans-Ruedi Künsch, EWTLeHamburg wind tunnel data was analysed in the Master thesis “Heavy tails and self-similarity of wind turbulence data” by Jongkil Kim. The aim of the work was to examine whether the data fits the “normal inverse Gaussian distribution” for the increments as it was examined in Barndorff-Nielsen et al., [2004].

This *normal inverse Gaussian distribution* has a location and scale parameter. It is based on the normal distribution and the parameters depend on the increment τ . The data which was available at that time was *wind tunnel* inflow data of the *Hamburg campaign* and the corresponding *field data* from the NDR-pylon in Hamburg-Billwerder (the “Hamburg Weather Mast”).⁹⁷

The field data showed *heavy tails* and *little skewness* and applicability of the Barndorff-Nielsen distribution. The wind tunnel data fits well to the *Gaussian distribution*, even for *small* time lags, so it was not analysed further. Also, *joint distributions* of *consecutive* velocity values were examined and an indication of tail dependence was found. Furthermore, the data analysis indicated *dependence* of *extreme value* properties on *1-minute average wind speeds*. However, this requires further examination.

- **Geomorphological dynamics:** The hill shape analysis has clearly shown strong *sensitivity* to slight changes in the representation of the *hill shape*, especially *sharpness of the front edge*. Thus, for long-term predictions or modelling atmospheric boundary layer flow over hills over a long period of time, *geomorphological processes* can be *significant*, such as erosion etc. In other words, a model for flow over hills in which the shape of the topography remains constant refers to a *snapshot* of the geomorphological *reality* with respect to large time scales. (Multiyear simulations may require suitable accounting of the local geomorphological dynamics.)

⁹⁷ See also: <http://wettermast-hamburg.zmaw.de/> (as of 03/10/2012)

Standard Bayesian framework

This section is a summary of [Weisberg, 2012] with some extensions by G.P.. Probabilities can be formalised as *numbers that are assigned to possible outcomes* of a situation, an experiment, a game etc. The *outcome set* can be denoted with Ω and possible *outcomes* are *elements* in Ω (pp. 41). For example, the *outcome set* of the *roll* for a *six-sided dice* can be described as $\Omega = \{1,2,3,4,5,6\}$. The assignment of probabilities as numbers to elements of the outcome space can be formalized with a mapping $P: \Omega \rightarrow \mathbb{R}$. For example, the assignment for a perfectly fair dice with outcome set, $\Omega=\{1,2,3,4,5,6\}$ would be: $P(\{1\}) = 1/6$, $P(\{2\}) = 1/6$, $P(\{3\}) = 1/6$, $P(\{4\}) = 1/6$, $P(\{5\}) = 1/6$, $P(\{6\}) = 1/6$.

A mathematician who wants to work with this function will ask for *properties* of the function or of the outcome set. This is the motivation to define a *probability space*. The usual way to do this is to demand a certain *structure* on the *outcome*, the σ -algebra (called “sigma-algebra”). Recall that the *outcome space* was denoted by an ordered pair (Ω, σ) , and the *probability space* as ordered triple (Ω, σ, p) . For the definition of a σ -algebra and a *probability function*, see pp. 41. For these definitions basic *set theoretical* notions are pre-assumed and not discussed here. Instead of relying on a set-theoretical approach, probabilities can be defined in many different ways, e.g. by means of *sentences* and *logic operators*, see e.g. Weisberg, [2012]. It is important that the *elements* of the *outcome space* can be interpreted as *sentences*. This leads to the fact that *probability* machinery can be used to analyse a *degree of logical entailment* (also denoted: “degree of believe”) [Weisberg, 2012]. Here, this will be introduced for the purpose of quantification of model impact – for examining how *confirmation and evidence* for *scientific theories* can be analysed within the framework of *Bayesianism*.

Definition: Conditional probability

Let $A, B \in \sigma$. The *conditional probability* of B given A is written $p(B|A)$, and is defined by

$$p(B|A) := \frac{p(A \cap B)}{p(A)},$$

when $p(A) \neq 0$.

—/

One way to handle probability is interpreting it as a *logical property*. This is especially useful if the elements of the *outcome space* are interpreted as *sentences* and set-theoretical operators are interpreted as *logical operators*.

For example:

- if A is logical true, $p(A)=1$.
- If A is false, $p(A)=0$.

The values in between can be thought of as *degrees of logical truth*. Now, from logical perspective, the notion of *conditional probability* needs to be connected to logical entailment since " $p(A \text{ entails } B)=p(B|A)$ " is the same as " $p(A \cap B) / p(A)$ " for $p(A) \neq 0$.

Following the *logical interpretation* of probabilities as *truth values*, then: if A entails B that means $p(B|A)=1$. If A entails not B then $p(B|A)=0$. Thus, $p(B|A)$ can be understood as *degree* to which A entails B. The discussion, how a "degree of logical entailment" fits into the classical understanding of logic, is skipped at this point.

Another way to understand probabilities is the *degree of belief* interpretation, e.g. based on Ramsey and de Finetti. This means that probabilities can be understood as a subject's level of certainty. Then, $p(1), p(2)$ and $p(3)$ can be read as *rational rules*.

For example, a wind forecast predicting 70 percent probability for wind speeds between 10-15 m/s and at the same time promising 70 percent probability for wind speeds between 5-9 m/s, would *violate* our understanding of *rationality*.

Probability theory seems to follow our *rules of rationality* – at first sight – however, in practice it seems that the human mind does not strictly follow the rules (or probability theory does not follow the rationality of the human mind). For example, the prominent *conjunction fallacy problem* illustrates this. Tversky and Kahneman, [1982], analyse that in certain circumstances, people tend to believe $p(A \cap B) > p(A)$, for certain A,B. This is in

contradiction to the mathematical rules.⁹⁸ Hence, for discussion on *rationality* with regard to “probability”, it has to be considered that there may be different “probabilities” and that the human mind can be apt to handle *probabilities* distinct from the rationality according to the *mathematical rules*.

There are also *non-epistemic* interpretations of *probabilities* as *frequencies* and *chances*. According to the *frequency interpretation*, the *probability of an event* can be assigned by *frequency with which such things occur*, [Weisberg, 2012]. This means that a probability function can be understood as a *limit of an empiric probability density function* with sample size towards infinite. For example, in case of a perfectly fair dice, probability would converge to 1/6 for every number 1,...,6 if the sample size of rolls of the dice increases towards infinity. Please note that this expectation is due to our *idealised definition* of a *fair* dice which of course, in reality, does *not* exist. Also, probabilities can be interpreted as *physical chances*. This means that probabilities can be interpreted as objective *physical properties of objects and events*. However, whereas *frequencies* or *empirical knowledge* of physical properties can usually be interpreted as *probabilities of elements* in a certain *outcome space* – the other way around it is not clear if *probabilities* can always be interpreted as *frequencies* or *physical properties*. (Do we want to assign the probability that one person falls in love with another as an *objective physical property*? – or as a *frequency*?)

⁹⁸ The empirical outcome of the experiments, concerning the conjunction fallacy, might be due to misunderstanding of the question. The most cited example for the conjunction fallacy is the following case: Assume Linda is 31 years old, single, outspoken, and very bright. She majored in philosophy. As a student, she was deeply concerned with issues of discrimination and social justice, and also participated in anti-nuclear demonstrations. Which is more probable?

1. Linda is a bank teller.

2. Linda is a bank teller and is active in the feminist movement.

According to Tversky and Kahneman, [1982], around 85 percent of those asked chose option 2. However, there is on-going discussion on many sources of misunderstanding, see e.g. Hertwig et al., [2008]

Principle of indifference and ambiguities

Another question is how probabilities should be *assigned* if *no evidence* is given and *no degree of belief* is *preferred*. This can be done following the *principle of indifference*. It states:

- Given a finite outcome set Ω with cardinality N , if you have no (relevant) evidence then assign $p(\omega_i)=1/N$ to each singleton $\omega_i \in \Omega$.

The *principle of indifference* can be extended to continuous Ω by use of appropriate technical tools including a probability density function and the *integration* over subsets of Ω . In the 1-dimensional case, the length of an interval can be assigned as a probability of the interval.

For defining a *unique* probability, the probability should be *independent of the choice of parameterization* of Ω . This is *not* always the case. There are examples of probabilistic questions in which *no invariant density function exists* – invariant under parameterization of the space. In other words: the problem can occur that the *choice of parameterization* of the outcome space *influences* the result. For an illustrative example see Weisberg, [2012, p. 40]. Hence it should be kept in mind that the *determination* of the *outcome space* can influence the result. The interesting aspect here is that the “rationality” which determines the *degree of belief* is not only a question of the *rules* that can or cannot be applied to the probability space. Even if it is agreed on using the mathematical rules of probabilities instead of other conceptions of probability, still, the *modelling* of the *outcome space* is subject to individual preferences and will determine the results.

Appendix according to §7 paragraph 4 of the Doctoral Degree Regulations of the MIN Faculty:

Short summary of the results in English:

See p. 265 - 267.

Short summary of the results in German:

Fundamentaler Teil:

Ein atmosphärischer Grenzschichtwindkanal kann interpretiert werden als *Vermittler* zwischen Theorien und Realität; (Theorien aus Gebieten der Strömungsdynamik und der Meteorologie einerseits und der Realität der atmosphärischen Grenzschichtströmung andererseits). Im Hinblick auf die verfügbaren Theorien wird die Navier-Stokes Gleichung in dieser Arbeit als *Kern* der modernen Strömungsdynamik angesehen. Sie kann vor dem historischen Kontext der Theoriebildung in der Strömungsmechanik als *Spezialisierung* der Euler Gleichung verstanden werden, da sie die *Viskosität* von Fluiden einführt. (*Kern* und *Spezialisierung* sind hier Begriffe aus dem *Strukturalismus*, einer Rahmentheorie zur Analyse von Theorien in der Wissenschaftstheorie.) Die Analysen der Strömungsdynamik in zwei technischen Meta-Rahmentheorien, nämlich im (bereits genannten) *Strukturalismus* und in Gärdenfors' *begrifflichen Räumen*, bringen ein ähnliches Resultat hervor: Die mengentheoretische Rekonstruktion (strukturalistisch) und die geometrische Analyse (Gärdenfors-räumlich) werden vereinigt in den differentialgeometrischen Objekten (Mannigfaltigkeiten), die (möglicherweise) die Navier-Stokes Gleichungen lösen.

In dieser Arbeit wird argumentiert, dass Modelle genutzt werden um eine Lücke zwischen Theorien und Beobachtungen in der Welt zu schließen, und dass durch das (maschinengestützte) Modellieren eine Art „künstlicher“ Erfahrung erschaffen wird, indem Theorien mit einer solch großen Anzahl von Modell- und Natur-Daten verbunden und Modell-Resultate als Erfahrungswerte geliefert werden, wie es für den Menschen ohne Hilfsmittel niemals möglich wäre. Das Verständnis von Modellen als *Vermittler zwischen Theorien und Realität* mithilfe von Datenvergleichen kann für den Aufbau methodologischer Rahmenkonzepte zur Qualitätsabschätzung von Windprognose-Werkzeugen als Fundament

genutzt werden, zum Beispiel für die Anwendung in der Windenergie. Der Modell-Vergleich muss allerdings von einer qualitativen (strukturellen) Analyse und dem Vergleich der involvierten Theorien begleitet werden. Der Vergleich von „Zahlen“ ist nicht hinreichend, da die *Akkuratesse* (Richtigkeit der Modelle im Vergleich mit der Realität) nicht quantifizierbar ist. (Die Begriffe *Akkuratesse* und *Präzision* werden in dieser Arbeit für die Kategorisierung von Modellunsicherheiten strikt getrennt.) Daten für die Modellvalidierung müssen für das jeweilig spezifische Modell geeignet sein. Zum Beispiel wird in dieser Arbeit gezeigt, dass Naturdaten nicht notwendigerweise zufriedenstellend „präzise“ sind um als Validierungsdaten Nutzen zu bringen – „präzise“ bezieht sich hier auf den Kontext der Theorien, die in dem jeweiligen Modell Anwendung finden. Die Ergebnisse aus dem fundamentalen Teil dieser Arbeit werden an einem konkreten experimentellen Teil verdeutlicht. Dieser ist zusammengefasst im folgenden Abschnitt.

Experimenteller Teil:

Glatte atmosphärische Grenzschichtströmung über dem steilen, dänischen Hügel Bolund wurde für zwei verschiedene Windrichtungen mit besonderem Augenmerk auf *Akkuratesse* (Naturähnlichkeit der Strömung) und *Präzision* (Wiederholbarkeit der Modell-Resultate) in einem großen Grenzschichtwindkanal (WOTAN in der Universität Hamburg) modelliert. Im Experiment zeigt sich, dass die mittlere Windströmung bereits eine Hügellänge vor dem Hügel messbar durch die Topographie beeinflusst ist. Das Einflussgebiet der Topographie auf die atmosphärische Grenzschicht erstreckt sich über dem Hügel um bis zu fünf Hügelhöhen vertikal und hinter dem Hügel in bis 1.5 Hügellängen horizontal. Der maximale „Speed-up“ von Bolund in WOTAN wird in 2-5 m Höhe über der Vorderkante gemessen. Die mittlere Geschwindigkeit erhöht sich um bis zu 40 Prozent gegenüber der mittleren Geschwindigkeit in der gleichen Höhe über Grund in der von der Topographie ungestörten atmosphärischen Grenzschicht. Auch die Statistiken der turbulenten Windschwankungen sind sensitiv für die Topographie: Die *Turbulenzintensität* verdoppelt sich in halber Hügelhöhe hinter dem Hügel; Die negative *Scher-Spannung* verfünffacht sich im Absolutbetrag an der Vorderkante und hinter dem Hügel; Die *Schiefte der Fluktuationsverteilungen* ist negativ im freien Anströmungsfeld und verfünffacht ihren Betrag im Negativen an der vorderen Luv-Kante des Hügels. Positiv ist die Schiefe dagegen in der Region der Strömungsverlangsamung vor der

steilen Vorderkante des Hügels und im – relativ zur ungestörten Grenzschichtströmung verlangsamen – Nachlauf hinter dem Hügel.

Es zeigt sich, dass die *Präzision* der oben genannten Ergebnisse stark von der lokalen Strömung abhängt (ob dies signifikant ist hängt von dem Zweck der Modellierung ab). Wie in der Pilotstudie „idealized Bolund“ gezeigt, kann sich die Streubreite der mittleren Geschwindigkeiten (berechnet durch Wiederholungsmessungen) an bestimmten Orten versiebenfachen. In der Pilotstudie wurde ferner gezeigt, dass die Strömung abhängig von der geometrischen Auflösung des Modells ist. Ein Ablösungswirbel über der Vorderkante wurde gefunden für eine räumliche Auflösung von 2.5 m in Naturmaßstab. Der Wirbel verschwand für runde Konturen. (Hier bedeuten 2.5 m Auflösung im Naturmaßstab in dimensionsloser Form $0.1H$ bzw. $0.01L$ für H := Hügelhöhe und L := Hügellänge.) Auch sind Ort und Ausdehnung des Speed-up-Gebiets über dem Hügel, die Blockierung vor dem Hügel und Nachlaufteffekte hinter dem Hügel abhängig von der *geometrischen Repräsentation* der Hügelform. Dies wurde in der Pilotstudie für eine Auflösung von 1.5 m im Naturmaßstab ($0.05H$ bzw. $0.01L$ hohe Stufen) untersucht. In einer weiterführenden statistischen Analyse zu der Strömung über der Vorderkante des Hügels wurde gezeigt, dass die *statistische Konvergenz höherer statistischer Momente* (der Ordnung 1 bis 4) stärker von der Sampling-Dauer als von der Resampling-Frequenz abhängt (innerhalb der hier untersuchten Resampling-Konfigurationen).

Zuletzt wurden offene Fragen herausgestellt, unter anderem ob die Analyse einzelner Zeitserien im Bolund-Naturdatensatz besser geeignet sein könnte um sie mit *statistisch stationären* Modelldaten zu vergleichen als die Anwendung von Ensemble-Mittelwerten (aufgrund der Inhomogenität des Datensatzes); wie LDA-Daten bestmöglich aufbereitet werden können für zukünftige „*fortgeschrittene*“ *statistische Analysen* im Hinblick auf klein-skalige Turbulenz (z.B. mithilfe von Differenzenanalyse, Strukturfunktionen und Extremwertstatistik) und ob ein *Bayesianischer Ansatz* hilfreich sein kann um Modellergebnisse zu interpretieren, vor dem Hintergrund der Tatsache, dass eine absolute Modellakkuratesse nicht quantifizierbar ist.

List of any earlier publications derived from the dissertation:

Petersen, G.; Leitl, B. and Schatzmann, M.: On proper physical simulation of turbulent atmospheric flow over hills;

EAWC proceedings, Brussels, 2011

Extended as:

Petersen, G.; Leitl, B. and Schatzmann, M.: Wind tunnel simulation: On Proper Physical Modelling of Atmospheric Boundary Layer Flow over Hills;

Windtech International; September 2011

Petersen, G.; Leitl, B. and Schatzmann, M.: ABL flow over hills: A review on theory and critics of recent wind tunnel studies;

ICWE 13, conference article, Amsterdam, 2011

Petersen, G.; Gähde, U.; Hoffman, M.; Leitl, B. and Schatzmann, M.: Models in Wind Energy Assessment;

PHYSMOD 2011 proceedings, 2011

Petersen, G. and Zenker, F.: From Euler to Navier Stokes: The Conceptual Space of 19th Century Fluid Dynamics;

submitted to History and Philosophy of Science, 2012

Fin of appendix